AFFTC-TIM-03-07

An Investigation of Open Loop Flight Control Equations of Motion Used to Predict Flight Control Surface Deflections at Non-Steady State Trim Conditions

(Project HAVE TRIM)

AFFTC

GARY D. MILLER
Captain, USAF
Project Manager

FABRIZIO BECCARISI
First Lieutenant, ITAF
Flight Test Engineer

MATTHEW W. HIGER
Captain, USAF
Project Pilot

E. JOHN TEICHERT
Captain, USAF
Project Pilot

PETER A. WENELL
Captain, USAF
Flight Test Navigator

DECEMBER 2003

FINAL TECHNICAL INFORMATION MEMORANDUM

Approved for public release; distribution unlimited.

AIR FORCE FLIGHT TEST CENTER
EDWARDS AIR FORCE BASE, CALIFORNIA
AIR FORCE MATERIEL COMMAND
UNITED STATES AIR FORCE

This Final Technical Information Memorandum (AFFTC-TIM-03-07), *An Investigation of Open Loop Flight Control Equations of Motion Used to Predict Flight Control Surface Deflections at Non-Steady State Trim Conditions* (Project HAVE TRIM), was submitted under Job Order Number (JON) M03C1400 by the Commandant, USAF Test Pilot School, Edwards AFB California 93524-6485.

Prepared By:

GARY D. MILLER
Captain, USAF
Project Manager / Flight Test Engineer

PETER A. WENELL
Captain, USAF
Project Flight Test Navigator

MATTHEW W. HIGER
Captain, USAF
Project Test Pilot

E. JOHN TEICHERT
Captain, USAF
Project Test Pilot

FABRIZIO BECCARISI
First Lieutenant, ITAF
Project Flight Test Engineer

Reviewed By:

RUSSELL E. ERB
Master Instructor, USAF TPS/EDP
Staff Monitor

MARK P. STUCKY
Lieutenant Colonel, USAF
Chief, Test Management Division

This Final Technical Information Memorandum has been approved for publication:

ERNIE H. HAENDSCHKE
Colonel, USAF
Commandant, USAF Test Pilot School

REPORT DOCUMENTATION PAGE

Form Approved
OMB No. 0704-0188

Public reporting burden for this collection of information is estimated to average 1 hour per response, including the time for reviewing instructions, searching existing data sources, gathering and maintaining the data needed, and completing and reviewing this collection of information. Send comments regarding this burden estimate or any other aspect of this collection of information, including suggestions for reducing this burden to Department of Defense, Washington Headquarters Services, Directorate for Information Operations and Reports (0704-0188), 1215 Jefferson Davis Highway, Suite 1204, Arlington, VA 22202-4302. Respondents should be aware that notwithstanding any other provision of law, no person shall be subject to any penalty for failing to comply with a collection of information if it does not display a currently valid OMB control number. PLEASE DO NOT RETURN YOUR FORM TO THE ABOVE ADDRESS.

1. REPORT DATE
12 Dec 03

2. REPORT TYPE
Final Technical Information Memorandum

3. DATES COVERED *(From - To)*
8 to 17 Oct 03

4. TITLE AND SUBTITLE
An Investigation of Open Loop Flight Control Equations of Motion Used To Predict Flight Control Surface Deflections at Non-Steady State Trim Conditions (Project HAVE TRIM)

5a. CONTRACT NUMBER

5b. GRANT NUMBER

5c. PROGRAM ELEMENT NUMBER

5d. PROJECT NUMBER

5e. TASK NUMBER

5f. WORK UNIT NUMBER

6. AUTHOR(S)
Miller, Gary D., Captain USAF
Wenell, Peter A., Captain USAF
Higer, Matthew W., Captain USAF
Teichert, E. John, Captain USAF
Beccarisi, Fabrizio, First Lieutenant ITAF

7. PERFORMING ORGANIZATION NAME(S) AND ADDRESS(ES)
Air Force Flight Test Center
412th Test Wing
USAF Test Pilot School
220 South Wolfe Ave
Edwards AFB CA 93524-6485

8. PERFORMING ORGANIZATION REPORT NUMBER
AFFTC-TIM-03-07

9. SPONSORING / MONITORING AGENCY NAME(S) AND ADDRESS(ES)
US Air Force Institute of Technology
2950 P Street
Wright Patterson AFB OH 45433-7765

10. SPONSOR/MONITOR'S ACRONYM(S)

11. SPONSOR/MONITOR'S REPORT NUMBER(S)

12. DISTRIBUTION / AVAILABILITY STATEMENT
Approved for public release; distribution unlimited.

13. SUPPLEMENTARY NOTES
CA: Air Force Flight Test Center Edwards AFB CA CC:012100

14. ABSTRACT
This report presents the results of Project HAVE TRIM, An Investigation of Open Loop Flight Control Equations of Motion Used To Predict Flight Control Surface Deflections at Non-Steady State Trim Conditions. The overall test objective was to validate the HAVE TRIM model through comparison of predicted control surface deflections with flight test measured control surface deflections at specified trimmed conditions. The USAF Test Pilot School, Class 03A, conducted 10 flights totaling 18.5 hours at Edwards AFB CA from 8 Oct to 17 Oct 03. All test objectives were met.

15. SUBJECT TERMS
Control Equations, Control Surfaces, Equations of Motion, Flight Control Surfaces, Flight Control Systems, Flight Test, Parameter Estimation, Stability Derivative, Stability Derivative Trim Testing

16. SECURITY CLASSIFICATION OF:			17. LIMITATION OF ABSTRACT	18. NUMBER OF PAGES	19a. NAME OF RESPONSIBLE PERSON LtCol David R. Jacques
a. REPORT UNCLASSIFIED	b. ABSTRACT UNCLASSIFIED	c. THIS PAGE UNCLASSIFIED	UNCLASSIFIED	184	19b. TELEPHONE NUMBER *(include area code)* (937) 255-7777 x 3329

Standard Form 298 (Rev. 8-98)
Prescribed by ANSI Std. Z39.18

20040722 035

PREFACE

The entire HAVE TRIM team thanks Mr Russ Easter, Mr Dave Vanhoy, Mr Chris Nagy, and Mr Mike Nelson for their invaluable guidance in the preparation for flight test, execution, data analysis, and reporting of these flight test data.

EXECUTIVE SUMMARY

The overall objective of the HAVE TRIM project was to validate the prediction of flight control surface deflections from model equations of motion in the unpublished Master's Thesis by Captain Gary D. Miller. To accomplish this, a sensitivity analysis was performed of the model's control surface deflection predictions to changes in stability derivatives. The Learjet 25 stability derivatives were updated to improve the accuracy of the model equations of motion. Project HAVE TRIM then compared the actual aircraft trimmed flight control surface deflections to the results predicted by the model equations of motion incorporating the updated stability derivatives.

Included in this document are the test and evaluation procedures, concepts, rationale, results and conclusions of the HAVE TRIM project. The responsible test organization was the 412th Test Wing. The HAVE TRIM Test Team, members of the USAF Test Pilot School Class 03A, accomplished all test and evaluation. This project was part of the curriculum for both the USAF Test Pilot School and the Air Force Institute of Technology.

A technical review board and safety review board were accomplished per Air Force Flight Test Center procedures. Also prior to flight test, the HAVE TRIM team determined the sensitivity of model results to variations in the Learjet 25 stability derivatives. From this investigation, the most critical stability derivatives were determined. These critical stability derivatives were the primary focus of the Learjet 25 aerodynamic stability derivatives updates.

Project HAVE TRIM included ten flights (18.5 flight hours) in the Advanced Information Engineering Services (formerly Veridian) Learjet 25. The flights occurred at the Air Force Flight Test Center, Edwards AFB, CA, during 8-17 October 2003 with support from Advanced Information Engineering Services.

A portion of flight test was used to update the longitudinal and lateral-directional stability derivatives of the Learjet 25 aircraft. These higher fidelity stability derivatives were then incorporated into the model equations of motion predictions for control surface deflections.

Finally, the HAVE TRIM team compared control surface deflection predictions to flight test data as a function of eight variables. The effects of aircraft center of gravity, velocity, altitude, asymmetric thrust and sideslip angle were investigated in trimmed, straight and level flight. Flight path angle variations were then used to determine trimmed climbing/descending flight effects. Trimmed turn conditions were investigated by varying bank angle or load factor. Finally, pitch-pointing capability was examined by changing the pitch rotation rate.

All test objectives were met.

This page intentionally left blank.

TABLE OF CONTENTS

PREFACE iv
EXECUTIVE SUMMARY v
TABLE OF CONTENTS vii
LIST OF FIGURES ix
LIST OF TABLES xii
INTRODUCTION 1
GENERAL 1
BACKGROUND 1
PROGRAM CHRONOLOGY 2
TEST ITEM DESCRIPTION 2
TEST OBJECTIVES 2
TEST AND EVALUATION 3
GENERAL 3
Flight Test Data Capture And Processing 3
Flight Envelope Regimes 4
Independent Variables 4
Model EOM Sensitivity To Variations In Aerodynamic Stability Derivatives 5
Aerodynamic Stability Derivatives Determination 5
Parallel δ And Aerodynamic Stability Derivatives Testing 5
TEST OBJECTIVES 6
Determine sensitivity of model EOM results to stability derivative variation 6
Determine δ_e sensitivity to stability derivative variation 7
Determine δ_a and δ_r sensitivity to stability derivative variation 8
Determine test aircraft stability derivatives 10
Derivatives as a function of α 12
Derivatives as a function of β 13
Derivatives as a function of M 14
Derivatives as a function of q 14
Derivatives as a function of flight regime (indicated by α) 15
Comparison of flight test δ's to model predictions of δ's at trimmed flight conditions 16
Compare δ(CG) to model predictions 16
Compare δ(V) to model predictions 18
Compare δ(PA) to model predictions 19
Compare δ(Asymmetric T) to model prediction 20
Compare $\delta(\gamma)$ to model prediction 21
Compare $\delta(\beta)$ to model prediction 22
Compare $\delta(\phi)$ to model prediction 22
Compare δ(Q) to model prediction 23
Determine the influence on the model accuracy of the non-linear aircraft response when flying close to the stall condition and the transonic region 24
CONCLUSIONS AND RECOMMENDATIONS 25
APPENDIX A – FLIGHT ENVELOPE AND FLIGHT LIMITS 29

APPENDIX B – FLIGHT REGIMES 31
APPENDIX C – TEST CONDITION MATRIX 33
APPENDIX D – PLOTS SUPPORTING COMPARISON OF FLIGHT TEST δ TO PREDICTED δ 39
APPENDIX E – SAMPLE MODEL PREDICTIONS 69
APPENDIX F – PLOTS SUPPORTING DETERMINATION OF TEST AIRCRAFT STABILITY DERIVATIVES 71
APPENDIX G – DERIVATIVES LIST 141
APPENDIX H – PLOTS SUPPORTING DETERMINATION OF MODEL SENSITIVITY TO STABILITY DERIVATIVE VARIATION 150
APPENDIX I – THESIS FLIGHT CONTROL EQUATIONS 154
APPENDIX J – PARAMETERS LIST 156
APPENDIX K – WORKING WITH PEST 158
APPENDIX L – PROGRAMMED TEST INPUT DESCRIPTION 161
APPENDIX M – GROUND SIM AND PTI SHAPING 163
APPENDIX N – IN FLIGHT LESSONS LEARNED 165
APPENDIX O – POINTS OF CONTACT 167
LIST OF ABBREVIATIONS, ACRONYMS, AND SYMBOLS 169
REFERENCES 171
DISTRIBUTION LIST 172

LIST OF FIGURES

Figure A1: Flight Envelope and Limits 29
Figure B1: Flight Regimes 31
Figure C1: Test Condition Matrix 33
Figure D1: Learjet 25 Elevator Deflection Weight Effects, Project HAVE TRIM 40
Figure D2: Learjet 25 Angle of Attack Weight Effect, Project HAVE TRIM 41
Figure D3: Learjet 25 Pitch Angle Weight Effect, Project HAVE TRIM 42
Figure D4: Learjet 25 Elevator Deflection Velocity Effect, Project HAVE TRIM 43
Figure D5: Learjet 25 Angle of Attack Velocity Effect, Project HAVE TRIM 44
Figure D6: Learjet 25 Pitch Angle Velocity Effect, Project HAVE TRIM 45
Figure D7: Learjet 25 Regime 1 Elevator Deflection Altitude Effect, Project HAVE TRIM 46
Figure D8: Learjet 25 Regime 2 Elevator Deflection Altitude Effect, Project HAVE TRIM 47
Figure D9: Learjet 25 Regime 1 Angle of Attack Altitude Effect, Project HAVE TRIM 48
Figure D10: Learjet 25 Regime 1 Pitch Angle Altitude Effect, Project HAVE TRIM 49
Figure D11: Learjet 25 Regime 2 Angle of Attack Altitude Effect, Project HAVE TRIM 50
Figure D12: Learjet 25 Regime 2 Pitch Angle Altitude Effect, Project HAVE TRIM 51
Figure D13: Learjet 25 Rudder Deflection Asymmetric Thrust Effect, Project HAVE TRIM 52
Figure D14: Learjet 25 Aileron Deflection Asymmetric Thrust Effect, Project HAVE TRIM 53
Figure D15: Learjet 25 Elevator Deflection Asymmetric Thrust Effect, Project HAVE TRIM 54
Figure D16: Learjet 25 Sideslip Angle Asymmetric Thrust Effect, Project HAVE TRIM 55
Figure D17: Learjet 25 Bank Angle Asymmetric Thrust Effect, Project HAVE TRIM .. 56
Figure D18: Learjet 25 Elevator Deflection Flight Path Angle Effect, Project HAVE TRIM 57
Figure D19: Learjet 25 Angle of Attack Flight Path Angle Effect, Project HAVE TRIM 58
Figure D20: Learjet 25 Pitch Angle Flight Path Angle Effect, Project HAVE TRIM 59
Figure D21: Learjet 25 Rudder Deflection Sideslip Angle Effect, Project HAVE TRIM 60
Figure D22: Learjet 25 Aileron Deflection Sideslip Angle Effect, Project HAVE TRIM61
Figure D23: Learjet 25 Bank Angle Sideslip Effect, Project HAVE TRIM 62
Figure D24: Learjet 25 Rudder Deflection Bank Angle Effect, Project HAVE TRIM 63
Figure D25: Learjet 25 Aileron Deflection Bank Angle Effect, Project HAVE TRIM ... 64
Figure D26: Learjet 25 Sideslip Bank Angle Effect, Project HAVE TRIM 65
Figure D27: Learjet 25 Elevator Deflection Pitch Rate Effect, Project HAVE TRIM 66
Figure D28: Learjet 25 Angle of Attack Pitch Rate Effect, Project HAVE TRIM 67
Figure F1: Longitudinal Time History Comparison, Project HAVE TRIM 72
Figure F2: Learjet 25 $C_{m\alpha}$ vs α, Project HAVE TRIM 73
Figure F3: Learjet 25 $C_{L\alpha}$ vs α, Project HAVE TRIM 74

Figure F4: Learjet 25 C_{L0} vs α, Project HAVE TRIM 75
Figure F5: Learjet 25 C_{mq} vs α, Project HAVE TRIM 76
Figure F6: Learjet 25 $C_{m\delta e}$ vs α, Project HAVE TRIM 77
Figure F7: Learjet 25 $C_{m\alpha}$ vs Mach Regime 1, Project HAVE TRIM 78
Figure F8: Learjet 25 $C_{m\alpha}$ vs Mach Regime 2, Project HAVE TRIM 79
Figure F9: Learjet 25 $C_{L\alpha}$ vs Mach Regime 1, Project HAVE TRIM 80
Figure F10: Learjet 25 $C_{L\alpha}$ vs Mach Regime 2, Project HAVE TRIM 81
Figure F11: Learjet 25 C_{L0} vs Mach Regime 1, Project HAVE TRIM 82
Figure F12: Learjet 25 C_{L0} vs Mach Regime 2, Project HAVE TRIM 83
Figure F13: Learjet 25 C_{mq} vs Mach Regime 1, Project HAVE TRIM 84
Figure F14: Learjet 25 C_{mq} vs Mach Regime 2, Project HAVE TRIM 85
Figure F15: Learjet 25 $C_{m\delta e}$ vs Mach Regime 1, Project HAVE TRIM 86
Figure F16: Learjet 25 $C_{m\delta e}$ vs Mach Regime 2, Project HAVE TRIM 87
Figure F17: Learjet 25 $C_{m\alpha}$ vs q Regime 1, Project HAVE TRIM 88
Figure F18: Learjet 25 $C_{m\alpha}$ vs q Regime 2, Project HAVE TRIM 89
Figure F19: Learjet 25 $C_{L\alpha}$ vs q Regime 1, Project HAVE TRIM 90
Figure F20: Learjet 25 $C_{L\alpha}$ vs q Regime 2, Project HAVE TRIM 91
Figure F21: Learjet 25 C_{L0} vs q Regime 1, Project HAVE TRIM 92
Figure F22: Learjet 25 C_{L0} vs q Regime 2, Project HAVE TRIM 93
Figure F23: Learjet 25 C_{mq} vs q Regime 1, Project HAVE TRIM 94
Figure F24: Learjet 25 C_{mq} vs q Regime 2, Project HAVE TRIM 95
Figure F25: Learjet 25 $C_{m\delta e}$ vs q Regime 1, Project HAVE TRIM 96
Figure F26: Learjet 25 $C_{m\delta e}$ vs q Regime 2, Project HAVE TRIM 97
Figure F27: Learjet 25 Lateral-Directional Time History Comparison, Project HAVE TRIM 98
Figure F28: Learjet 25 $C_{n\beta}$ vs. β Regime 1, Project HAVE TRIM 99
Figure F29: Learjet 25 $C_{n\beta}$ vs. β Regime 2, Project HAVE TRIM 100
Figure F30: Learjet 25 C_{nr} vs. β Regime 1, Project HAVE TRIM 101
Figure F31: Learjet 25 C_{nr} vs. β Regime 2, Project HAVE TRIM 102
Figure F32: Learjet 25 $C_{n\delta r}$ vs. β Regime 1, Project HAVE TRIM 103
Figure F33: Learjet 25 $C_{n\delta r}$ vs. β Regime 2, Project HAVE TRIM 104
Figure F34: Learjet 25 $C_{l\beta}$ vs. β Regime 1, Project HAVE TRIM 105
Figure F35: Learjet 25 $C_{l\beta}$ vs. β Regime 2, Project HAVE TRIM 106
Figure F36: Learjet 25 C_{lp} vs. β Regime 1, Project HAVE TRIM 107
Figure F37: Learjet 25 C_{lp} vs. β Regime 2, Project HAVE TRIM 108
Figure F38: Learjet 25 $C_{l\delta a}$ vs. β Regime 1, Project HAVE TRIM 109
Figure F39: Learjet 25 $C_{l\delta a}$ vs. β Regime 2, Project HAVE TRIM 110
Figure F40: Learjet 25 $C_{n\beta}$ vs. Mach Regime 1, Project HAVE TRIM 111
Figure F41: Learjet 25 $C_{n\beta}$ vs. Mach Regime 2, Project HAVE TRIM 112
Figure F42: Learjet 25 C_{nr} vs. Mach Regime 1, Project HAVE TRIM 113
Figure F43: Learjet 25 C_{nr} vs. Mach Regime 2, Project HAVE TRIM 114
Figure F44: Learjet 25 $C_{n\delta r}$ vs. Mach Regime 1, Project HAVE TRIM 115
Figure F45: Learjet 25 $C_{n\delta r}$ vs. Mach Regime 2, Project HAVE TRIM 116
Figure F46: Learjet 25 $C_{l\beta}$ vs. Mach Regime 1, Project HAVE TRIM 117

Figure F47: Learjet 25 $C_{l\beta}$ vs. Mach Regime 2, Project HAVE TRIM 118
Figure F48: Learjet 25 C_{lp} vs. Mach Regime 1, Project HAVE TRIM 119
Figure F49: Learjet 25 C_{lp} vs. Mach Regime 2, Project HAVE TRIM 120
Figure F50: Learjet 25 $C_{l\delta a}$ vs. Mach Regime 1, Project HAVE TRIM 121
Figure F51: Learjet 25 $C_{l\delta a}$ vs. Mach Regime 2, Project HAVE TRIM 122
Figure F52: Learjet 25 $C_{n\beta}$ vs. q Regime 1, Project HAVE TRIM 123
Figure F53: Learjet 25 $C_{n\beta}$ vs. q Regime 2, Project HAVE TRIM 124
Figure F54: Learjet 25 C_{nr} vs. q Regime 1, Project HAVE TRIM 125
Figure F55: Learjet 25 C_{nr} vs. q Regime 2, Project HAVE TRIM 126
Figure F56: Learjet 25 $C_{n\delta r}$ vs. q Regime 1, Project HAVE TRIM 127
Figure F57: Learjet 25 $C_{n\delta r}$ vs. q Regime 2, Project HAVE TRIM 128
Figure F58: Learjet 25 $C_{l\beta}$ vs. q Regime 1, Project HAVE TRIM 129
Figure F59: Learjet 25 $C_{l\beta}$ vs. q Regime 2, Project HAVE TRIM 130
Figure F60: Learjet 25 C_{lp} vs. q Regime 1, Project HAVE TRIM 131
Figure F61: Learjet 25 C_{lp} vs. q Regime 2, Project HAVE TRIM 132
Figure F62: Learjet 25 $C_{l\delta a}$ vs. q Regime 1, Project HAVE TRIM 133
Figure F63: Learjet 25 $C_{l\delta a}$ vs. q Regime 2, Project HAVE TRIM 134
Figure F64: Learjet 25 $C_{n\beta}$ vs. α, Project HAVE TRIM 135
Figure F65: Learjet 25 C_{nr} vs. α, Project HAVE TRIM 136
Figure F66: Learjet 25 $C_{l\beta}$ vs. α, Project HAVE TRIM 137
Figure F67: Learjet 25 C_{lp} vs. α, Project HAVE TRIM 138
Figure F68: Learjet 25 $C_{n\delta r}$ vs. α, Project HAVE TRIM 139
Figure F69: Learjet 25 $C_{l\delta a}$ vs. α, Project HAVE TRIM 140
Figure H1: Learjet 25 C_{m0} vs α, Project HAVE TRIM 151
Figure H2: Learjet 25 $C_{y\beta}$ vs α, Project HAVE TRIM 152
Figure K1: Response Page (longitudinal case) 159
Figure K2: Response Page (lateral-directional case) 160
Figure L1: Programmed Test Input 161

LIST OF TABLES

Table 1: Results of Stability Derivatives Sensitivities 6
Table 2: Sensitivity of δ_e to Longitudinal Stability Derivatives 7
Table 3: Sensitivity of δ_a to Lateral-Directional Derivatives 8
Table 4: Sensitivity of δ_r to Lateral-Directional Derivatives 10
Table 5: CG Subsets 17
Table 6: CG Determination 17
Table 7: Regimes Comparison 24
Table A1: LEARJET-25 Sideslip Limits 30
Table C1: Test Matrix 37
Table G1: Longitudinal Derivatives – Regime 1 141
Table G2: Longitudinal Cramer-Rao Bounds – Regime 1 142
Table G3: Lateral-Directional Derivatives – Regime 1 143
Table G4: Lateral-Directional Cramer-Rao Bounds – Regime 1 144
Table G5: Longitudinal Derivatives – Regime 2 145
Table G6: Longitudinal Cramer-Rao Bounds – Regime 2 146
Table G7: Lateral-Directional Derivatives – Regime 2 147
Table G8: Lateral-Directional Cramer-Rao Bounds – Regime 2 148
Table M1: PTI Summary 164

INTRODUCTION

GENERAL

USAF Test Pilot School (TPS) and the Air Force Institute of Technology (AFIT) sponsored the HAVE TRIM project as part of a joint curriculum in support of a Master's degree thesis. This project was conducted under the authority of the Commandant, USAF TPS. Additional guidance and technical requirements were provided by AFIT.

This thesis was based on six-degree-of-freedom flight control equations of motion (EOM) model developed to predict trimmed flight conditions for the Advanced Information Engineering Services (formerly Veridian) Learjet 25. These equations are referred to in the remainder of this report as "the model" or the "model EOM". The model was incorporated into a Matlab® routine that output the predicted required aircraft control surface deflections (δ's[1]) to achieve a specified orientation and flight path of the vehicle. Prior to flight testing, the model was used to determine the sensitivity of the predictions to uncertainties in the stability derivatives. Then, flight test data were used to refine the Learjet-25 stability derivatives for incorporation into and refinement of the model. Finally, flight test results were compared to the model predictions.

BACKGROUND

Automatic flight control systems were a vital part of many current aircraft designs. The control system decreased pilot workload and increased flight safety, and was increasingly used to stabilize aircraft that otherwise would not be stable. Also, with the increased use of Unmanned Aerial Vehicles (UAVs), the automatic flight control system was vital to achieve the required performance. Traditionally, automatic flight control systems have used linearized EOM to simplify aircraft motion around an equilibrium point. Linearization methods have been studied extensively and implemented on many current aircraft. To eliminate limitations created by linearization, the aircraft EOM were solved directly for the δ's necessary to achieve a desired flight path.

"Trimmed flight" in the HAVE TRIM project was defined as zero net moments on the aircraft, resulting in no angular acceleration. Straight and level, unaccelerated flight (SLUF), the typical definition of "trim", was a subset of the HAVE TRIM definition of trimmed flight. In SLUF maneuvers, the sum of the forces was assumed to be zero, resulting in no accelerations on the aircraft.

In the HAVE TRIM project the model EOM were solved for δ's at trimmed flight conditions and compared to flight test results of δ's. The ability to directly calculate δ's for a given flight condition would reduce computational processing time that would be spent refining δ's in an iterative process to set the specified flight condition.

[1] For clarity, the phrase "control surface deflections" will be replaced by the symbol δ or δ's throughout the remainder of the HAVE TRIM TIM. This designation either refers to flight control surface deflections generically or to the combination of the elevator (δ_e), aileron (δ_a), and rudder (δ_r) surface deflections. Symbols δ_e, δ_a, and δ_r in the HAVE TRIM TIM refer specifically to the identified control surface only.

PROGRAM CHRONOLOGY

Flight testing was conducted from the Air Force Flight Test Center (AFFTC) at Edwards AFB California, in the R-2508 complex, from 8 to 17 October 2003. Flight testing was conducted by the HAVE TRIM test team, USAF TPS Class 03A (The CENTURIONS). All testing was conducted under job order number (JON) M03C1400. The Responsible Test Organization (RTO) was the 412th Test Wing. Flight testing consisted of ten Learjet-25 sorties totaling 18.5 flight hours.

TEST ITEM DESCRIPTION

The test item was the flight control system of a Learjet-25 owned and operated by Advanced Information Engineering Services (formerly Veridian) and registered in the civilian experimental category. It was capable of in-flight simulation of the flight control system and flight dynamics of other aircraft via the Variable Stability System (VSS). The left cockpit flight controls were production standard reversible Learjet-25.

The right set of flight controls was mechanically disconnected from the standard Learjet-25 flight control system and connected to the flight controls via a fly-by-wire, hydraulically assisted, irreversible system via the VSS. Control feel on the right side controls was variable through the VSS and hydraulic actuators. Control force and position plus sensor signals were input into the VSS computer that computed the δ's required to simulate the flight dynamics of the aircraft. Disengagement of the fly-by-wire system was achieved by shutting off the hydraulic power to the flight control surface actuators and opening dual bypasses around each actuator.

For the HAVE TRIM project, the control feel had nominal characteristics and the flight dynamics were that of the unaugmented Learjet-25. The VSS computer was configured to accept "open-loop" control position information and Programmed Test Inputs (PTIs) sculpted by the HAVE TRIM team.

TEST OBJECTIVES

The overall test objective was to validate the HAVE TRIM model through comparison of predicted δ's with flight test measured δ's at specified trimmed conditions. HAVE TRIM project had three primary objectives in support of the overall objective. These primary objectives were:

- Evaluate model sensitivity to aerodynamic stability derivative changes.
- Determine the aerodynamic stability derivatives of the test aircraft.
- Compare model δ's predictions to flight test δ's results.

All the test objectives were met.

TEST AND EVALUATION

GENERAL

Prior to flight testing, mathematical computations were performed to determine the sensitivity of the model equations of motion (EOM) to variations in the stability derivatives. This was accomplished prior to flight test to provide additional focus for data collection and analysis.

The longitudinal and lateral-directional aerodynamic stability derivatives used in the model EOM were determined from data collected during flight test. Aerodynamic stability derivative determination was a function of five variables: dynamic pressure (q), Mach number (M), angle of attack (α), sideslip angle (β) and flight regime. The aerodynamic stability derivatives were calculated for each trimmed flight condition.

The heart of the HAVE TRIM project incorporated the results from the sensitivity analysis and the newly determined test aircraft stability derivatives into the model EOM. The model EOM are Matlab® routines developed in Captain Miller's draft Air Force Institute of Technology (AFIT) Master's Thesis. This thesis was based on a six-degree-of-freedom flight control EOM model developed to predict trimmed flight conditions. These equations are referred to in the remainder of this report as "the model" or the "model EOM".

The HAVE TRIM project compared the predicted control surface deflection (δ) results from the model EOM for specified trimmed flight conditions to the actual aircraft flight test δ results. Eight variables were adjusted in trimmed flight conditions for data collection. These eight variables were aircraft CG, true airspeed (V), pressure altitude (PA and/or h), asymmetric thrust (T), flight path angle (γ), sideslip angle (β), bank angle (ϕ) and pitch rate (Q).

Flight Test Data Capture And Processing

Flight test data were collected by the on-board Learjet 25 data collection system. Aerodynamic parameters (α, β, θ, ϕ, W, h, V, T, γ, M, n_x, n_y, n_z, P, Q, and R) and δ's from flight test were provided by Advanced Information Engineering Services (formerly Veridian) in Matlab® files. Parameter Estimation (PEST) was used to calculate stability derivatives. For details on working with PEST and the HAVE TRIM PEST lessons learned, refer to Appendix K. All other data processing and results presentation were done using Matlab®.

Flight Envelope Regimes

The Learjet-25 flight envelope (see Appendix A for a detailed description of the flight envelope) was divided into the following three flight regimes or regions listed in priority order and characterized by different combinations of q and M. These regions are further detailed in Appendix B. Due to data collection time constraints during HAVE TRIM execution, data were not collected in Regime 3. This did not prevent completion of all test objectives.

1) Medium M (0.29 – 0.57) and medium q (0.76 psi – 1.53 psi)
2) Low M (0.21 - 0.38) and low q (0.31 psi – 0.76 psi)
3) High M (>0.44) and high q (>1.53 psi)

The model EOM were developed for Regime 1, the priority (center) region, where all model EOM assumptions were valid. Data were collected outside Regime 1 to test the validity and influence of the assumptions on the accuracy of the δ predictions. The priority for the three regimes was set based on the relative importance of model EOM per regime to the Capt Miller's Thesis.

For each regime a center test point was defined at 15,000 ft PA and a specific velocity. Testing for the model EOM evaluation at Regime 1 was centered on the velocity of 220 knots indicated airspeed (KIAS) (approximately 0.44 M). Flight testing in Regime 2 was centered on 150 KIAS (approximately 0.30 M), this corresponds to approximately 1.3 times stall airspeed (1.3 V_{stall}[2]).

The effects on the δ's of each of the eight variables mentioned above were examined separately, thus neglecting the combined influence of the variables. The results from the investigation in Regime 2 were used to evaluate the capability of the model to predict the δ's in a flight condition close to V_{stall} where the model assumptions begin to lose accuracy. The evaluation in Regime 2 determined how flexible the model was in predicting the δ's in a non-linear region. The results of this analysis helped define the applicable envelope of the model.

Independent Variables

The effects of the eight variables investigated started with CG, h, and V. Then the effects of the other variables were examined one at time. Thus, a build up approach was followed for evaluating the influence of the eight variables on the δ's, going from less demanding maneuvers[3] to more demanding maneuvers. Overall, CG effects were examined between approximately 14% and 21%[4]. Altitude sensitivity was investigated between 8,800 and 20,000 ft PA. Velocity effects were determined between 135 KIAS (approximately 1.15 V_{stall}) and 250 KIAS (0.50 M) at 15000 ft PA. The effect of asymmetric thrust was examined by varying the thrust from each engine up to the

[2] The stall speed was computed based on a gross weight of 13,500 lbs. All test points in Region 2 were based on this speed. If the weight was different when the test points were flown, the stall speed was re-computed in flight. The test points were not changed and were flown if within test limits.
[3] The analysis of CG, h, and V influence needed only a set of SLUF trim shots.
[4] This CG range corresponded to aircraft gross weight between 10,000 and 15,000 lbs.

maximum asymmetric thrust or the maximum β test limit (see Appendix A for details on sideslip limits). The effects of β were evaluated from zero to maximum sideslip test limit (see Appendix A), left and right. The longitudinal pointing capability with respect to the rate of climb/descent was determined by varying θ from 15° nose high to 5° nose low. The lateral pointing capability was investigated through trimmed level turns by varying ϕ from 5° to 60° (β in the turns was approximately zero; maximum load factor (g) 2.5). Finally, the pitch pointing capability of the aircraft was investigated by testing negative pitch rates up to approximately 5.6 degrees per second (°/sec). This range was limited by the minimum load factor test limit of +0.2g.

Model EOM Sensitivity To Variations In Aerodynamic Stability Derivatives

Prior to the flight test, the sensitivity of the model EOM to the aerodynamic stability derivative variations was determined. This determination was also used in the evaluation of the aerodynamic stability derivatives, since a bad estimation of a specific aerodynamic stability derivative would be insignificant if the impact on the model EOM was small. Also, the analysis conducted for this objective helped separate the effects of the derivatives inaccuracy from the effects of the model EOM inaccuracy.

Aerodynamic Stability Derivatives Determination

The aerodynamic stability derivatives were calculated to update and refine the model EOM. Both longitudinal and lateral-directional doublet PTIs were performed at each trim condition. Aircraft response was captured via the variable stability system (VSS) resident on the Learjet-25. The different combinations of M and q in both regimes was representative of the aerodynamic flow energy, and was used as a variable for the derivatives determination. The flow energy (or flight regime; they are synonymous in this context), affected the derivatives by modifying the aerodynamic flow around the tail. At low M and q (Regime 2), the flow energy was expected to be lower than in Regime 1. The maximum α the aircraft could reach, the control surfaces control power (both longitudinal and lateral/directional), and the damping (both longitudinal and lateral/directional) were affected by the different flow energy and different combinations of q and M. In each regime the effects of q, M, α and β were investigated.

Parallel δ And Aerodynamic Stability Derivatives Testing

At the start of project HAVE TRIM, the only aerodynamic stability derivatives available were referenced to SLUF at 15,000 ft PA and 250 KIAS. Therefore the aerodynamic stability derivatives data collection and the trimmed δ investigation was performed simultaneously. These aerodynamic stability parameters were incorporated into the model EOM. This updated model was used to calculate δ's. The comparison between predicted and flight test data δ's was used to evaluate the model EOM accuracy and the aerodynamic stability derivatives accuracy. In order to determine the source of errors in both the model EOM and the stability derivatives, the aerodynamic stability derivatives accuracy were also evaluated by using the 10 Times Cramer-Rao Parameter (10CRP) and expert insight.

TEST OBJECTIVES

Determine sensitivity of model EOM results to stability derivative variation

Sensitivity analysis of the longitudinal and lateral-directional stability derivatives was performed using the original baseline stability derivatives. The sensitivity of the stability derivatives is summarized in Table 1 below. Each stability derivative was varied up to ±40% or the variation that resulted in a corresponding ±1.0° δ, whichever occurred first. Variations in stability derivatives ±0 to 10% that resulted in a ±1.0° δ displayed "Extreme Sensitivity". Variations in stability derivatives ±10 to 20% that resulted in a ±1.0° δ displayed "Significant Sensitivity". Variations in stability derivatives ±20 to 30% that resulted in a ±1.0° δ displayed "Moderate Sensitivity". Variations in stability derivatives ±30 to 40% that resulted in a ±1.0° δ displayed "Slight Sensitivity". Stability derivatives not listed in Table 1 below did not produce a ±1.0° δ with a ±40% variation. The stability derivatives in Table 1 are listed in order of decreasing sensitivity with the most sensitive on top.

Extreme Sensitivity (±0 to 10%)	Significant Sensitivity (±10 to 20%)	Moderate Sensitivity (±20 to 30%)	Slight Sensitivity (±30 to 40%)
Cmo (SLUF and Climbs)	$C_{n\delta r}$ (Sideslip)	$C_{L\alpha}$ (SLUF)	Cmα (SLUF and Climbs)
$C_{n\delta r}$ (Bank)	$C_{l\beta}$ (Sideslip)	$C_{l\delta r}$ (Sideslip)	
$C_{y\beta}$ (Bank)	$C_{l\delta a}$ (Bank)		
$C_{n\beta}$ (Bank and Sideslip)	$C_{l\delta a}$ (Sideslip)		
$C_{l\beta}$ (Bank)	$C_{l\delta r}$ (Bank)		

Table 1: Results of Stability Derivatives Sensitivities

Determine δ_e sensitivity to stability derivative variation.

Table 2 below displays the longitudinal stability derivative variations at a given condition that resulted in a δ change of $\pm 1°$ are listed under the "Error (Condition)" column along with the condition at which they occurred. Those stability derivatives whose variations of 40% did not result in a δ change of $\pm 1°$ are listed under the "Error (Condition)" column as "> 40%".

SLUF, sideslip, climbing, and turning conditions were examined by varying the stability derivatives within the Matlab® routine ± 40% and determining the resulting change in δ_e. All longitudinal stability derivatives described in Appendix J were examined.

Variable	Error (Condition)
C_{mo}	± 10% (SLUF and Climbs) > ± 40% (Sideslips and Turns)
$C_{L\alpha}$	- 23.8% (SLUF) > + 40% (SLUF) > ± 40% (Climbs, Sideslips, and Turns)
$C_{m\alpha}$	± 31% (SLUF and Climbs) > ± 40% (Sideslips and Turns)
C_{L0}	> ± 40% (All)
C_{D0}	> ± 40% (All)
C_{mq}	> ± 40% (All)
$C_{m\delta e}$	> ± 40% (All)

Table 2: Sensitivity of δ_e to Longitudinal Stability Derivatives

Only three stability derivatives resulted in a δ_e change that reached $\pm 1°$ when varied ±40%. During SLUF and the climbing conditions a change in C_{mo} of only ±10% resulted in the limiting δ_e. This indicated an extreme sensitivity. Even a slight error in the stability derivate value would produce a δ_e error of greater than 1°. During SLUF, a change of $C_{L\alpha}$ of -23% resulted in the limiting δ_e. This derivative exhibited a moderate level of sensitivity. During SLUF and climbing conditions a change in $C_{m\alpha}$ of ±31% resulted in the limiting δ_e. The derivative exhibited a slight level of sensitivity with only a large error creating more than 1° of δ_e. $C_{m\delta e}$ and C_{mq} were expected to be critical, but were less than slight sensitivity.

Determine δ_a and δ_r sensitivity to stability derivative variation.

The results are summarized in Table 3 for the δ_a and Table 4 for the δ_r. The lateral directional stability derivative variations at a given condition that resulted in a δ change of $\pm 1°$ are listed under the "Error (Condition)" column along with the condition at which they occurred. Those stability derivatives whose variations of 40% did not result in a δ change of $\pm 1°$ are listed under the "Error (Condition)" column as "> 40%".

The stability derivatives listed in each table have the most sensitive stability derivatives at the top and are listed in order of decreasing sensitivity. SLUF, sideslip, and turning conditions were examined for the limiting δ_a and δ_r. Stability derivatives were varied within the Matlab® routine ±40% and the resulting changes in δ_a and δ_r were determined. All lateral directional stability derivatives described in Appendix J were examined.

Variable	Error (Condition)
$C_{l\beta}$	± 6.9% (Bank) ± 17.1% (Sideslip) > ± 40% (SLUF)
$C_{y\beta}$	- 11.0% (Bank) > + 40% (Bank) > ± 40% (Sideslip and SLUF)
$C_{l\delta a}$	- 11.1% (Bank) +14.6% (Bank) - 18.7% (Sideslip) + 30.0% (Sideslip) > ± 40% (SLUF)
$C_{n\delta r}$	- 13.2% (Bank) + 18.6% (Bank) -22.1% (Sideslip) > + 40% (Sideslip) > ± 40% (SLUF)
$C_{n\beta}$	± 15.4% (Bank) ± 28.6% (Sideslip) > ± 40% (SLUF)
$C_{l\delta r}$	± 15.6% (Bank) ± 28.6% (Sideslip) > ± 40% (SLUF)
C_{lp}	> ± 40% (All)
C_{nr}	> ± 40% (All)
$C_{n\delta a}$	> ± 40% (All)
C_{lr}	> ± 40% (All)
C_{np}	> ± 40% (All)

Table 3: Sensitivity of δ_a to Lateral-Directional Derivatives

No stability derivative when varied ± 40% produced a change of 1° of δ_a in SLUF. For a banked condition $C_{l\beta}$ produced a δ_a change of 1° with only a ± 6.9% variation. This condition and stability derivative exhibited extreme sensitivity. Even a very slight error in this stability derivative would produce a δ_a error of greater than 1°. The next five stability derivatives listed in Table 3 produced an δ_a change of 1° with less than a ± 20% variation for a banked condition. $C_{l\beta}$ and $C_{l\delta a}$ produced a δ_a change of 1° with less than a ± 20% variation for a sideslip condition. These stability derivatives indicated a significant level of sensitivity, with only slight errors in the stability derivatives creating more than 1° of δ_a error. $C_{n\delta r}$, $C_{n\beta}$, and $C_{l\delta r}$ produced an δ_a change of 1° with less than a ± 30% variation for a sideslip condition. These three stability derivatives indicated a moderate level of sensitivity during sideslip. Moderate errors in these stability derivatives would produce more than 1° of δ_a. $C_{n\delta a}$ was expected to be critical, but it was not. $C_{l\beta}$, $C_{y\beta}$, and $C_{n\beta}$ were not expected to be critical, but proved otherwise.

Variable	Error (Condition)
$C_{n\delta r}$	± 4.6% (Bank) ± 10.4% (Sideslip) > ± 40% (SLUF)
$C_{y\beta}$	- 4.8% (Bank) + 5.6% (Bank) > ± 40% (Sideslip and SLUF)
$C_{n\beta}$	± 5.0% (Bank) ± 9.3% (Sideslip) > ± 40% (SLUF)
$C_{l\beta}$	> ± 40% (All)
$C_{l\delta a}$	> ± 40% (All)
$C_{l\delta r}$	> ± 40% (All)
C_{lp}	> ± 40% (All)
C_{nr}	> ± 40% (All)
$C_{n\delta a}$	> ± 40% (All)
C_{lr}	> ± 40% (All)
C_{np}	> ± 40% (All)

Table 4: Sensitivity of δ_r to Lateral-Directional Derivatives

No stability derivative when varied ±40% produced a change of 1° of δ_r in SLUF. But, the first three stability derivatives listed in Table 4 produced a δ_r change of 1° with less than a ±5% variation for a banked condition. $C_{n\delta r}$ and $C_{n\beta}$ also produced a δ_r change of 1° with less than a ±10% variation for a sideslip condition. These conditions and stability derivatives exhibited an extreme sensitivity. Even very slight errors in any of these stability derivatives would produce a δ_r error of greater than 1°. $C_{n\delta a}$, $C_{l\delta a}$, and $C_{l\delta r}$ were expected to be critical, but they were not. $C_{y\beta}$ and $C_{n\beta}$ were not expected to be critical, but displayed extreme sensitivity. Figures F34, F35, H2, F38, F39, F32, F33, F28, and F29 show the most critical derivatives: $C_{l\beta}$, $C_{y\beta}$, $C_{l\delta a}$, $C_{n\delta r}$, $C_{n\beta}$.

Determine test aircraft stability derivatives

Elevator and combination rudder/aileron doublets were performed after each trim shot to collect time history responses required for computing the stability derivatives. The doublets were applied by using a programmed test input (PTI). PTI details are discussed in Appendix M. This procedure was used on all sorties.

Appendix G summarizes the longitudinal and lateral-directional stability derivatives at each trim condition. All the derivatives were standardized to a CG position equal to 22% of the mean aerodynamic cord. Flight conditions and the corresponding derivatives are presented. The 10CRP are also displayed. Figures in Appendix F present, for each point, the 95% confidence interval, related to the 10CRP bounds calculated by Parameter Estimation (PEST). A hand faired curve was drawn through the points and the equation of the curve was presented, whenever possible. The plots as function of M, β

and q are presented separately for Regime 1 and Regime 2. This isolated the effects of M, q and β (where applicable) from the effects of the different trimmed δ_e in the two regions. These different trimmed δ_e resulted from different ranges of α.

The Appendix G table is derived from PEST output generator data base page. Since the settings for the data base did not permit display of more than six digits for each number, some derivatives and 10CRP's were truncated. This PEST limitation had the greatest effects on stability derivatives with magnitudes of 0.00010 or less. Refer to Appendix K – Working With PEST for more details. Stability derivatives with values less than 0.00010 were C_{D0}, $C_{n\delta a}$ and $C_{l\delta r}$. In some cases $C_{l\delta a}$ and $C_{n\delta r}$ also had values of 0.00010 or less.

Data were first evaluated by comparing the time histories calculated by PEST and the time histories collected onboard. Figure F1 shows an example of a longitudinal time history comparison, and Figure F27 shows an example of a lateral-directional time history comparison, taken from the PEST output generator frame. The dotted lines were calculated by PEST and the solid lines were those collected from flight test. The characteristics to examine when evaluating the quality of the match between the two curves were the amplitude of the peaks after the PTI was applied and the time between the peaks. The time histories matched very well. However, a slight time delay was observed in all the α and β time histories. PEST predicted the initial change in α and β after the PTI starting prior to the initial change in flight test data time histories. Since PEST was able to closely match all other parameters this apparent discrepancy is most likely the result of acceleration effects on the α and β measurment systems and/or the incorrect compensation for these acceration effects via the onboard data acquisition system. **Determine the source of and correct for the discrepancy between PEST predictions of α and β and onboard data acquisition values of α and β prior to future stability derivative determination on the test aircraft (R1)**[5].

Both longitudinal and lateral-directional stability derivatives were determined as a function of q and M. Longitudinal derivatives were also determined as a function of α and trimmed δ_e. Lateral-directional derivatives were also determined as a function of β. Figures F2 to F26 show respectively $C_{m\alpha}$, $C_{L\alpha}$, C_{L0}, C_{mq} and $C_{m\delta e}$ as a function of α, M and q. Figures F28 to F69 show respectively $C_{n\beta}$, C_{nr}, $C_{n\delta r}$, $C_{l\beta}$, C_{lp} and $C_{l\delta a}$ as a function of β, M and q. The accuracy of the longitudinal and directional derivatives were satisfactory, while the accuracy for the lateral derivatives was marginal; especially $C_{l\beta}$ and $C_{l\delta a}$. In the following section each plot will be examined.

Figures F2, F3, and Figure H1 show the most critical longitudinal stability derivatives, $C_{m\alpha}$, $C_{L\alpha}$ C_{mo}, as a function of α. The figures indicate that even though these derivatives heavily affected the quality of the predictions in the δ_e, they were calculated with satisfactory accuracy to minimize the effects of the sensitivity on the model results.

[5] Numerals preceded by any **R** within parentheses at the end of a paragraph correspond to the recommendation numbers tabulated in the Conclusions and Recommendations section of this report.

Figures F28, F29, F32 thru F35, F38 thru F41, F44 thru F47, F50 thru F53, F56 thru F59, F62 thru F64, F66, F68, F69, and H1 show the most critical lateral directional stability derivatives, $C_{l\beta}$, $C_{y\beta}$ $C_{l\delta a}$, $C_{n\delta r}$, $C_{n\beta}$ and $C_{l\delta r}$,as functions of β, M, q, and α. The effect of these stability derivatives on the model results are discussed below.

The profile drag coefficient (C_{D0}) plus the adverse yaw and the roll due to rudder deflection coefficients ($C_{n\delta a}$ and $C_{l\delta r}$ respectively) were characterized by significant scatter, thus making their determination elusive. Therefore plots of these derivatives are not presented. As discussed in the sensitivity analysis above, determination of these derivatives was not critical to the accuracy of the model. **Determine the source of, and correct for, the significant data scatter of C_{D0}, $C_{n\delta a}$ and $C_{l\delta r}$ prior to future attempts at determination of these specific stability derivatives (R2).**

Overall, the quality of the data collected, as assessed by time history evaluation during PEST, was satisfactory for the longitudinal and directional axis. The lateral data quality was marginal using the same evaluation source.

Data quality was also evaluated by using the 10CRP's, which were plotted for each data point in all figures of Appendix F. The 10CRP's indicated the 95% confidence interval for each point. Overall, the 10CRP's shown indicated most derivative calculation accuracies were satisfactory. Exceptions are further examined below.

As will be detailed below, the quality of the data was additionally evaluated by looking at the δ comparison results. In this evaluation the model EOM trimmed δ's calculated using the derivatives obtained from PEST were compared with the flight data. The trimmed longitudinal and lateral δ's closely matched with the model EOM, resulting in another indication of satisfactory accuracy of the longitudinal and lateral derivatives calculated. However, A marginal match was found in the lateral axis. This confirmed that the lateral derivatives estimation presented some issues.

Finally, the data quality was assessed by soliciting expert's opinions on the results. Mr Chris Nagy, NASA Dryden aeromodeling and PEST expert, concurred with the assessment of derivative calculations performed during project HAVE TRIM.

Therefore, in order to improve the quality of the model predictions, either the accuracy of the dihedral effect and aileron control power should be improved or the impact these derivatives on the model should be limited.

Derivatives as a function of α

The $C_{m\alpha}$ plot (Figure F2) shows that the pitch moment coefficient was negative, as was expected since the airplane was speed stable. It also shows a positive slope, indicating that as α increased the aerodynamic center of the airplane moved forward, thus reducing the distance between the aerodynamic center and the CG, which reduced the longitudinal stability margin. For positively cambered wings, like the Learjet-25, this result matched the predictions. The 10CRP indicated the results were satisfactory.

The $C_{L\alpha}$ plot (Figure F3) shows that the lift slope coefficient was positive and the slope was negative. This resulted in flattening of the lift curve as α increased and approached α_{stall}. The 10CRP's indicated the data collected presented more uncertainty around the center values than the data shown in the $C_{m\alpha}$ plot, but were satisfactory because the time histories matched well between prediction and reality.

The C_{L0} plot (Figure F4) shows that the zero lift coefficient slightly increased with α. This characteristic was caused by lift produced by the horizontal tail that caused the lift curve slope to decrease in the region well below stall where theory predicted a constant slope. The lift curve was actually a greater order curve, resulting in a slight change of the zero lift coefficient with α. The 10CRP accuracy of the data collected indicated that at high α the derivative estimation was less accurate than at low α. The data were marginal.

The C_{mq} plot (Figure F5) shows that the pitch damping did not change significantly with α. The 10CRP's bounds were larger than for other derivatives, but C_{mq} was expected to be hard to precisely determine. This data were also considered satisfactory.

The $C_{m\delta e}$ plot (Figure F6) shows that the elevator control power coefficient was negative, as expected. It also shows that the slope of the curve was negative. This indicated as α increased, the down wash produced by the main wing incident on the tail increased. This resulted in a decrease of the local α on the tail and consequently an increase of lift produced by the elevator (the elevator load is opposite the main wing lift). This behavior matched theory. In addition, the accuracy indicated by the 10CRP's indicated that the data were satisfactory.

Derivatives as a function of β

The $C_{n\beta}$ and C_{nr} plots (Figures F28 through F31) show the weathercock stability and directional damping were basically constant with the β. This was expected since the range of β was not large enough to present a significant change in the rudder lateral force that could modify the directional stability. The 10CRP's indicated that the results were satisfactory.

The $C_{n\delta r}$ plots (Figures F32 and F33) show that the directional control power was constant with β. The quality of the data was marginal, since the 10CRP bounds showed a significant level of uncertainty.

The $C_{l\beta}$ plots (Figures F34 and F35) show that the dihedral effect was essentially constant with β. The quality of the data, according to the 10CRP's, was satisfactory. However, the points in Regime 2 demonstrate more scattering than the points in Regime 1. It was possible that the α influence at low speeds affected the trimmed flight condition with β more than at higher speed.

The C_{lp} and $C_{l\delta a}$ plots (Figures F36 through F39) show that for both Regime 1 and Regime 2 the lateral damping and aileron control power were nearly constant with β. The quality of data was satisfactory.

Derivatives as a function of M

The $C_{m\alpha}$, $C_{L\alpha}$, C_{L0}, C_{mq}, and $C_{m\delta e}$ plots as a function of M are displayed in Figures F7 through F16. The $C_{n\beta}$ and C_{nr} plots as a function of M are displayed in Figures F40 through F43. The $C_{n\delta r}$ and $C_{l\beta}$ plots as a function of M are displayed in Figures F44 through F47. These plots showed that for both Regime 1 and Regime 2 the associated stability derivatives were basically constant with the Mach number. This was as expected because the flight conditions were far from the transonic region of the envelope. Therefore, there were no effects on the aircraft stability derivatives induced by shock waves, the shift of the aerodynamic center, or the variation of lateral force on the rudder with M. The lift coefficient of an airfoil increases with M close to the transonic region; therefore, the lateral force on the rudder could be influenced by this factor. The 10CRP's indicated that the results were satisfactory.

The C_{lp} plots (Figures F48 and F49) show that for Regime 2 that the lateral damping was basically constant with the M. However, for Regime 1, the measurements C_{lp} increased with M. Although unlikely since the M range in Regime 1 did not approach a classically defined transonic region, the increase of C_{lp} was deemed possible.

The $C_{l\delta a}$ plots (Figures F50 and F51) show the same characteristics of C_{lp}, with a trend for the aileron control power, especially in Regime 1, to increase with M. The theory does not support the results; therefore further data analysis was suggested. One possible explanation could be the limited number of significant digits assigned by PEST to the derivatives. If the numbers were not rounded, the plot would probably be different. **Refine $C_{l\delta a}$ as a function of M in Regime 1 during future test aircraft stability derivative determination (R3).**

Derivatives as a function of q

The $C_{m\alpha}$, $C_{L\alpha}$, C_{L0}, and C_{mq} plots as a function of q are displayed in Figures F17 through F24. The plots showed that for both Regime 1 and Regime 2 the associated stability derivatives were essentially constant with q. This was as expected because the flight conditions were far from a high q region, where structural loads may bend the airplane and modify the aerodynamic response. The 10CRP's indicated the results were satisfactory.

The $C_{m\delta e}$ plots (Figures F26 and F25) show that for Regime 2 the elevator control power was nearly constant with q. However, for Regime 1, the plot showed a decrease with q, as if the elevator was subject to bending from the q. Although unlikely, the decrease of the control power with increased q, was possible.

The $C_{n\beta}$, C_{nr}, $C_{n\delta r}$, $C_{l\beta}$, C_{lp} and $C_{l\delta a}$ plots (Figures F52 through F63) show that for both Regime 1 and Regime 2 that all lateral-directional stability derivatives were basically constant with the q. This was expected since the flight conditions were far from

a high q region, where the airplane might be subject to structural deformation. The only exception was in Regime 2 where C_{lb} decreased with q. The dynamic pressure was not expected to have any influence on the stability derivatives, in Regime 2. **Refine $C_{l\beta}$ as a function of q in Regime 2 during future test aircraft stability derivative determination (R4).** Overall, the 10CRP's showed a relatively small 95% confidence interval, indicating that the PEST estimation of the derivatives was reliable.

Derivatives as a function of flight regime (indicated by α)

Overall, the estimation accuracy of the longitudinal derivatives did not present significant differences between Regime 1 and Regime 2. However, the data were characterized by more scatter in Regime 2 than in Regime 1. As highlighted in the previous sections, the 10CRP's were almost the same between the two regimes, and the variation of the derivatives with α, M and q, except for $C_{m\delta e}$, was consistent and predictable. However, the flight regime seemed to influence the absolute value of the derivatives calculated. If the derivatives were not plotted separately, an unexpected variation with Mach number or dynamic pressure would be noted, indicating that the flight regime affected the aerodynamic model. The most important influence of the flight regime on the derivatives was that in Regime 1 the α used to evaluate M and q effects on the aerodynamic model were significantly different than in Regime 2. If the maneuvers in Regime 1 and Regime 2 were flown at same α, the difference between the two regimes would probably be negligible. The stabilator position was also changed between Regime 1 and Regime 2. The position of the stabilator had an effect on the elevator trim values, and may have changed the derivatives between the two regimes. **Investigate the effect of test aircraft stabilator position on the stability derivatives (R5).**

Overall, the estimated accuracy of the lateral derivatives did not present significant differences between Regime 1 and Regime 2. As highlighted in the previous sections, the 10CRP's were almost the same between the two regimes. The variation of the derivatives with β, M and q, except for a few cases, was consistent and predictable. However, the flight regime seemed to influence the absolute value of the derivatives calculated. If the derivatives were not split into two regimes and plotted separately, an unexpected variation with β, M or q was noted. This indicated that unless the derivatives were normalized not only for the same CG position but also for the same flight regime (trimmed δ and α range), then the flight regime affected the aerodynamic model. The effect of the stabilator position may have also contributed to the discrepancies.

Figures F64 through F69 show $C_{n\beta}$, C_{nr}, $C_{l\beta}$, C_{lp}, $C_{n\delta r}$, and $C_{l\delta a}$, each as a function of α. As predicted, the α influenced the value of the lateral-directional derivatives. $C_{n\beta}$ (Figure F64) slightly increased with the α, indicating that the blanking effect to the rudder was compensated by a decrease in the destabilizing effect of the fuselage. C_{nr} and $C_{n\delta r}$ (Figures F65 and F68) were almost constant with the α, confirming that the rudder was not subject to significant blanking by the fuselage as α increased. The lateral derivatives seemed more heavily affected by the α; this could explain the scatter observed in the previous analysis. $C_{l\beta}$ (Figure F66) increased with α. C_{lp} and $C_{l\delta a}$

(Figures F67 and F69) decreased with α, as expected since the wing lift coefficient, for a given camber (δ_a) tends to decrease with α.

The α was responsible for the different absolute value of the derivatives between the two regimes. As previously discussed, a compensation for the different α probably would have made the differences between the two regimes negligible.

Ways to isolate the M and q effects from the α effects include flying the FTT's in a wind-up turn, so that α could be held in a specific interval with minimal changes in M or q. Another way could be to normalize the derivatives not only for CG position, but also for α and fly the FTT's for evaluating the M and q effects at the same α. Then, normalize the longitudinal derivatives for CG and for α in order to reduce the flight regime influence.

Finally, the number of lateral directional time histories usable for running PEST was significantly less than in the longitudinal case, mostly because the time spacing between the aileron doublets and the rudder doublets was often not short enough to permit a good estimation of the derivatives[6].

Comparison of flight test δ's to model predictions of δ's at trimmed flight conditions

The trimmed δ's were determined at each test point and compared to the predictions from the model EOM. The results were plotted for each trim condition outlined below. Plots of the results are in Appendix D. The model δ values were plotted for an average flight condition for each test regime. The averaged flight condition calculated from flight test points was 13879 pounds for the aircraft weight, 12712 feet PA, 475 feet per second (ft/s) true airspeed in Regime 1, and 315 ft/s true airspeed in Regime 2. Stability derivatives used in the model EOM were the average values from each of Regime 1 and Regime 2.

Compare δ(CG) to model predictions.

Data from trim shots at the center test conditions were analyzed to determine the influence of CG position on the aircraft aerodynamic parameters and δ's (see Test Matrix for details, Appendix C). The aircraft parameters and δ's were evaluated in three different CG position subsets. These subsets were each characterized by a center value, a maximum and a minimum. As the aircraft CG entered a new subset during the each test sortie, a trim shot was performed at the prescribed flight condition. Table 5 defines the CG subsets.

CG subsets			
Subsets	**CG1**	**CG2**	**CG3**
Max	21.2	18.1	15.3
Center value	19.6	16.7	14.7
Min	18.1	15.3	14

[6] Refer to Appendix K and L for more details regarding PEST capabilities and using the program.

Table 5: CG Subsets

Table 6 was used by the test team to determine the CG position during flight, as a function of zero fuel weight (with four people on board), total fuel weight and the weight of fuel stored in the fuselage.

zero fuel weight (lbs)	total fuel weight (lbs)	fuselage weight (lbs)	gross weight (lbs)	CG position
9570	5200	500	14770	21.1%
9570	1700	500	11270	18.1%
9570	1700	0	11270	15.3%
9570	1200	0	10770	14.6%

Table 6: CG Determination

The CG position varied linearly with the total fuel between 5200 lbs and 1700 lbs. Then the fuel stored in the fuselage was transferred to the wings. Due to time and return fuel constraints, all test points were flown before the fuel was transferred to the wings.

The effect of changing the aircraft weight and CG was compared to the predictions from the model EOM. Since CG was a linear function of the aircraft weight for all test points, the δ's were plotted as a function of weight. Figure D1 shows the combined results for Regime 1 and Regime 2.

For Regime 1 the flight test results were almost all within ±0.5° of the theoretical prediction. However, the flight test results did not show a significant relationship between δ_e and variations in weight; δ_e was constant. According to theory, a 3000 pound increase in weight would produce a 1.0° decrease in δ_e in Regime 1, but this was not observed during flight test.

In Regime 2 the data were more scattered and also did not match the predicted trend. The Regime 2 flight test results were on average about 1.0° higher than the predicted value. Again the flight test δ_e were nearly constant for all weights in the test envelope. Theoretically, a 1500 pound increase in weight would produce a 1.0° decrease in δ_e in Regime 2. Overall, the impact of aircraft weight did not have a measurable effect on the δ_e value from flight test data. Theoretically the impact was expected to be small, but not as small as the actual data indicated. The significant difference between Regime 1 and Regime 2 δ_e were the result of a change in trimmed stabilator position.

The δ_a and δ_r were predicted to be zero in trimmed flight. Small values of δ_a and δ_r were measured in flight. These deviations result from the impossibility to be perfectly trimmed with no lateral-directional inputs during actual flight test. There were no significant values of δ_a and δ_r in the weight investigation data points.

The plot of α verses weight is shown in Figure D2. Both Regime 1 and Regime 2 are shown on the plot. Figure D3 shows the effect of weight on θ. For Regime 1, the flight test data are scattered within 2° of the predicted curve, with all the θ data points within 1° of the expected values. The α values were directly affected by the airspeed at

which the test point was flown. A 10 ft/s change in true airspeed resulted in an average 0.5° to 1.5° change in α. The α and θ values were more constant than the predicted curve. The accuracy of the in-flight α and θ measurements contributed to the scatter in the data. The α measurement varied ±1.0° to 2°, and the θ measurement varied up to ±1.0°. Therefore, the weight effect on these flight parameters was not as large as expected.

In Regime 1 the flight test data were consistently 1° to 2° lower than the predicted values. The flight test data showed the same scatter in Regime 2 as in Regime 1, with θ nearly linear around the average value and α scattered more about the average value. The larger discrepancy for α and θ in Regime 2 may be due to the fact that the equations were developed for R1, and small aerodynamic non-linearities and the changed position of the stabilator could cause an error in the predictions.

The test point set-up had a major impact on variations between the flight test data and the theoretical predictions. The flight test velocity had the largest impact on changes in the δ_e values. Small variations in test point velocity produced a large change in δ_e values. The effect of W variations was less significant, and the effect of changing PA was very small. The test set-up variations in β and flight path angle from the specified test conditions were generally less than ±1.0° for all test points and did not significantly impact the results. The bank angle varied up to ±8.0° from the specified test conditions. Often there was a small P (±0.5°/sec), that was not observed in flight, but impacted the flight test data. The ϕ measurement also had the largest oscillations about the steady-state value, up to a ±1.0°. The combined errors in ϕ values had a significant impact on the lateral-directional results. Combining variations resulted in a combined change in the δ value, which accounts for some of the scatter seen in the flight test data.

Overall, the effect of α produced a larger change in the measured δ_e than the change in aircraft weight (and corresponding CG). The weight effect was masked by the changes in α from the predicted values. Airspeed also had a large effect on δ_e measurements in flight. The scatter in the data, especially in Regime 2, could be explained by the variances in the α and velocity at each test point from the ideal condition used for the model EOM calculation. When the identical flight condition parameters were used in the model EOM the δ values closely matched the flight test data (see Appendix E for examples).

Compare δ(V) to model predictions.

The effect of changing the aircraft velocity in flight test was compared to the theoretical prediction. The results for both Regime 1 and Regime 2 are plotted in Figure D4. The flight test data followed the same trend predicted by the model EOM, with a small bias. The data bias was more pronounced in Regime 2.

In Regime 1, the flight test δ_e was consistently higher than the theoretical prediction by approximately 0.25°. All flight test data were within 0.0° to 0.5° of the model EOM prediction. The effect of velocity was not affected by small changes in the

aircraft weight and test point altitude. Therefore, the effect of velocity on δ_e had the greatest impact on the straight and level flight results. In Regime 2 the flight test δ_e was consistently 0.75° higher than the predicted curve. The flight test data were tightly grouped around the average trend-line and showed the strong effect that a change in velocity had in a change in the δ_e value. The larger difference between predicted and flight test data in Regime 2 was similar to the results as discussed above for δ(CG).

The α and θ results are plotted in Figures D5 and D6. The flight test results matched the theoretical predictions within ±1.0°, except at the slowest airspeeds in Regime 2. The data were in a nearly continuous curve across both regimes. There was a slight jump in the theoretical curve between Regime 1 and Regime 2 of less than 0.2°. Again there was more scatter in the α flight test results than in the θ values. The α and θ flight test data matched the model very closely. The velocity effect dominated and the data were scattered by the other factors.

Overall, there was a strong correlation between changes in true airspeed and δ_e. The correlation was also seen in α and θ. Velocity measurement accuracy was one of the key indicators of δ_e prediction accuracy. Example calculations showing the accuracy using actual flight conditions are shown in Appendix E.

Compare δ(PA) to model predictions.

A trim shot was flown to establish the conditions outlined for each point in the Test Matrix (see Appendix C). The test points were distributed approximately on the same dynamic pressure line (constant airspeed), and have different Mach numbers.

The altitude effect on the flight test parameters was compared to the predictions. The results were very scattered with little correlation. Therefore the data were further separated into three aircraft velocity bands. The flight test results in Regime 1 closely matched the predicted values, while the Regime 2 flight test data were biased from the predicted curves.

Figure D7 shows the δ_e flight test data in Regime 1 with an overlay of the predicted δ_e for three true airspeed values. The low speed region (V_t = 460 ft/s) described a much more shallow curve than theory predicted. The mid-speed region (V_t = 475 ft/s), matched the predicted curve with a +0.2° bias for all altitudes. The high speed region (V_t = 490 ft/s), matched the predicted curve, with about the same +0.2° bias, but was more scattered than the mid-speed data. Overall the flight test data matched the predicted data with a small amount of variation.

In Regime 2 the flight test data differed from the predicted curve by almost +1.0° on average for all three velocity bands (see Figure D8). The flight test data were also more scattered than in Regime 1. Overall the data in Regime 2 shows the same general trend as the predicted curves, but the correlation was not strong. The altitude effect on δ_e was very small, and was masked by other factors, especially small changes in airspeed.

The altitude effect on α and θ was also not very strong. Figures D9 and D10 show the plot of flight test data in Regime 1 for α and θ, respectively, with the model EOM predictions shown for the same three true airspeed bands. The data in all three bands were characterized by a lot of scatter in the flight test data. All data were within 2° of the predicted curves. As was discussed in previous analysis, the θ values were closer to the predicted curves and did not have as much scatter as α. In Regime 2, the data were again scattered, increasing in error as the altitude increased (see Figures D11 and D12). The flight test data were also biased -2° to -3° from the predicted value curves. Also the α values were more scattered than the θ values at each altitude.

The altitude effect on the δ's was very small. The data points were scattered by other effects and the predicted trends were difficult to match to the model predictions. The effect of altitude variations does not have a significant impact on the result errors.

Compare δ(Asymmetric T) to model prediction.

Thrust from one of the two engines was progressively reduced and thrust on the other engine was progressively increased while keeping the wings level and the airspeed within the required tolerance. Data were collected at each asymmetric thrust setting. The data were plotted as the percentage of total thrust from the right engine.

Limited data were collected, especially in Regime 2. The data were very scattered, and did not match the predicted values very closely for lateral-directional δ's values. Figures D13 and D14 show the δ_r and δ_a values, respectively, from flight test compared to the predicted theoretical values for both regimes. The theory predicted a larger asymmetric thrust influence on δ_r (slope -0.5° per 10% change in asymmetric thrust, verses less than 0.1° per 10% for the averaged values of the flight test data in Regime 1). The δ_r results were about the same in Regime 2. The δ_a results showed the opposite trend result. The theory predicted about a -0.1° change per 10% change in asymmetric T, while the averaged flight test data had a slope of about -0.5° per 10% change in asymmetric T. The data had a lot of noise and stable points were difficult to achieve in asymmetrical conditions. The ϕ measurements also had a lot of noise and were accurate to within only a degree or two of the averaged value at most test points. These errors may account for the inaccuracies between the flight test results and the theoretical predictions.

The δ_e values were tabulated and compared to the theoretical predictions. Theoretically the δ_e was constant for all asymmetric thrust test points. Figure D15 shows that in Regime 1, all δ_e values were within ±0.3° of the theoretical value. If the four data points with large changes in ϕ were discarded, the average flight test data δ_e was -0.03° from the theoretical δ_e and all flight test points were within ±1.0° of the predicted value. In Regime 2 the flight data δ_e value was biased -1.0° with very little scatter in the data.

The lateral-directional δ errors also were increased because the test points were not exactly in perfect trim condition in most cases. Figure D16 and D17 show the plot of β and ϕ, respectively, for each test point. The theoretical values for the ϕ were expected

to be 0.0° because the maneuver was designed for wings level flight. Flight test points were not perfectly trimmed to wings level, straight flight, so this plot is a measure of the error due to non-ideal flight test conditions. The errors in ϕ were all less than ±4.0°. The offsets from trim would also contribute to the errors in lateral-directional δ's. The ϕ errors were largest for the points around 50% asymmetric T, which correspond to the largest errors on the δ plots (Figures D16 and D17). Also the ϕ errors tended to be more negative as asymmetric thrust approached 0%, and more positive as asymmetric thrust approached 100%. This was also observed in the δ_a and δ_r values at the extreme asymmetrical thrust conditions.

The lateral-directional stability derivatives had a much larger uncertainty than the longitudinal stability derivatives. This lateral-directional stability derivative uncertainty contributed to variations in model δ's as indicated by the sensitivity analysis. The most critical stability derivatives ($C_{n\delta r}$, $C_{y\beta}$, $C_{n\beta}$ and $C_{l\beta}$) created a large error for a small variation. Finally, a bias was observed in both the δ_a and δ_r values. For Flight 10, a constant +1.6° bias was observed in all straight and level test cases. The δ_a had a small bias of about 0.3° for Flight 10. The δ_a and δ_r were manually trimmed, and the small error could not be detected from the cockpit. The trim error contributed directly to an error in the δ's results.

Overall the asymmetric thrust flight test data did not match the theoretical predictions. The correct trend was seen in the data, but the flight test results had large differences from the expected values. The difficulty in establishing trimmed flight in an asymmetrical flight condition and the inaccuracy in the bank angle measurement aggravated the errors. A sample calculation of the δ's using exact flight conditions for an asymmetrical thrust case can be found in Appendix E.

Compare $\delta(\gamma)$ to model prediction.

A sawtooth climb/descent was flown for each pitch angle to establish the conditions outlined for each point in the Test Matrix (see Appendix C) to investigate γ.

The γ effect on δ_e is shown in Figure D18. The γ effect on δ_e was predicted to be very small, and the flight test data matched the predictions. In Regime 1, all the flight test data were within ±0.25° of the theoretical curve. In Regime 2 the flight test δ_e was biased +0.7° from the predicted value. The flight test data were also more scattered about the average value in Regime 2 than in Regime 1. Overall, the predicted γ correlation to δ_e matched flight test results, but the impact of γ on δ_e was very small.

Figures D19 and D20 shows the comparison of flight test γ effect on α and θ respectively to the theoretically predicted relationship. In Regime 1, all flight test data for both α and θ were within ±1.0° of the model EOM prediction for all γ values. In Regime 2 the flight test data were within ±2.0° of the predicted value, with a slight bias of about -1.0°. As seen for other longitudinal investigations, the scatter in the α data points was larger than the scatter in the θ values.

Overall, the flight test data correlated with the predicted values for all γ. The impact of γ was not significant, but was predicted properly by theory.

Compare $\delta(\beta)$ to model prediction.

A steady heading sideslip was flown to establish the conditions outlined for each point in the Test Matrix (see Appendix C). The maneuver was not a dynamic maneuver. At each test point data were recorded with the aircraft in a stable condition. Data were graphed, comparing degrees of δ_a and δ_r to the steady-state β that resulted from the deflections, and compared β to ϕ.

Regime 1 and Regime 2, δ_a and δ_r were compared to the δ_a and δ_r predicted by the model EOM. The δ_r is shown in Figure D21 and δ_a is shown in Figure D22. The flight test data for δ_a and δ_r were linear, as was predicted by the model. In addition, the slopes of the flight test data had similar slopes to that predicted by the model. When the slopes did vary from the model predictions, the slope of the flight test data were higher, but only by approximately 0.1° of δ per degree of β. It was also noted that at $\beta = 0°$ δ_a was negative and δ_r was positive. The deflection at $\beta = 0°$ had much more effect on moving the data away from the prediction than the slopes of the data. The rudder showed zero deflection at approximately $\beta = -2°$, and the ailerons showed no deflection at approximately β = -0.5°. It is unknown if this was an instrumentation issue, a slightly bent aircraft, or some other phenomenon.

The ϕ flight test data were also graphed for the steady-heading sideslips, as seen in Figure D23. For Regime 1 and Regime 2, the slope from the flight test data were approximately 2.5 times greater than the predicted slope.

Overall, the data quality from flight test was good and showed a linear relationship between δ's and β, and ϕ to β. The slopes of the δ's to β closely matched model prediction, while the slope of ϕ to β differed from the model by a factor of 2.5.

Compare $\delta(\phi)$ to model prediction.

Sustained coordinated level turns at different ϕ were flown at the conditions outlined for each point in the Test Matrix (see Appendix C).

Figure D24 shows the δ_r and Figure D25 shows δ_a as a function of ϕ for Regime 1 and Regime 2. Regime 1 δ_a increased approximately 0.13° per 10° of bank. Additionally, a positive δ_a (stick to the right) was required to maintain a right bank. This indicated a small magnitude of positive spiral stability. Zero ϕ required zero δ_a, which was to be expected. Regime 2 δ_r increased approximately 0.04° per 10° of bank. However, at ϕ=1°, the rudder indicated a deflection of just greater than 1°. This indicated a slight bias of the neutral rudder position. Regime 2 δ_a data were scattered and did not show a definite trend. Regime 2 δ_r data were also scattered with no trend information. Part of the lack of trend information available for Regime 2 was that there were a very limited amount of ϕ data in Regime 2 and a very small spread of ϕ's examined.

The dynamic flight test maneuvers were not well predicted by the equation models. The 1g model assumption was violated. Therefore, the model was not able to match the flight test results. Including the load factor in the model equations may improve the prediction accuracy. Flight test data from less dynamic maneuvers matched the predicted results with small errors. In general the closer the trimmed flight test point was to straight and level flight the more closely the flight test results matched the prediction.

The theoretical predictions did not match the flight test data in either region. This was due to the model assumption of 1-g flight, while the flight test was performed in level turns with an increasing load factor. This caused the model to break down and a comparison to flight test data useless.

Compare δ(Q) to model prediction.

A symmetric push-over was flown from approximately 15° nose-high to 5° nose low at different g (or Q). Data were collected while the aircraft passed through approximately level with the horizon, at the required load factor.

Flight test data showed a linear relationship between δ_e and pitch rate. Figure D27 shows that a trailing-edge down δ_e resulted in a pitch over, as would be expected, and a greater control surface input resulted in a higher Q. The model for δ_e showed that δ_e was nearly invariant with respect to Q. This was due to the fact that the model was written for 1.0 g flight. This assumption makes the data from the model not comparable to the flight data and no conclusions may be drawn.

The other model comparison that the test team compared flight data to and graphed was Q and α. Figure D28 shows that there was a linear relationship between α and Q. When the theoretical data were calculated from the model, α was constant for a given pitch rate. This, again, was a problem with the model, for the model was set up for 1.0 g flight, where a given α would result in Q=0°/sec (level flight). Consequently, comparison of the data to the model was not useful without having the model incorporate flight conditions at other than 1.0 g. **Apply load factor effects to the model EOM and re-compare to flight test data (R6).**

Determine the influence on the model accuracy of the non-linear aircraft response when flying close to the stall condition and the transonic region.

For each flight regime, the average error of the δ as a function of each variable (W, h, V, γ, ϕ, β, Q, asymmetric T) was calculated. Table 7 summarizes the results.

	Regime 1			Regime 2		
	δ_e (deg)	δ_a (deg)	δ_r (deg)	δ_e (deg)	δ_a (deg)	δ_r (deg)
h	3.37	n/a	n/a	3.50	n/a	n/a
KTAS	0.18	n/a	n/a	1.01	n/a	n/a
W	1.24	n/a	n/a	2.04	n/a	n/a
ΔT	0.07	0.53	0.97	0.99	0.27	1.64
phi	1.97	0.43	0.21	4.30	1.85	2.12
Q	5.06	n/a	n/a	2.90	n/a	n/a
beta	0.2	0.30	0.64	0.39	0.23	1.33
gamma	n/a	n/a	n/a	0.6	n/a	n/a

Table 7: Regimes Comparison

The data showed, for each regime and for each variable, the absolute value for the average difference between the calculated and the predicted δ's. Overall, since the two regimes were characterized by a different range of α (so the hypothesis of linear aerodynamic flow was not applicable in Regime 2), the model prediction showed a better estimation in Regime 1 than in Regime 2. However, only in a few cases was the difference larger than 1°; in both cases the load factor was different from 1.0 g. The model equations were already deemed to be inapplicable with load factor different from 1.0 g, as discussed above. Therefore, if the comparison between the two regimes ignored the two cases where the equations were not applicable, the model showed a relatively good flexibility, despite the different flight regimes.

CONCLUSIONS AND RECOMMENDATIONS

Determination of Model Sensitivity to Stability Derivative Variation

In the longitudinal axis, C_{m0}, $C_{m\alpha}$ and $C_{L\alpha}$ were the most critical derivatives because a small percentage difference in their estimation yielded a difference in the elevator defection greater than one degree. This issue did not affect the quality of the model predictions because sensitivity analysis performed concluded the longitudinal derivatives estimation was satisfactory.

In the lateral-directional axis, $C_{l\beta}$, $C_{y\beta}$, $C_{l\delta a}$, $C_{n\delta r}$, $C_{n\beta}$ were found to be the most critical. More specifically the rudder control power was the most critical in the rudder deflection prediction, while the dihedral effect and the aileron control power were the most critical in the aileron deflection prediction. $C_{y\beta}$ was found to significantly impact the prediction in both aileron and rudder deflections. These results affected the quality of the model predictions because the estimations of $C_{l\beta}$ and $C_{l\delta a}$ were marginal. On the other hand, $C_{y\beta}$ and the directional derivatives estimations were found satisfactory.

Determination of Test Aircraft Stability Derivatives

Overall, the quality of the data collected was satisfactory in the longitudinal and the directional axis, and marginal in the lateral axis. The variations of the derivatives with angle of attack, sideslip, Mach number and dynamic pressure were deemed predictable, except for two cases: the aileron control power as function of Mach in Regime1, and the dihedral effect as function of dynamic pressure in Regime 2.

For the first case, it was possible that the data base PEST produced assigned too few significant digits (only six) to the derivatives and the 10CRP's which skewed the data. For the second case no valid explanations were found.

The time history comparison showed that the angle of attack and the angle of sideslip gauges needed better compensation for the time delay for the aircraft normal, longitudinal and lateral accelerations. This characteristic did not significantly affect the accuracy of the predictions. However, for future testing, to further improve the aerodynamic model, it was recommended to compensate for these factors.

R1 Determine the source of and correct for the discrepancy between PEST predictions of α and β and onboard data acquisition values of α and β prior to future stability derivative determination on the test aircraft. (Page 11)

The zero lift, the adverse yaw and the roll due to the rudder deflection coefficients were characterized by significant scatter and were not plotted. The lack of accuracy in these derivatives was predictable and further data analysis was suggested.

R2 Determine the source of, and correct for, the significant data scatter of C_{D0}, $C_{n\delta a}$ and $C_{l\delta r}$ prior to future attempts at determination of these specific stability derivatives. (Page 12)

The flight regime seemed to affect the derivatives mostly because the angles of attack at which the flight test techniques were flown in the two regimes were significantly different. If the maneuvers were performed at the same angles of attack, the influence of the flight regime probably would have been negligible. For future testing, it was suggested to normalize the data collected for the CG position and for the angle of attack. Moreover, it was suggested to fly the flight test techniques where Mach number or dynamic pressure effects are evaluated, at the same angle of attack. For example performing the maneuvers in a wind up turn could better isolate Mach, dynamic pressure and angle of sideslip from angle of attack.

The stabilator position was also changed between Regime 1 and Regime 2. The position of the stabilator had an effect on the elevator trim values, and may have changed the derivatives between the two regimes.

R5 Investigate the effect of test aircraft stabilator position on the stability derivatives. (Page 15)

The $C_{l\delta a}$ tends to increase with M. Theory does not support this result; therefore further data analysis was suggested. One possible explanation could be the limited number of significant digits assigned by PEST to the derivatives.

Refine $C_{l\delta a}$ as a function of M in Regime 1 during future test aircraft stability derivative determination (R4).

In Regime 2 C_{lb} decreased with q. The dynamic pressure was not expected to have any influence on the stability derivatives, in Regime 2.

Refine $C_{l\beta}$ as a function of q in Regime 2 during future test aircraft stability derivative determination (R5).

Comparison of Flight Test δ's to Predicted δ's

Overall, the measured control surface deflections, satisfactorily compares to the model equations of motion predicted surface deflections. The longitudinal cases matched for all of the trim conditions except for δ(Q). The lateral-directional cases did not show as much correlation between the flight test data and the predicted results as the longitudinal cases. For a specific case with the exact flight test conditions input into the model equations, the predicted control surface deflections matched the flight test measurements to within 1.0° for a majority of the cases. The model predictions were also more accurate for straight and level flight conditions.

The test point set-up had a major impact on variations between the flight test data and the theoretical predictions. The flight test velocity had the largest impact on changes in the elevator defection values. Small variations in test point velocity produced a large change in elevator deflection values. The bank angle varied up to ±8.0° from the specified test conditions. Often there was a small roll rate (±0.5°/sec), that was not observed in flight, but that impacted the flight test data. The bank angle measurement also had the largest oscillation about the steady-state value, with up to a ±1.0° oscillation about the steady-state value. The combined errors in bank angle values had a significant impact on the lateral-directional results. Combining variations resulted in a combined change in the control surface value, which accounts for some of the scatter seen in the flight test data.

The flight test data and equations of motion predictions matched much better in the longitudinal cases than in the lateral-directional cases. The variations in lateral-directional cases were caused by the small variations in test point set-up, the higher uncertainty of the lateral-directional stability derivatives, and the biases in trim of the lateral-directional control surfaces. The lateral-directional test points were generally more difficult to establish in a steady trim condition than the longitudinal test cases. Therefore, the lateral-directional flight test data tended to have more variations from the stable trim condition. The bank angle variations also caused a significant impact on lateral-directional control surface deflection values. Finally, a bias was observed in both the aileron and rudder deflection values. For Flight 10, a constant +1.6° bias was observed in all straight and level test cases where the actual flight test results were input. The aileron had a small bias of about 0.3° for Flight 10. The rudder and aileron were manually trimmed, and the small error could not be detected from the cockpit. The trim error contributed directly to an error in the control surface deflection results.

The dynamic flight test maneuvers were not well predicted by the equation models. The model assumptions were violated both bank angle variations and symmetric push overs to generate pitch rate. Therefore, the model was unable to match the flight test results. The less dynamic maneuvers flight test data matched the predicted results with small errors. In general, the closer the trimmed flight test point was to straight and level flight the more closely the flight test results matched the predictions.

R6 Apply load factor effects to the model EOM and re-compare to flight test data. (Page 24)

Project recommendations are repeated below in a prioritized order:

- **Apply load factor effects to the model EOM and re-compare to flight test data (R6).**
- **Determine the source of and correct for the discrepancy between PEST predictions of α and β and onboard data acquisition values of α and β prior to future stability derivative determination on the test aircraft (R1).**
- **Determine the source of, and correct for, the significant data scatter of C_{D0}, $C_{n\delta a}$ and $C_{l\delta r}$ prior to future attempts at determination of these specific stability derivatives (R2).**
- **Investigate the effect of test aircraft stabilator position on the stability derivatives (R3).**
- **Refine $C_{l\delta a}$ as a function of M in Regime 1 during future test aircraft stability derivative determination (R4).**
- **Refine $C_{l\beta}$ as a function of q in Regime 2 during future test aircraft stability derivative determination (R5).**

APPENDIX A – FLIGHT ENVELOPE AND FLIGHT LIMITS

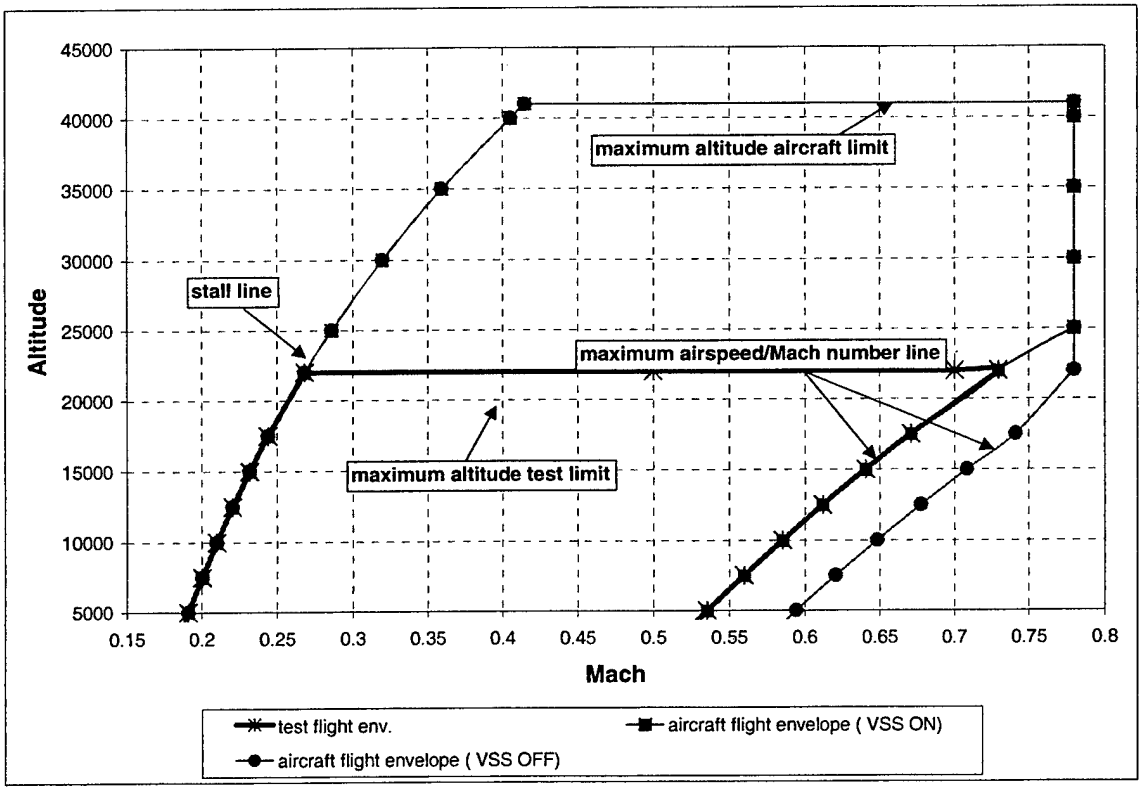

Figure A1: Flight Envelope and Limits

Figure A1 shows the flight envelope that was used during flight test. The left line was the stall speed line. The flight manual indicated that at 13,500 lbs gross weight, in the clean configuration, 108 KIAS was stall speed. For weights different than 13,500 lbs, the following formula was used:

$$V_s = \text{sqrt}\ (0.97 * n_z * W),$$

where W was the aircraft gross weight in lbs, n_z was the load factor normal to the flight path and the result was in knots.

The top line of Figure A1 indicates the 22,000 ft PA line. The stall warnings for the Learjet changed above 22,000 ft PA, so in order to keep the same gains and settings in the flight control system, all FTT's were flown at the maximum sortie altitude of 22,000 ft. The minimum altitude was 5,000 ft above ground level (AGL) for any FTT.

The right line of Figure A1 indicates the maximum airspeed, which was 325 KIAS with the VSS engaged. The maximum Mach number with the VSS on was 0.78 M, which would not be reached until 25,000 ft. The maximum velocity to be flown was 310

KIAS, approximately 95% of the maximum airspeed limit. The maximum airspeed with the VSS disengaged was the lesser of 361 KIAS or 0.78 M.

The load factor limits was +0.15 to +2.8 (with the flight control system engaged). The load factor limits with the VSS disengaged were –1.0g to +4.0g.

The maximum sideslip angle was a function of the airspeed and the rudder deflection:

$$(\beta \text{ limit}) = -0.25 * (\delta_r \text{ limit for } \beta=0) + (\beta \text{ limit for } \delta_r=0)$$

Table 3 defines the sideslip limit at no rudder and the rudder limit with no sideslip at different velocities. This was used as input for the above equation to calculate the maximum allowable sideslip:

KIAS	β limit for δ_r=0	δ_r limit for β=0
≤214	15.0°	30°
225	13.4°	26.8°
250	11.0°	22.0°
275	9.4°	18.8°
300	7.8°	14.6°
350	5.6°	10.6°

Table A1: LEARJET-25 Sideslip Limits

APPENDIX B – FLIGHT REGIMES

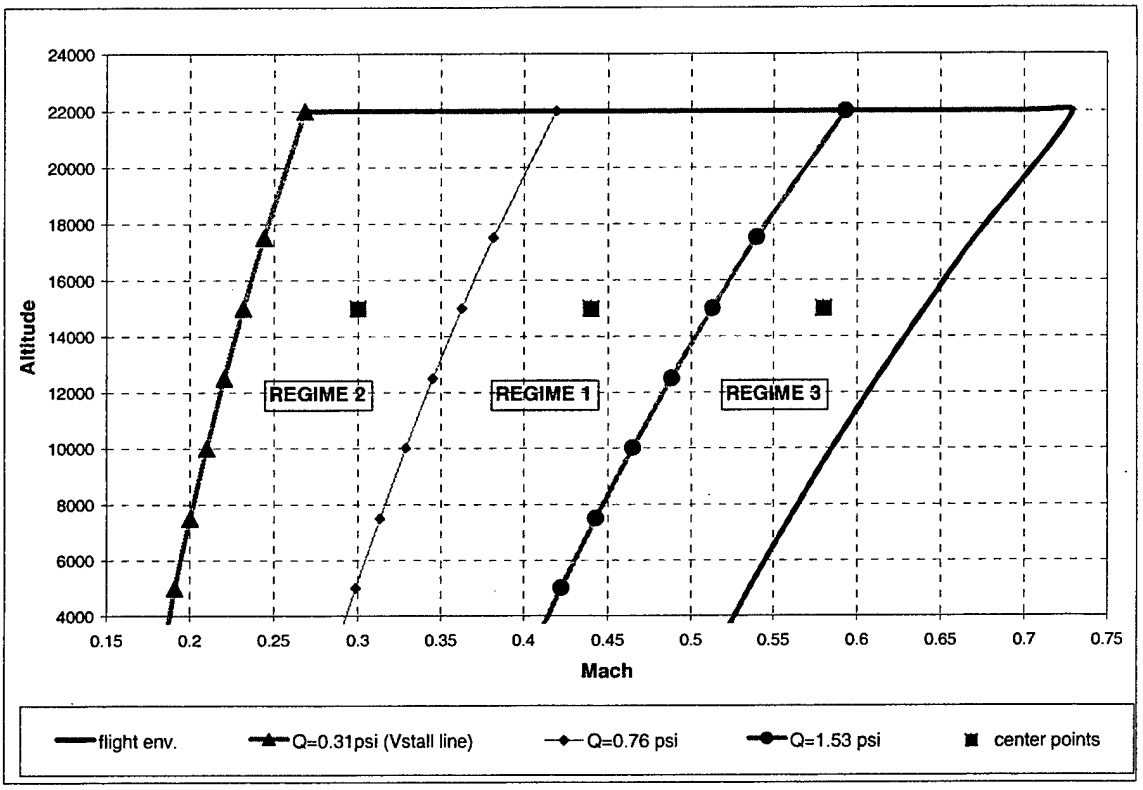

Figure B1: Flight Regimes

Figure B1 shows the flight envelope (solid line) and the flight regimes. The flight envelope was divided into three subsets, each of them characterized by a different combination of dynamic pressure and Mach number. The purpose of dividing the flight envelope into three regimes was to be able to determine the accuracy of the model in predicting the δ's in flight conditions where the assumption of linear flow was no longer accurate. From an aerodynamic model determination point of view, the purpose was to investigate the combined influence of q and M together, as well as the influence of a different flow around the elevator, especially in the surface control power and in the damping.

The flight regimes were defined as:

2) Low M (0.21 - 0.38), low q (0.31 psi – 0.76 psi).
1) Medium M (0.29 – 0.57), medium q (0.76 psi – 1.53 psi).
3) High M (>0.44), high q (>1.53 psi).

Constant q lines delineate the three regions. The square markers indicate the center flight condition for each regime.

This page intentionally left blank

APPENDIX C – TEST CONDITION MATRIX

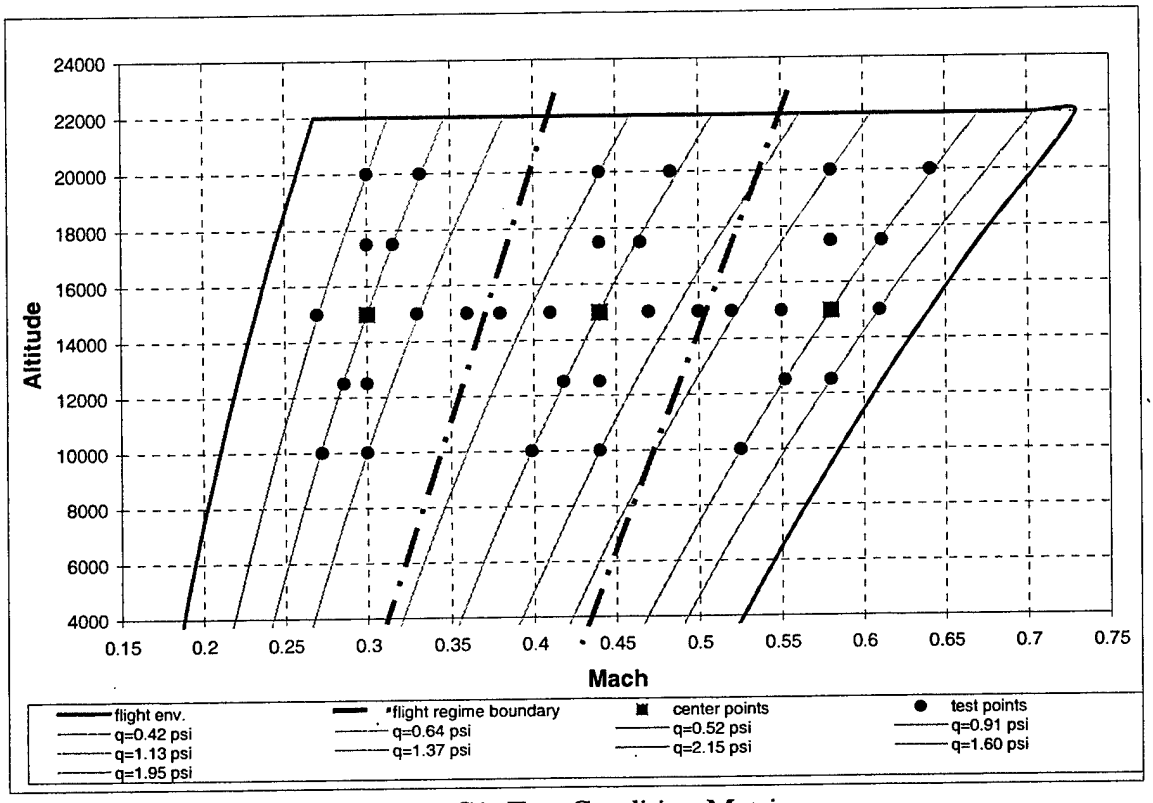

Figure C1: Test Condition Matrix

Figure C1 shows the entire series of desired test points to be flown. Due to time constraints, only data in Regime 1 and Regime 2 were collected during flight test. The dotted straight lines define the three flight regimes and replace the constant dynamic pressure lines for simplicity. The thick solid line indicates the flight envelope of the test aircraft. The points shown cover both the aerodynamic model determination and the equation of motion validation objective. For each flight regime the center points (square markers), the q line across the center points and the maximum and minimum q tested are plotted. The points along the center points q lines were used to evaluate the influence of Mach number on the derivatives (constant dynamic pressure) and the influence of altitude on the trimmed δ's (the points along the constant center points indicated airspeed lines are almost the same as the points along the constant q lines because, within the altitude range available, the density doesn't change significantly; it was assumed that they coincide within the tolerances fixed for each sortie). The points along straight horizontal lines investigated the effect of true airspeed on trimmed deflections. The points along a vertical line investigated the effect of q on the derivatives (constant M).

The square points indicate the center test points. The circles indicate the points where h, V, q and M influence were evaluated. The most important difference between these points is that the circles indicate that only a set of pitch and rudder/aileron doublets in SLUF were required. The δ's were estimated as a function of h and V, while the

aerodynamic stability derivatives were estimated as a function of q and M. At the square points the block of maneuvers to be flown was more complex. The pitch and rudder/aileron doublets were applied in a SLUF trim condition, in a climb/descent, in a stable turn at different load factors, in a push-over, in an asymmetric thrust investigation, and in a stable condition with steady sideslip.

See the Test Matrix in Table C1 for more details.

OBJ./ MOP	Var.	Test conditions (priority)	FTT required	Data band	Tolerance	Remarks	Test points:
1/1	CG	15000 ft, 220 KIAS (1) 15000 ft, 150 KIAS (2) 15000 ft, 295 KIAS (3)	Trim shot	H: ± 200 ft A/S: ± 5 KIAS CG: 21.2% - 14.0% W: 10000– 15000 lbs	H: ± 200 ft A/S: ± 5 KIAS VVI~0	The CG will be divided into three subsets. A trim shot with a pitch and rudder/aileron doublets will be performed any time the CG enters a new subset. The aircraft gross weight and the fuel fuselage weight will be used to figure out when the airplane enters a new subset.	**Regime 1, 2, 3** W1= 21.2% - 18.1% W2= 18.1% - 15.3% W3= 15.3% - 14.0%
1/2	KIAS	15000 ft	Trim shot	H: ± 200 ft A/S: 190 - 250 KIAS A/S: 131 - 180 KIAS A/S: 262 - 310 KIAS	H: ± 200 ft A/S: ± 5 KIAS CG: within one subset	Perform the trim shot, apply pitch and rudder/aileron doublets. The test points in the next cell are sorted out depending on the flight regime priority	**Reg. 1**: 190, 205, 220, 235, 250 **Reg. 2**: 135, 150, 165, 180 **Reg. 3**: 262, 278,290, 310
1/3	PA	220 KIAS (1) 150 KIAS (2) 295 KIAS (3)	Trim shot	A/S: ± 5 KIAS H: 10000 – 20000 ft	A/S: ± 5 KIAS ALT: ± 200 ft CG: within one subset	Perform the trim shot, apply pitch and rudder/aileron doublets.	**Reg. 1, 2, 3** : 10k, 12.5k, 15k, 17.5k, 20k
1/4	T	15000 ft, 220 KIAS (1) 15000 ft, 150 KIAS (2) 15000 ft, 295 KIAS (3)	Engine out FTT	H: ± 500 ft A/S: ± 5 KIAS T: 0 – max (one engine idle, one engine max thrust)	H: ± 500 ft A/S: ± 5 KIAS Heading: ± 5 deg Pitch: ± 5 deg Bank: ± 5 deg CG: within one subset	Wings level, apply asymmetric thrust; use rudder to stabilize at 5 points; apply pitch and rudder/aileron doublets	**Reg. 1, 2, 3:** 0%, 20%,40%, 60%, 80%, 98% (see MOP 1/6 for β limits)

OBJ./ MOP	Var.	Test conditions (priority)	FTT required	Data band	Tolerance	Remarks	Test points:
1/5	γ	15000 ft, 220 KIAS (1) 15000 ft, 150 KIAS (2) 15000 ft, 295 KIAS (3)	climb/ descent	H: 1000 ft A/S: ± 5 KIAS γ: -15 ÷ 15 deg	A/S: ± 5 KIAS γ: ± 2 deg CG: within one subset	Trim on the climb/descent; apply pitch doublets	**Reg. 1, 2, 3** : +5 deg, -5 deg, +10 deg, -10 deg, +15 deg, -15 deg
1/6	β	15000 ft, 220 KIAS (1) 15000 ft, 150 KIAS (2) 15000 ft, 295 KIAS (3)	SHSS	H: ± 500 ft A/S: ± 5 KIAS β: 0 – max	β: ± 2 deg H: ± 500 ft A/S: ± 5 KIAS Heading: ± 5 deg Pitch: ± 5 deg Bank: ± 5 deg CG: within one subset	The maneuver will be a stable one; trim or freeze controls at each trim condition; apply pitch and rudder/aileron doublets	**Reg. 1**: +3 deg, -3 deg, +6 deg, -6 deg, +9 deg, -9 deg **Reg. 2**: +3 deg, -3 deg, +6 deg, -6 deg, +9 deg, -9 deg **Reg. 3**: +2 deg, -2 deg, +5 deg, -5 deg,
1/7	ϕ	15000 ft, 220 KIAS (1) 15000 ft, 150 KIAS (2) 15000 ft, 395 KIAS (3)	Constant speed turn	H: ± 500 ft A/S: ± 5 KIAS Bank: 5 – 66 deg (load factor 1 – 2.5)	H: ± 500 ft A/S: ± 5 KIAS ϕ: ± 5 deg β: 0 ± 2 deg CG: within one subset	The maneuver will be a stable one; trim or freeze controls at each trim condition; apply pitch and rudder/aileron doublets	**Reg. 1, 2, 3** : 15 deg, 30 deg, 45 deg, 60 deg (1.2 load factor), 66 deg (2.5 load factor)
1/8	Q	15000 ft, 220 KIAS (1) 15000 ft, 150 KIAS (2) 15000 ft, 295 KIAS (3)	Push-over	H: ± 500 ft A/S: ± 5 KIAS Pitch: +5deg – -5deg N_z: +0.4 – 1.0	H: ± 500 ft A/S: ± 5 KIAS N_z: ± 0.1G CG: within one subset	Set a climb at 5 deg nose high; start pushing and freeze controls, whichever load factor reach at the top. Apply the pitch doublets when at 1 or 2 deg nose high, so the a/c response will develop at the top. Push until 5 deg nose low	**Reg. 1, 2, 3** : Load factor 0.8, 0.6, 0.4 **Reg. 2 (pitch rate):** 2.5; 3.4 ; 3.8 deg/sec **Reg. 1 (pitch rate):** 3.7 ; 4.9 ; 5.6 deg/sec **Reg. 3 (pitch rate):** 1.9 ; 2.5 ; 2.8 deg/sec

OBJ./ MOP	Var.	Test conditions (priority)	FTT required	Data band	Tolerance	Remarks	Test points:
1/9	Flight regime (non linear effects)	15000 ft, 220 KIAS (1) 15000 ft, 150 KIAS (2) 15000 ft, 295 KIAS (3)	No extra data to be collected	No extra data to be collected	No extra data to be collected	No extra data to be collected	No extra data to be collected
2/1	$C_{L\alpha}$, C_{L0}, C_{d0}, C_{m0}, $C_{m\alpha}$, C_{mq}, $C_{m\delta e}$	10000 - 20000 ft 0.27 - 0.58 M W: 10000 - 15000 lbs	pitch doublets	Extra data collected: Constant Mach number for each center test point	H: ± 200 ft M: ± 0.05 CG: within one subset	The test points are the same as in obj 1 plus the ones described here. The trim conditions where applying the doublets are the same used for obj. 1. Same priority order will be used. For each point apply the PTI; change amplitude and period if necessary	**Reg. 1**: 0.3 M @ 10k, 12.5k, 15k, 17.5k, 20k **Reg. 2**: 0.44 M @ 10k, 12.5k, 15k, 17.5k, 20k **Reg. 3**: 0.58 M @ 12.5k, 15k, 17.5k, 20k
2/2	$C_{n\beta}$ C_{nr} $C_{n\delta r}$ $C_{l\beta}$ C_{lp} $C_{l\delta a}$ $C_{n\delta\alpha}$	10000 - 20000 ft 0.28- 0.82 M W: 10000 – 15000 lbs	Rudder/ Aileron doublets	Extra data collected: Constant Mach number for each center test point	H: ± 200 ft M: ± 0.05 CG: within one subset	Same as MOP 2/1	**Reg. 1**: 0.3 M @ 10k, 12.5k, 15k, 17.5k, 20k **Reg. 2**: 0.44 M @ 10k, 12.5k, 15k, 17.5k, 20k **Reg. 3**: 0.58 M @ 12.5k, 15k, 17.5k, 20k
3/1	δ_e	15000 ft, 250 KIAS, 13500 lbs @ SLUF β 15 deg γ 15 deg N_z 2.5	Computer simulation	$C_{m\alpha}$, C_{mq} ,$C_{m\delta e}$ ± 40%		estimate the max percentage error in the derivatives that would allow the predictions of the model to be still acceptable.	
3/2	δ_a	15000 ft, 250 KIAS, 13500 lbs @ SLUF N_z 2.5	Computer simulation	$C_{l\delta a}$, $C_{l\beta}$,C_{lp} ± 40%		Same as MOP 3/1	
3/3	δ_r	15000 ft, 250 KIAS, 13500 lbs @ SLUF β 15 deg N_z 2.5	Computer simulation	$C_{n\beta}$, C_{nr} , $C_{n\delta r}$, $C_{n\delta a}$ ± 40%		Same as MOP 3/1	

Table C1: Test Matrix

This page intentionally left blank.

APPENDIX D – PLOTS SUPPORTING COMPARISON OF FLIGHT TEST δ TO PREDICTED δ

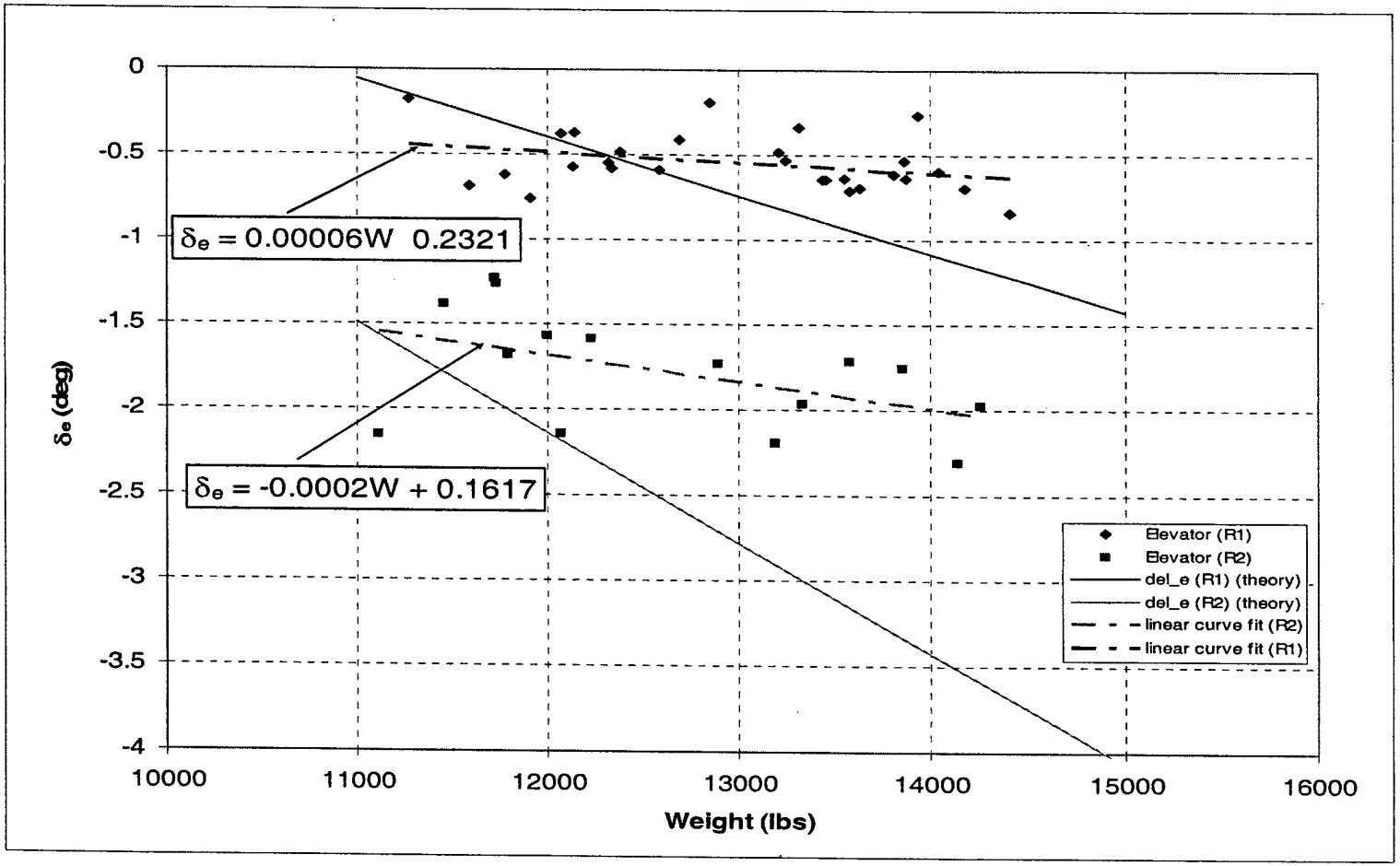

Figure D1: Learjet 25 Elevator Deflection Weight Effects, Project HAVE TRIM

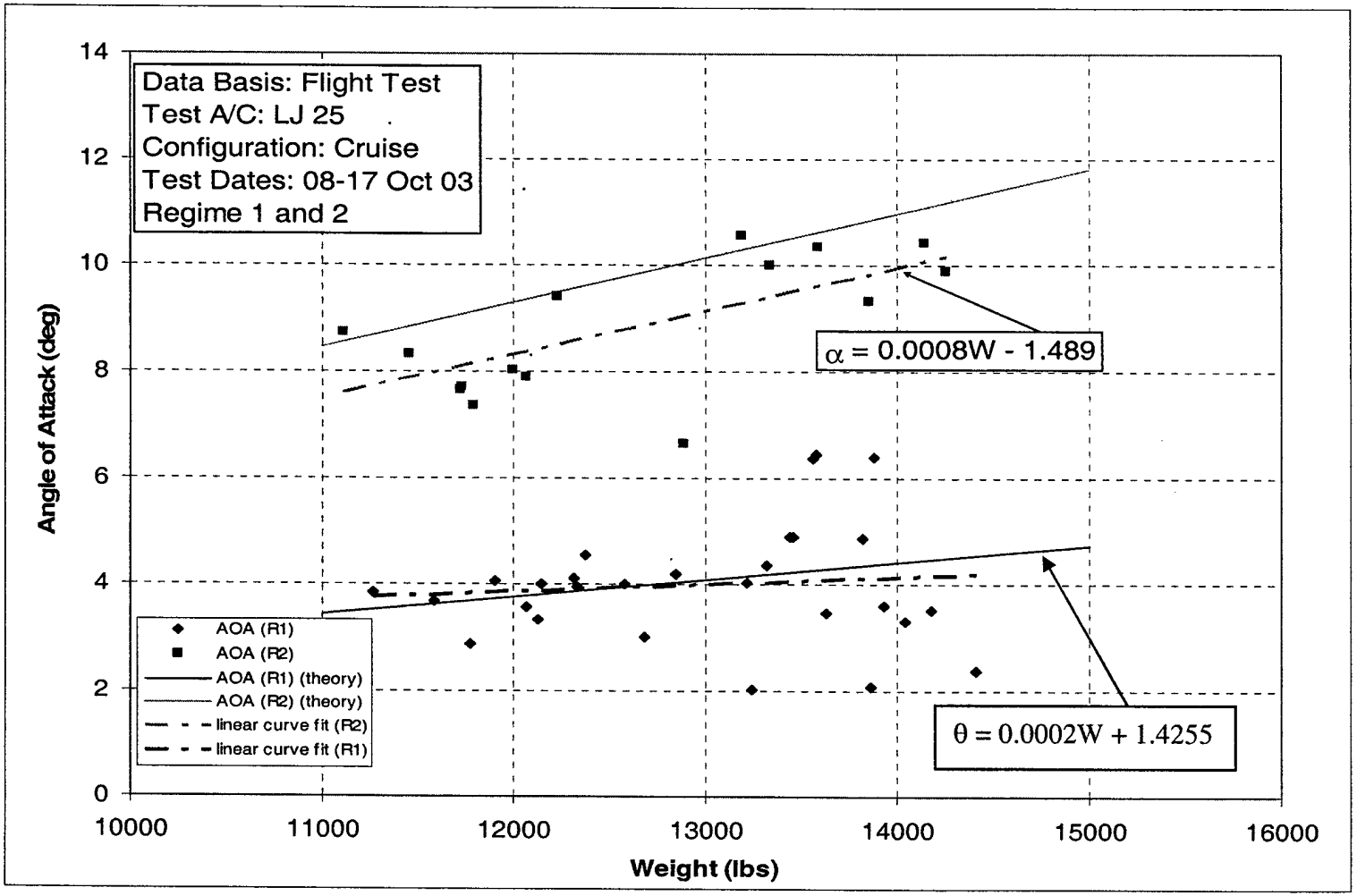

Figure D2: Learjet 25 Angle of Attack Weight Effect, Project HAVE TRIM

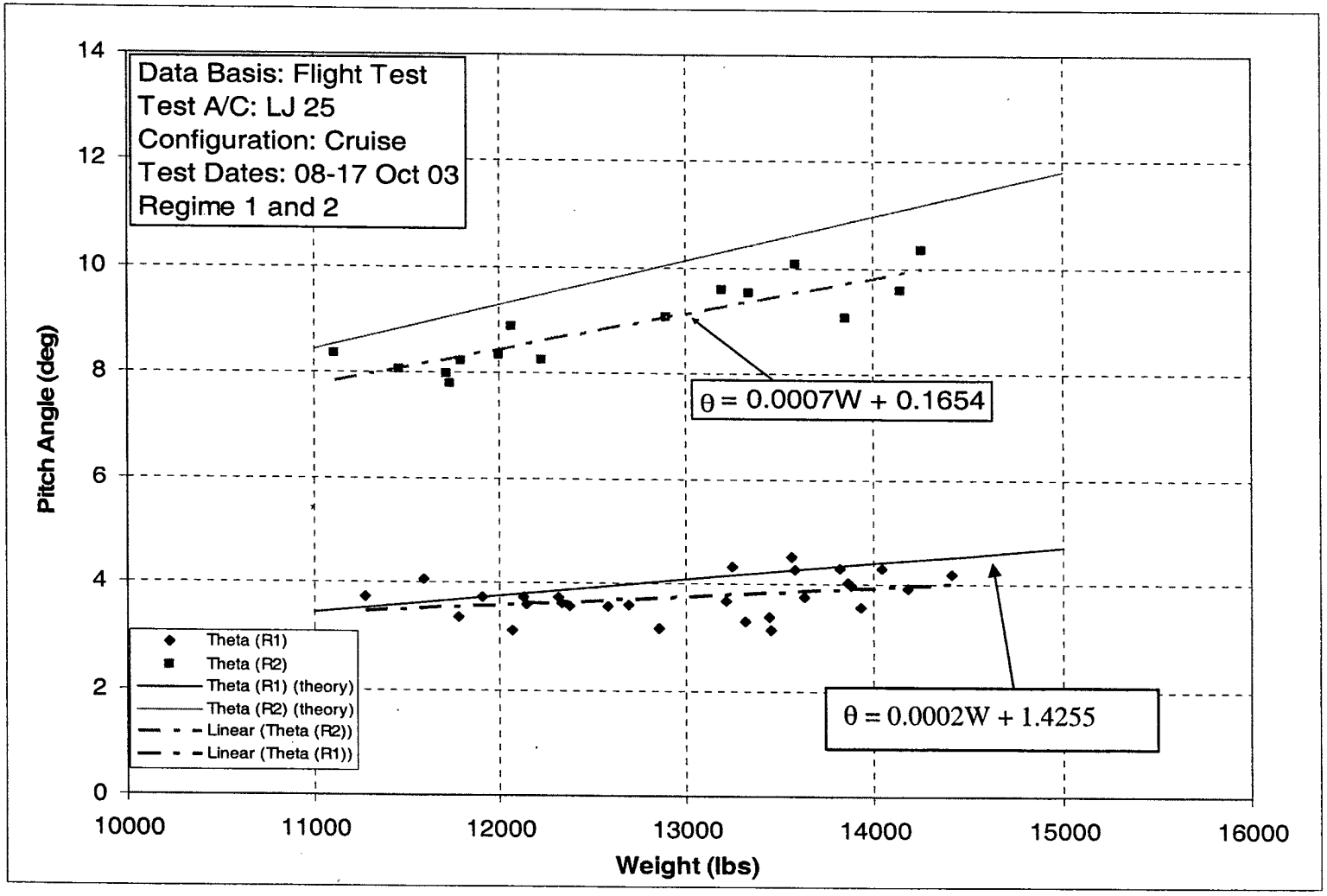

Figure D3: Learjet 25 Pitch Angle Weight Effect, Project HAVE TRIM

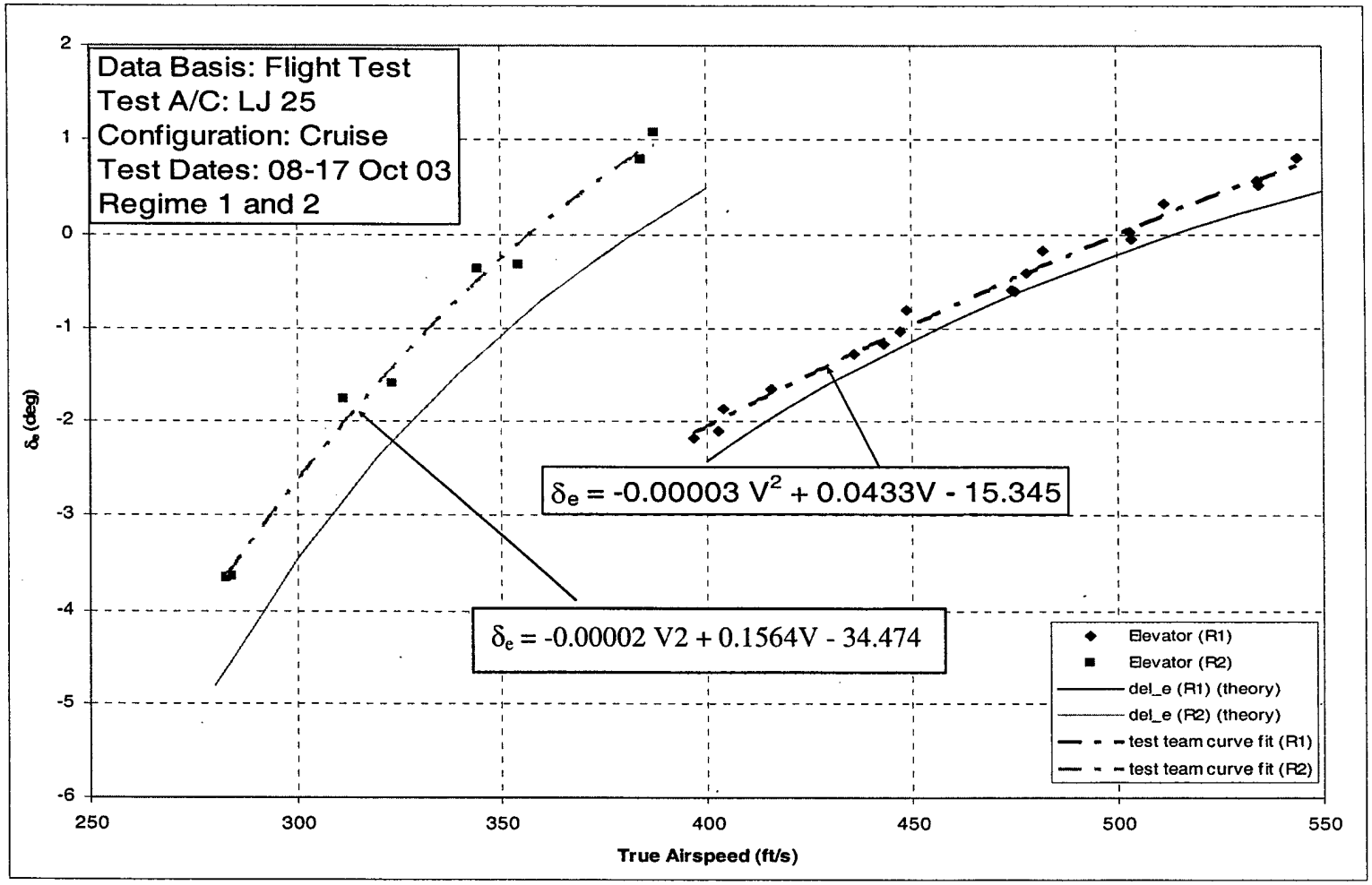

Figure D4: Learjet 25 Elevator Deflection Velocity Effect, Project HAVE TRIM

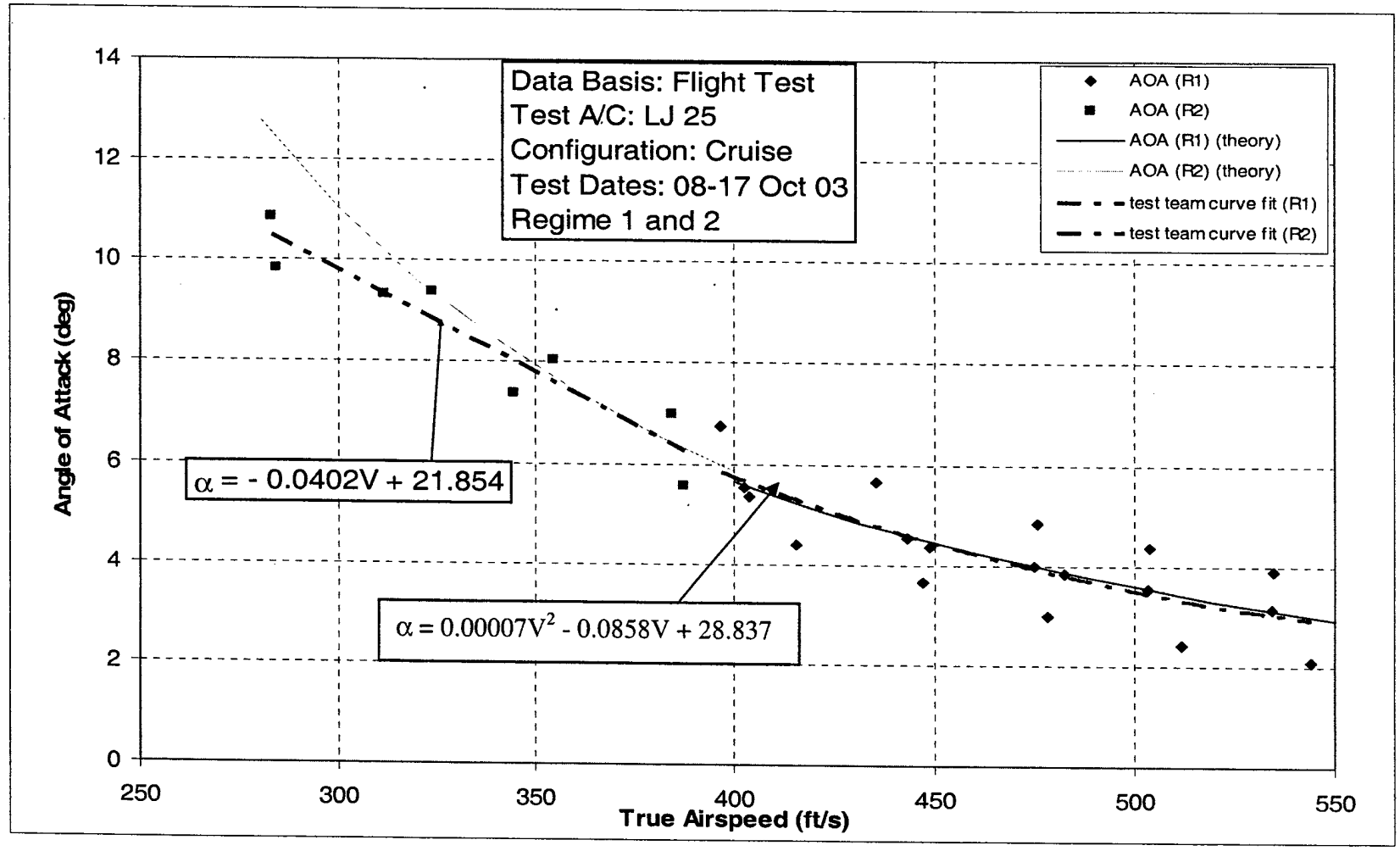

Figure D5: Learjet 25 Angle of Attack Velocity Effect, Project HAVE TRIM

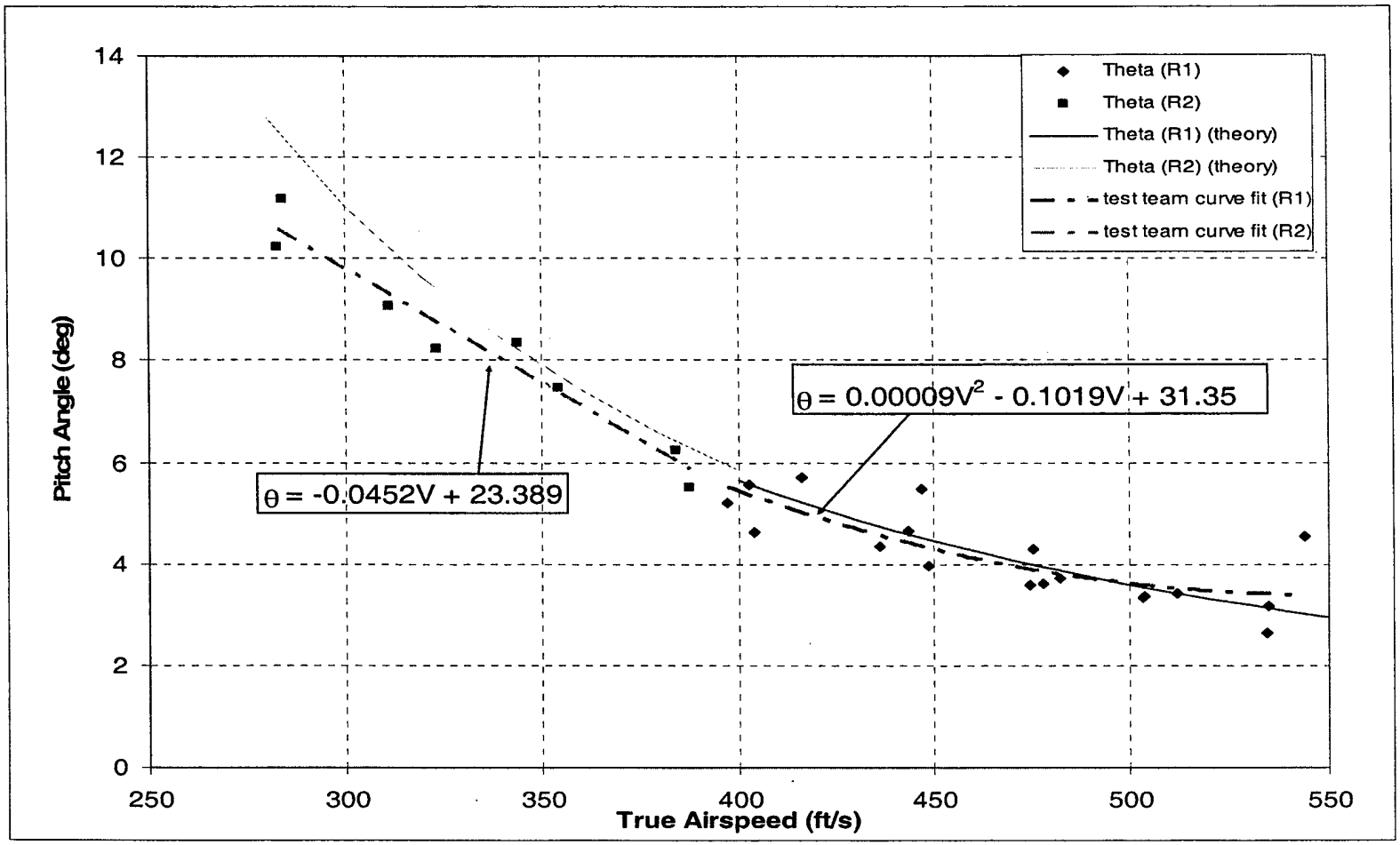

Figure D6: Learjet 25 Pitch Angle Velocity Effect, Project HAVE TRIM

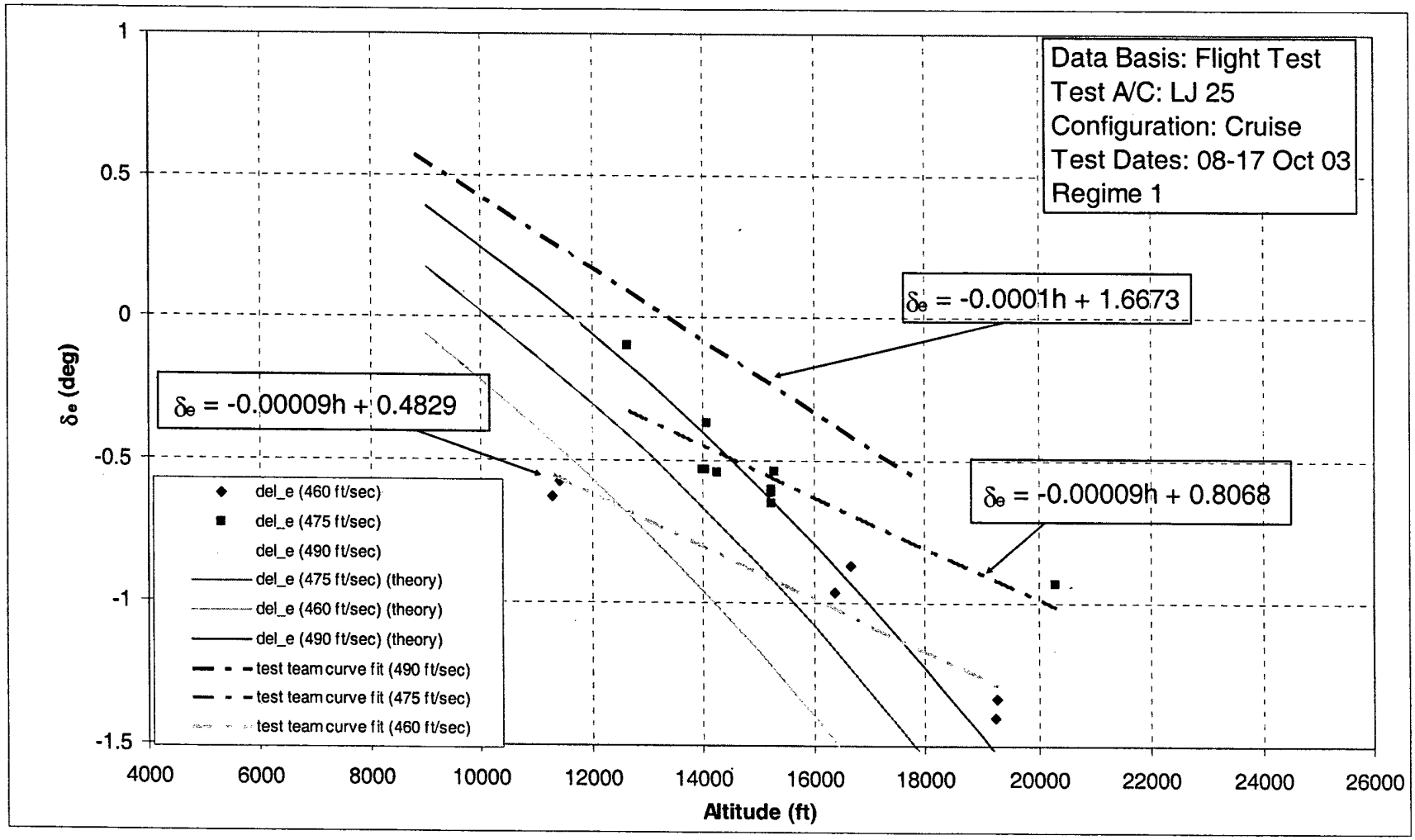

Figure D7: Learjet 25 Regime 1 Elevator Deflection Altitude Effect, Project HAVE TRIM

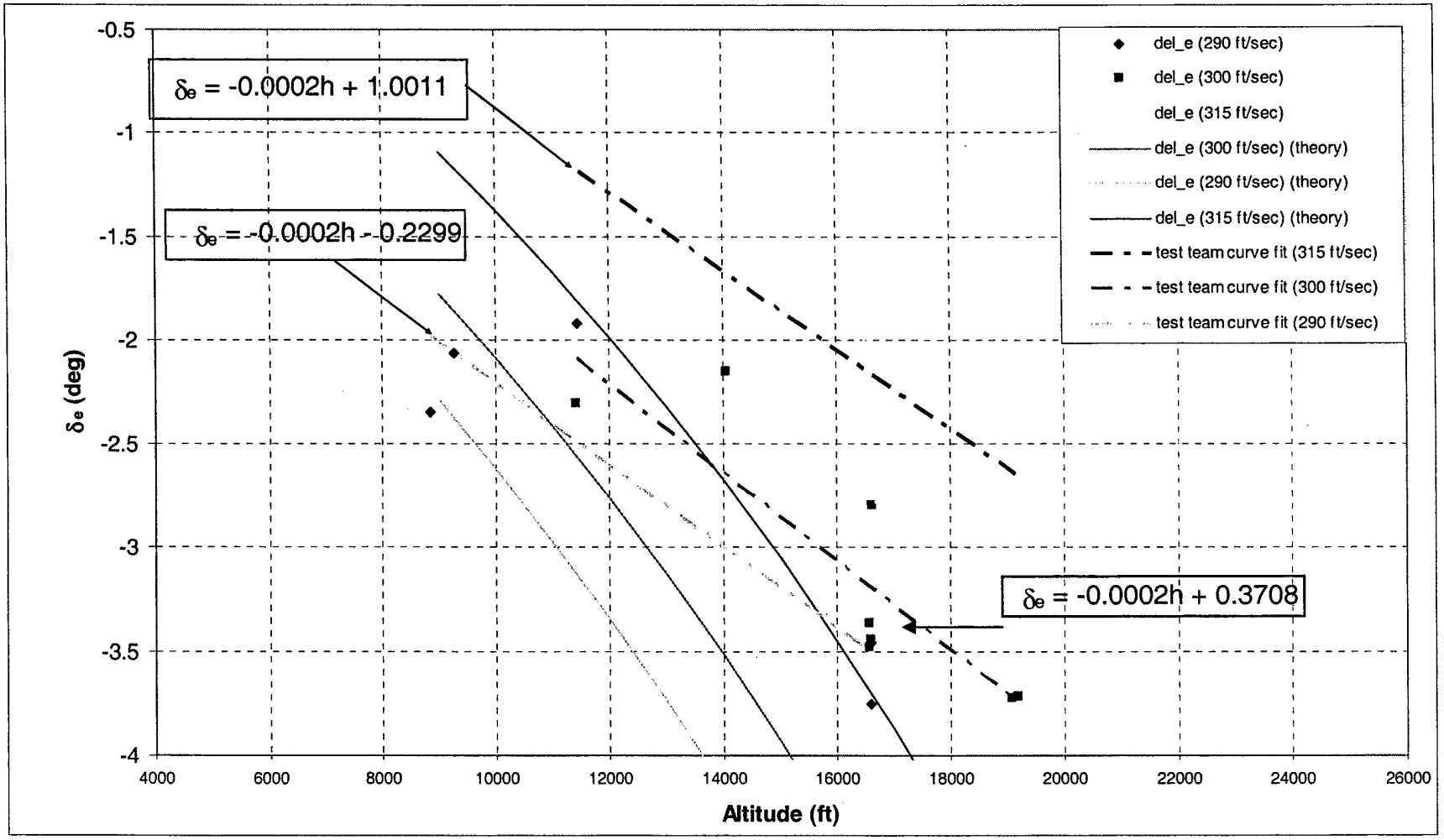

Figure D8: Learjet 25 Regime 2 Elevator Deflection Altitude Effect, Project HAVE TRIM

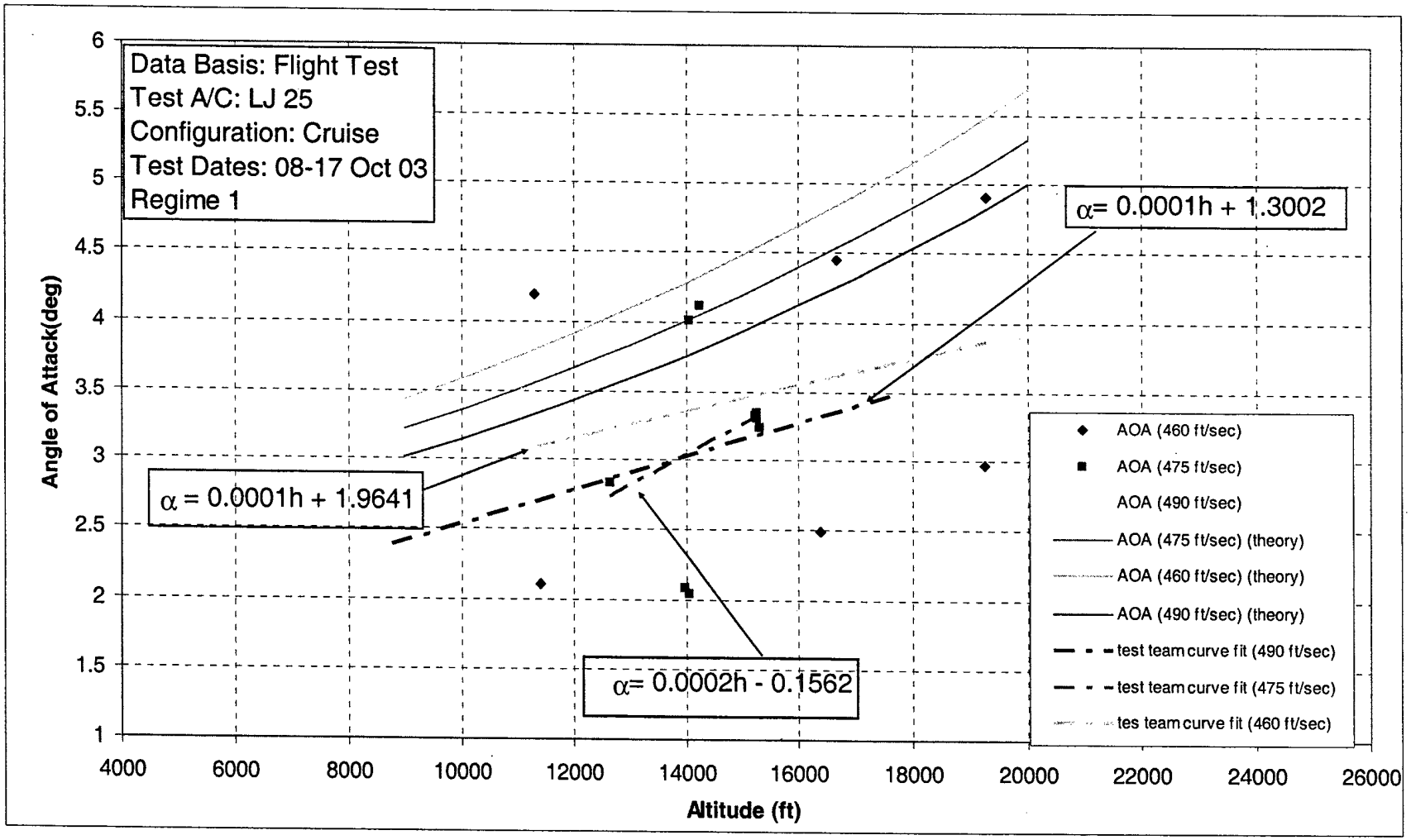

Figure D9: Learjet 25 Regime 1 Angle of Attack Altitude Effect, Project HAVE TRIM

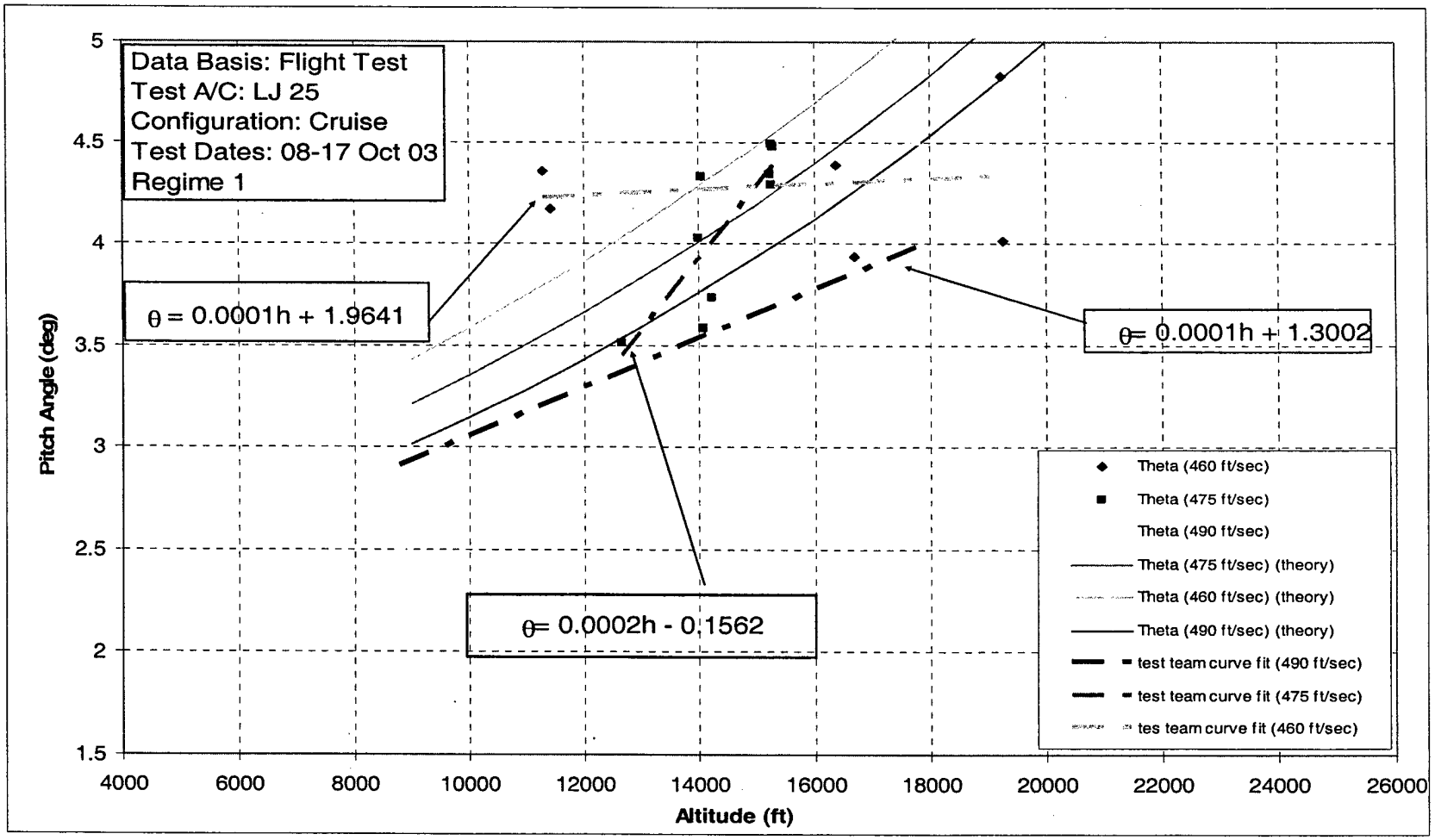

Figure D10: Learjet 25 Regime 1 Pitch Angle Altitude Effect, Project HAVE TRIM

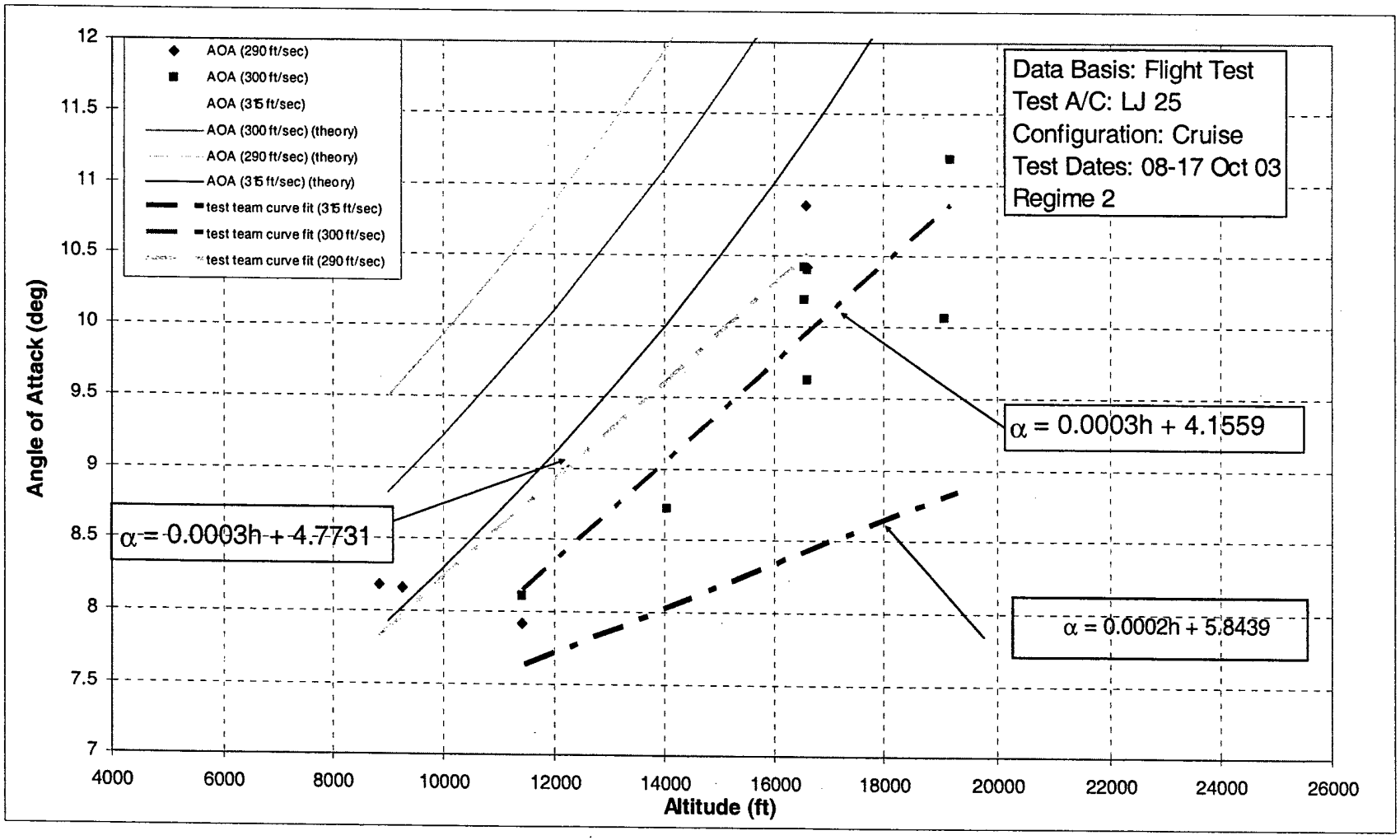

Figure D11: Learjet 25 Regime 2 Angle of Attack Altitude Effect, Project HAVE TRIM

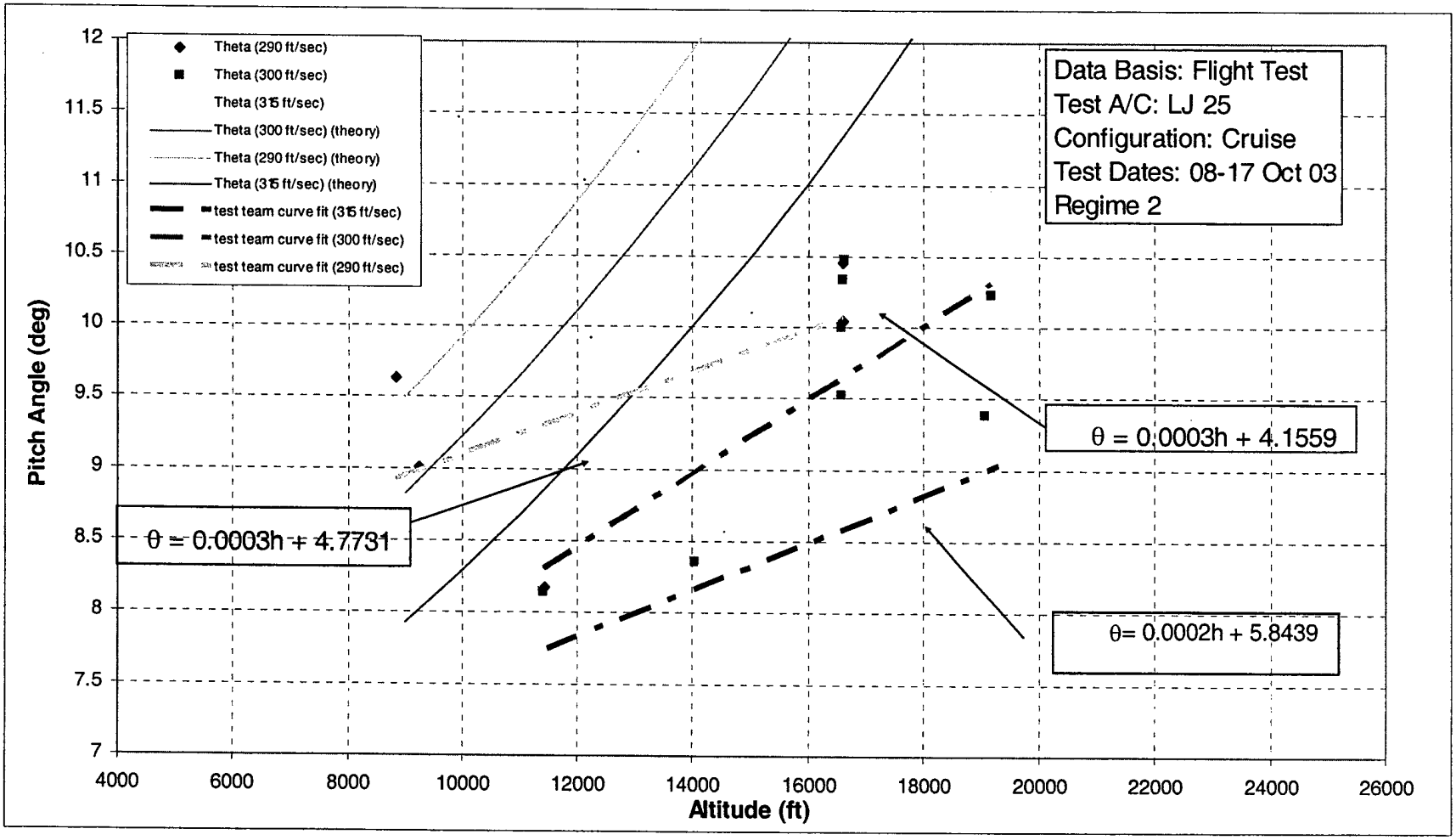

Figure D12: Learjet 25 Regime 2 Pitch Angle Altitude Effect, Project HAVE TRIM

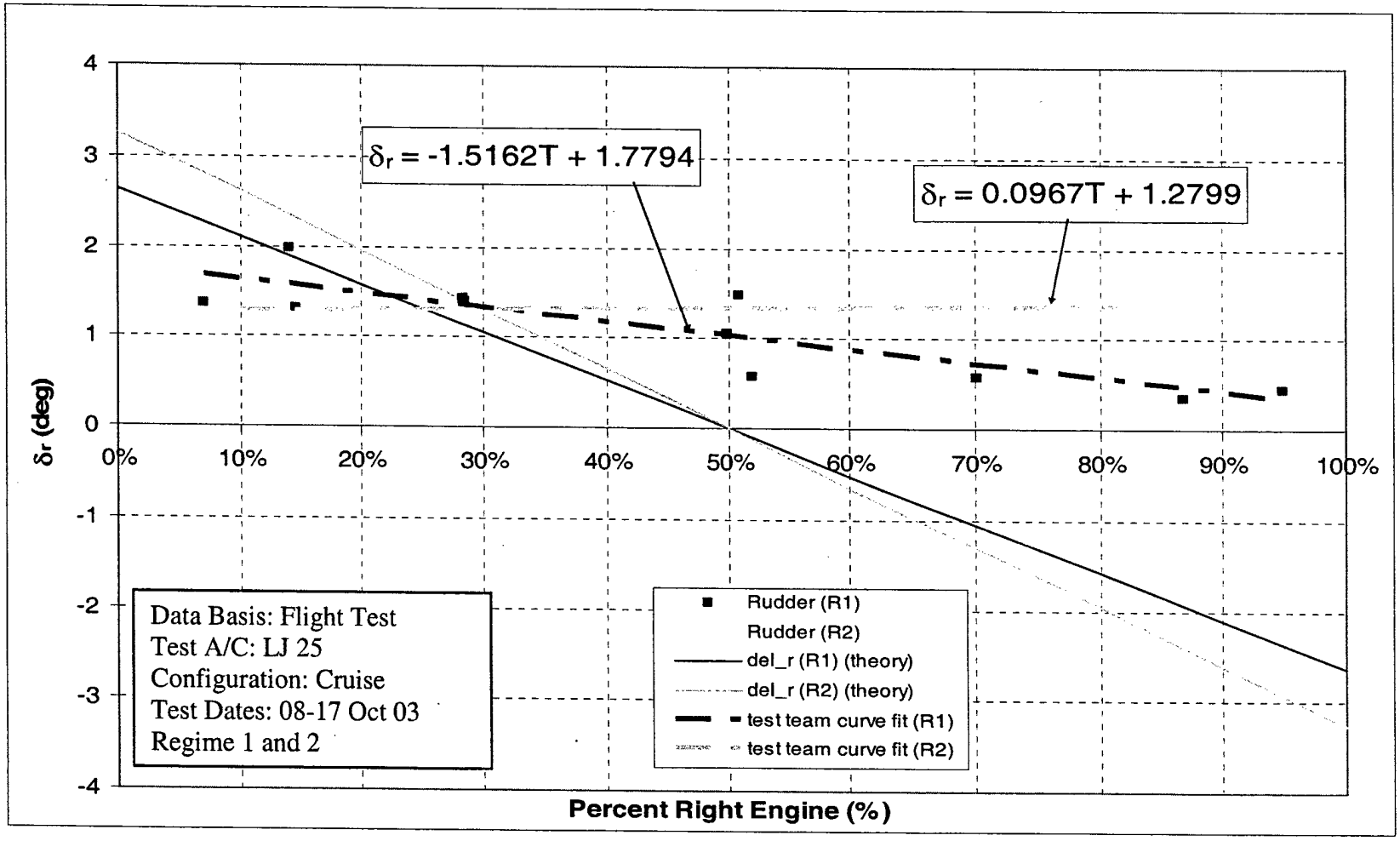

Figure D13: Learjet 25 Rudder Deflection Asymmetric Thrust Effect, Project HAVE TRIM

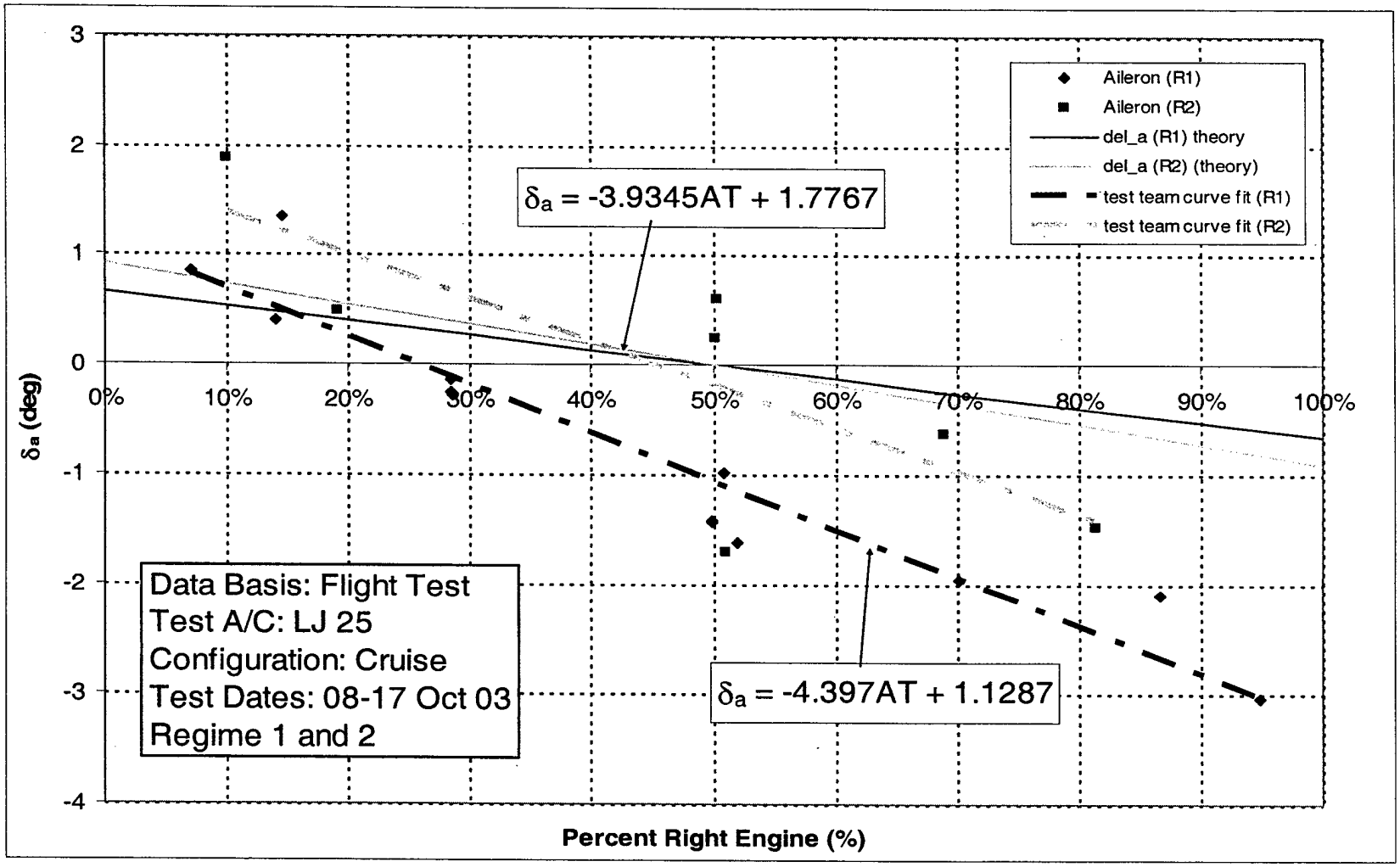

Figure D14: Learjet 25 Aileron Deflection Asymmetric Thrust Effect, Project HAVE TRIM

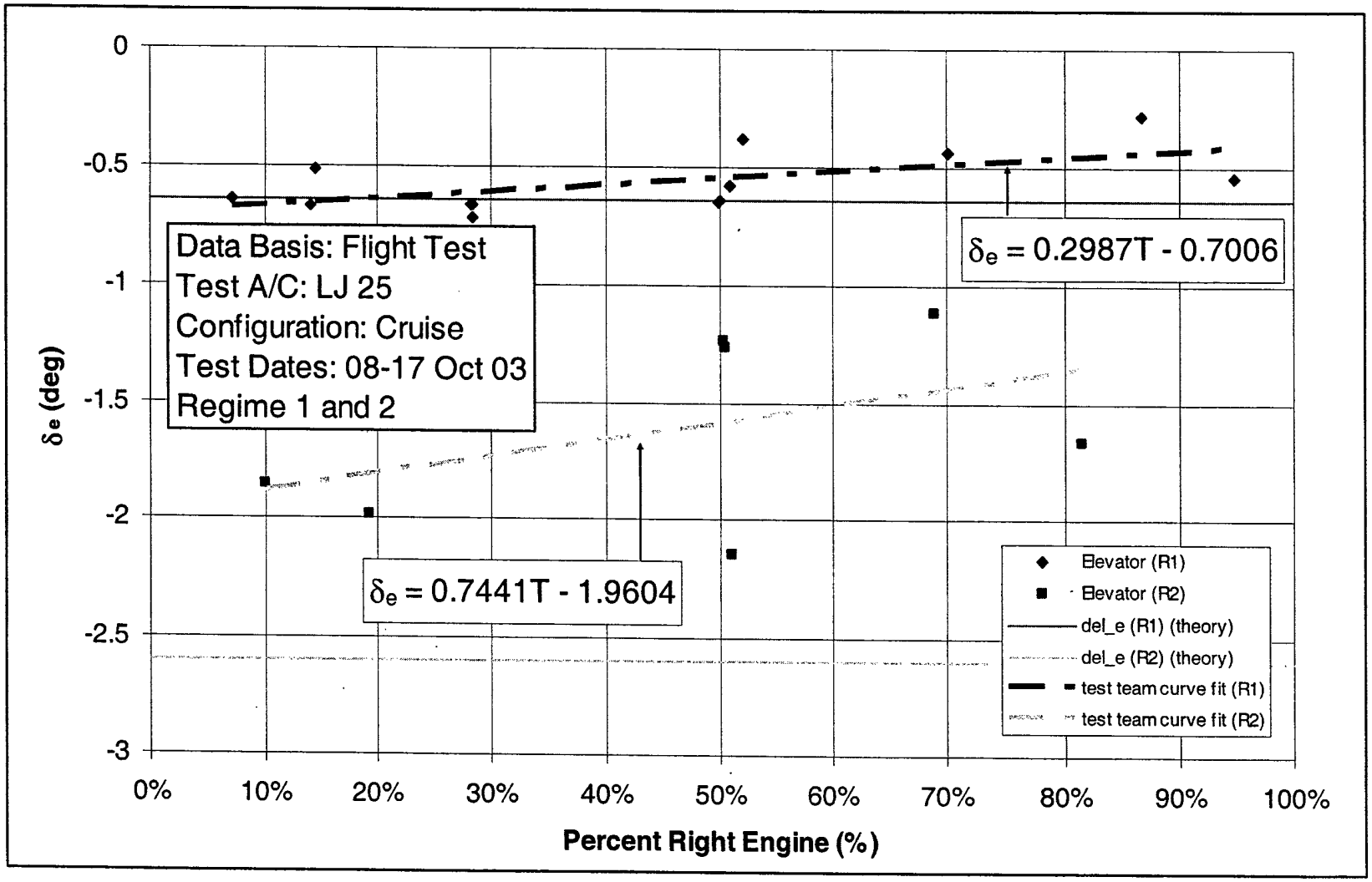

Figure D15: Learjet 25 Elevator Deflection Asymmetric Thrust Effect, Project HAVE TRIM

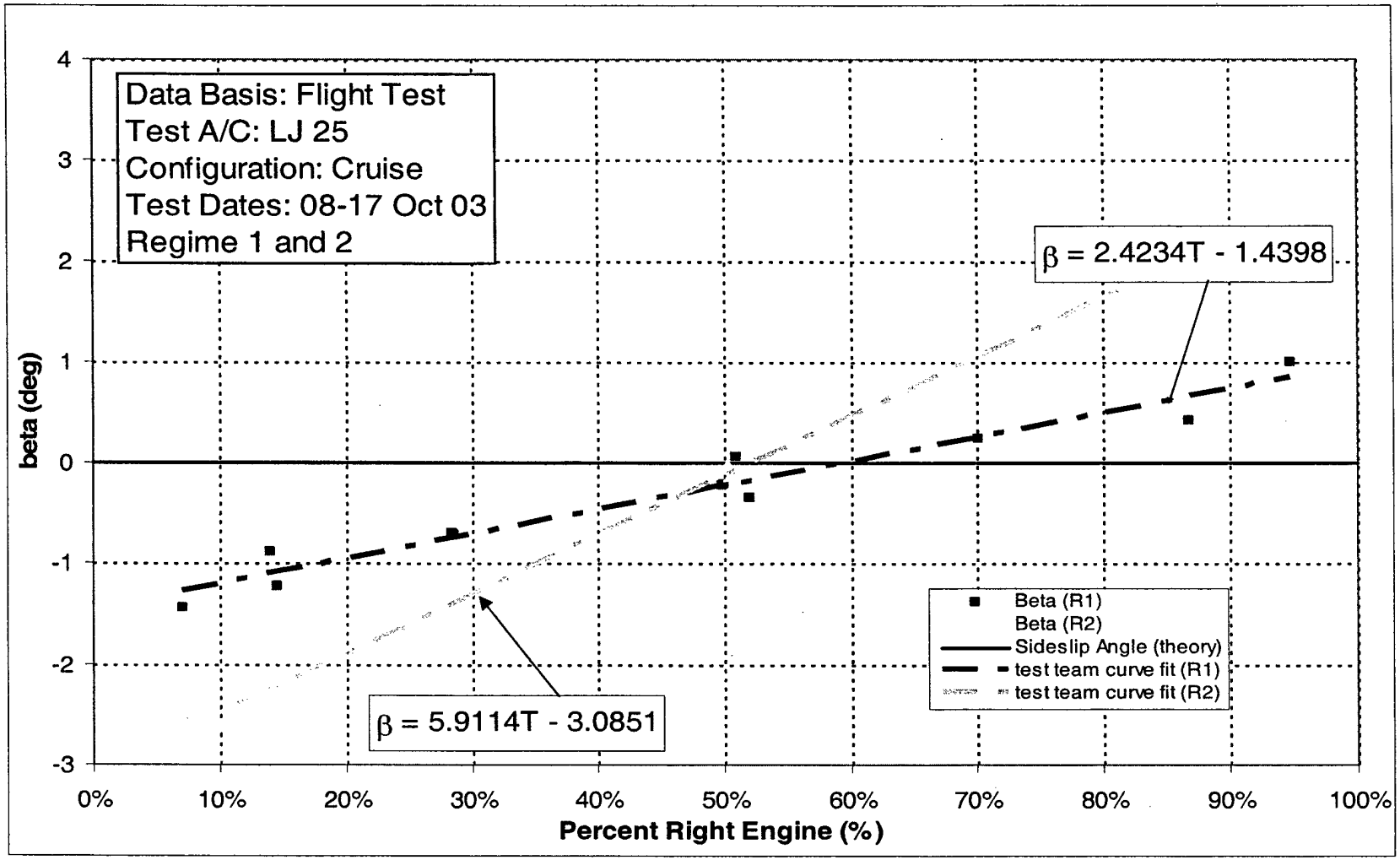

Figure D16: Learjet 25 Sideslip Angle Asymmetric Thrust Effect, Project HAVE TRIM

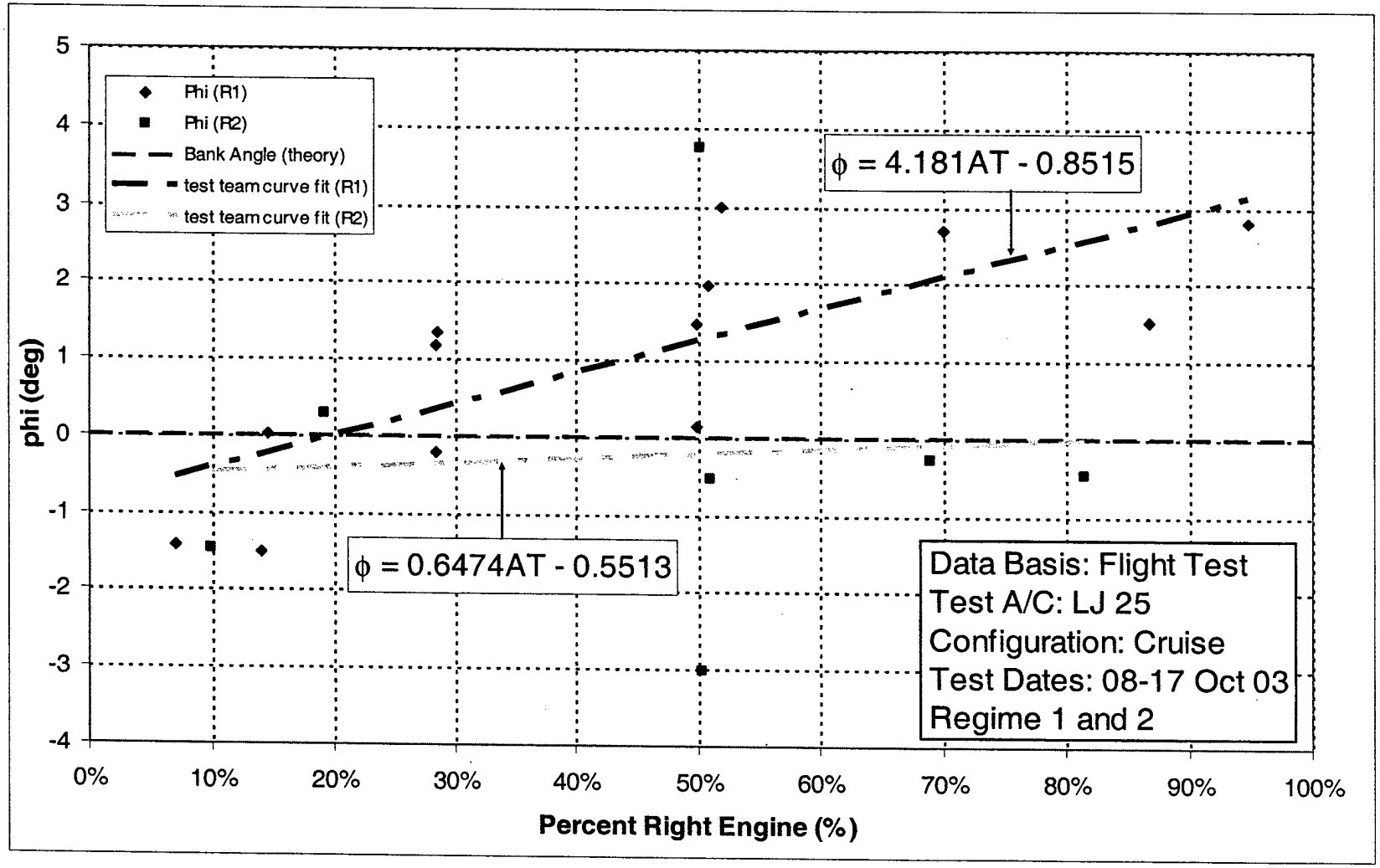

Figure D17: Learjet 25 Bank Angle Asymmetric Thrust Effect, Project HAVE TRIM

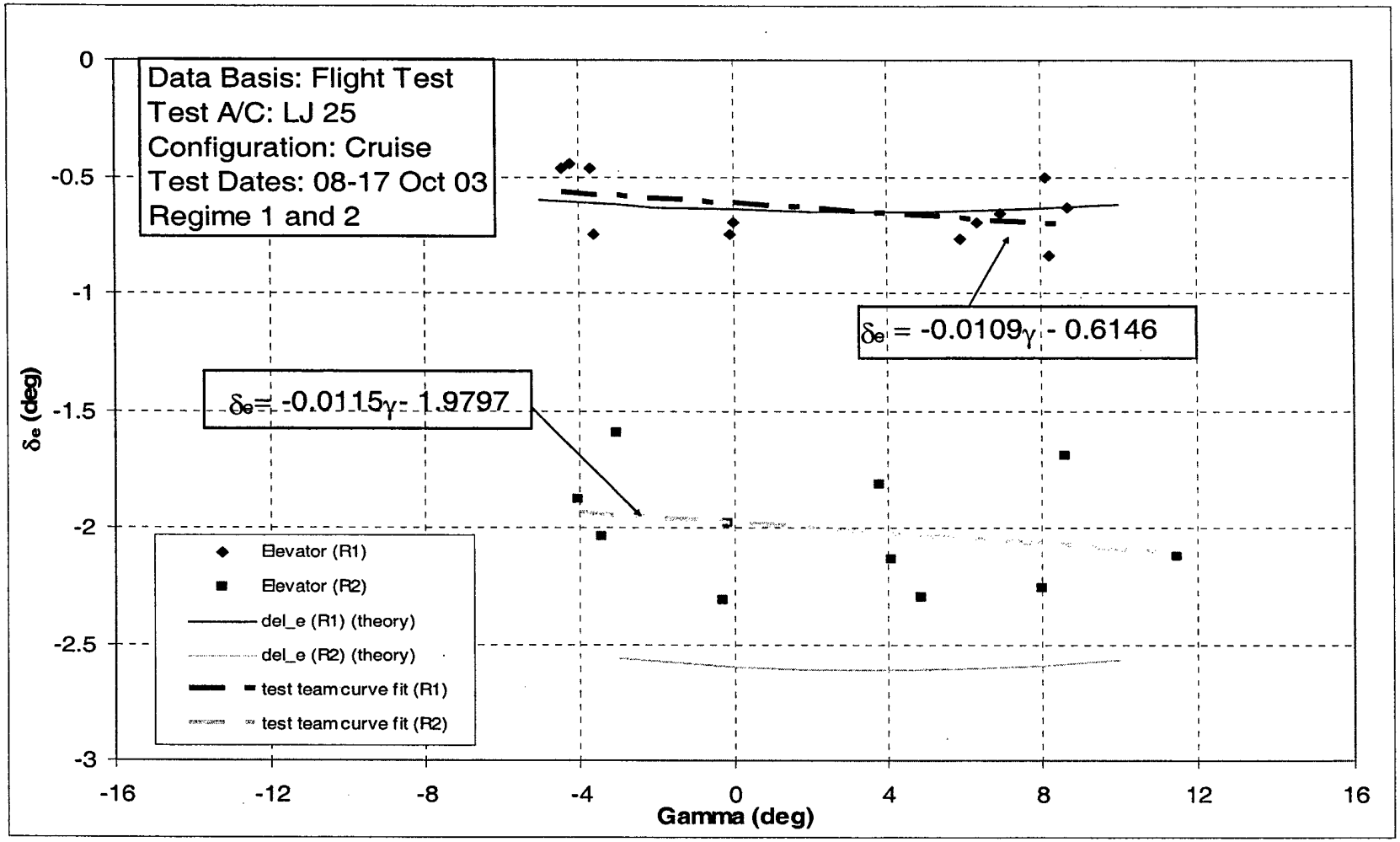

Figure D18: Learjet 25 Elevator Deflection Flight Path Angle Effect, Project HAVE TRIM

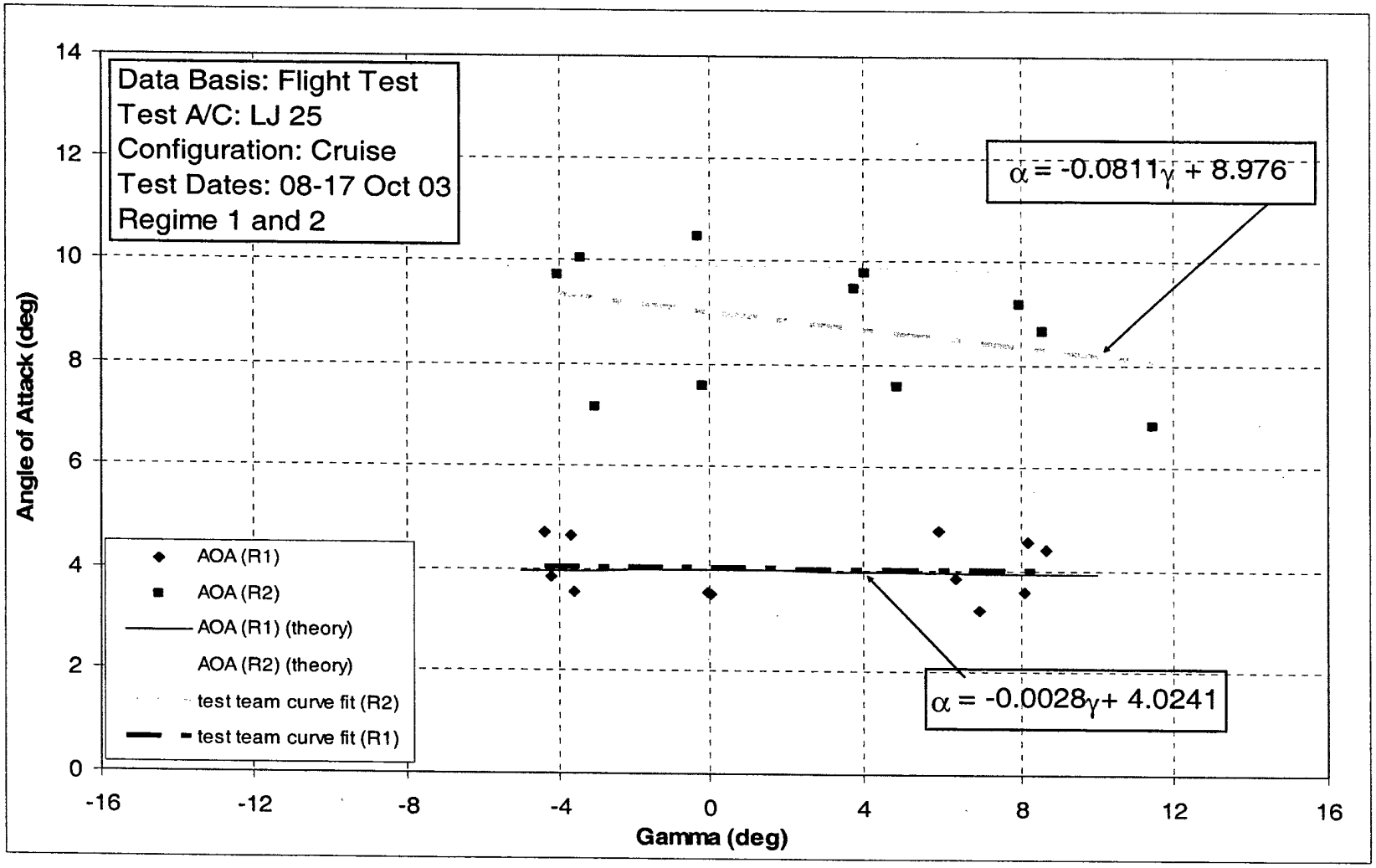

Figure D19: Learjet 25 Angle of Attack Flight Path Angle Effect, Project HAVE TRIM

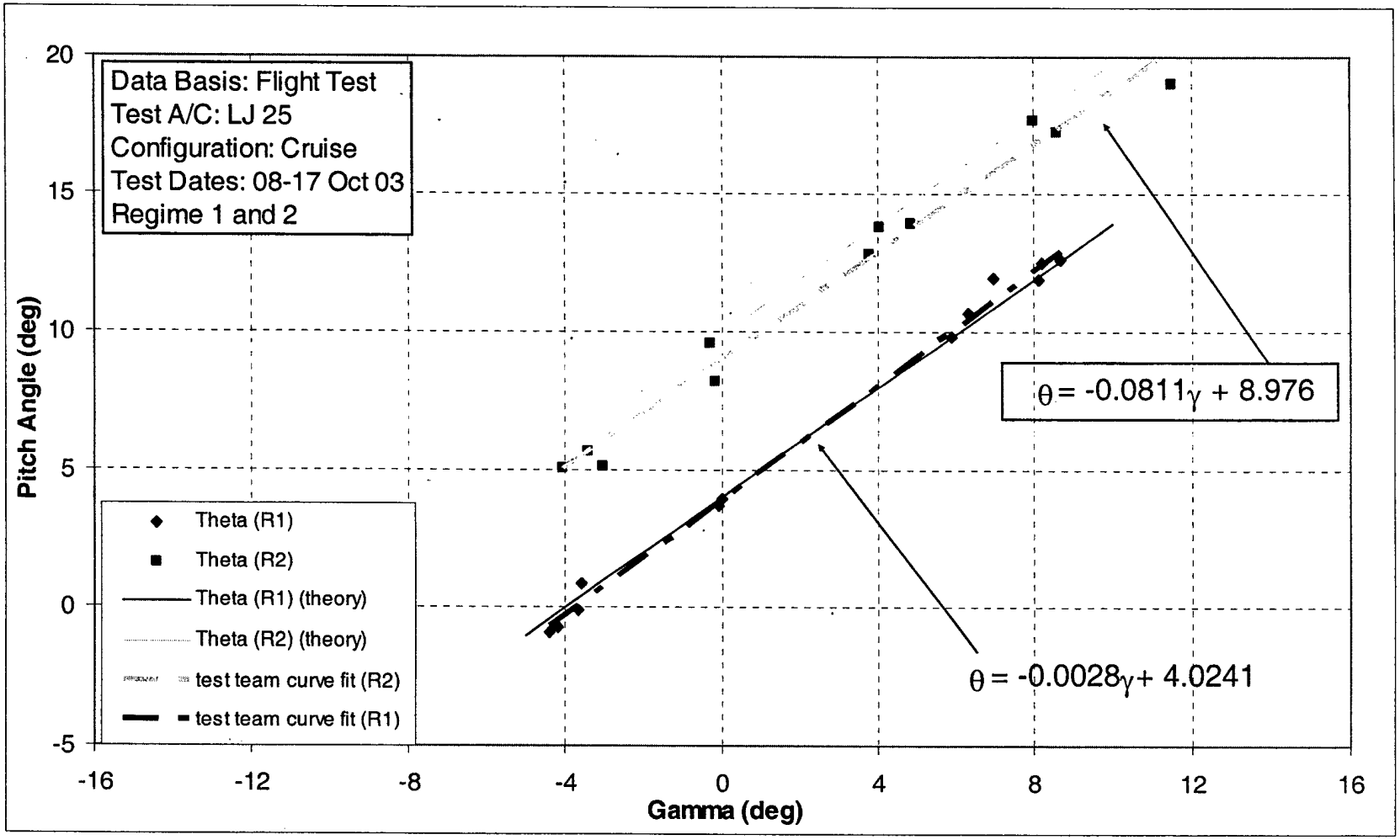

Figure D20: Learjet 25 Pitch Angle Flight Path Angle Effect, Project HAVE TRIM

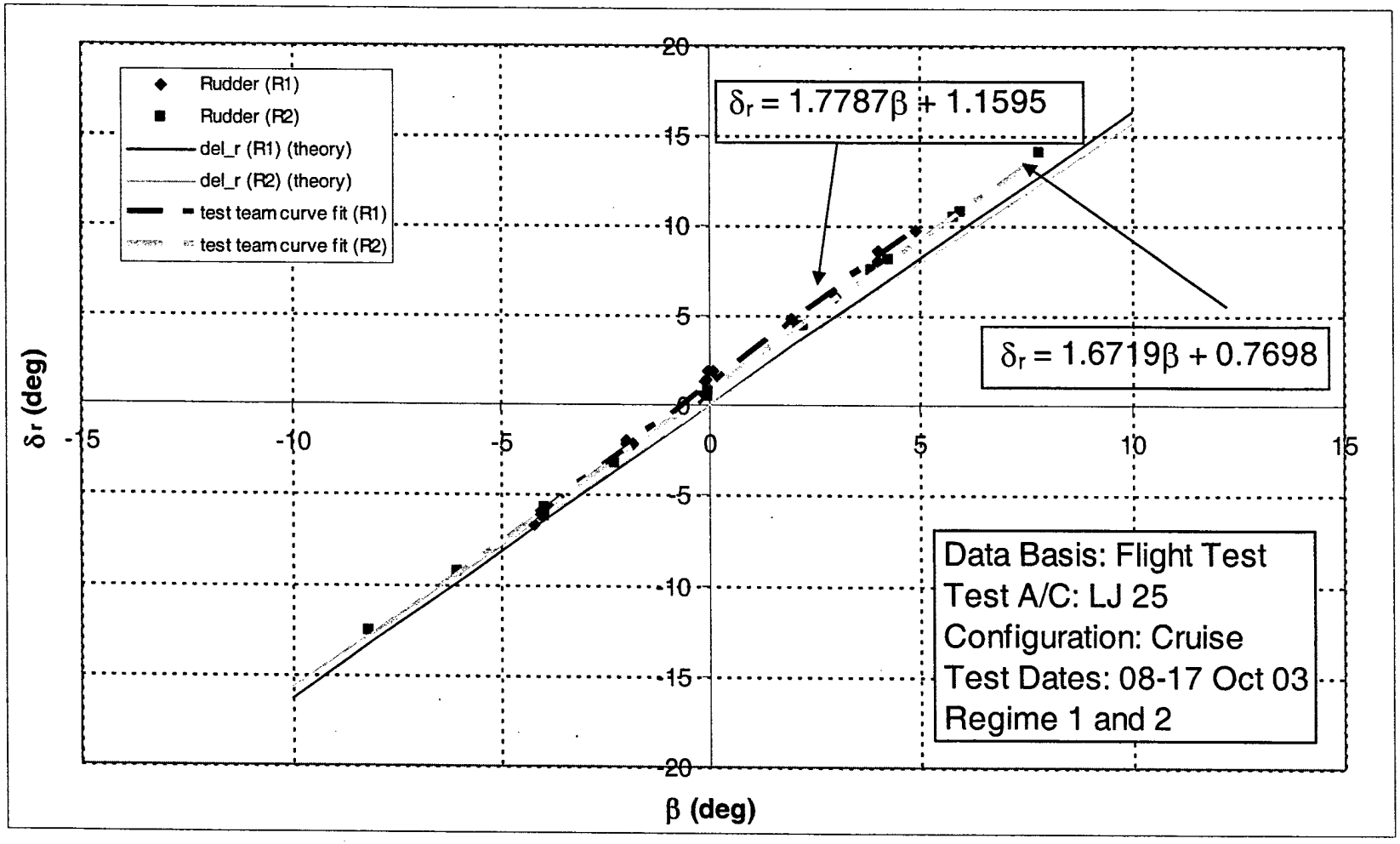

Figure D21: Learjet 25 Rudder Deflection Sideslip Angle Effect, Project HAVE TRIM

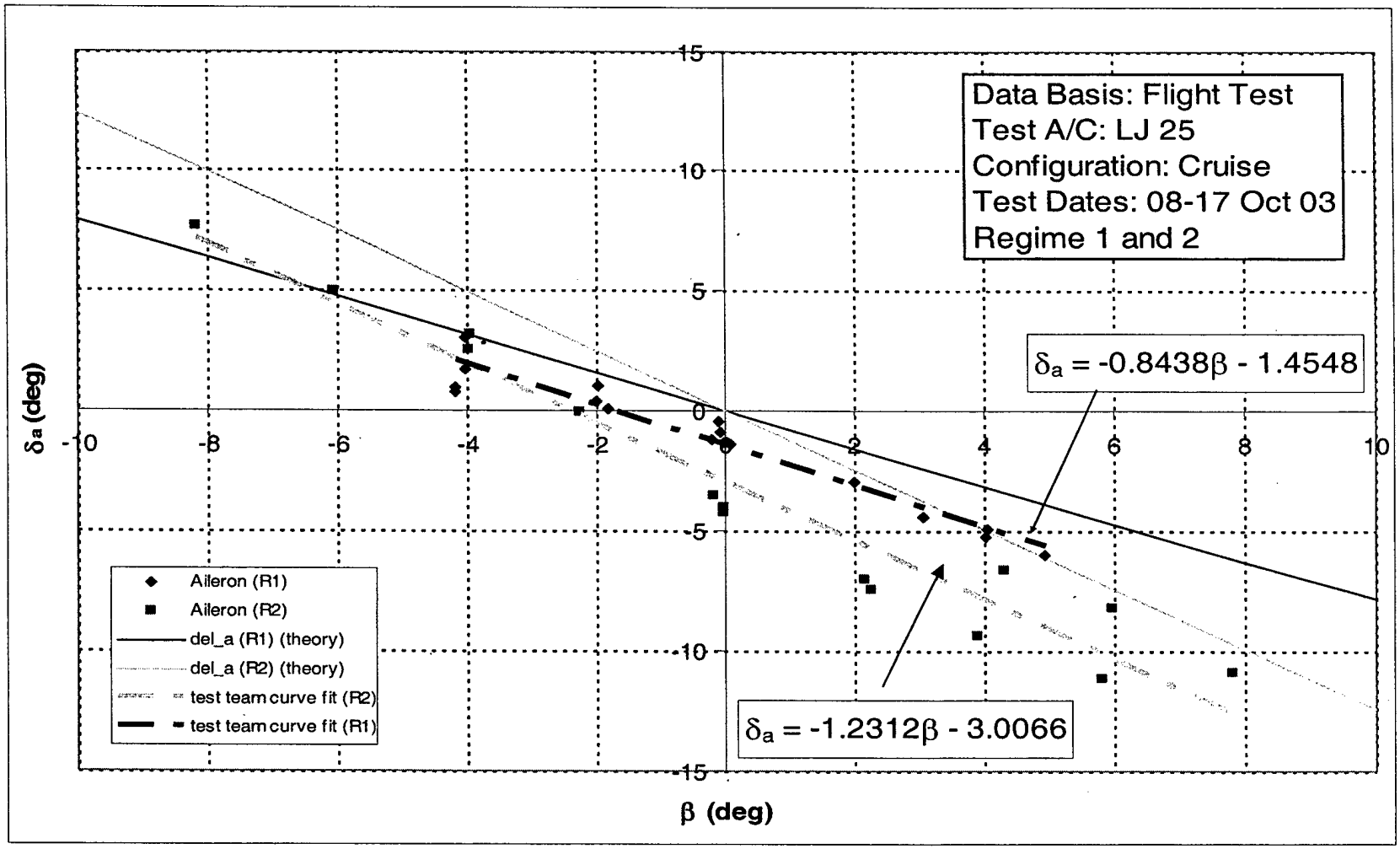

Figure D22: Learjet 25 Aileron Deflection Sideslip Angle Effect, Project HAVE TRIM

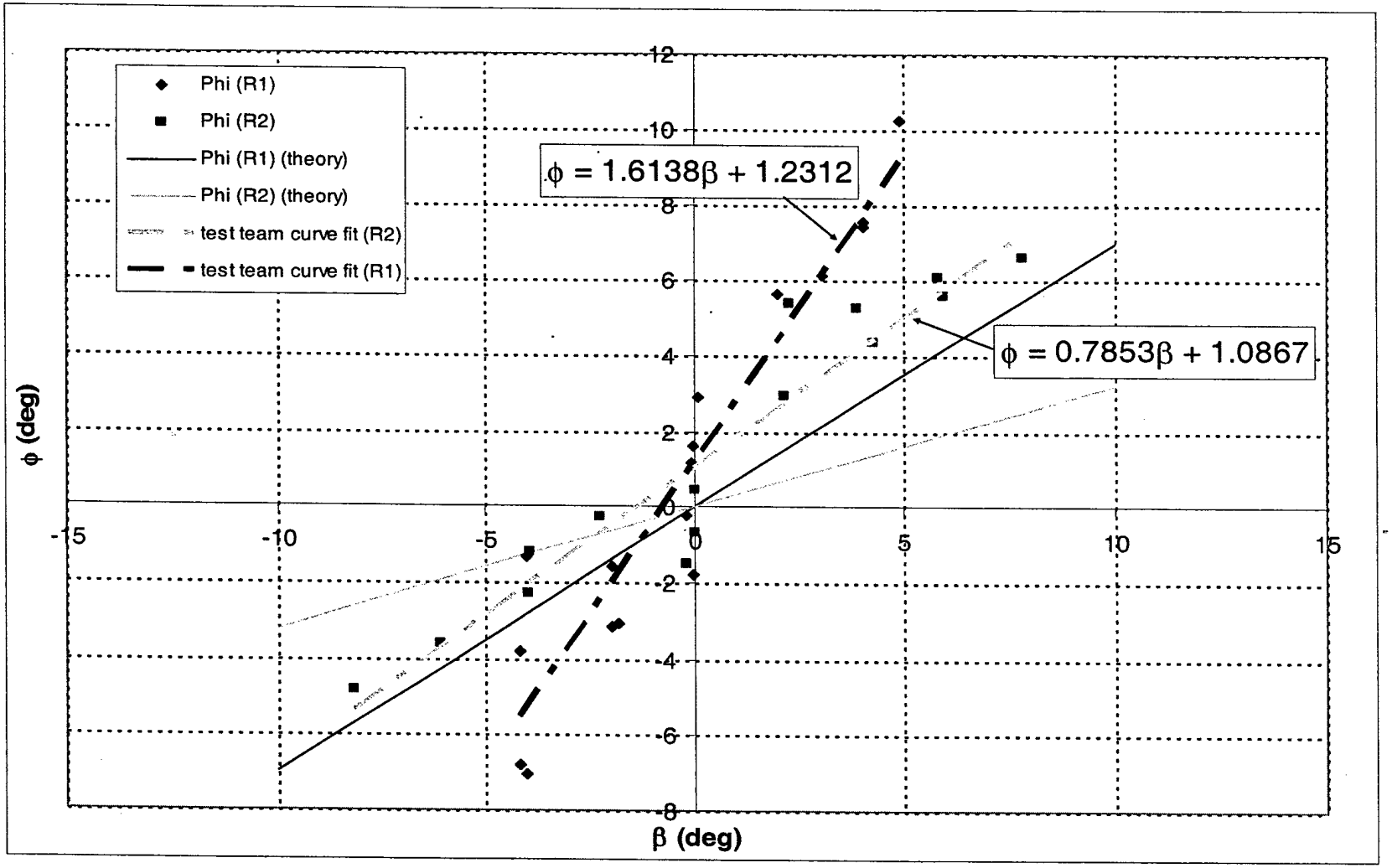

Figure D23: Learjet 25 Bank Angle Sideslip Effect, Project HAVE TRIM

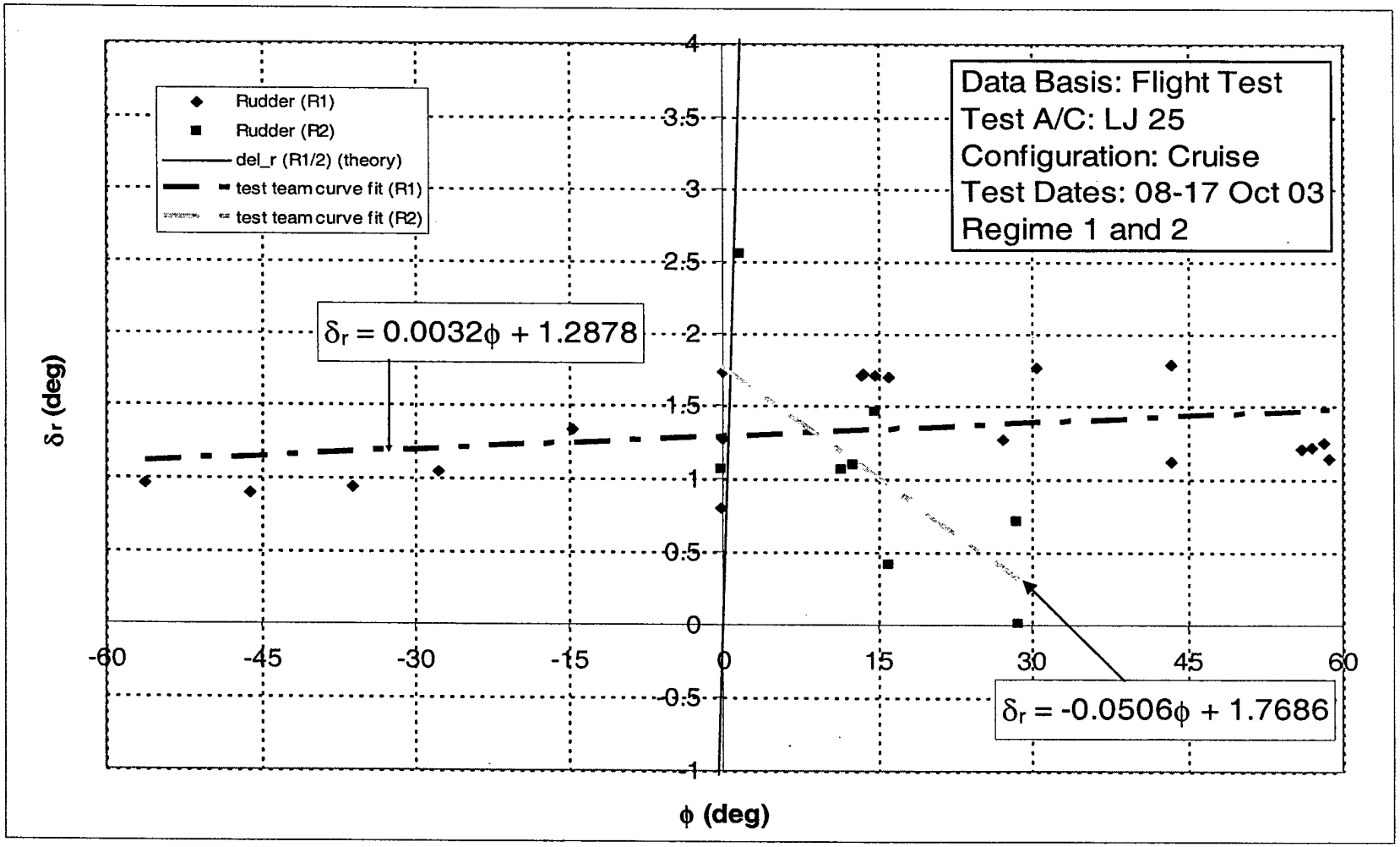

Figure D24: Learjet 25 Rudder Deflection Bank Angle Effect, Project HAVE TRIM

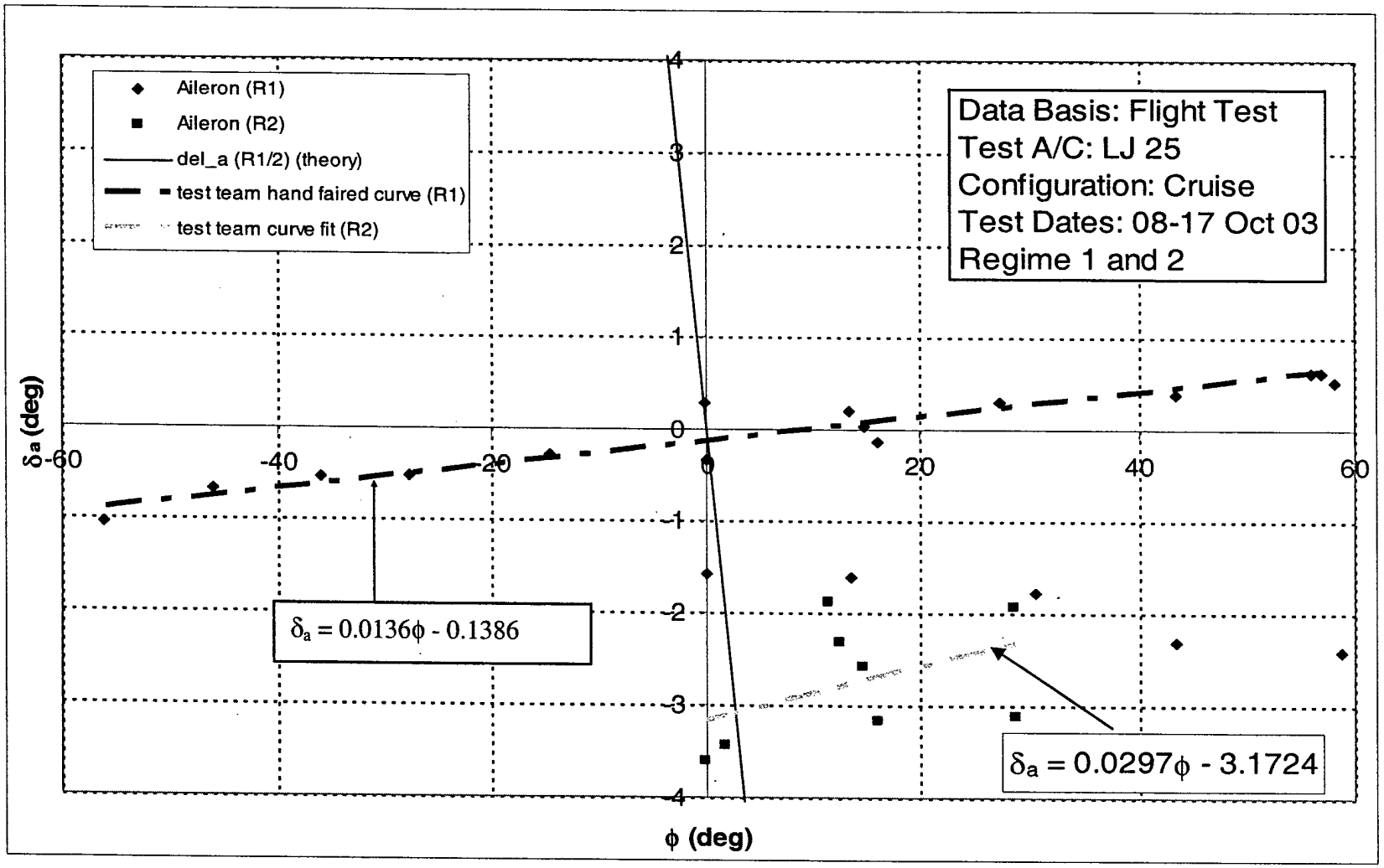

Figure D25: Learjet 25 Aileron Deflection Bank Angle Effect, Project HAVE TRIM

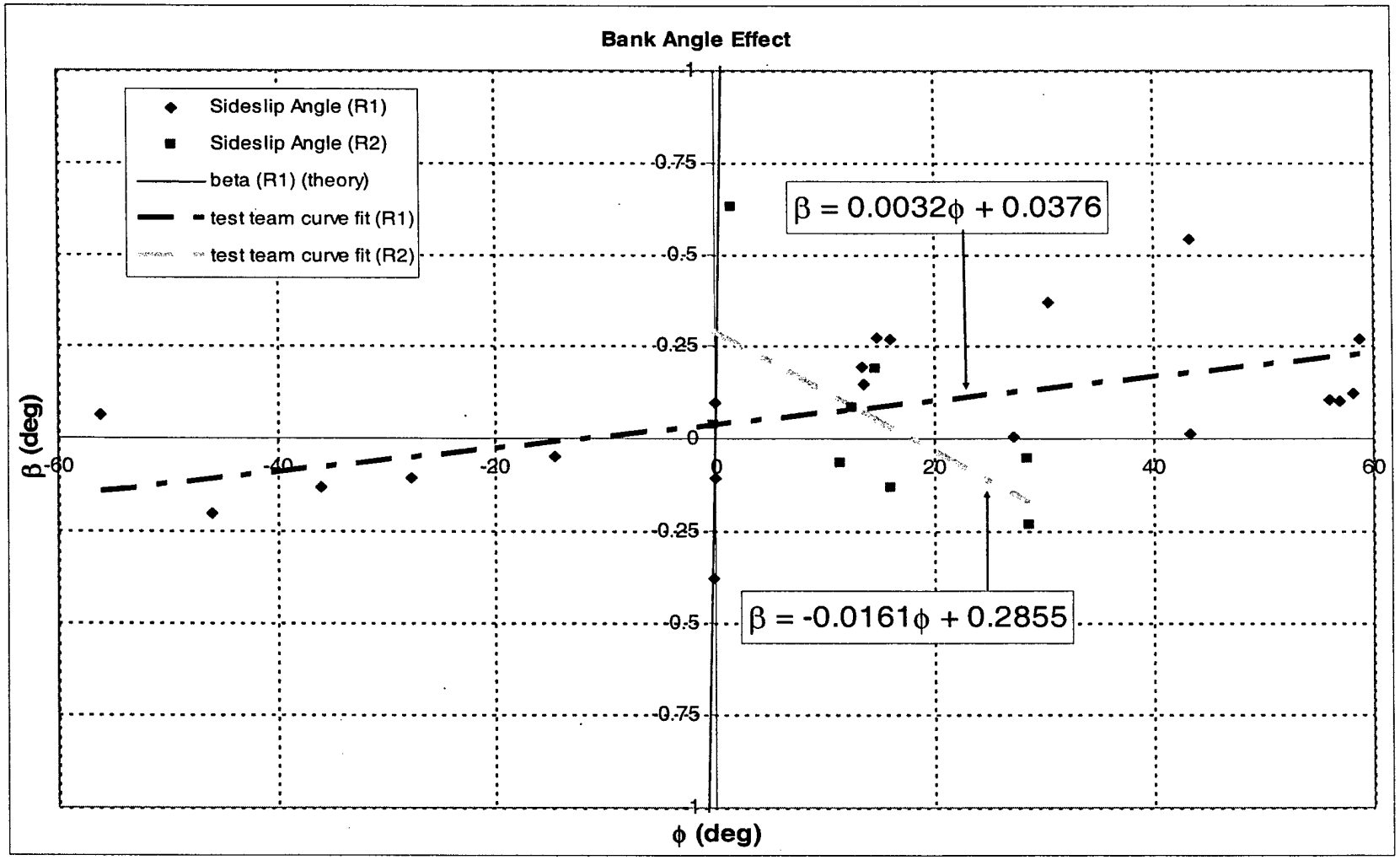

Figure D26: Learjet 25 Sideslip Bank Angle Effect, Project HAVE TRIM

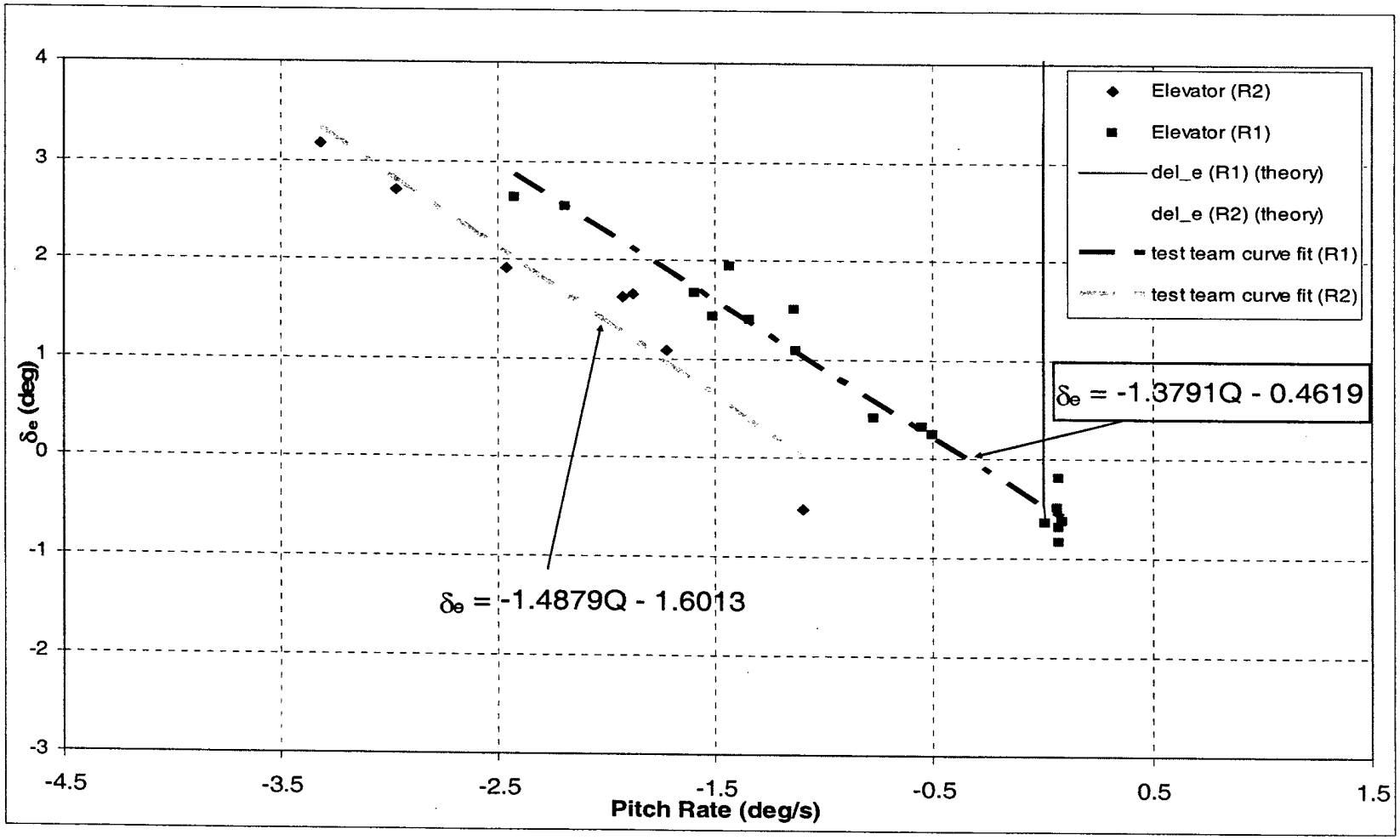

Figure D27: Learjet 25 Elevator Deflection Pitch Rate Effect, Project HAVE TRIM

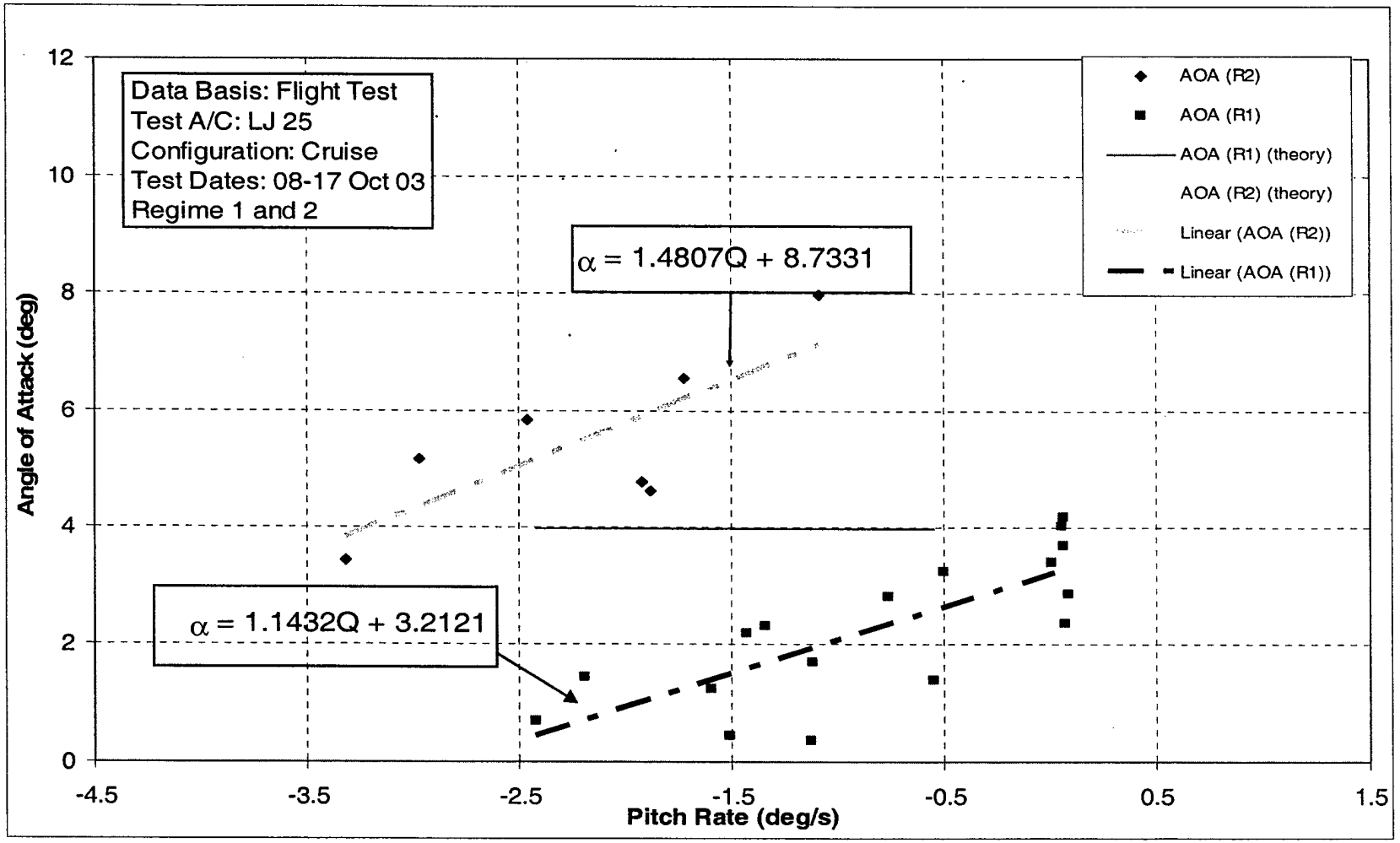

Figure D28: Learjet 25 Angle of Attack Pitch Rate Effect, Project HAVE TRIM

This page intentionally left blank.

APPENDIX E – SAMPLE MODEL PREDICTIONS

General

The model predictions were calculated for general test conditions to allow a comparison between flight test data and the model predictions. Small variations in the test point set-up caused significant impacts in the variation between flight test results and the model predicted values. All test cases used data that had as little noise as possible and flight test points with the smallest variations from the stable value. In Capt Miller's Master's thesis, individual test point conditions were investigated to determine the accuracy between the flight test data and the model using the actual flight test data. The point-by-point investigation determined the accuracy that the model can predict for the required control surface deflection. Example calculations are included below for comparison. At each test point, the calculated stability derivatives and the actual aircraft weight, altitude, airspeed, flight path angle, sideslip angle asymmetric thrust level and moments of inertia were input into the model. The model predictions for aircraft state (angle of attack, pitch angle, thrust settings, bank angle and angular rates) were calculated and then the control surface deflections were determined. The predictions were then compared to the flight test results.

Test Point 87 (Flight 10): The test point was at straight and level flight, flown at the center test position (15,000 feet, velocity 475 feet/second) with a reduced aircraft weight of 11,775 pounds. The predicted aircraft states were close to the expected measured flight test values. Angle of attack was predicted to be 3.900 degrees, which was 1.03 degrees greater than the flight test data. The predicted pitch angle was 4.002 degrees, which was 0.66 degrees higher than the measured value. The predicted bank angle was -0.016 degrees, 0.13 degrees higher than the measured flight test result. The thrust settings were both within a pound for both engines. The predicted angular rates were within 0.09 degrees per second for all three axes, with the yaw rate prediction exactly matching the flight test data. The elevator deflection prediction was -0.507 degrees, which was only 0.11 degrees greater than the flight test data and about equal to the measurement precision of 0.1 degree. The aileron deflection prediction (0.362 degrees) was within 0.03 degrees of the flight test value. The rudder deflection prediction was -0.383 degrees, which was 1.62 degrees higher than the flight test results. A 1.6 degree bias was observed in all straight and level test points for Flight 10, therefore the bias was probably caused by an asymmetrically trimmed rudder.

Test Point 60 (Flight 10): The test point was at a trim condition for the bank angle investigation, and was flown at the center test position (15,000 feet, 475 feet per second at 12,377 pounds) and with zero bank angle. Again the predicted aircraft states closely matched the flight test data. The predicted angle of attack was 4.04 degrees, which was 0.51 degrees below the flight test value. The predicted pitch angle was 3.959 degrees, which was 0.38 degrees higher than the measured results. The model bank angle was -0.248 degrees, which was within +0.14 degrees of the flight test data. The predicted flight test thrust was slightly less than the measured values, with just over 10 pounds more thrust on each engine. As in the previous case, the angular rates were within 0.07 degrees per second for all three axes, with the raw rate prediction exactly matching the

flight test data. The elevator deflection prediction was -0.658 degrees, only 0.17 degrees lower than the measured flight test results. The aileron deflection prediction of 0.618 degrees was 0.34 degrees higher than the flight test value. Finally the rudder deflection prediction was -0.887 degrees, which was 1.69 degrees lower than the flight test results. The bias was nearly equal to the bias in Test Point 87 of Flight 10.

Test Point 27 (Flight 10): The test point corresponds to a 10% asymmetric thrust point at the center test position. The point was a lateral-directional test point that incorporated more maneuvering flight than the straight and level stable condition. The aircraft state results matched closely, while the control surface deflections were invalid. The predicted angle of attack was 4.397 degrees, 0.46 degrees lower than the flight test data. The predicted pitch angle was 4.585 degrees, which was 0.81 degrees above the measured value. The model bank angle (3.552 degrees), differed significantly (+2.21 degrees) from the flight test results. The predicted thrust was slightly higher than the measured values (about 40 pounds on the left engine and 15 pounds on the right engine). Also in this case, the aircraft had larger angular accelerations (the largest was 0.275 degrees per second for yaw rate), but the errors were still under 0.09 degrees per second with a nearly perfect match in yaw rate. The control surface deflection predictions all exceeded the maximum deflection limits and were therefore invalid. Test Point 27 was one of the worst case scenarios, and will be investigated to attempt to determine the source of the error.

APPENDIX F – PLOTS SUPPORTING DETERMINATION OF TEST AIRCRAFT STABILITY DERIVATIVES

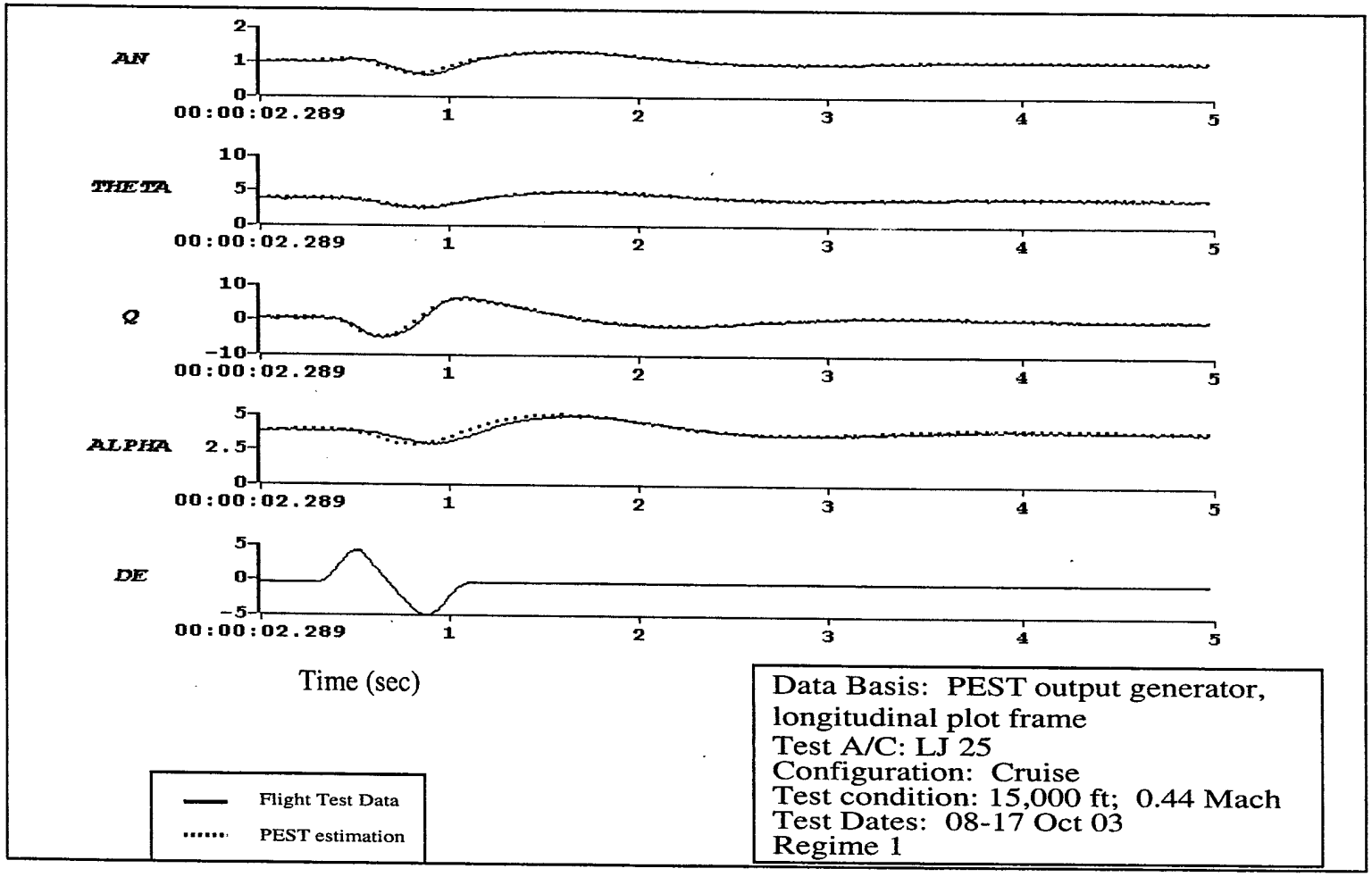

Figure F1: Longitudinal Time History Comparison, Project HAVE TRIM

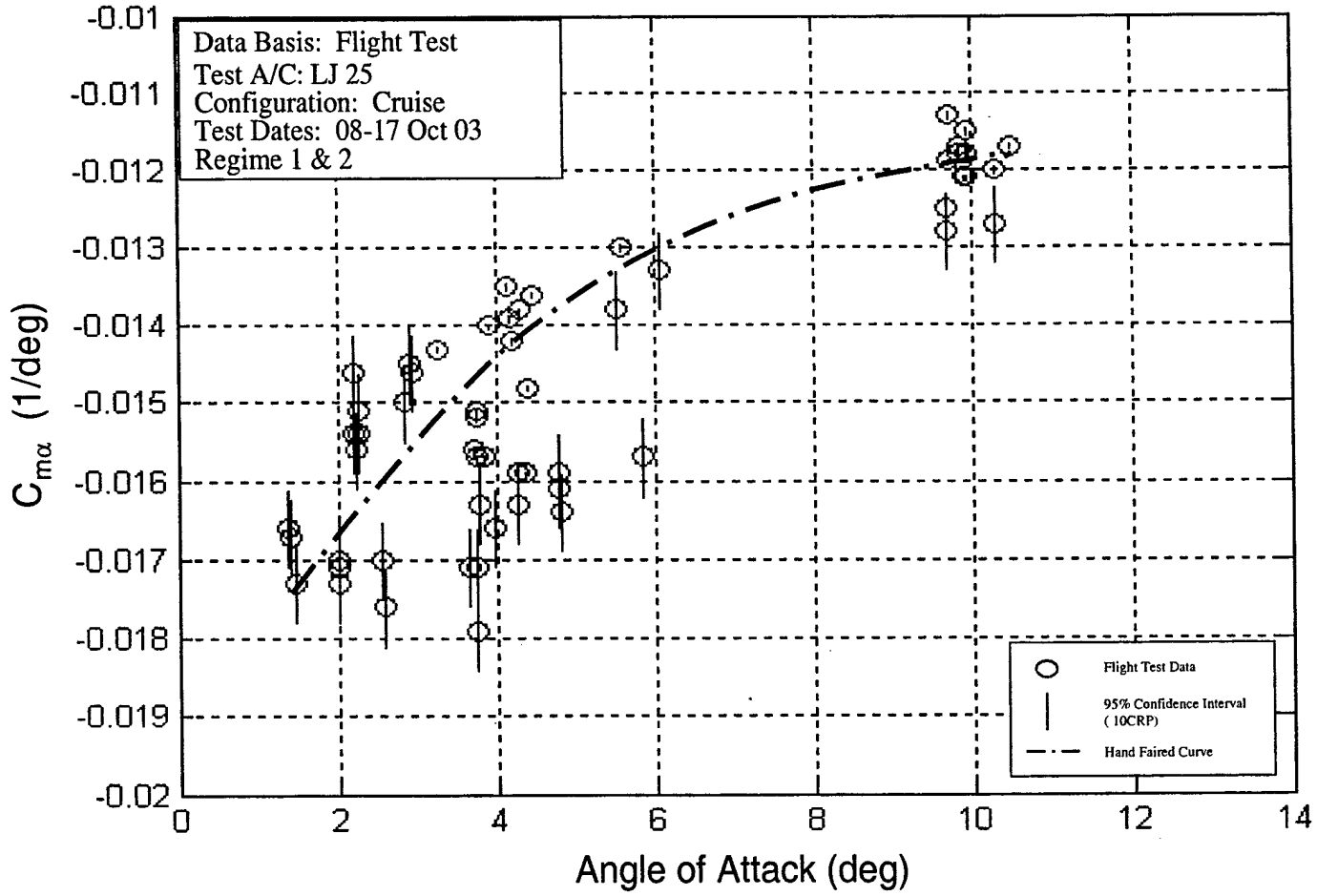

Figure F2: Learjet 25 $C_{m\alpha}$ vs α, Project HAVE TRIM

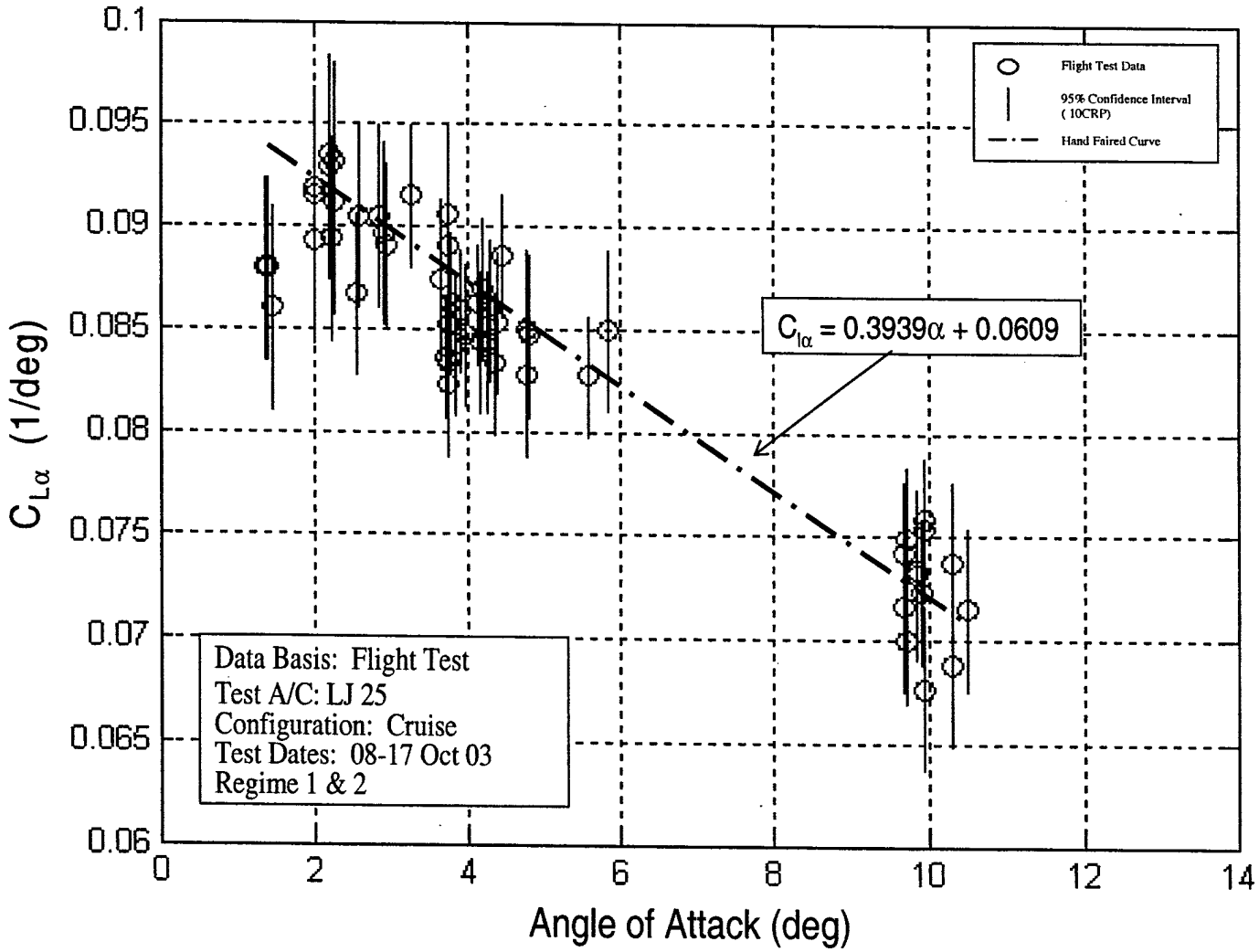

Figure F3: Learjet 25 $C_{L\alpha}$ vs α, Project HAVE TRIM

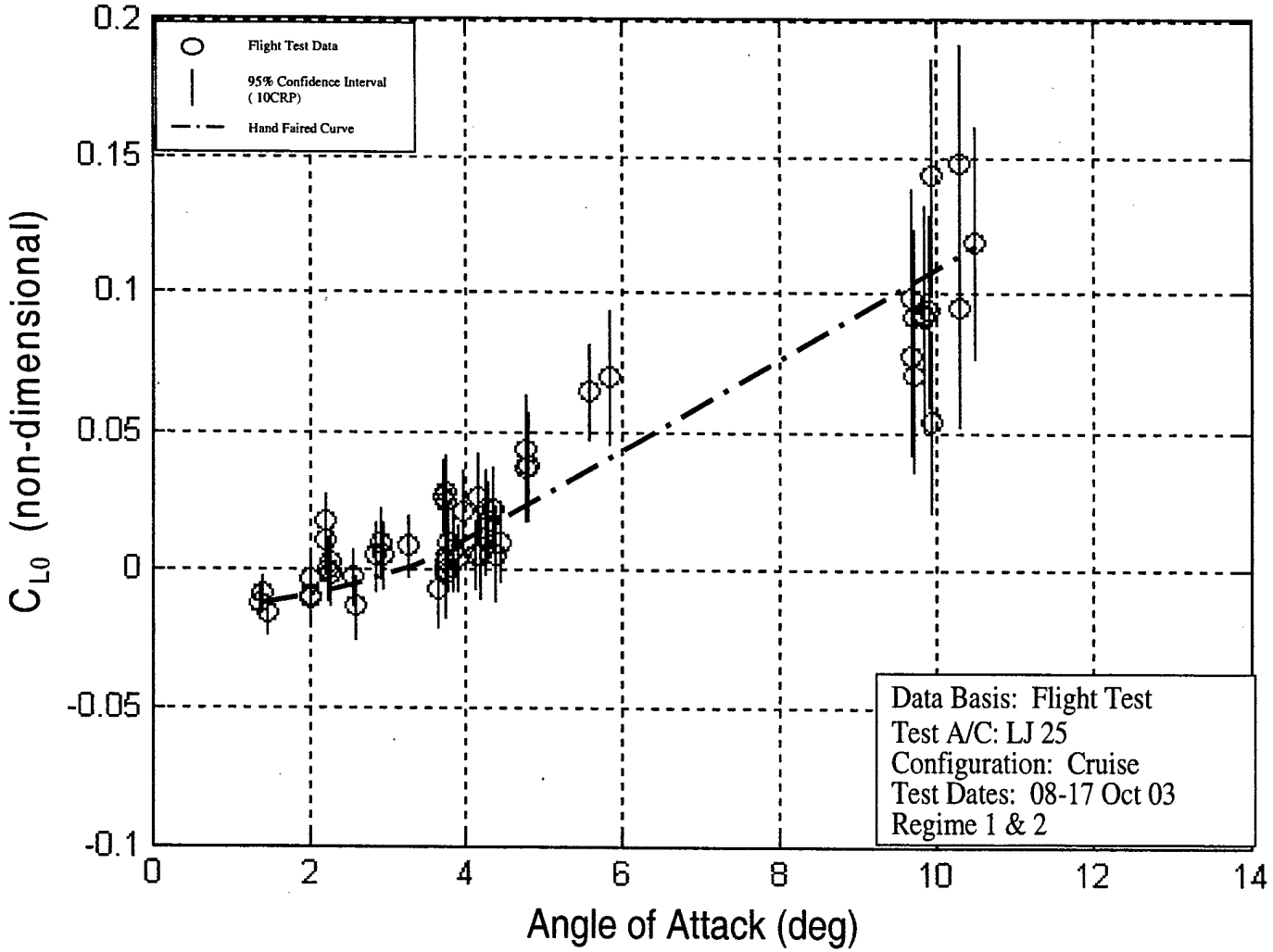

Figure F4: Learjet 25 C_{L0} vs α, Project HAVE TRIM

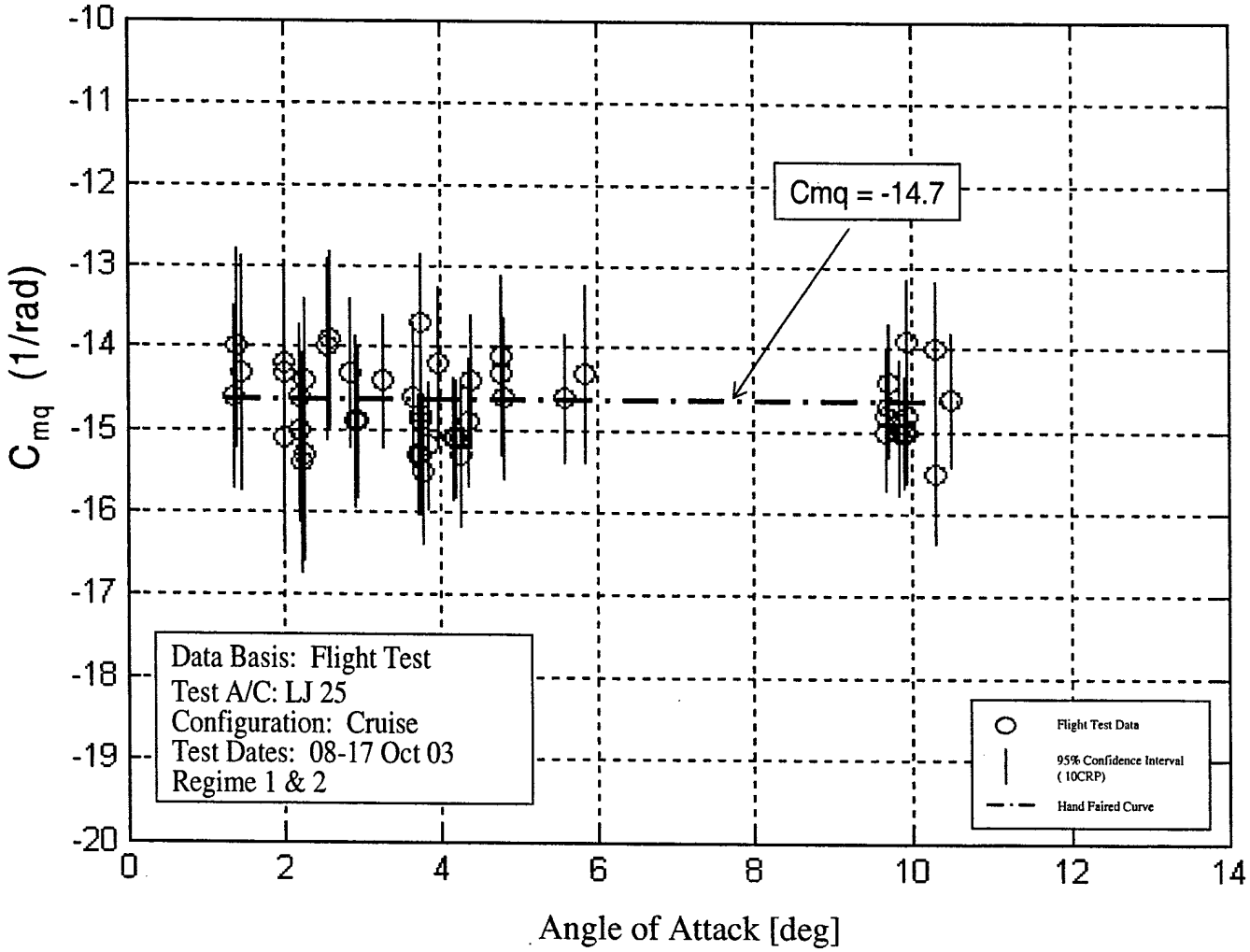

Figure F5: Learjet 25 C_{mq} vs α, Project HAVE TRIM

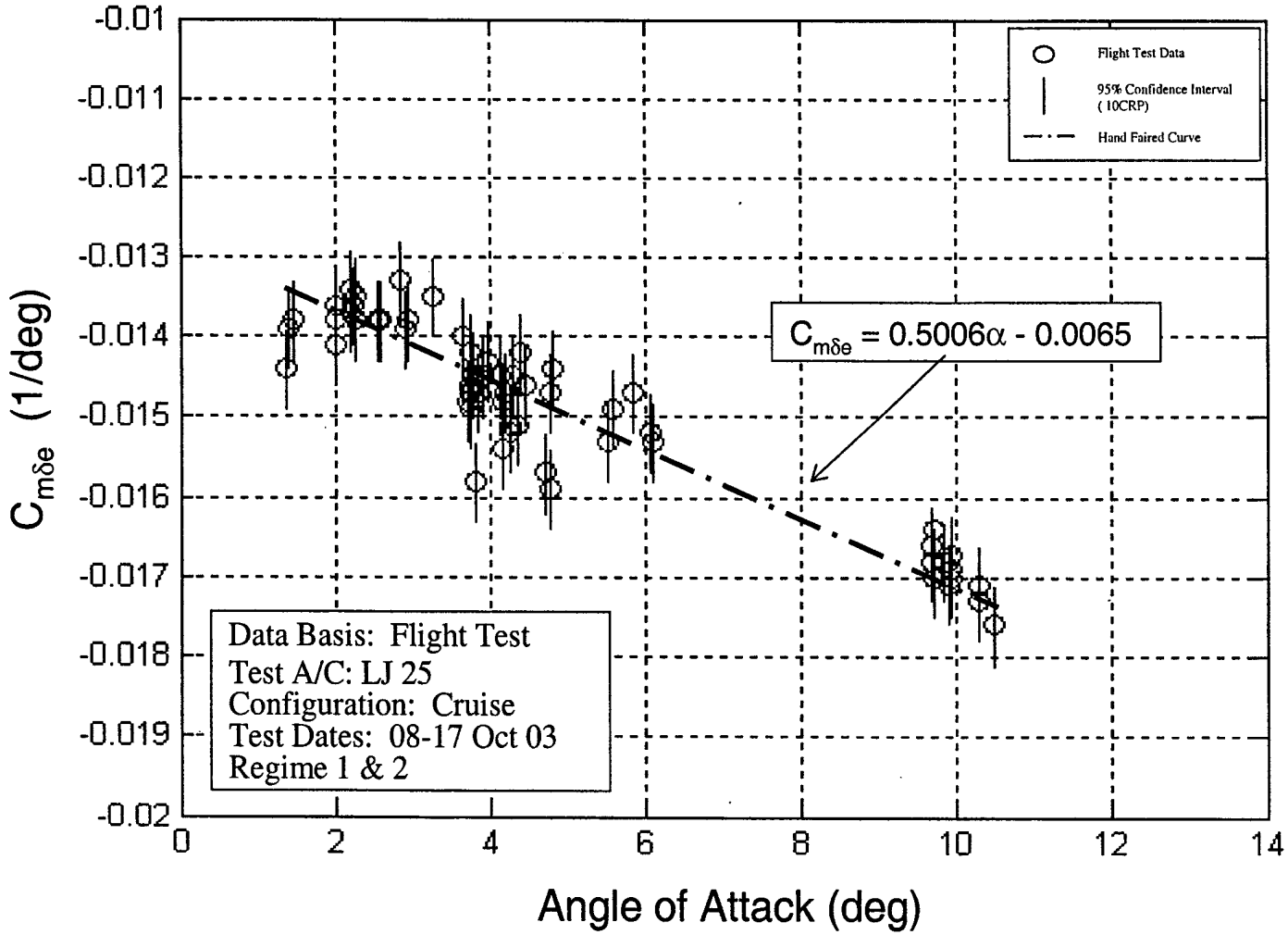

Figure F6: Learjet 25 $C_{m\delta e}$ vs α, Project HAVE TRIM

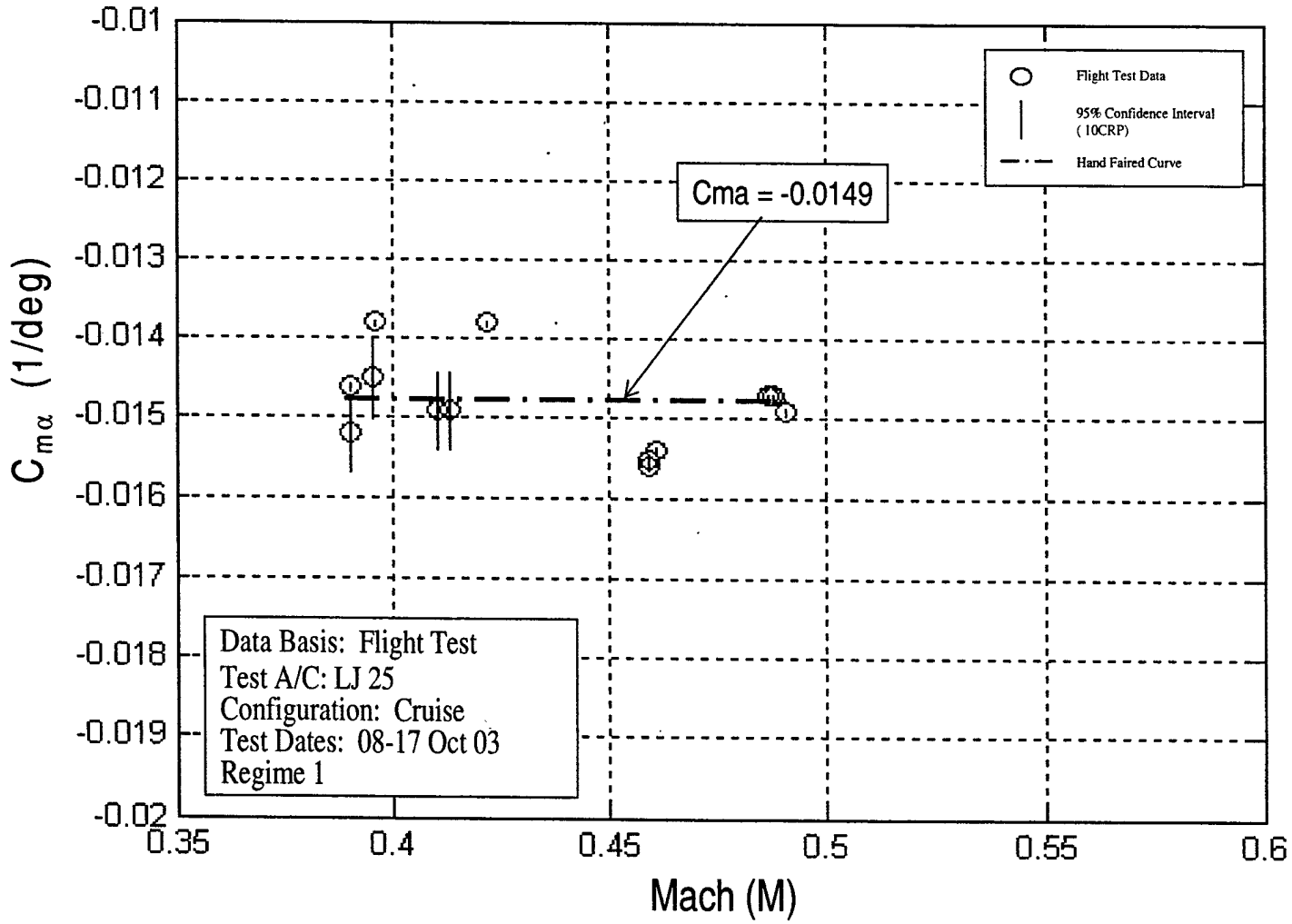

Figure F7: Learjet 25 $C_{m\alpha}$ vs Mach Regime 1, Project HAVE TRIM

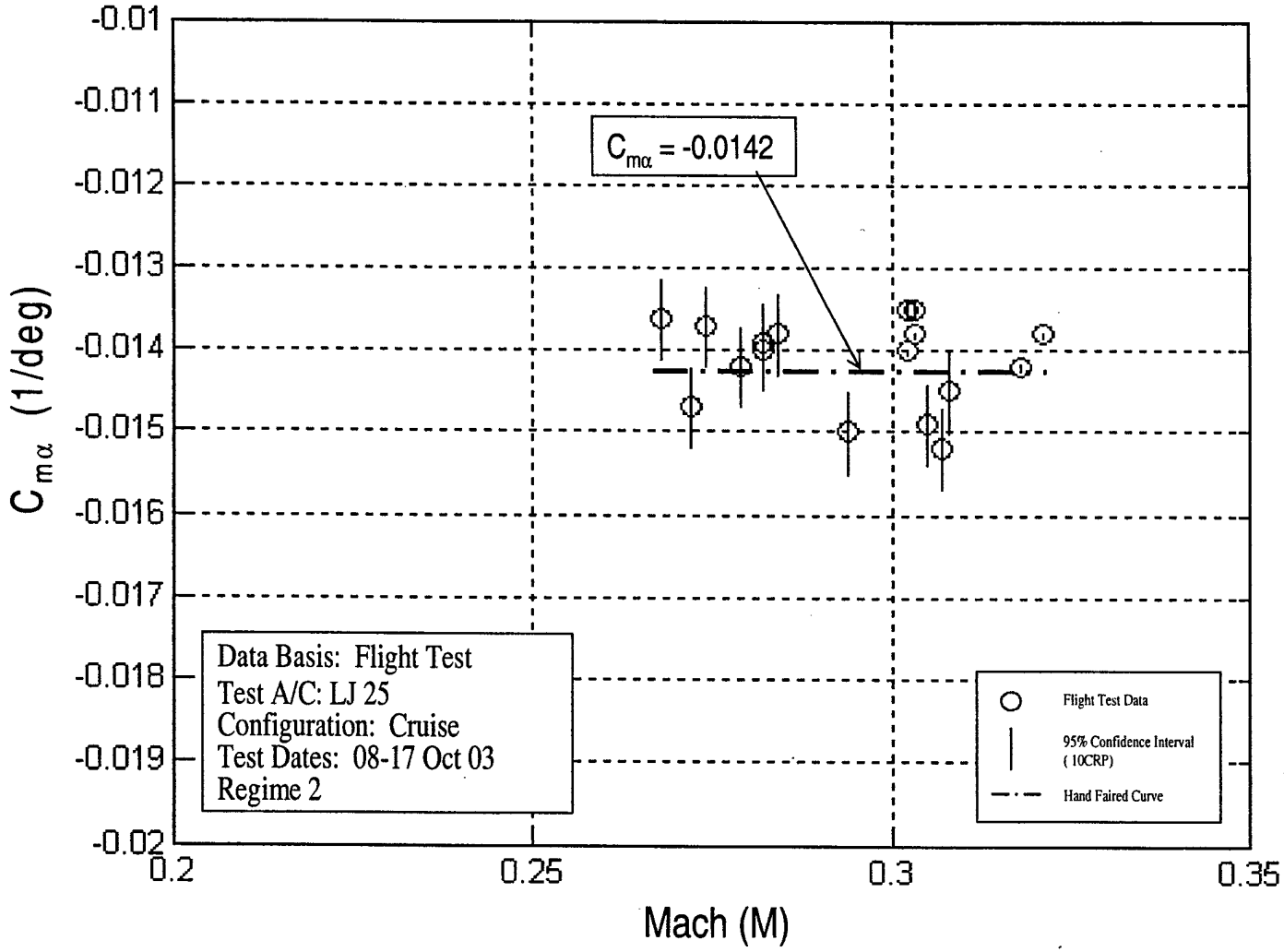

Figure F8: Learjet 25 $C_{m\alpha}$ vs Mach Regime 2, Project HAVE TRIM

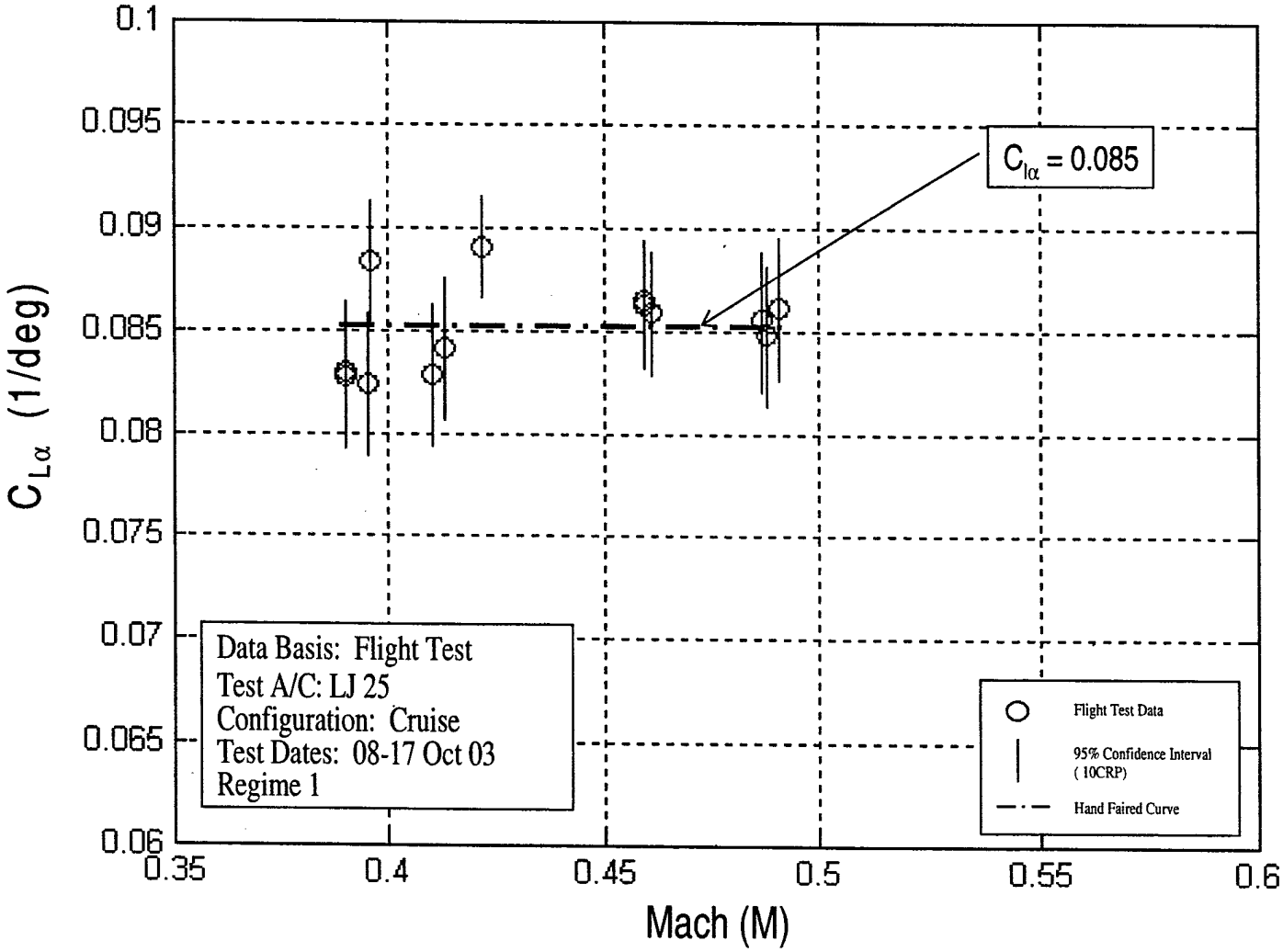

Figure F9: Learjet 25 $C_{L\alpha}$ vs Mach Regime 1, Project HAVE TRIM

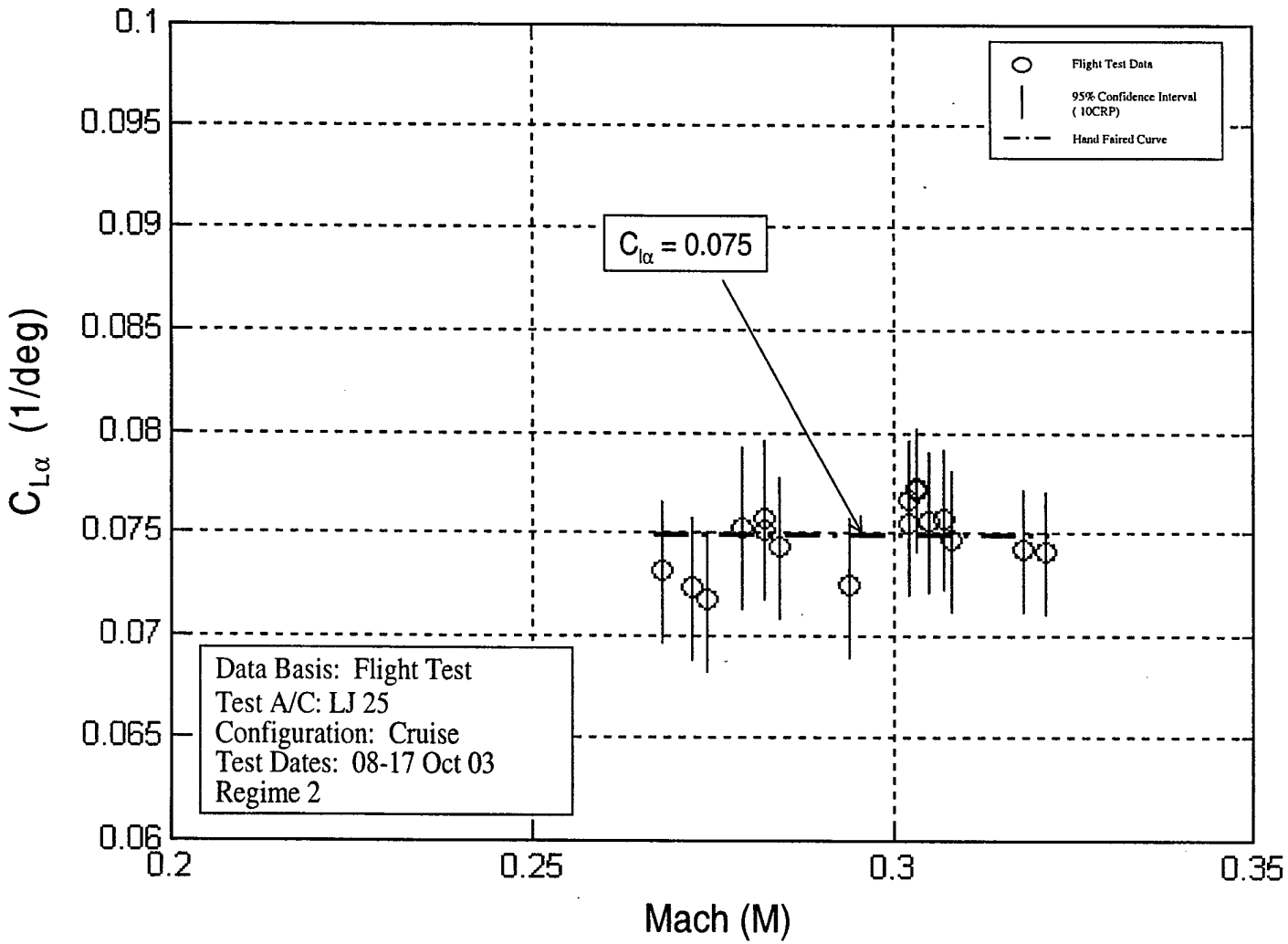

Figure F10: Learjet 25 $C_{L\alpha}$ vs Mach Regime 2, Project HAVE TRIM

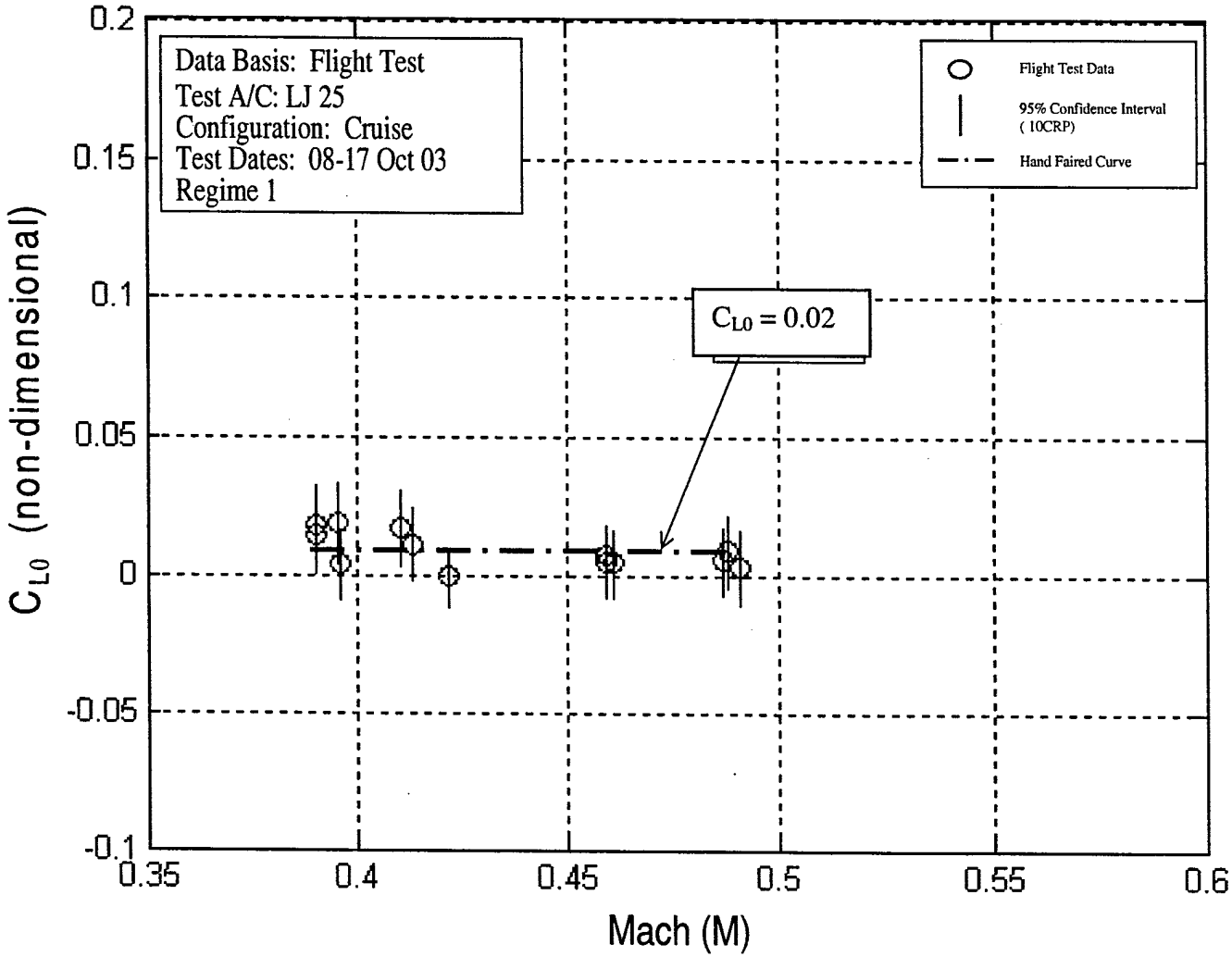

Figure F11: Learjet 25 C_{L0} vs Mach Regime 1, Project HAVE TRIM

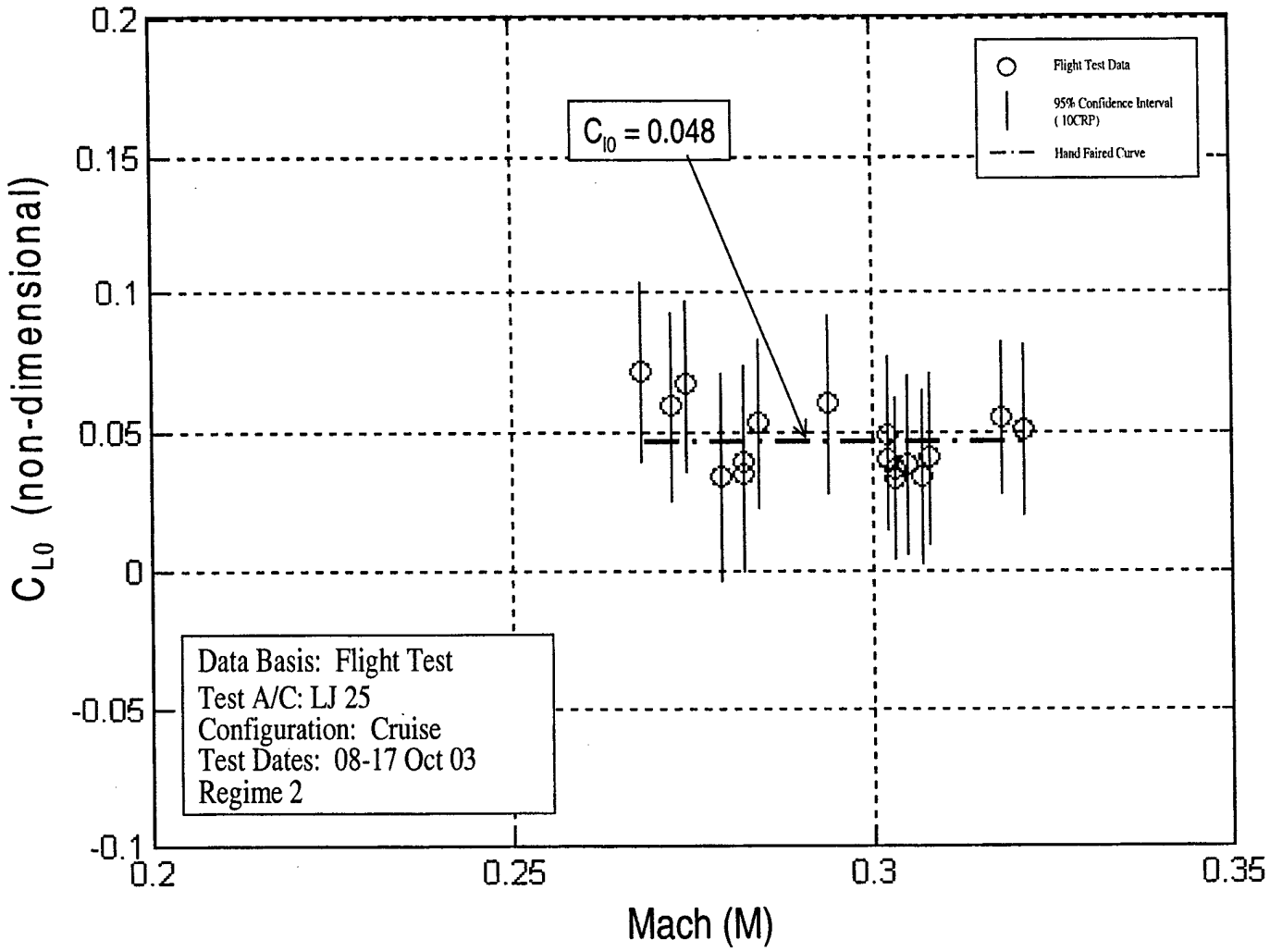

Figure F12: Learjet 25 C_{L0} vs Mach Regime 2, Project HAVE TRIM

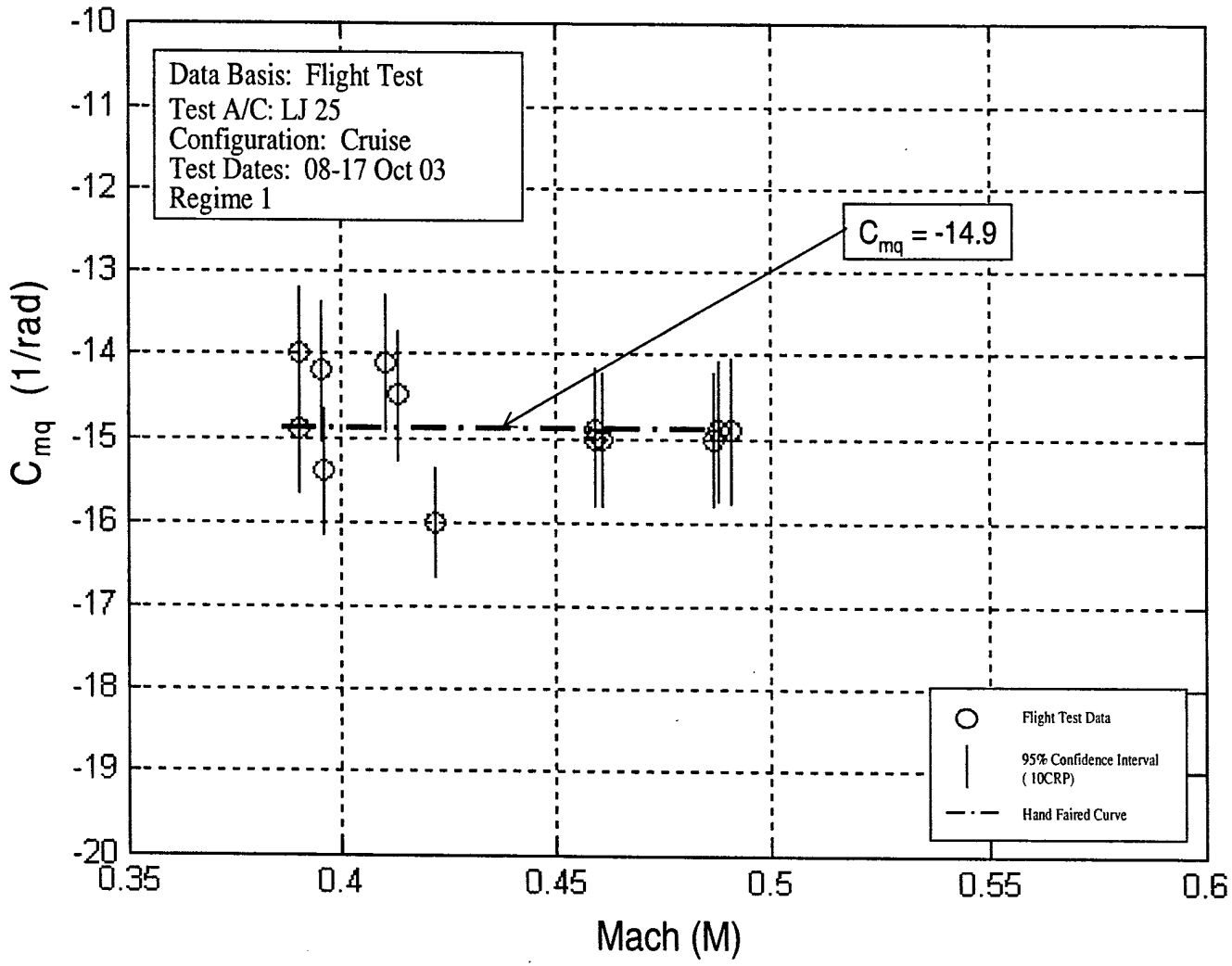

Figure F13: Learjet 25 C_{mq} vs Mach Regime 1, Project HAVE TRIM

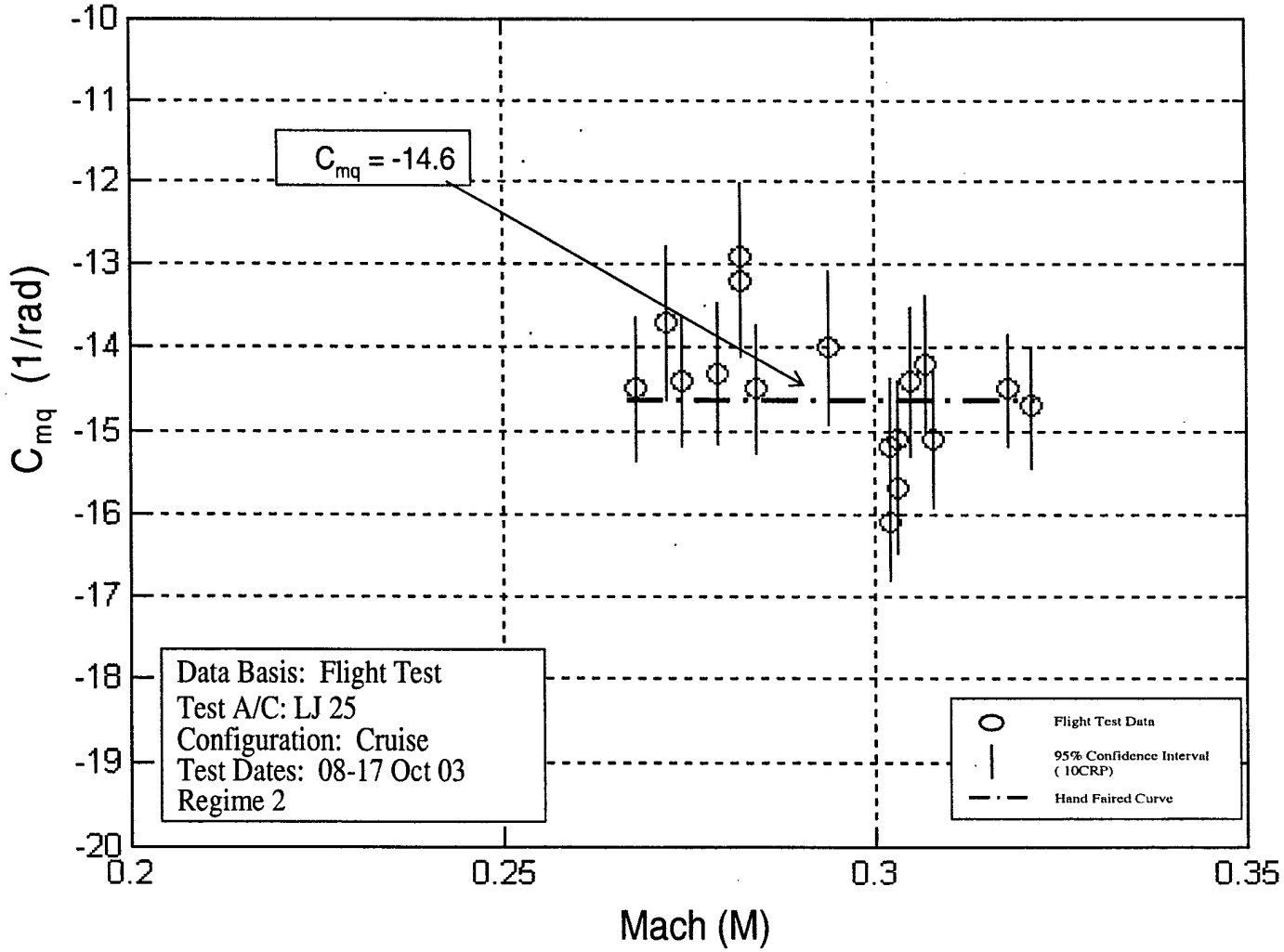

Figure F14: Learjet 25 C_{mq} vs Mach Regime 2, Project HAVE TRIM

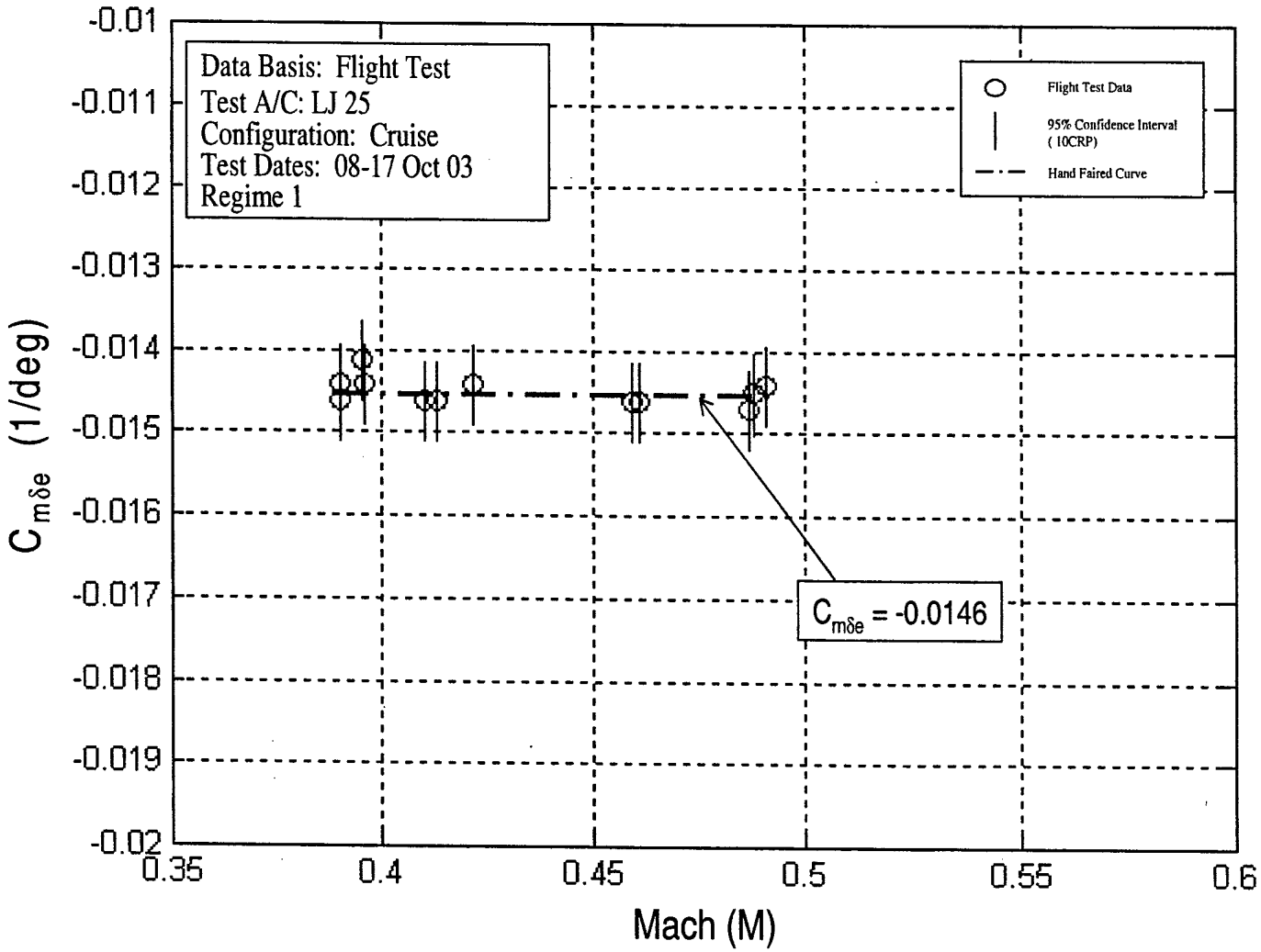

Figure F15: Learjet 25 $C_{m\delta e}$ vs Mach Regime 1, Project HAVE TRIM

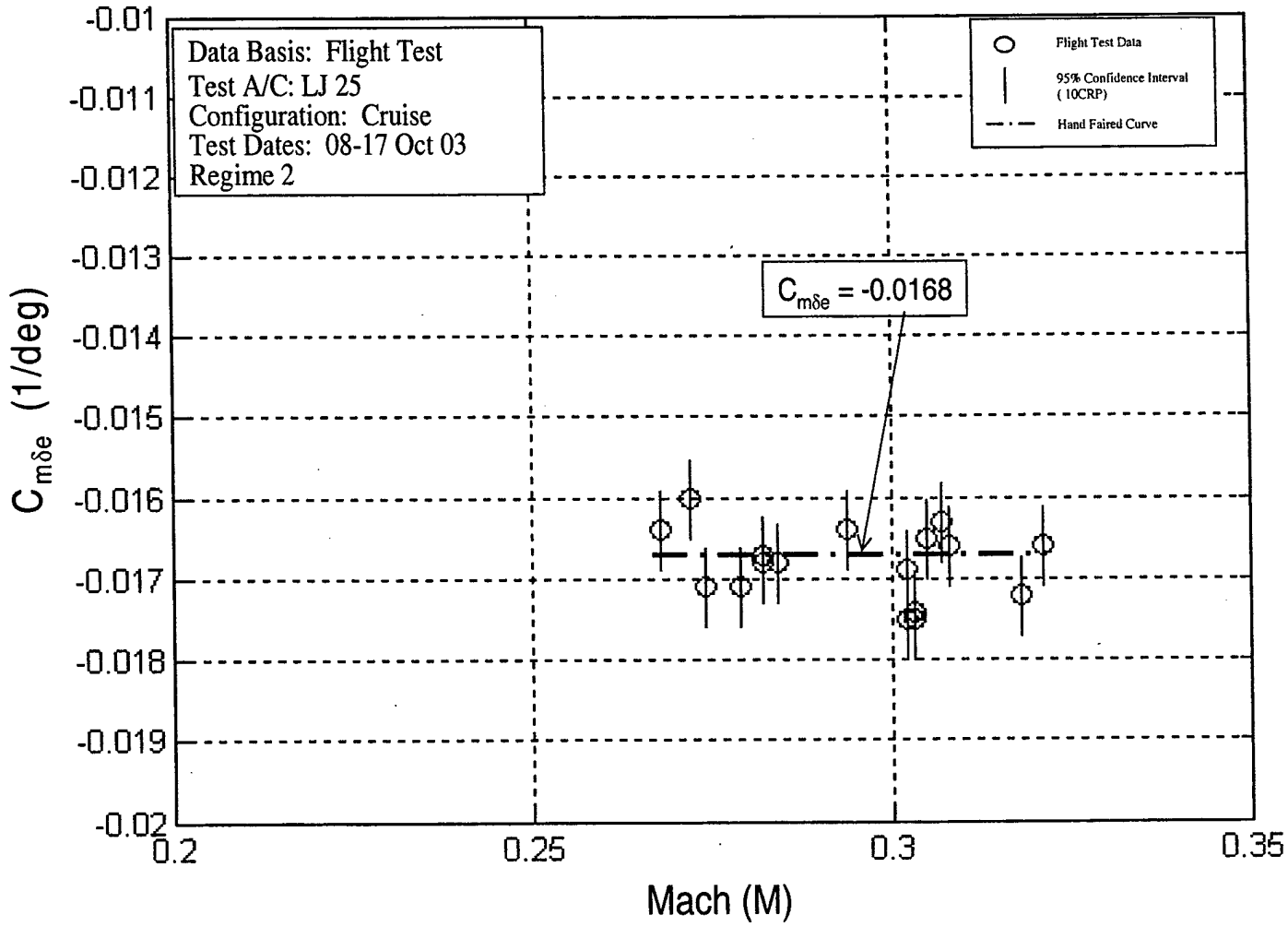

Figure F16: Learjet 25 $C_{m\delta e}$ vs Mach Regime 2, Project HAVE TRIM

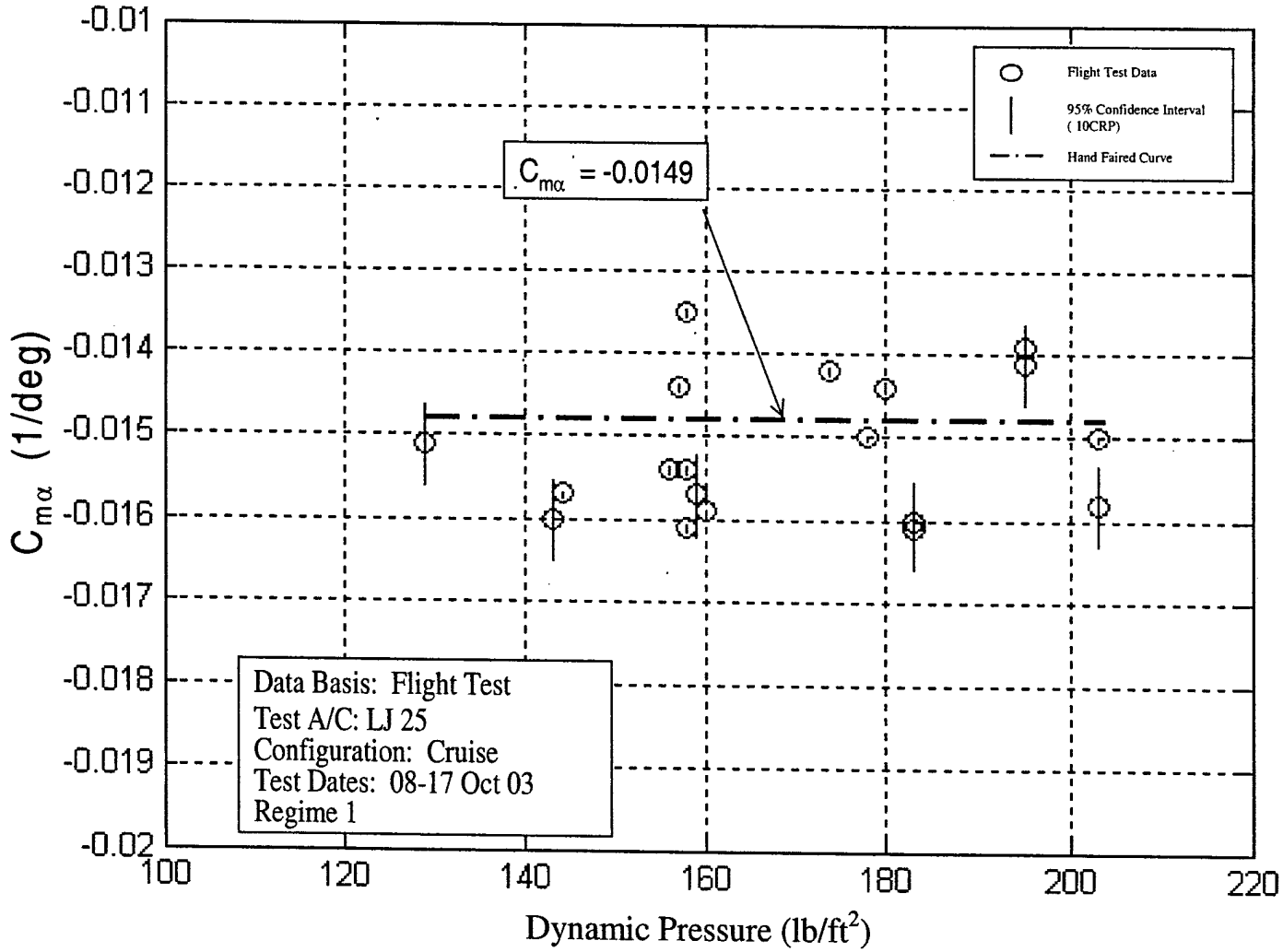

Figure F17: Learjet 25 $C_{m\alpha}$ vs q Regime 1, Project HAVE TRIM

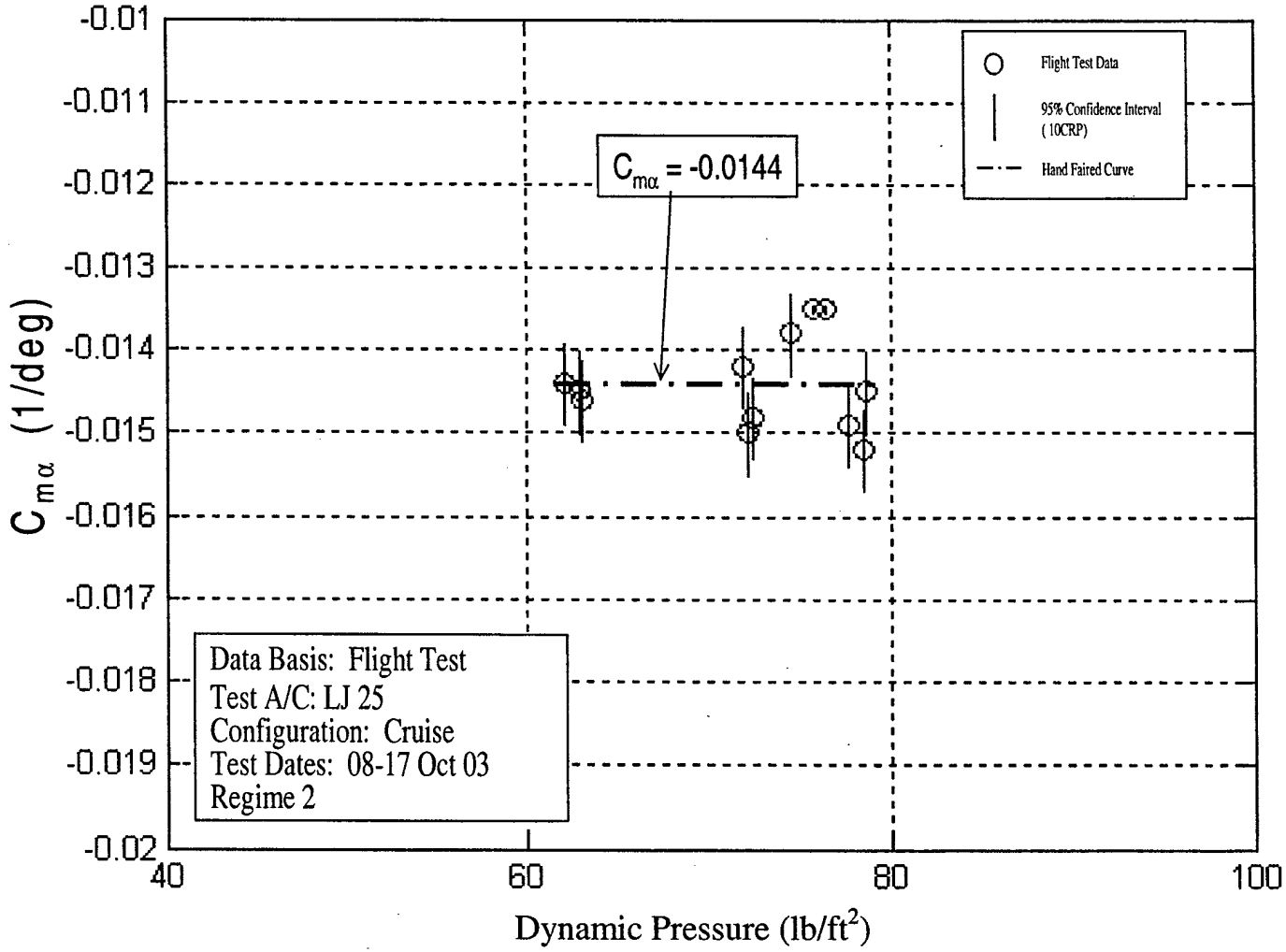

Figure F18: Learjet 25 $C_{m\alpha}$ vs q Regime 2, Project HAVE TRIM

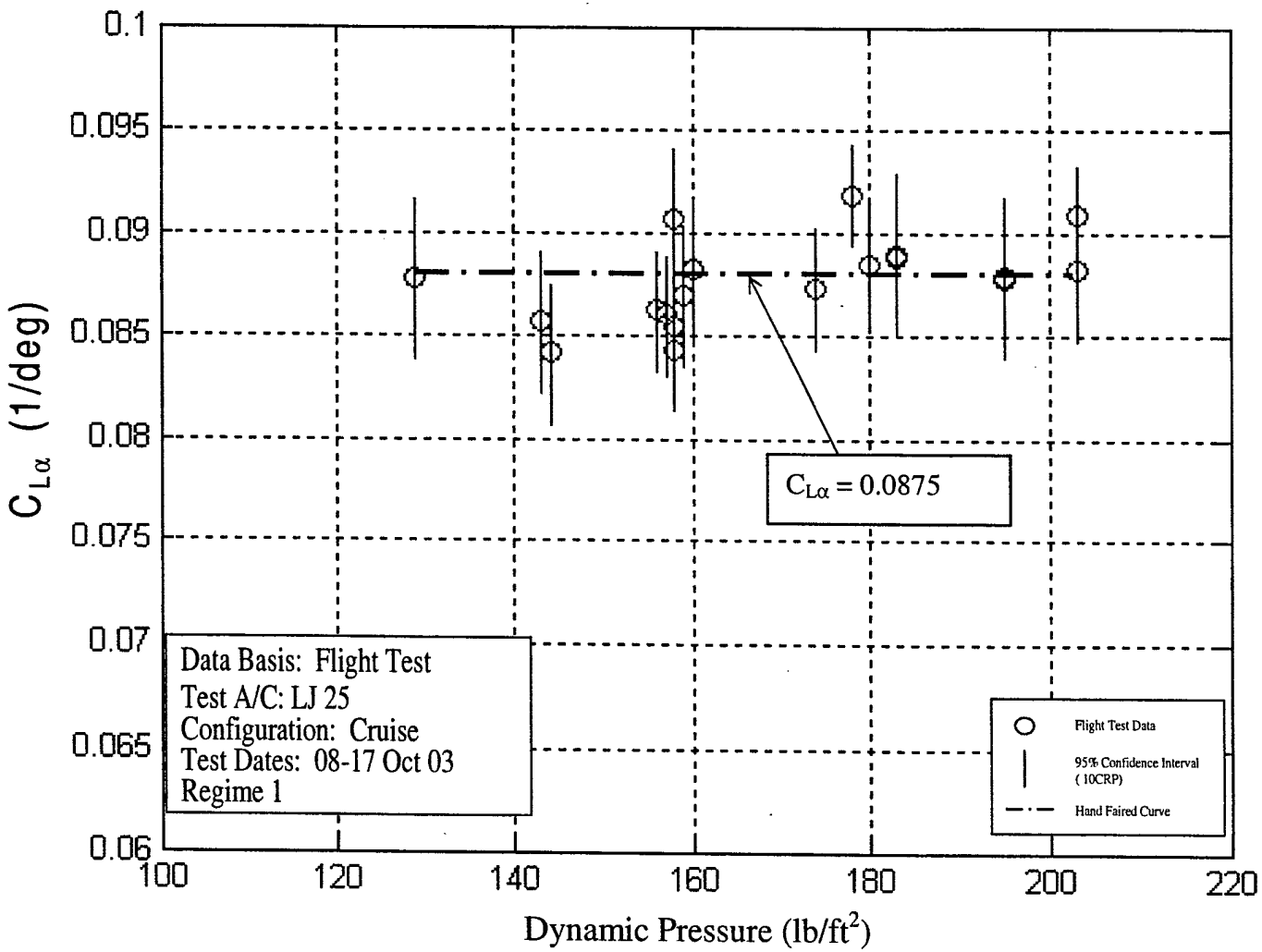

Figure F19: Learjet 25 $C_{L\alpha}$ vs q Regime 1, Project HAVE TRIM

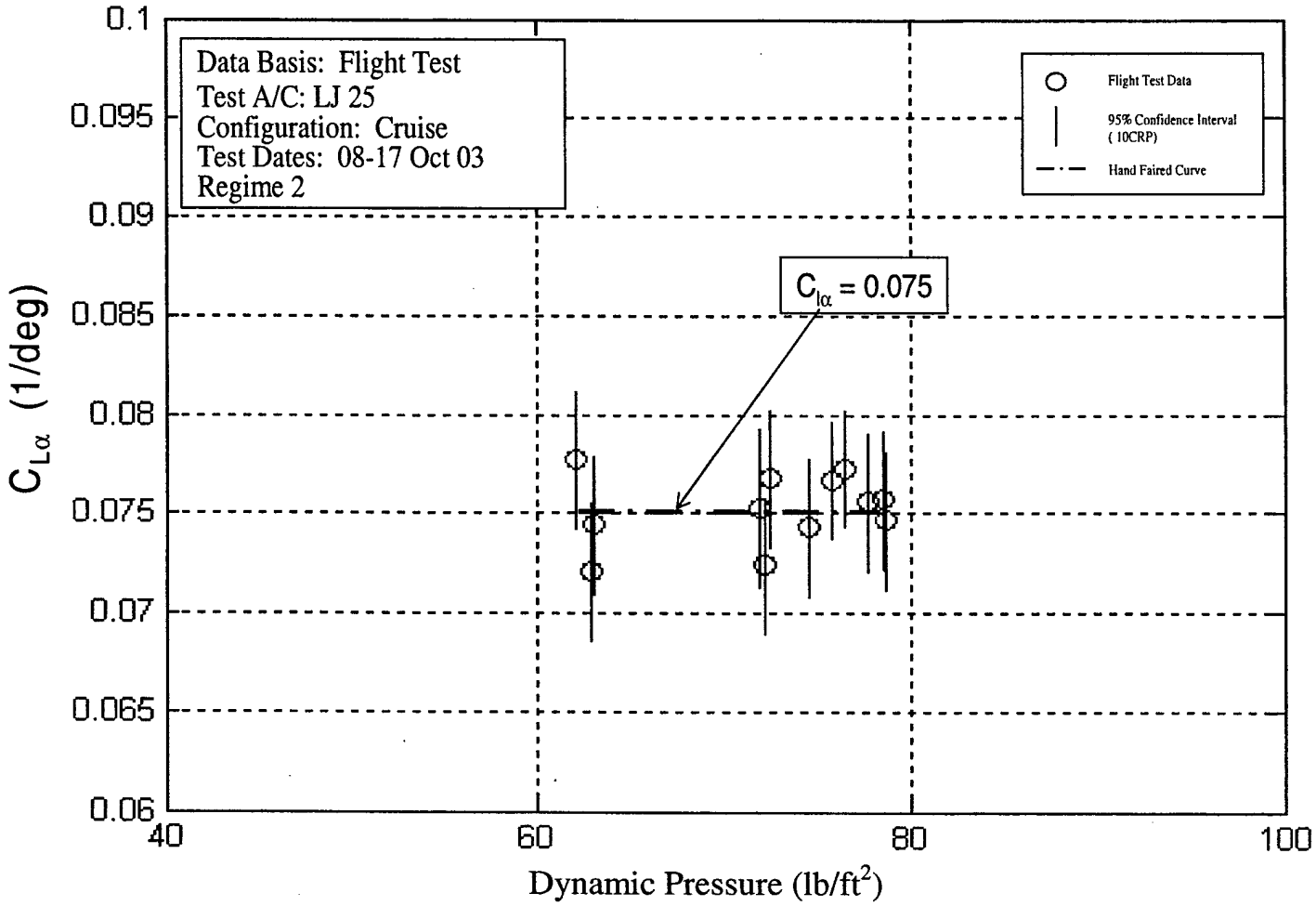

Figure F20: Learjet 25 $C_{L\alpha}$ vs q Regime 2, Project HAVE TRIM

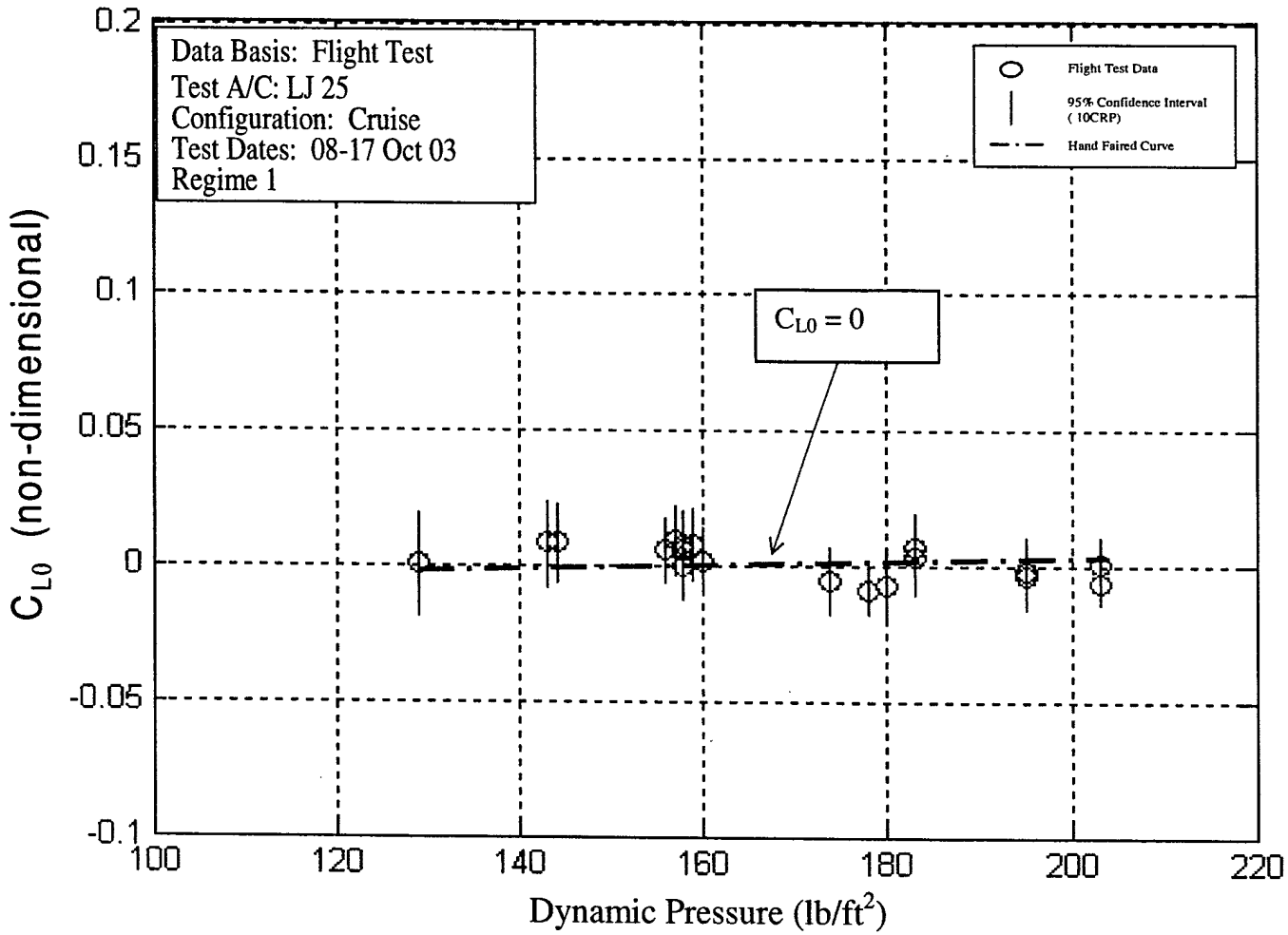

Figure F21: Learjet 25 C_{L0} vs q Regime 1, Project HAVE TRIM

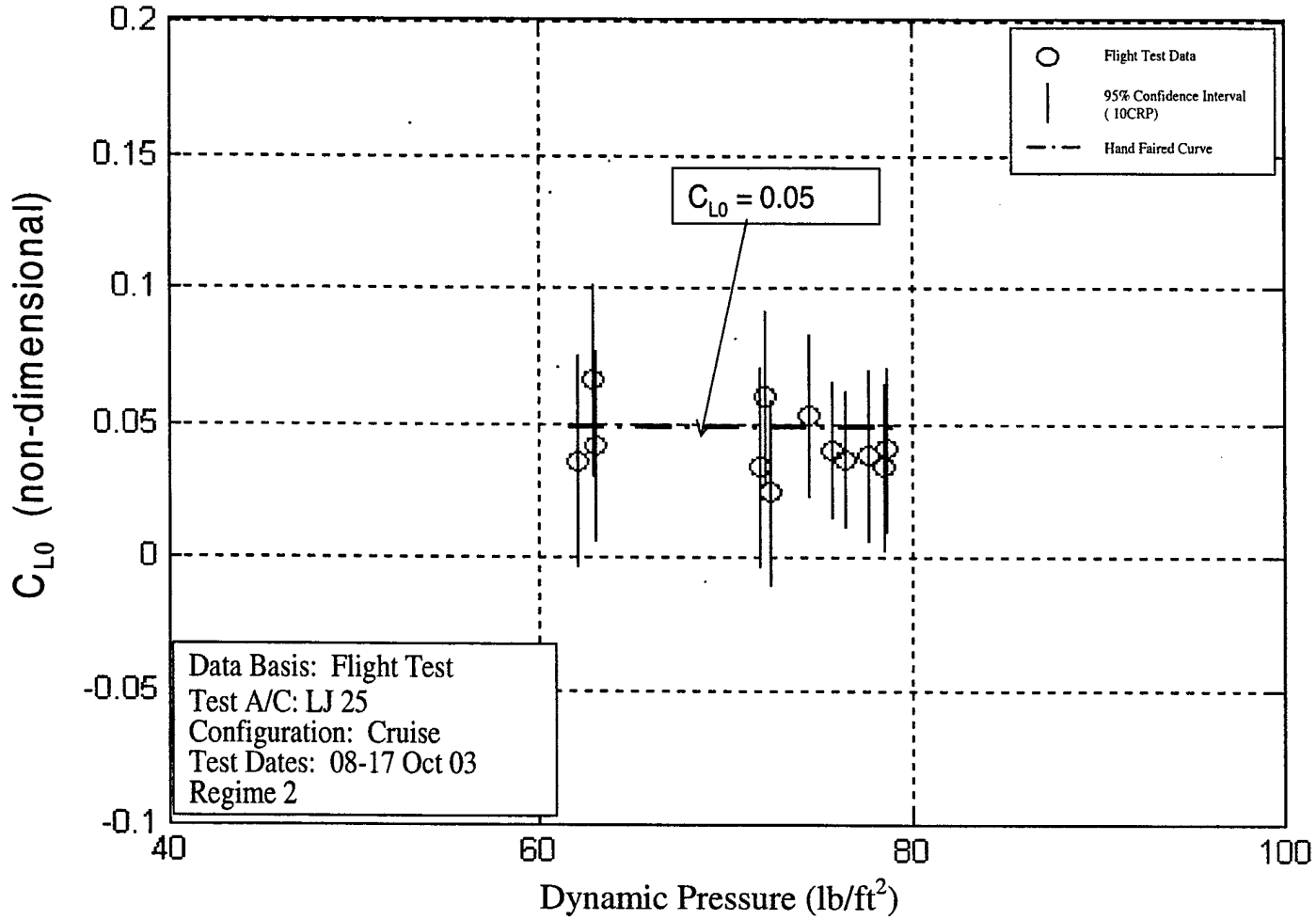

Figure F22: Learjet 25 C_{L0} vs q Regime 2, Project HAVE TRIM

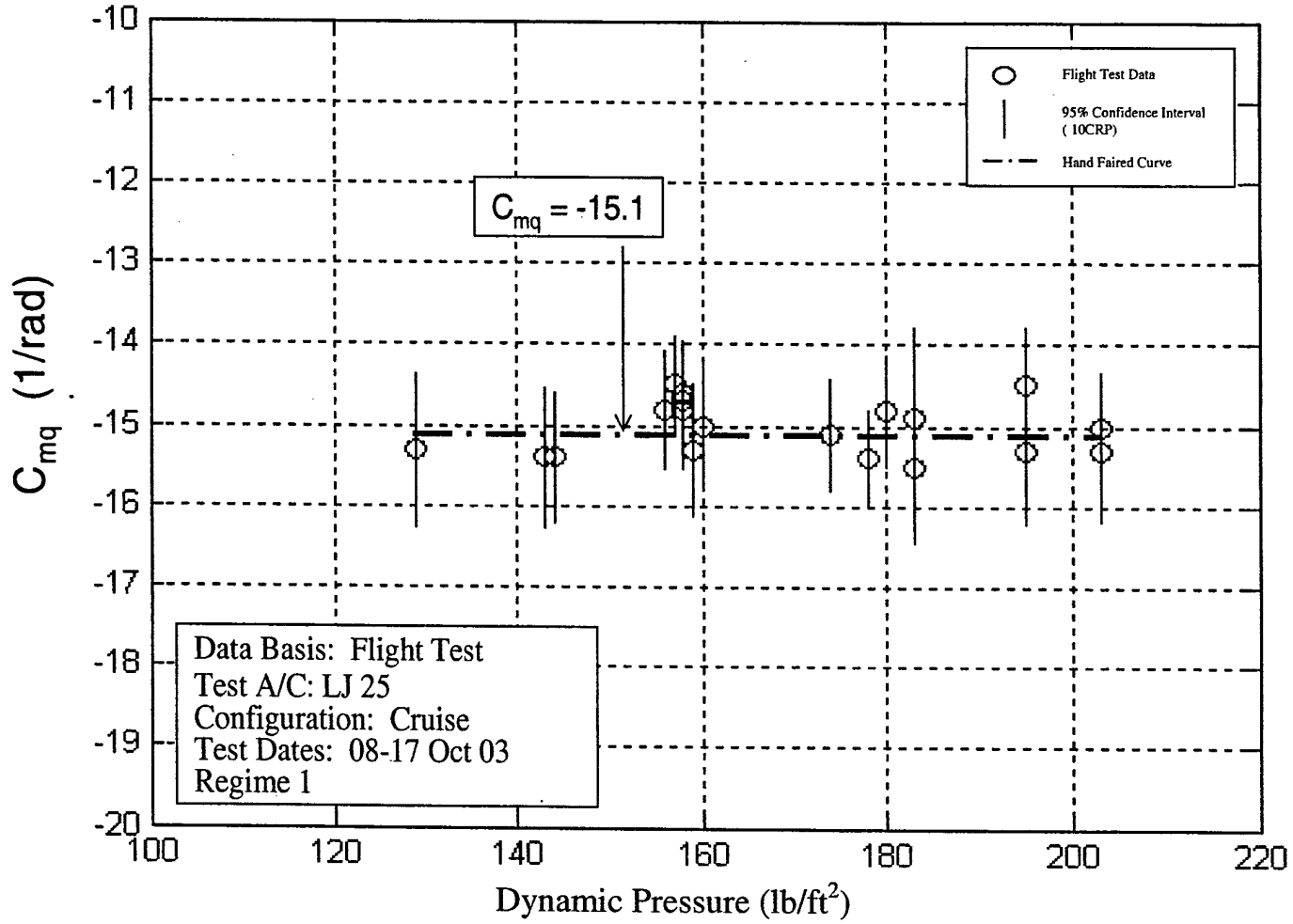

Figure F23: Learjet 25 C_{mq} vs q Regime 1, Project HAVE TRIM

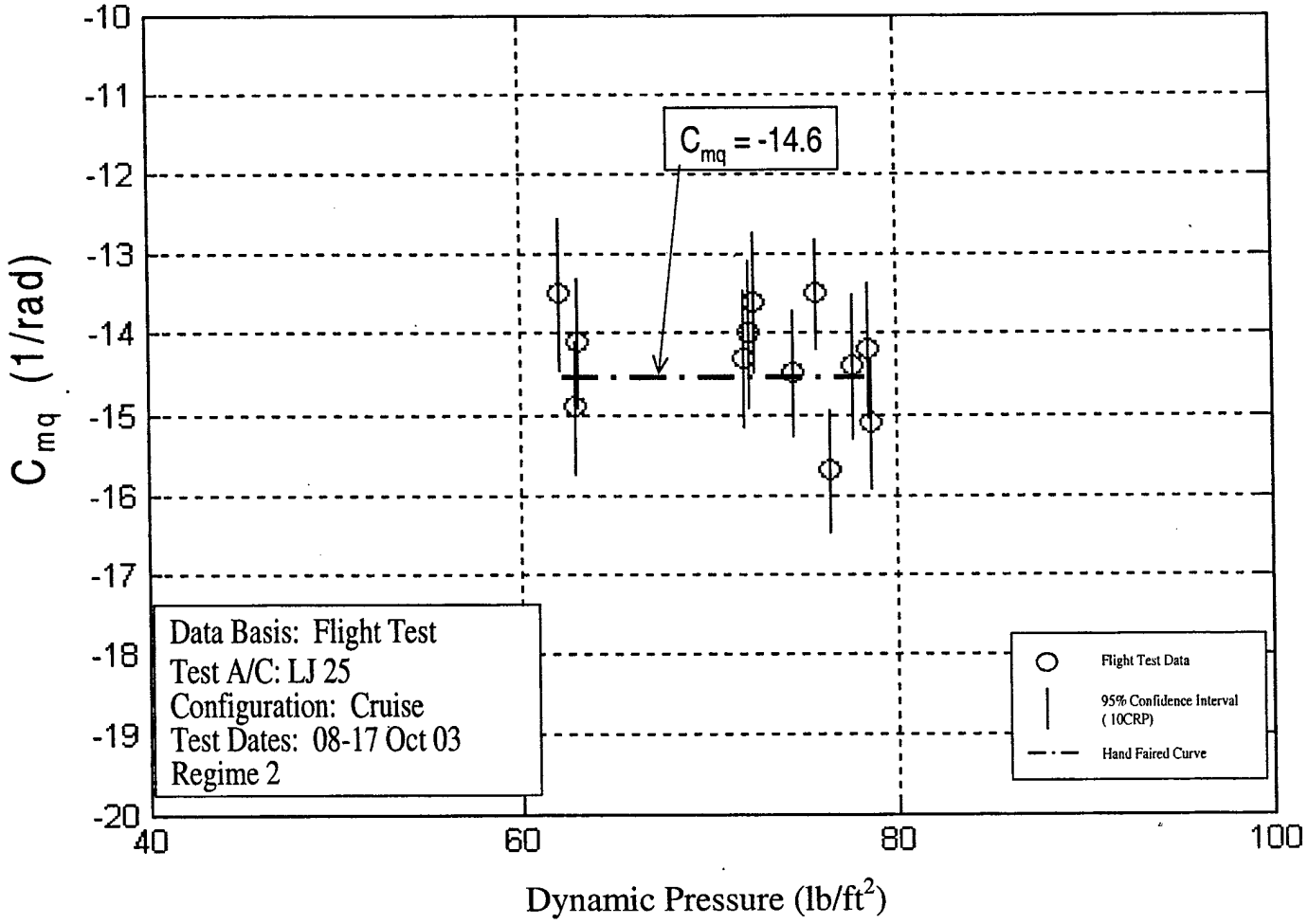

Figure F24: Learjet 25 C_{mq} vs q Regime 2, Project HAVE TRIM

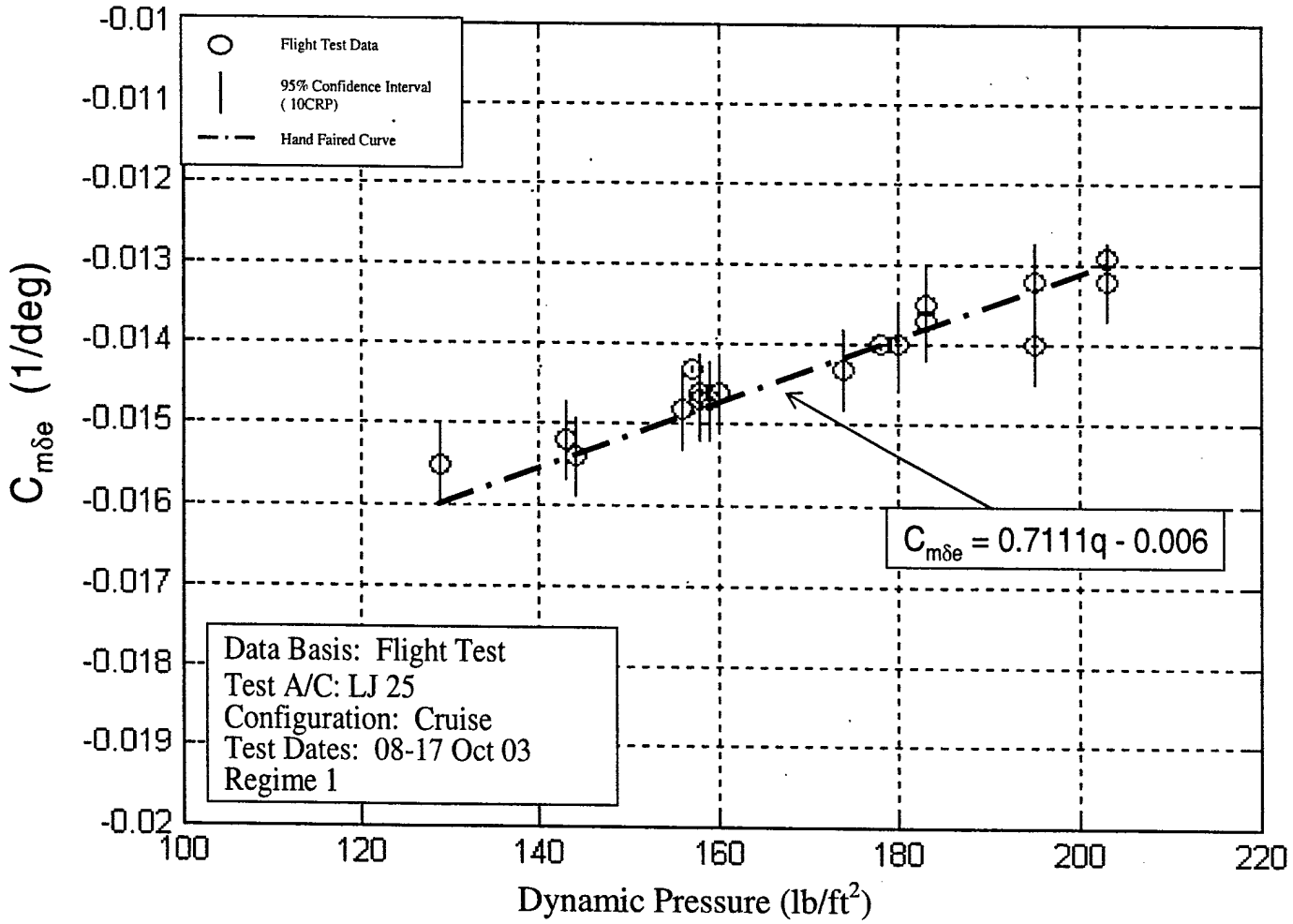

Figure F25: Learjet 25 $C_{m\delta e}$ vs q Regime 1, Project HAVE TRIM

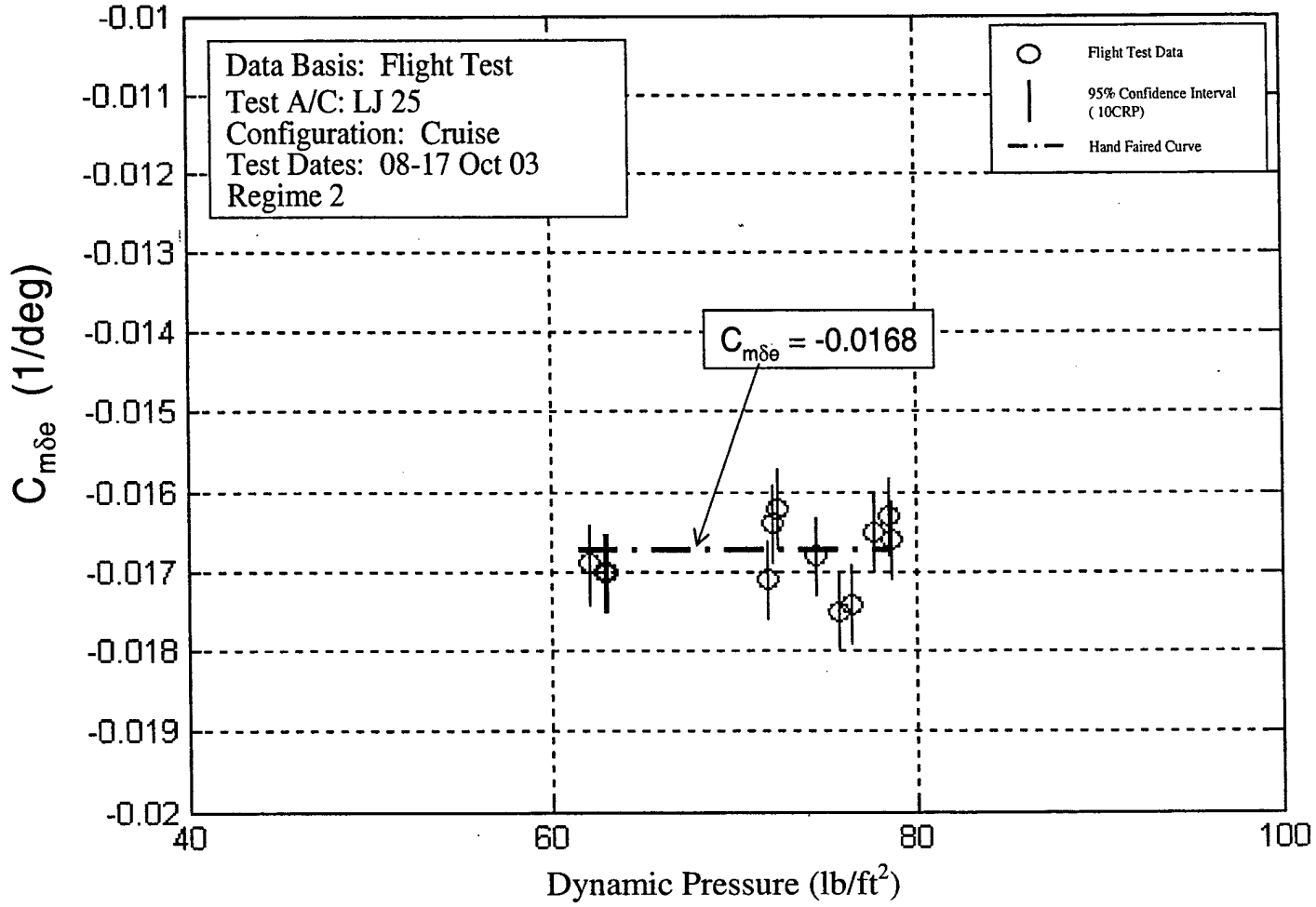

Figure F26: Learjet 25 $C_{m\delta e}$ vs q Regime 2, Project HAVE TRIM

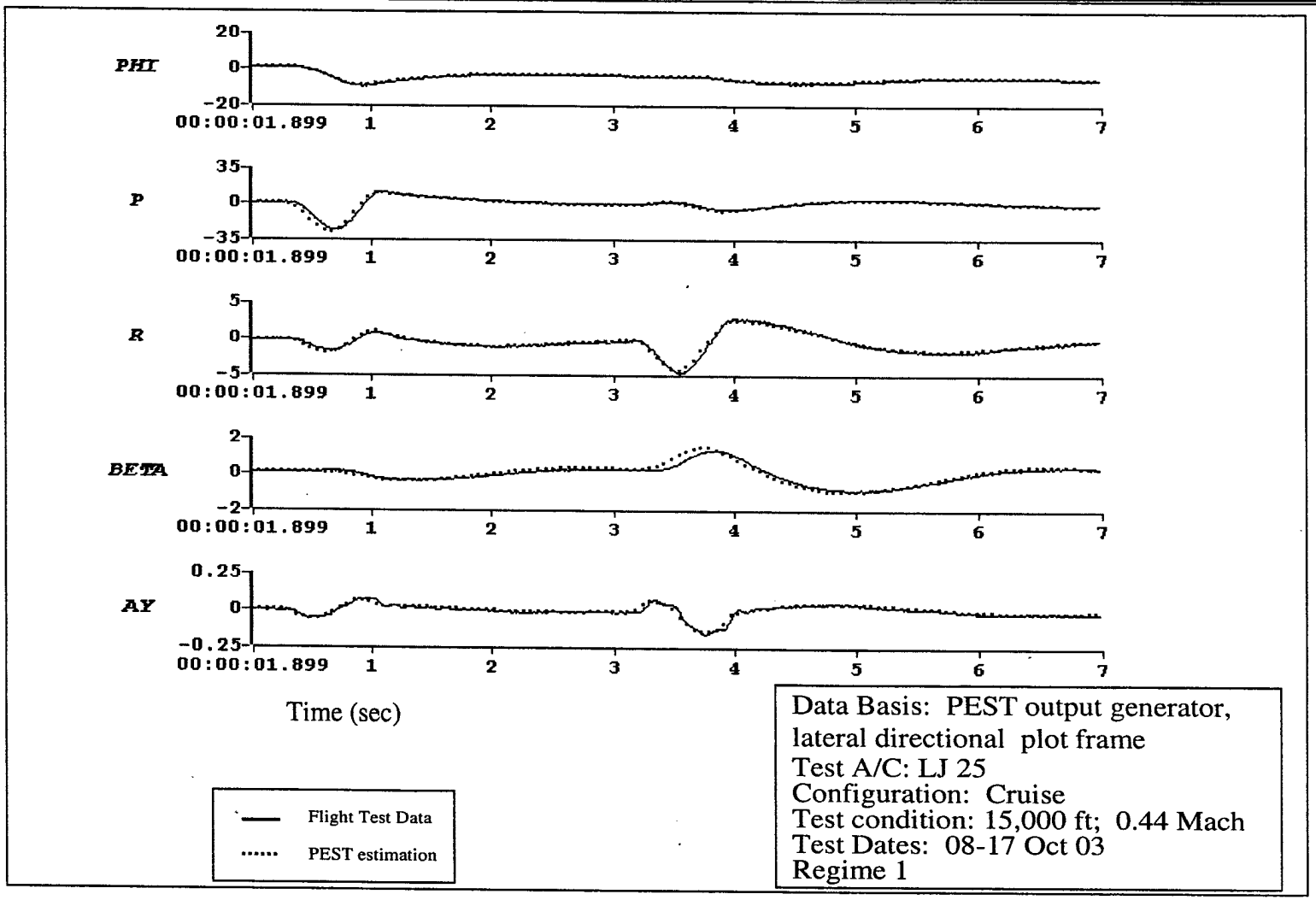

Figure F27: Learjet 25 Lateral-Directional Time History Comparison, Project HAVE TRIM

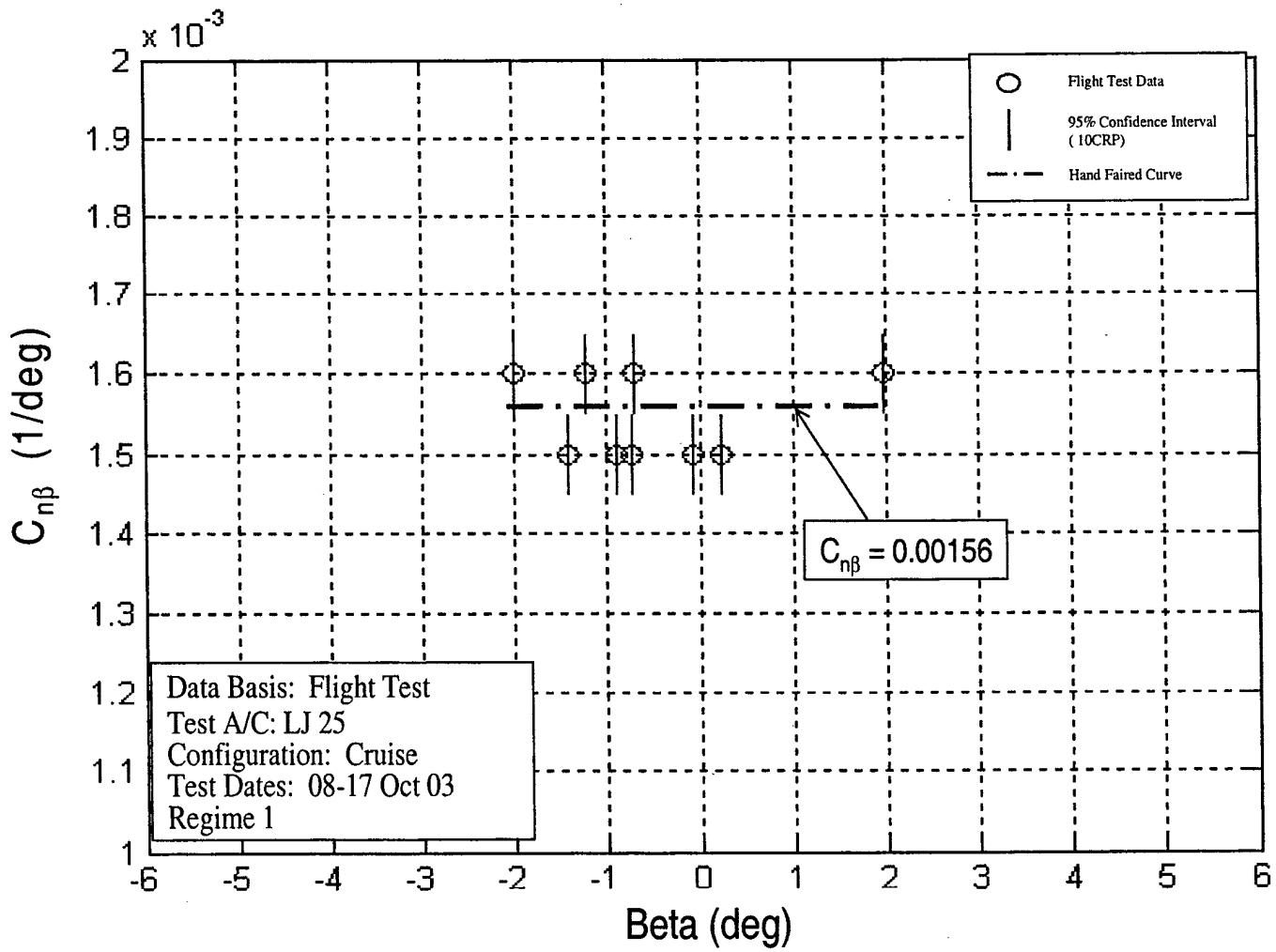

Figure F28: Learjet 25 $C_{n\beta}$ vs. β Regime 1, Project HAVE TRIM

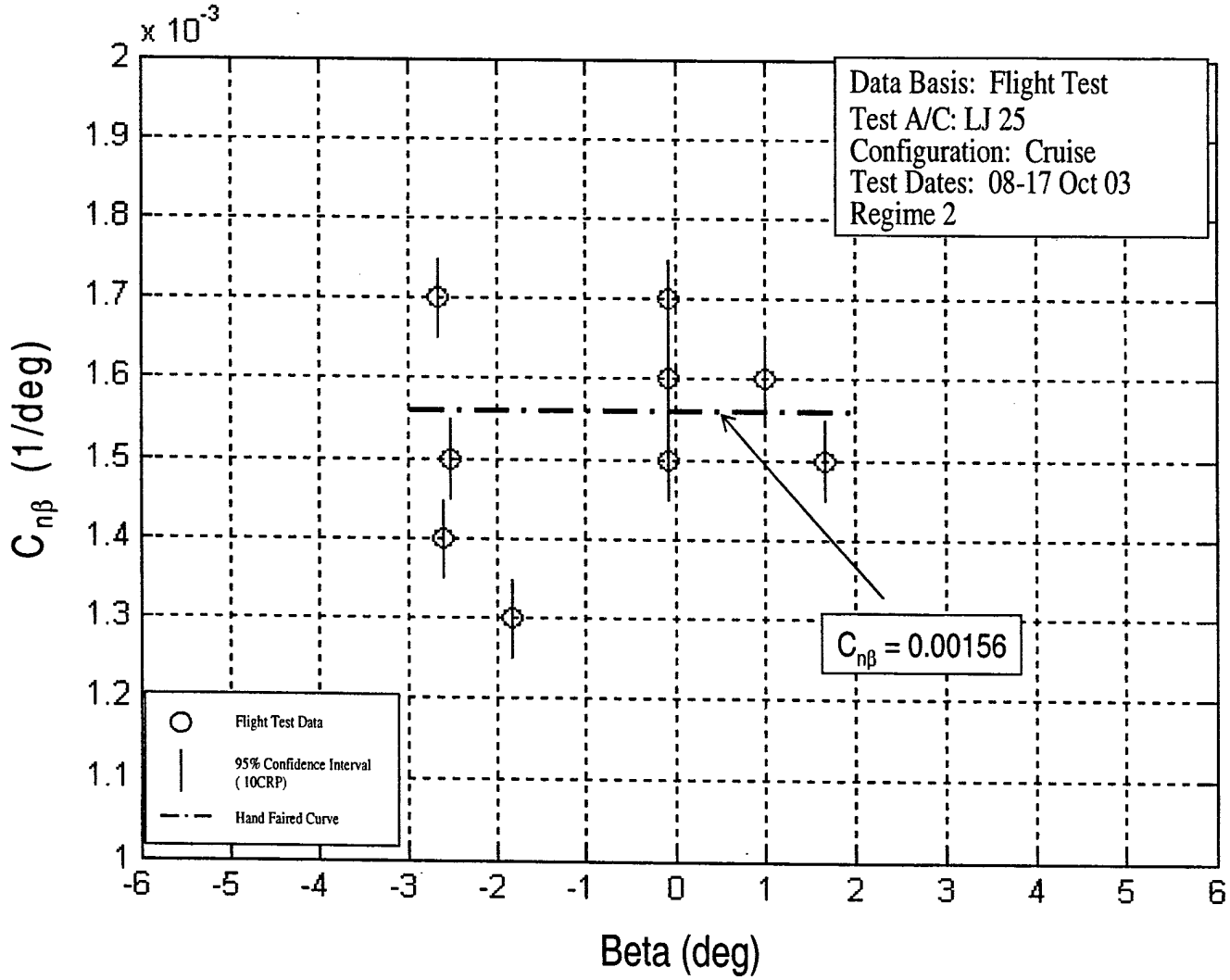

Figure F29: Learjet 25 $C_{n\beta}$ vs. β Regime 2, Project HAVE TRIM

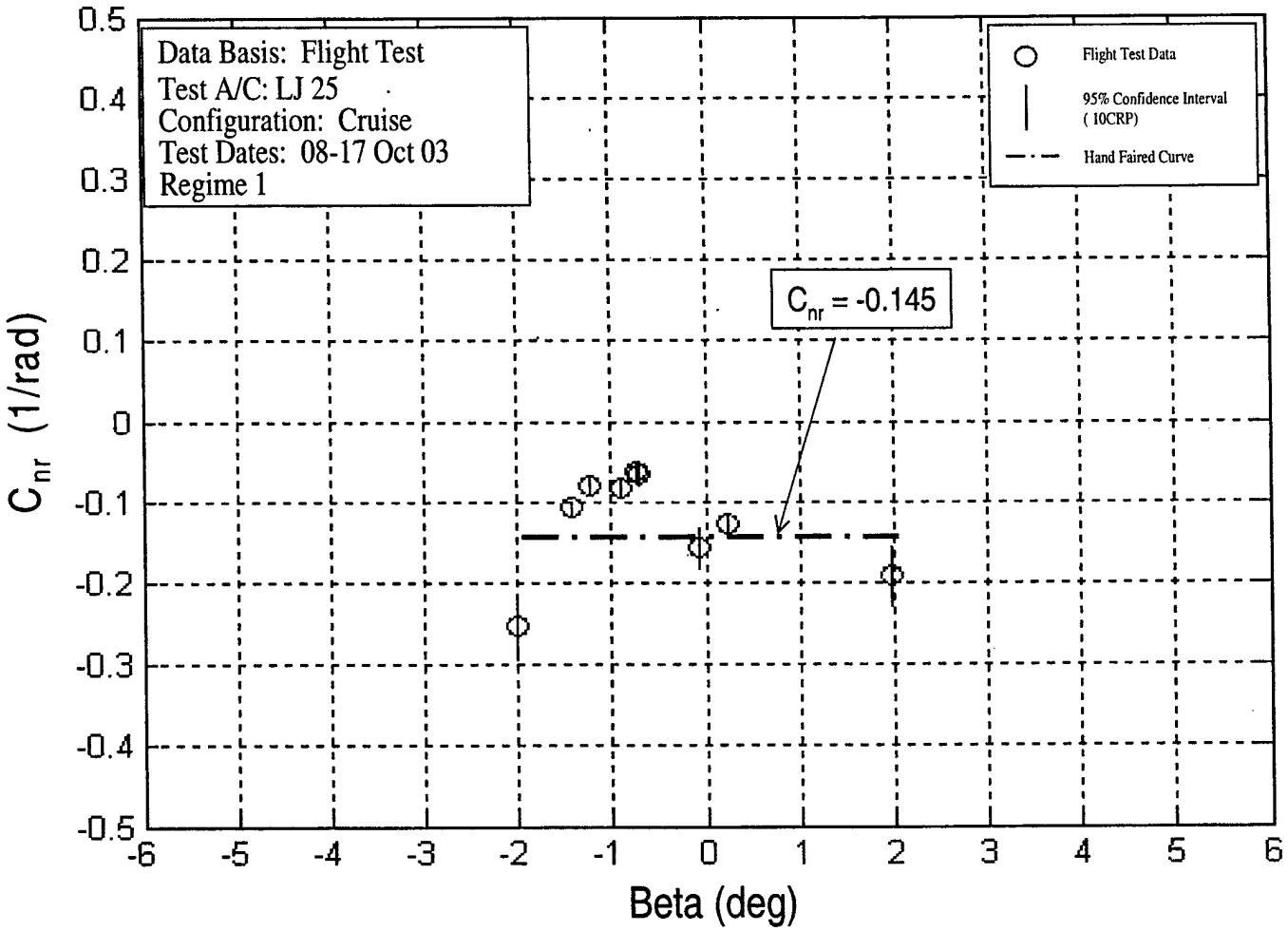

Figure F30: Learjet 25 C_{nr} vs. β Regime 1, Project HAVE TRIM

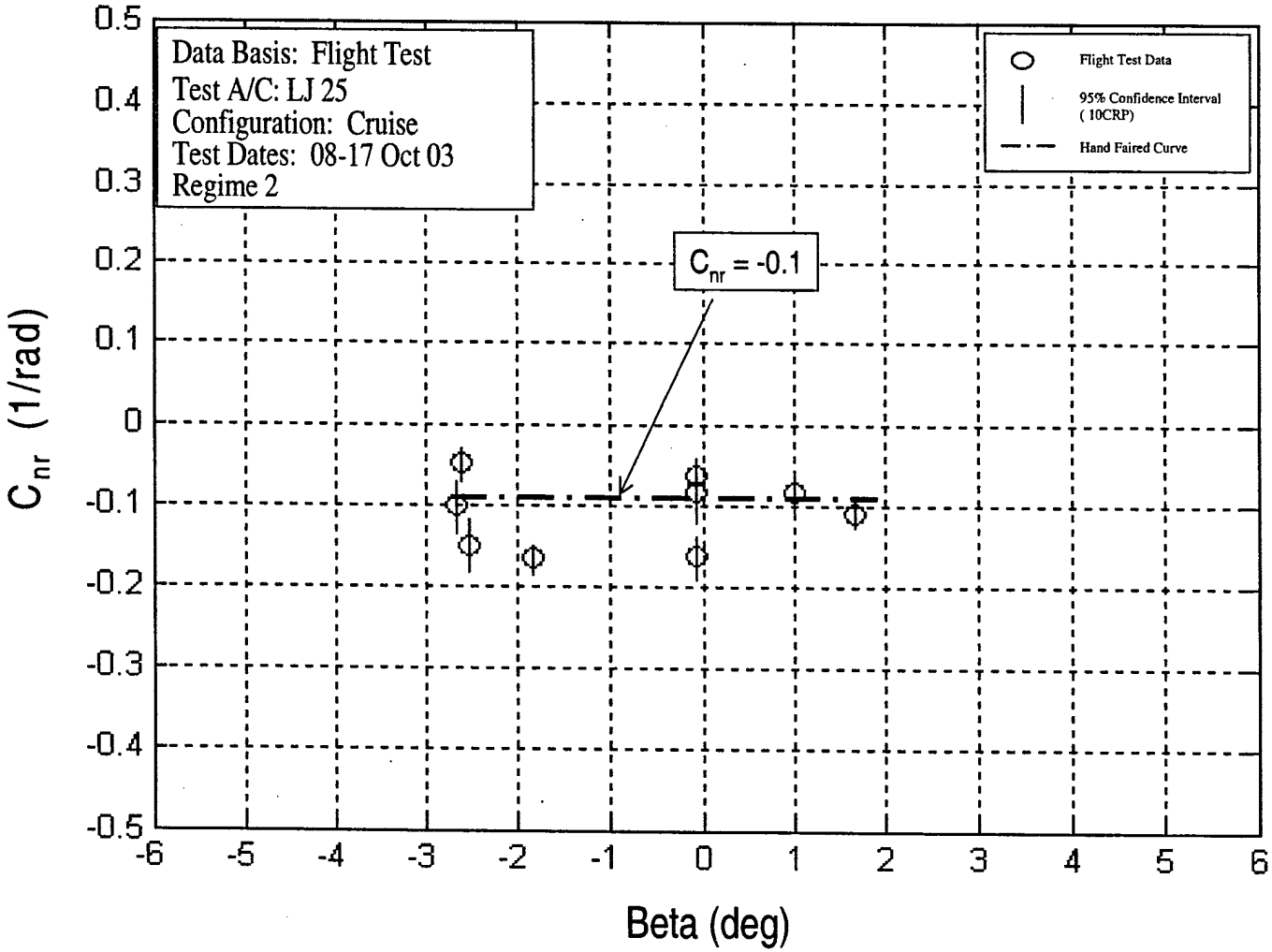

Figure F31: Learjet 25 C_{nr} vs. β Regime 2, Project HAVE TRIM

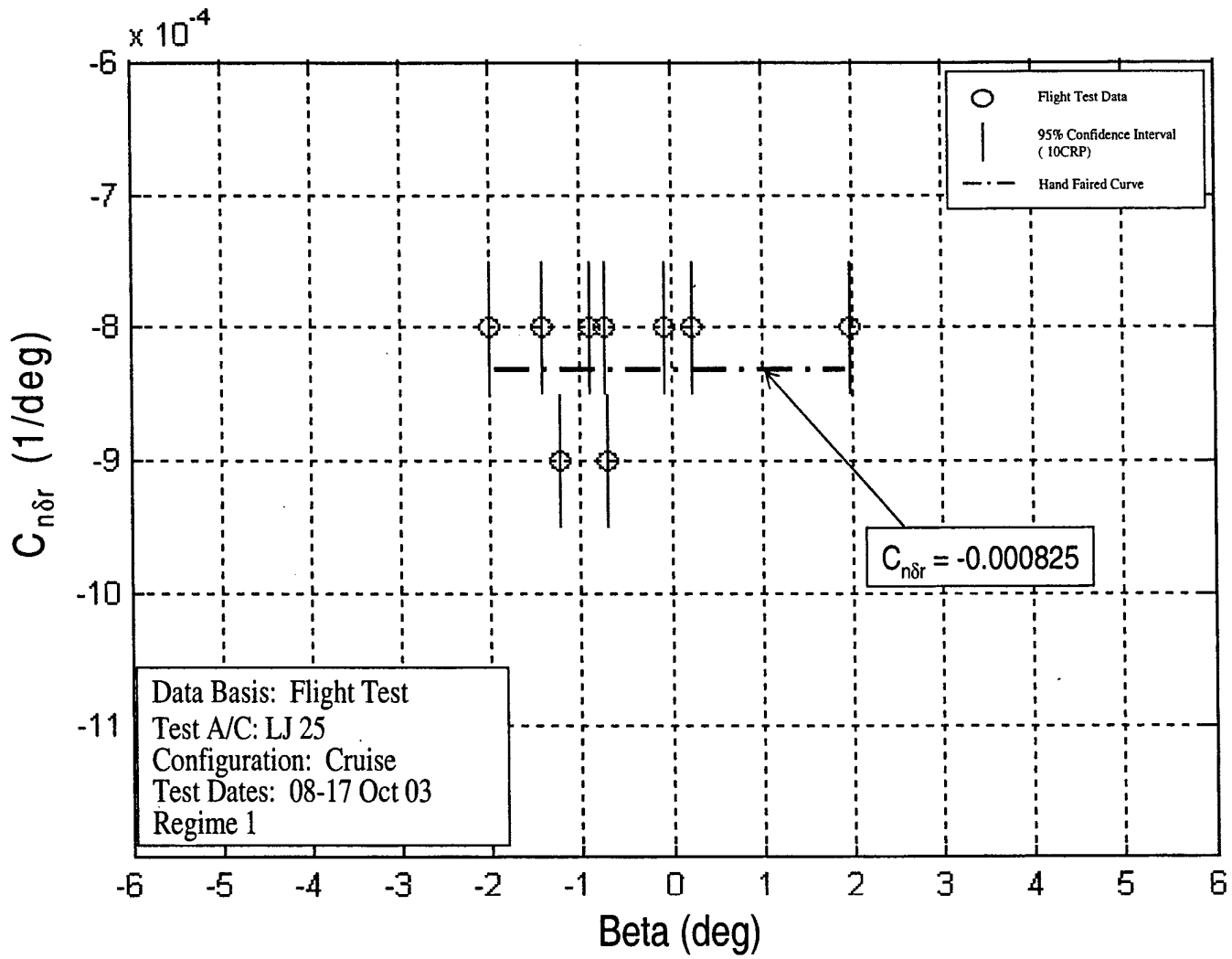

Figure F32: Learjet 25 $C_{n\delta r}$ vs. β Regime 1, Project HAVE TRIM

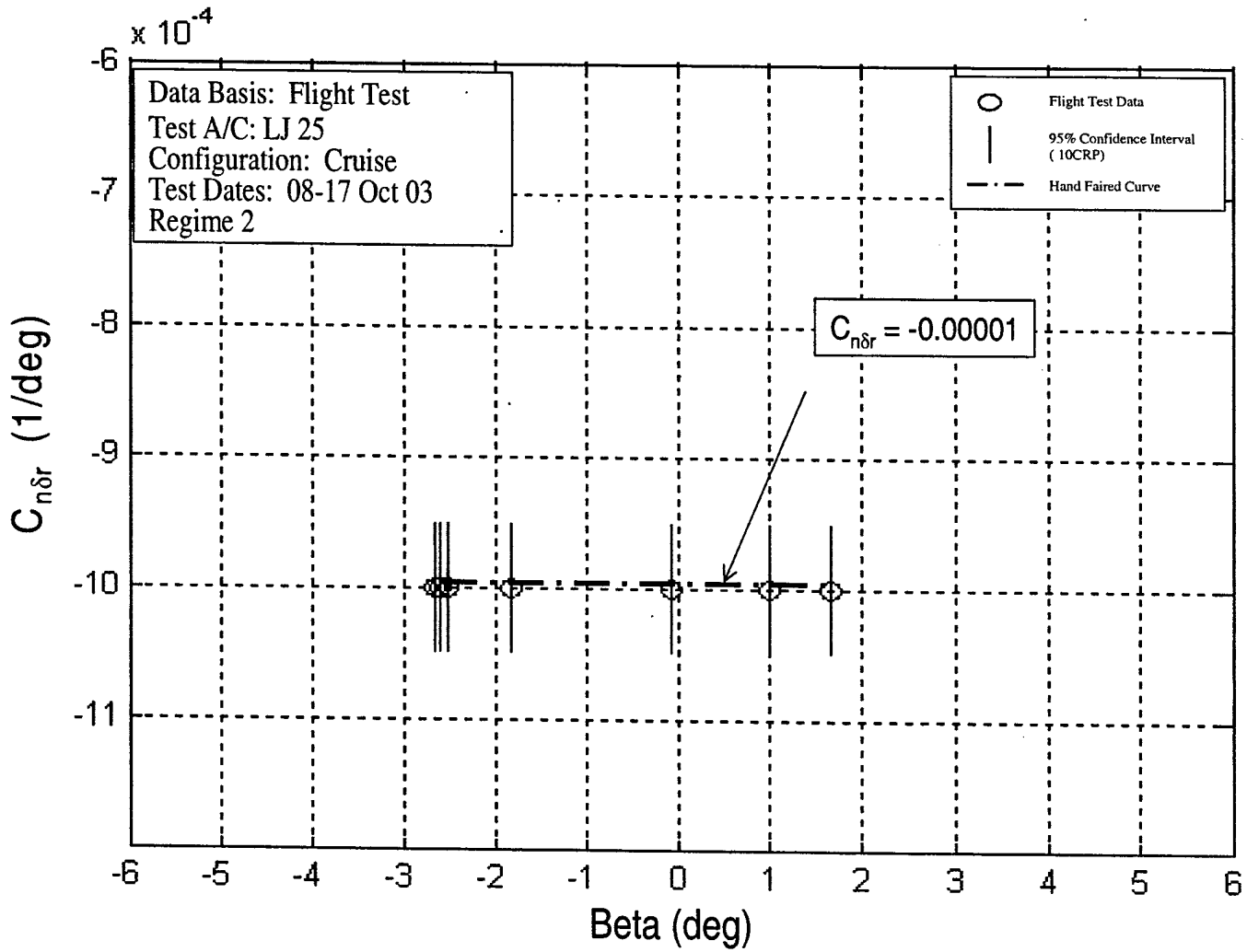

Figure F33: Learjet 25 $C_{n\delta r}$ vs. β Regime 2, Project HAVE TRIM

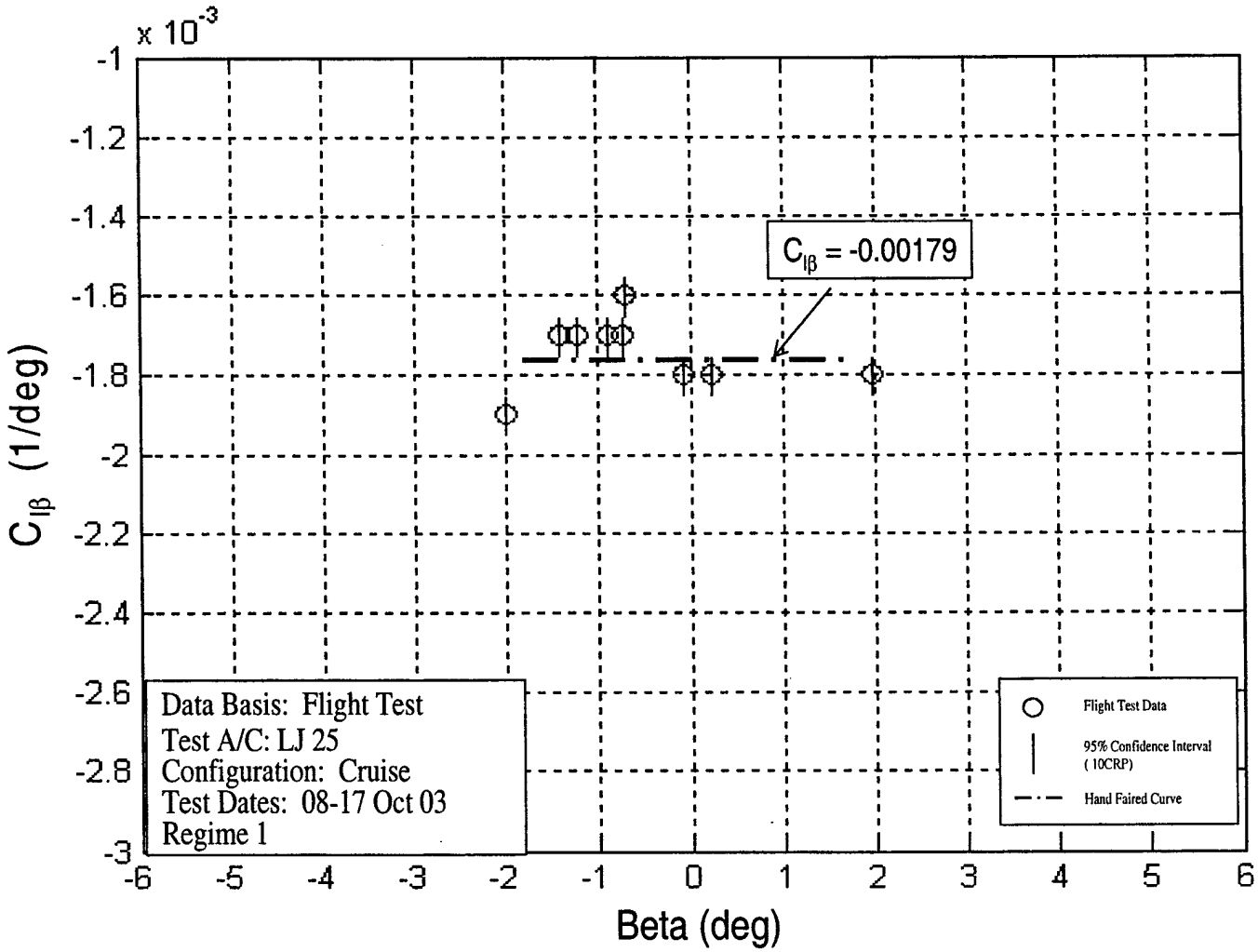

Figure F34: Learjet 25 $C_{l\beta}$ vs. β Regime 1, Project HAVE TRIM

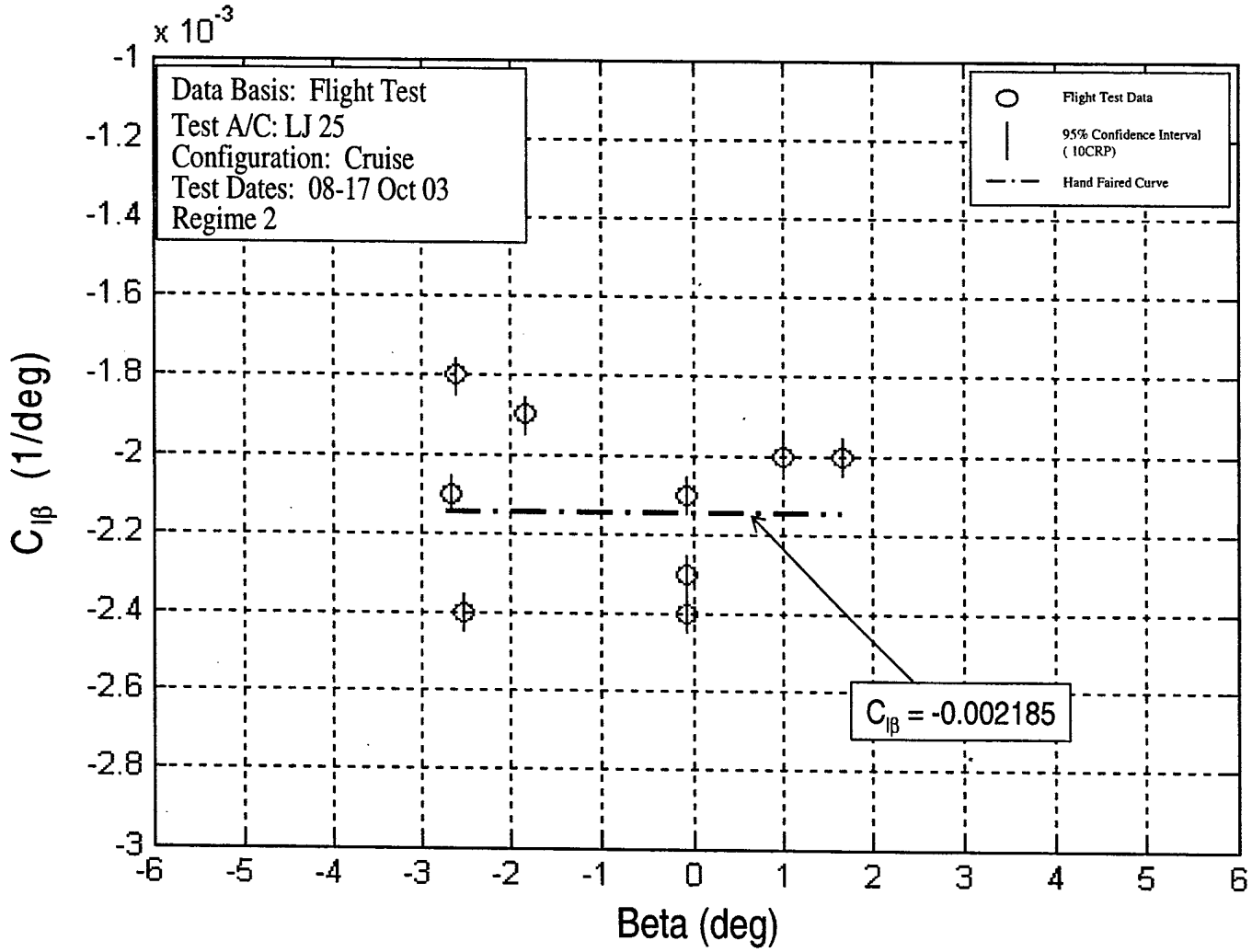

Figure F35: Learjet 25 $C_{l\beta}$ vs. β Regime 2, Project HAVE TRIM

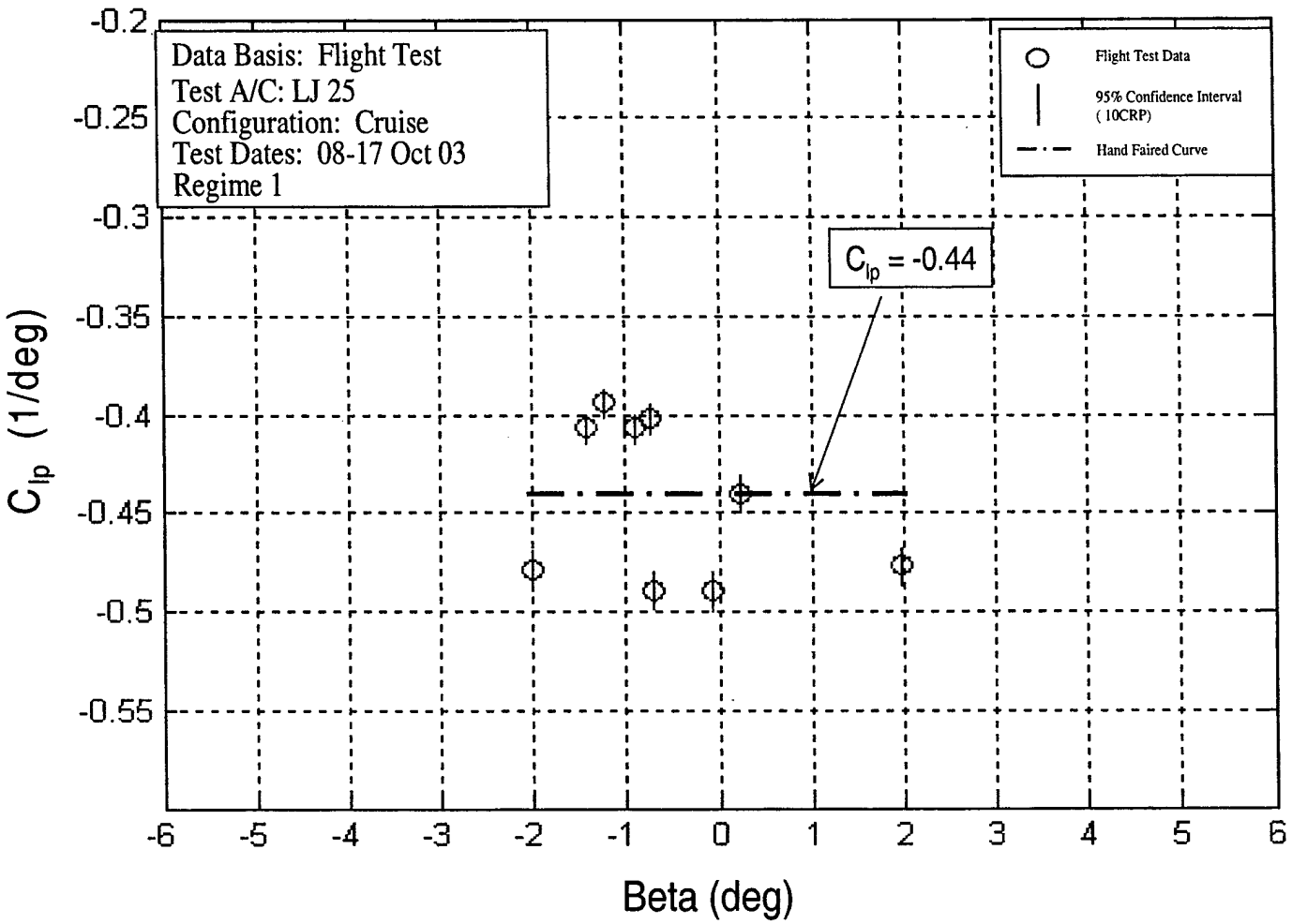

Figure F36: Learjet 25 C_{lp} vs. β Regime 1, Project HAVE TRIM

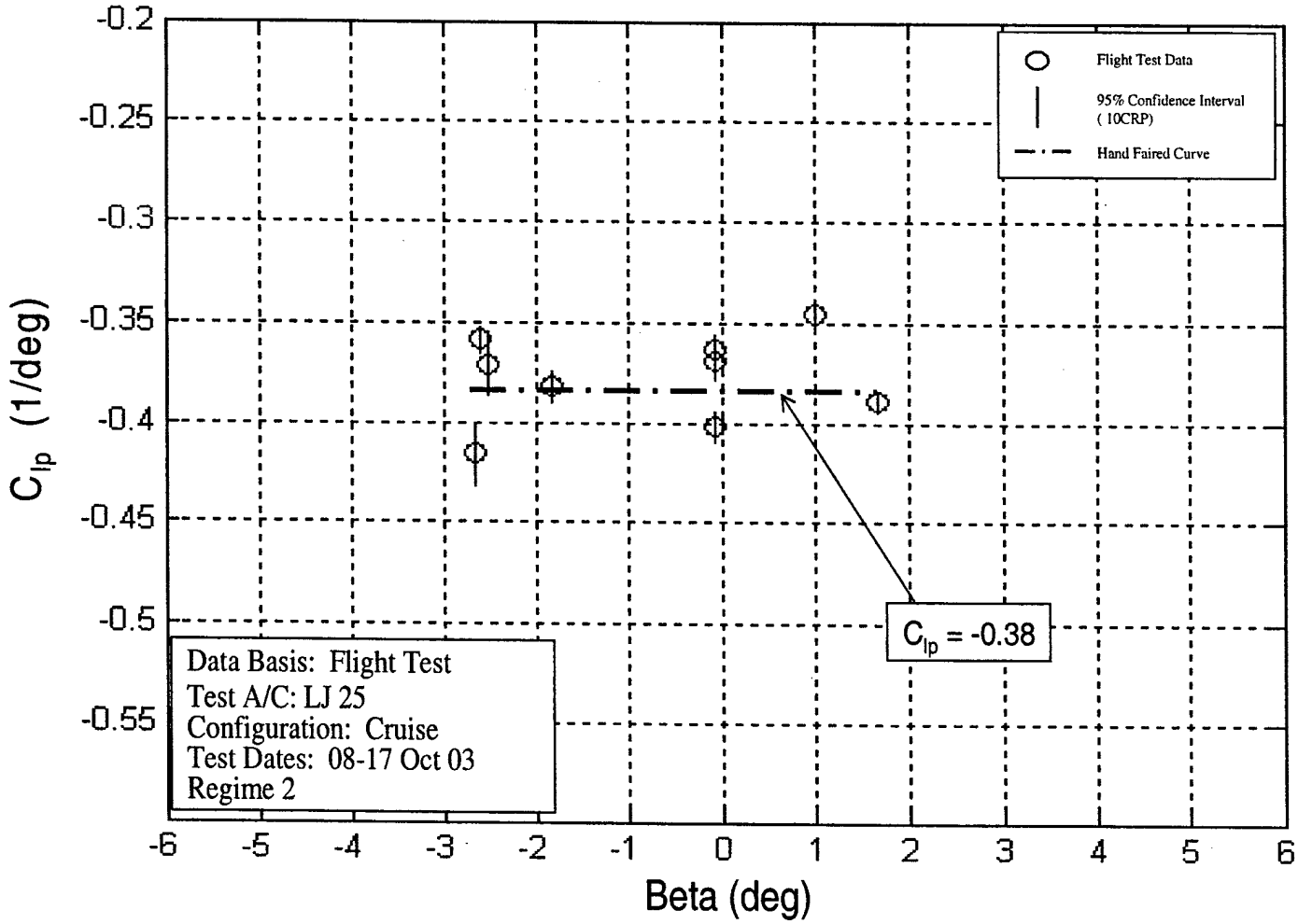

Figure F37: Learjet 25 C_{lp} vs. β Regime 2, Project HAVE TRIM

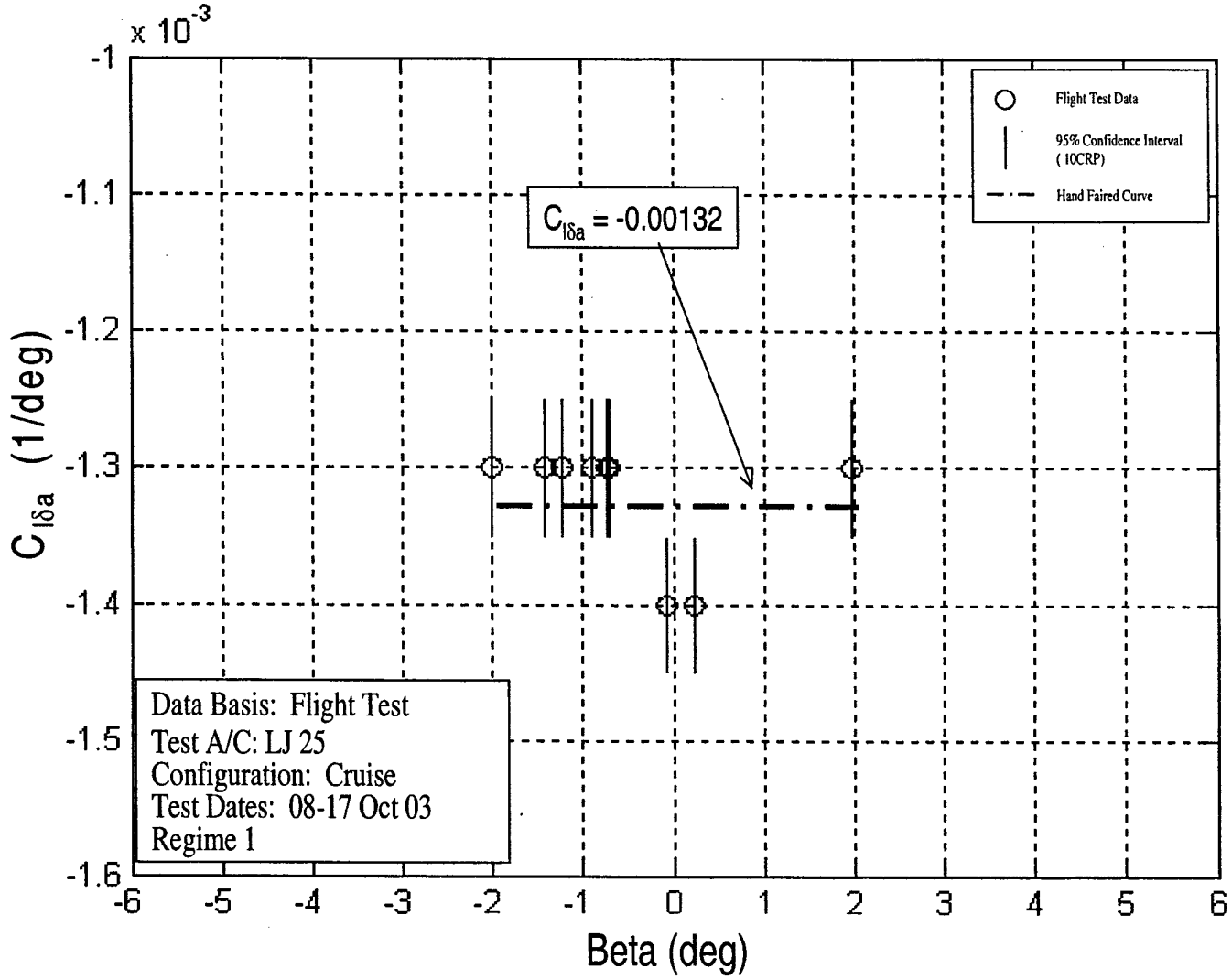

Figure F38: Learjet 25 $C_{l\delta a}$ vs. β Regime 1, Project HAVE TRIM

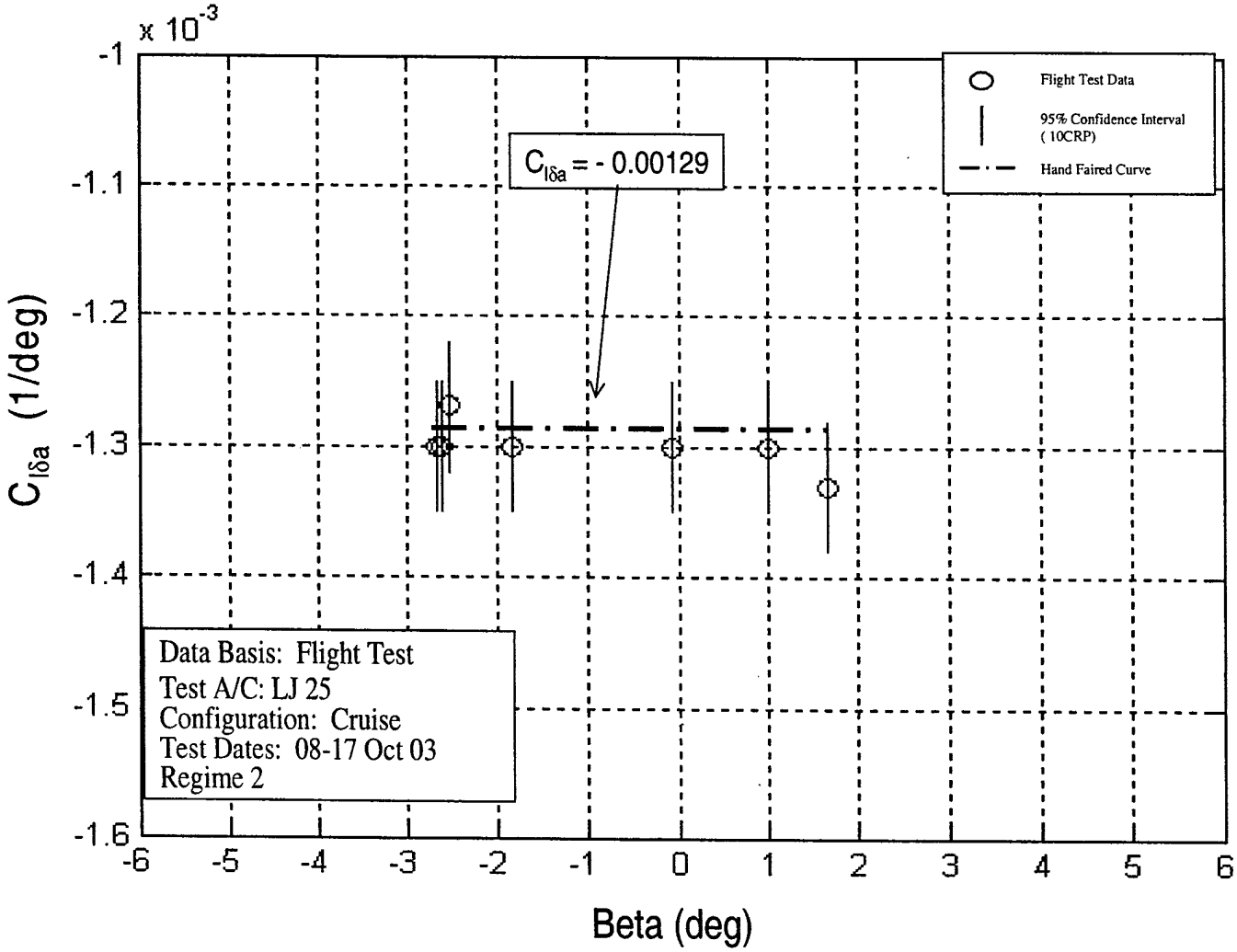

Figure F39: Learjet 25 $C_{l\delta a}$ vs. β Regime 2, Project HAVE TRIM

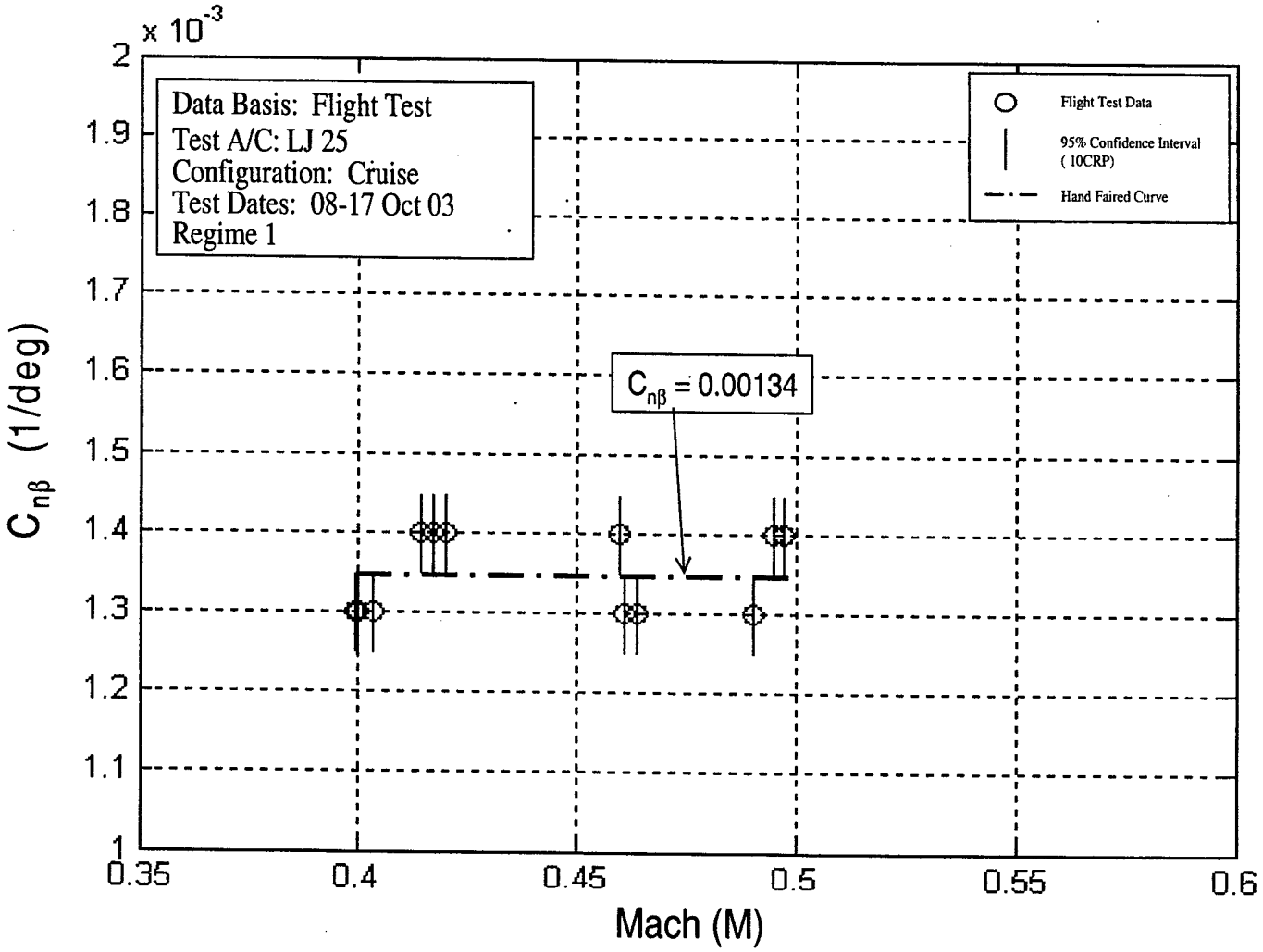

Figure F40: Learjet 25 $C_{n\beta}$ vs. Mach Regime 1, Project HAVE TRIM

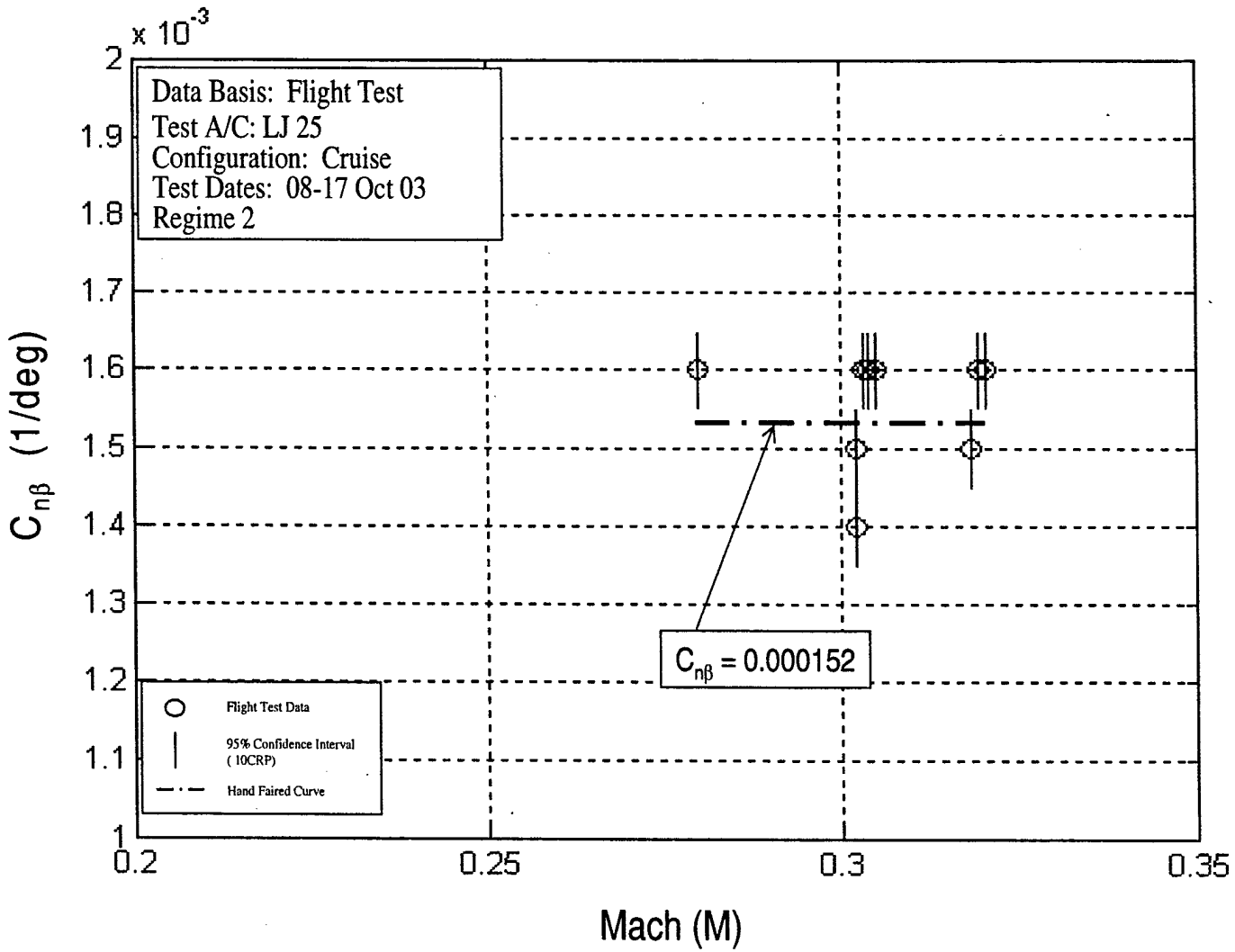

Figure F41: Learjet 25 $C_{n\beta}$ vs. Mach Regime 2, Project HAVE TRIM

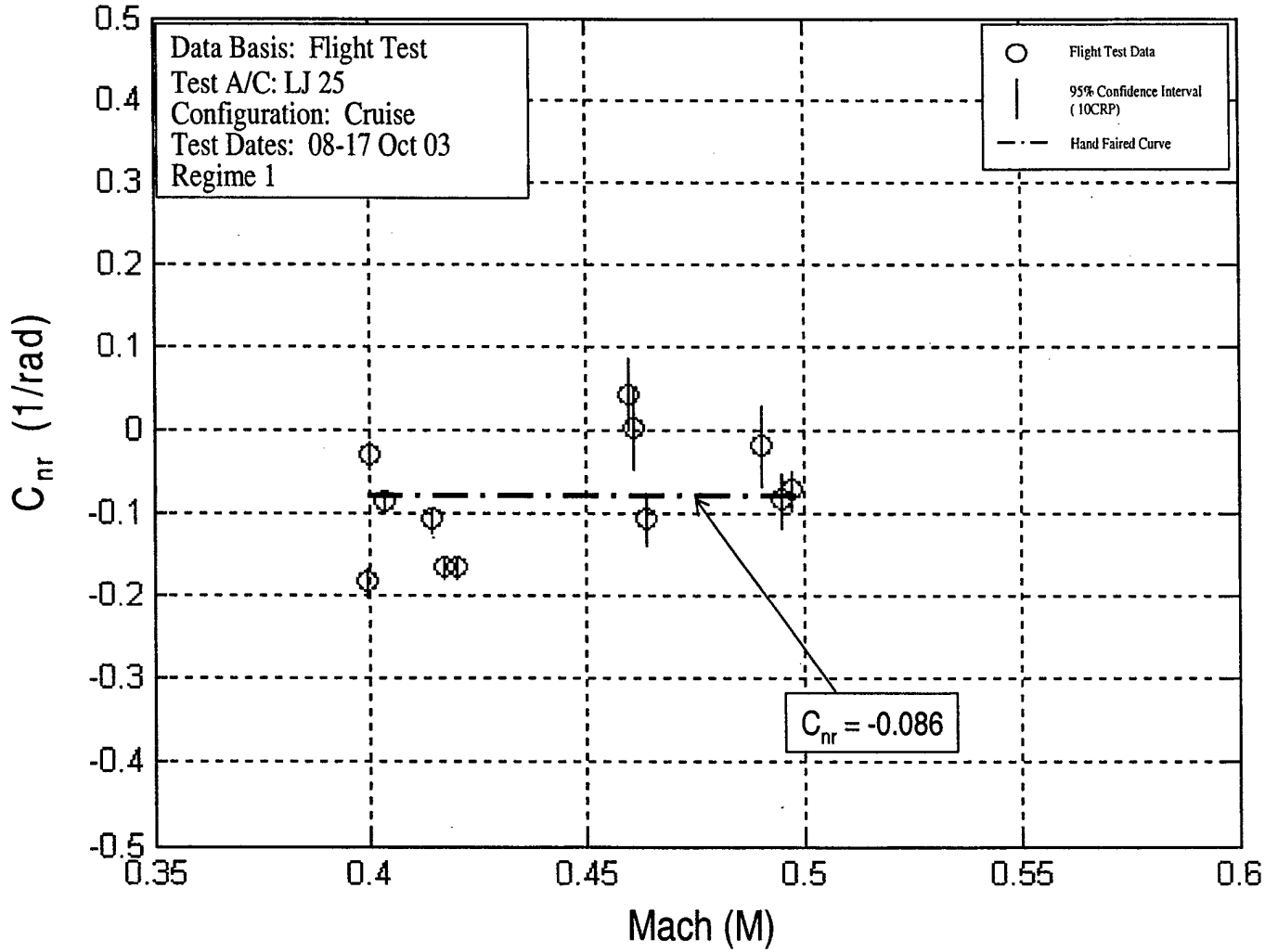

Figure F42: Learjet 25 C_{nr} vs. Mach Regime 1, Project HAVE TRIM

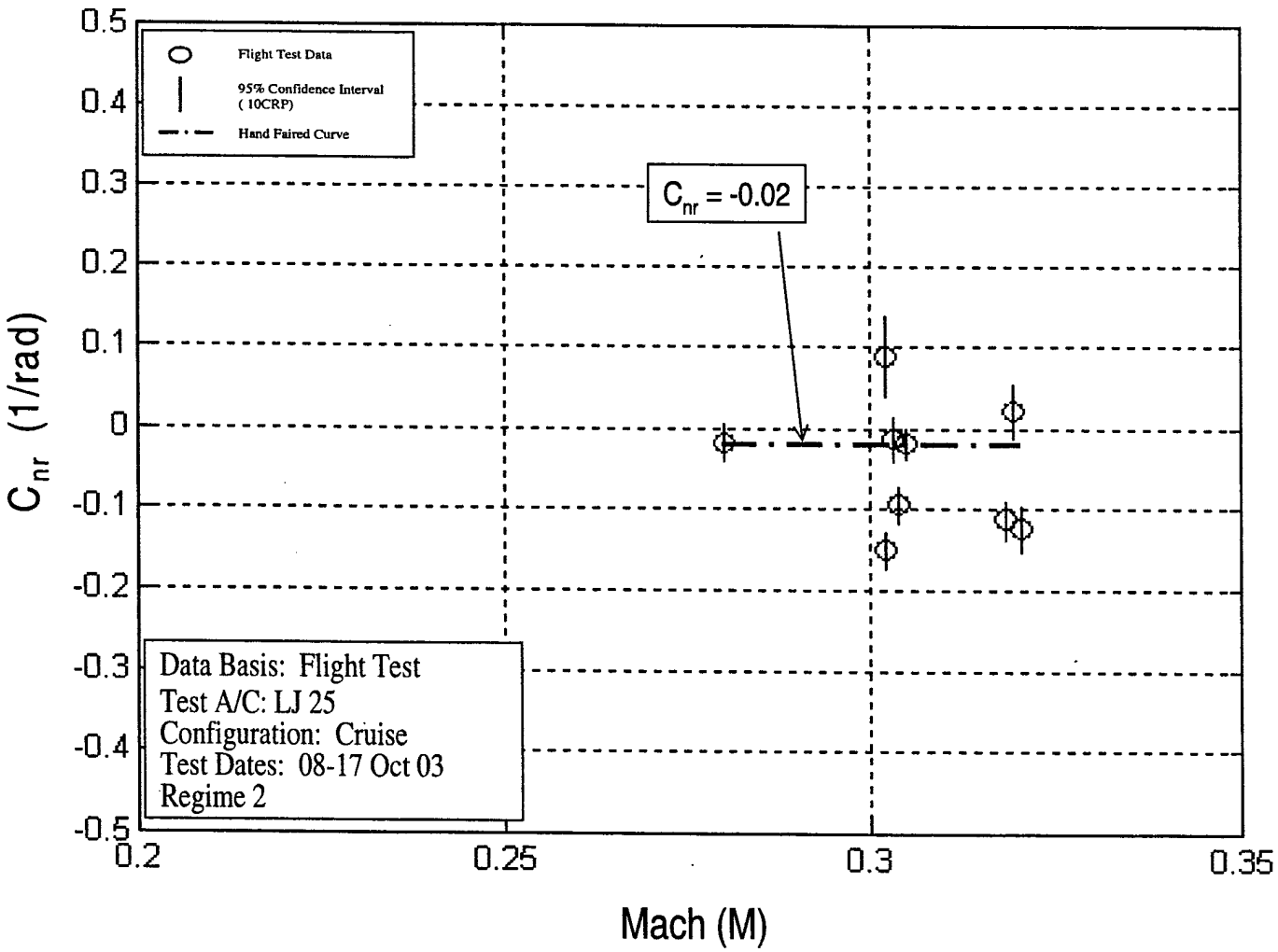

Figure F43: Learjet 25 C_{nr} vs. Mach Regime 2, Project HAVE TRIM

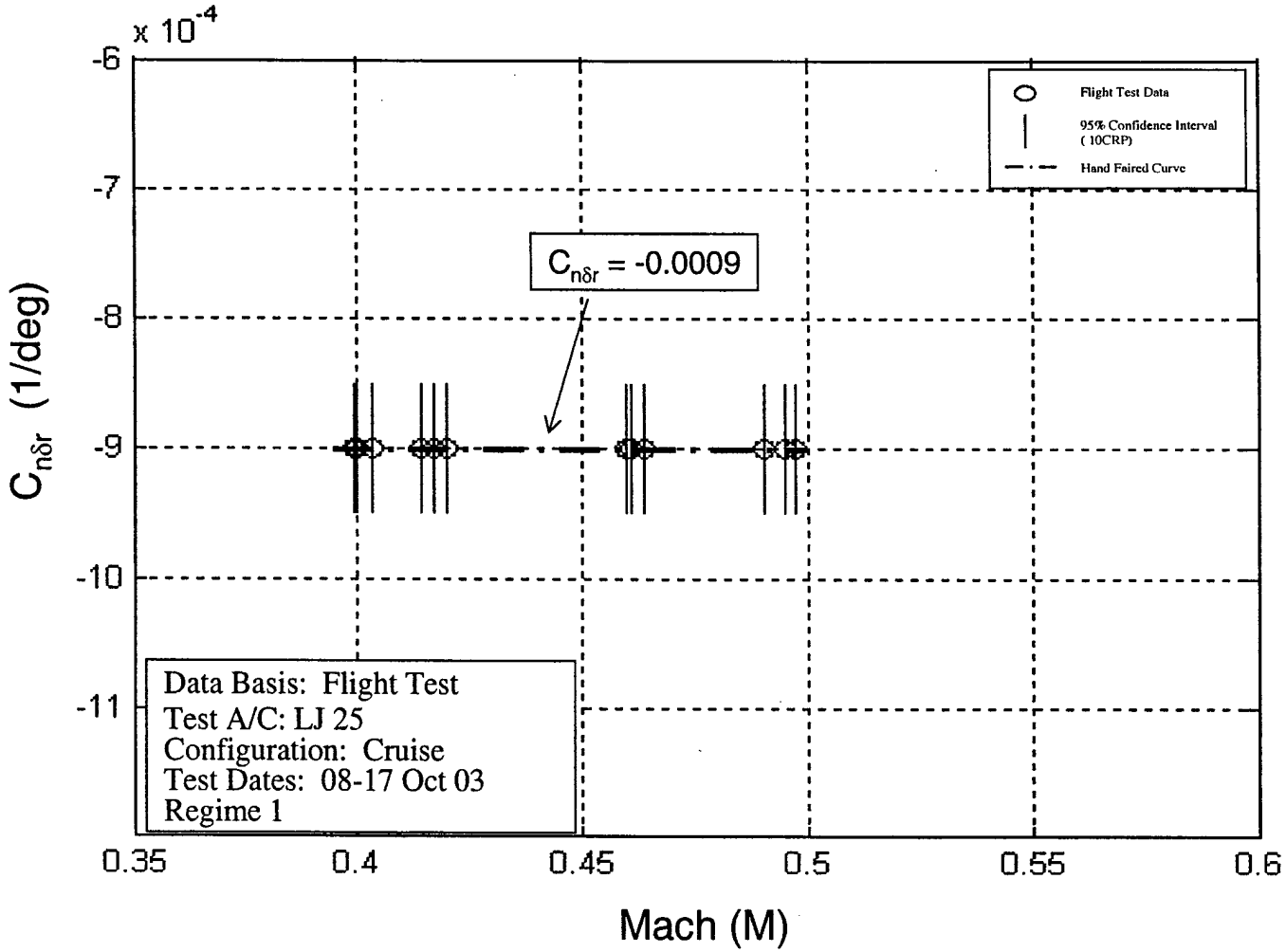

Figure F44: Learjet 25 $C_{n\delta r}$ vs. Mach Regime 1, Project HAVE TRIM

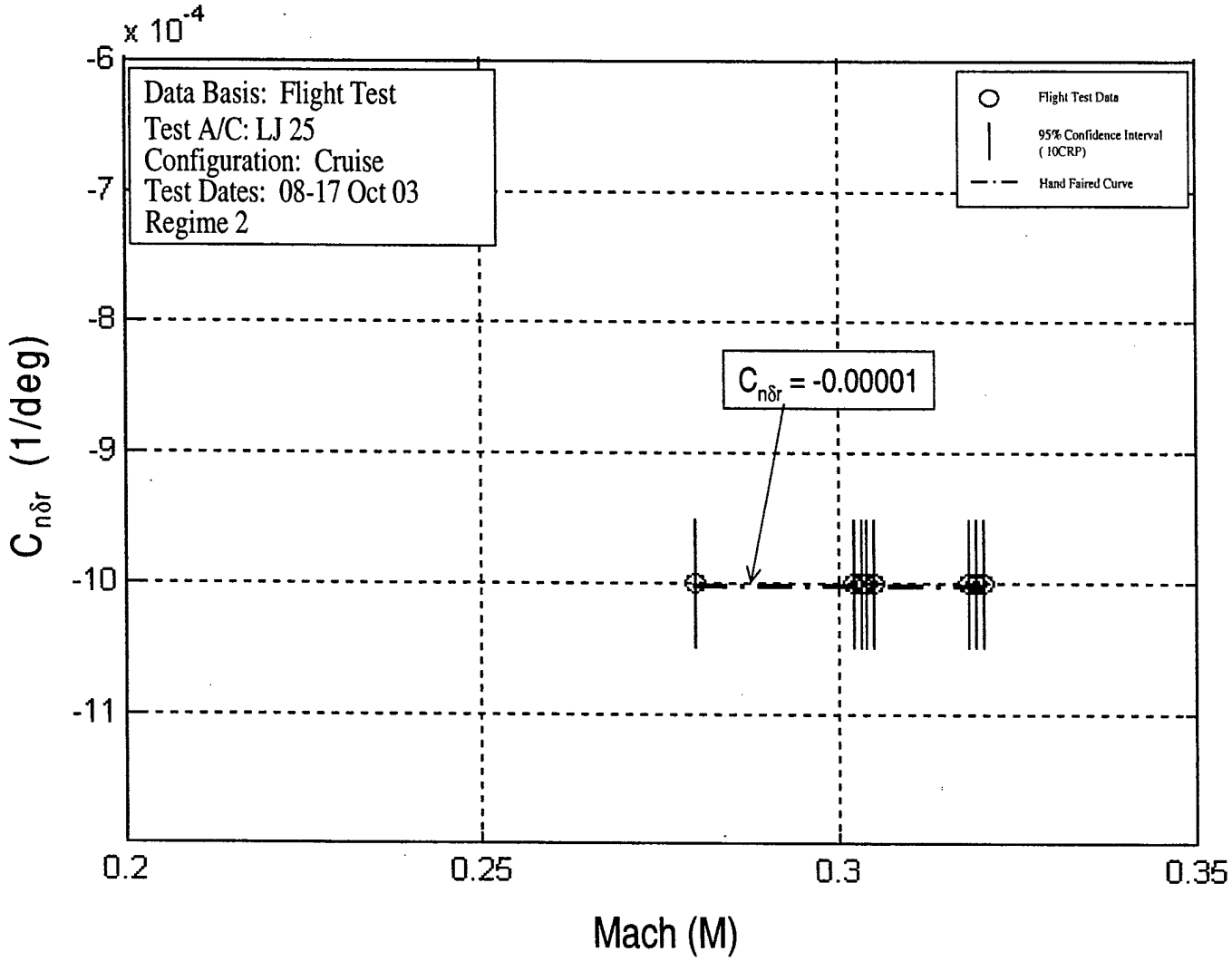

Figure F45: Learjet 25 $C_{n\delta r}$ vs. Mach Regime 2, Project HAVE TRIM

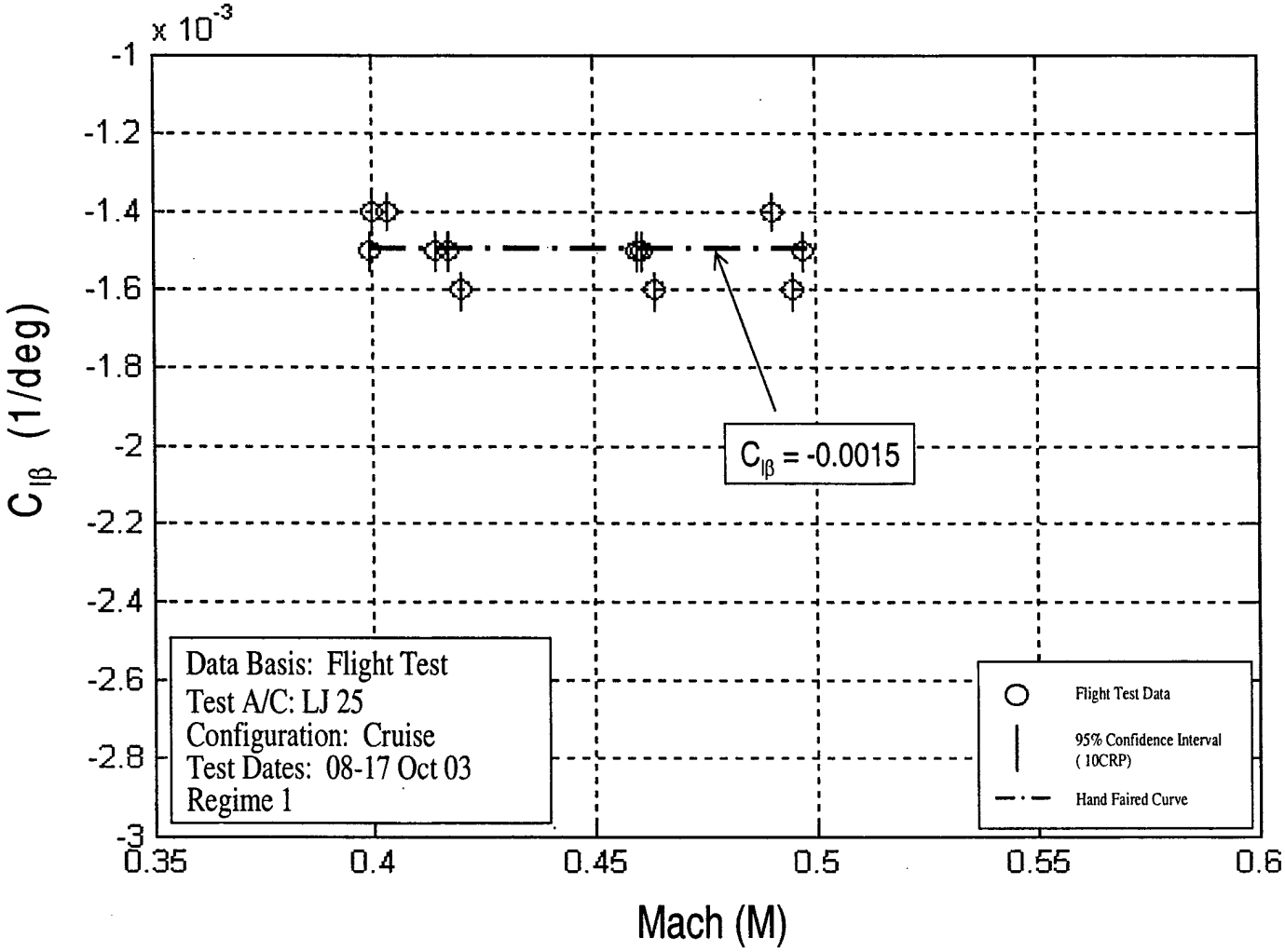

Figure F46: Learjet 25 $C_{l\beta}$ vs. Mach Regime 1, Project HAVE TRIM

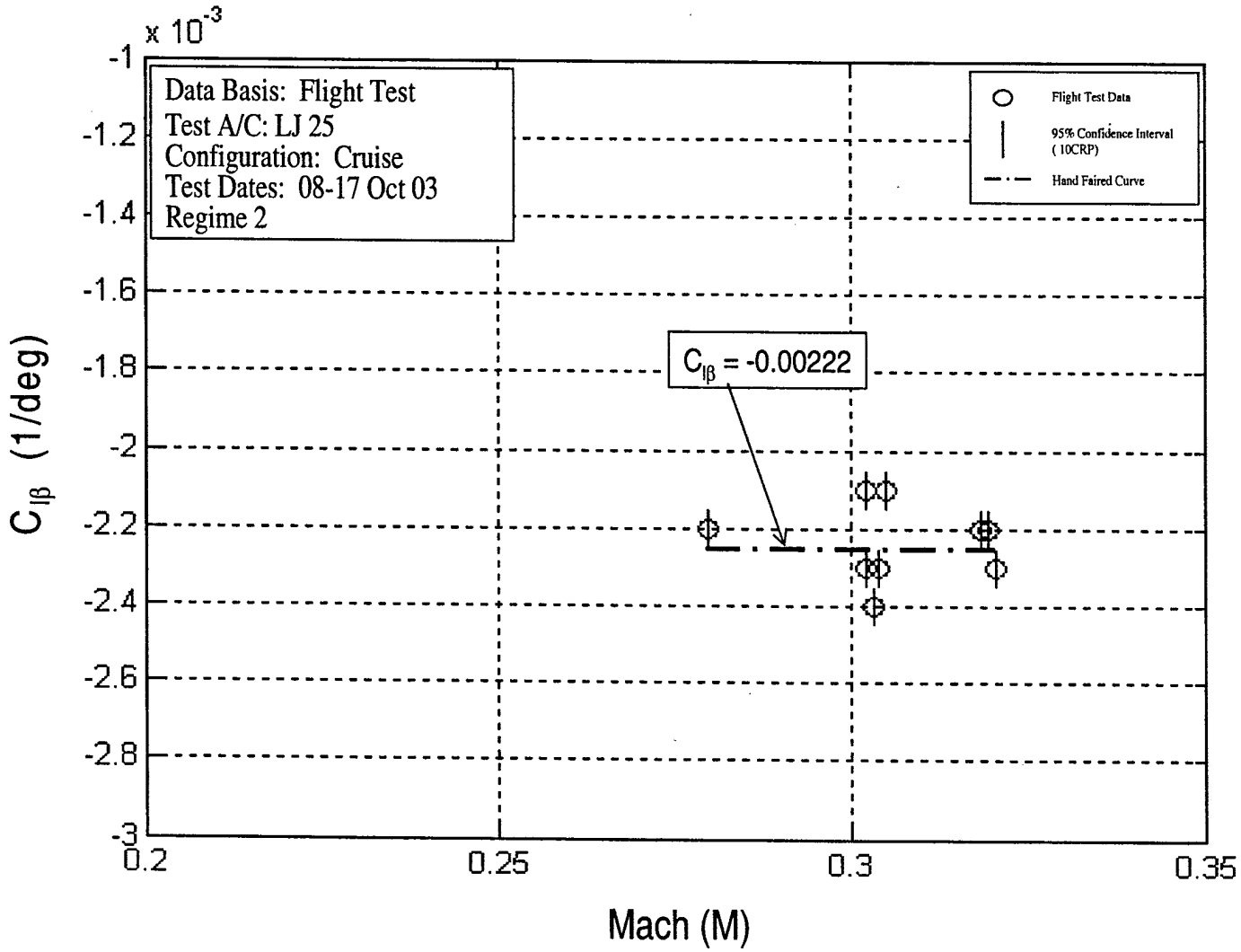

Figure F47: Learjet 25 $C_{l\beta}$ vs. Mach Regime 2, Project HAVE TRIM

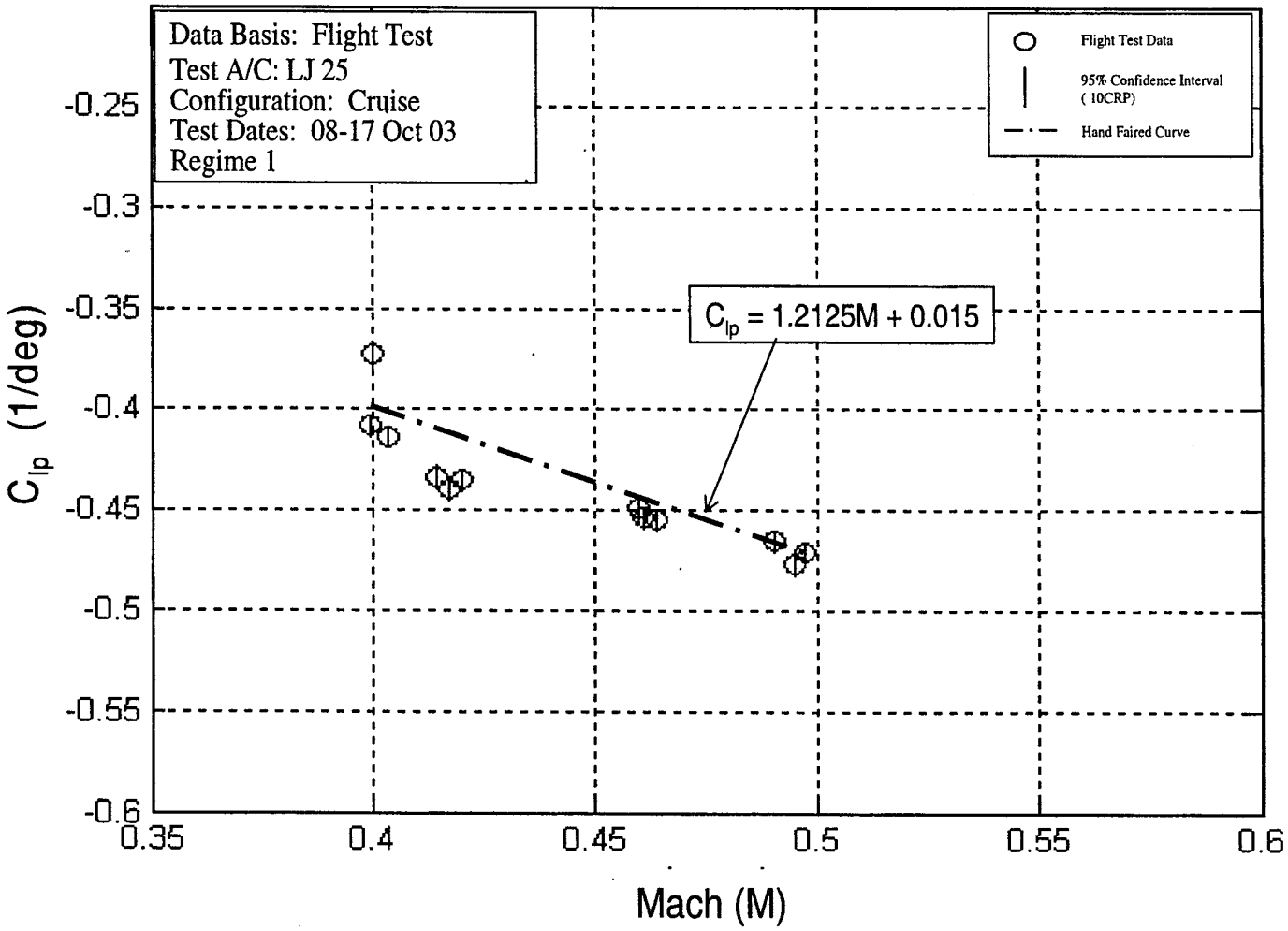

Figure F48: Learjet 25 C_{lp} vs. Mach Regime 1, Project HAVE TRIM

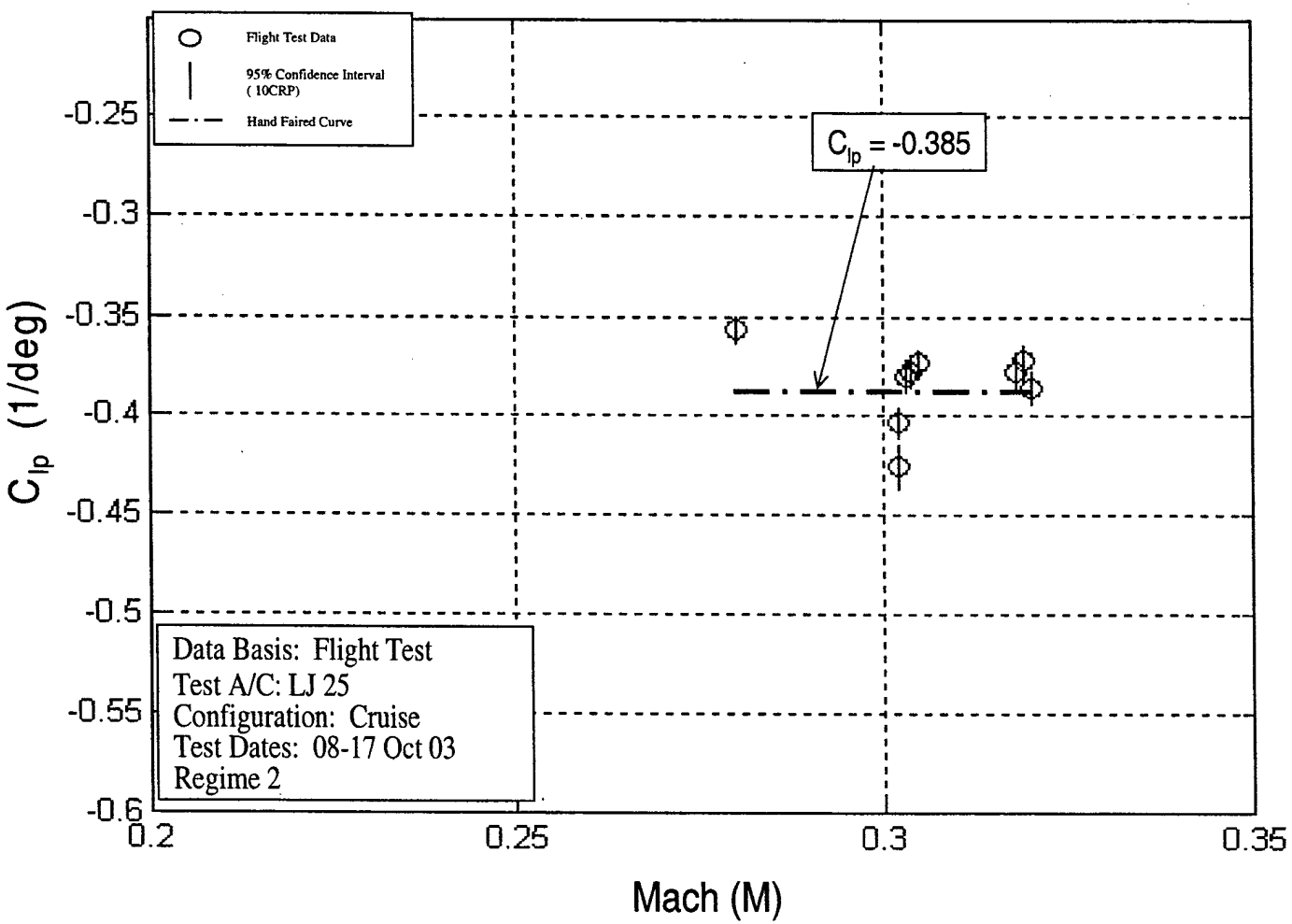

Figure F49: Learjet 25 C_{lp} vs. Mach Regime 2, Project HAVE TRIM

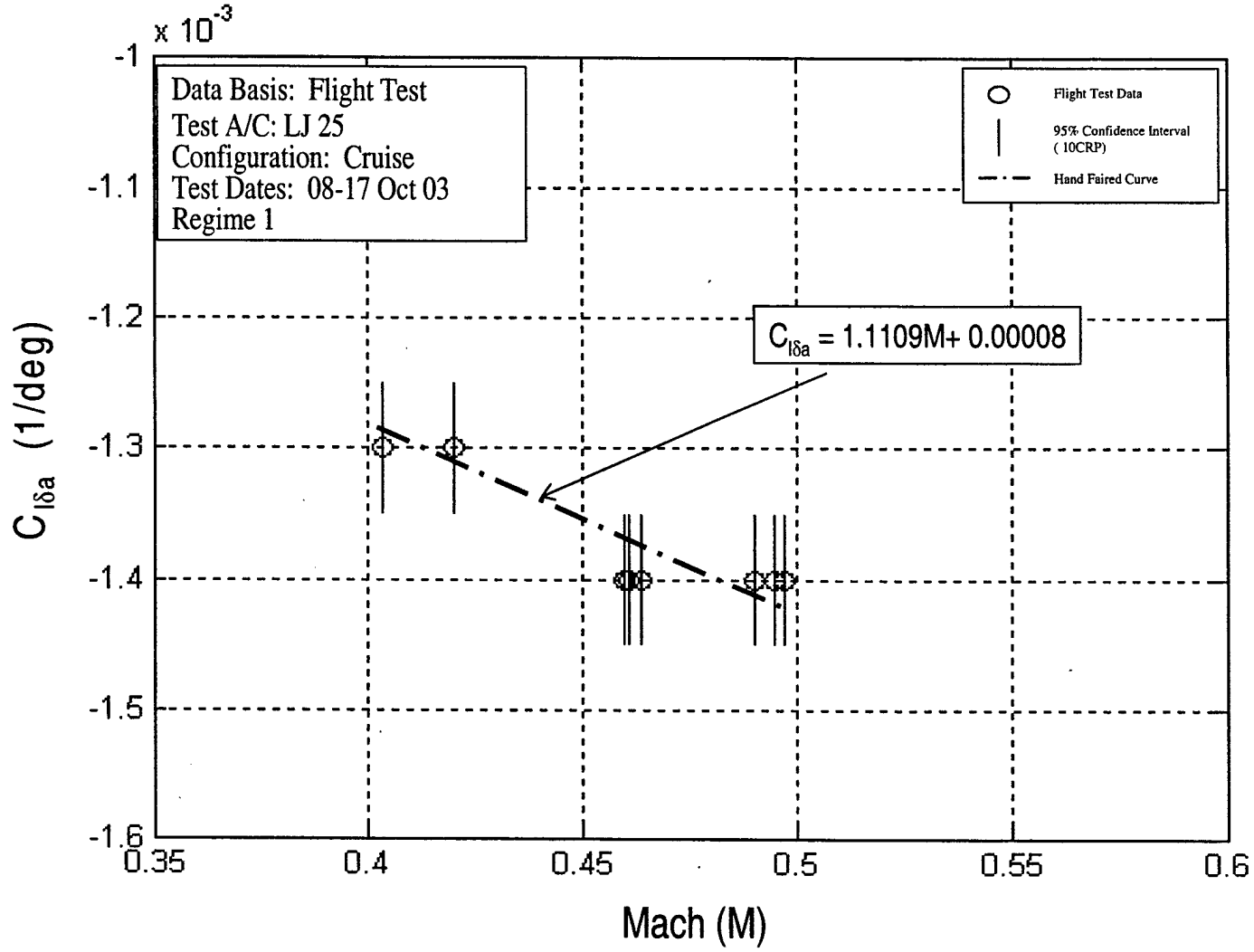

Figure F50: Learjet 25 $C_{l\delta a}$ vs. Mach Regime 1, Project HAVE TRIM

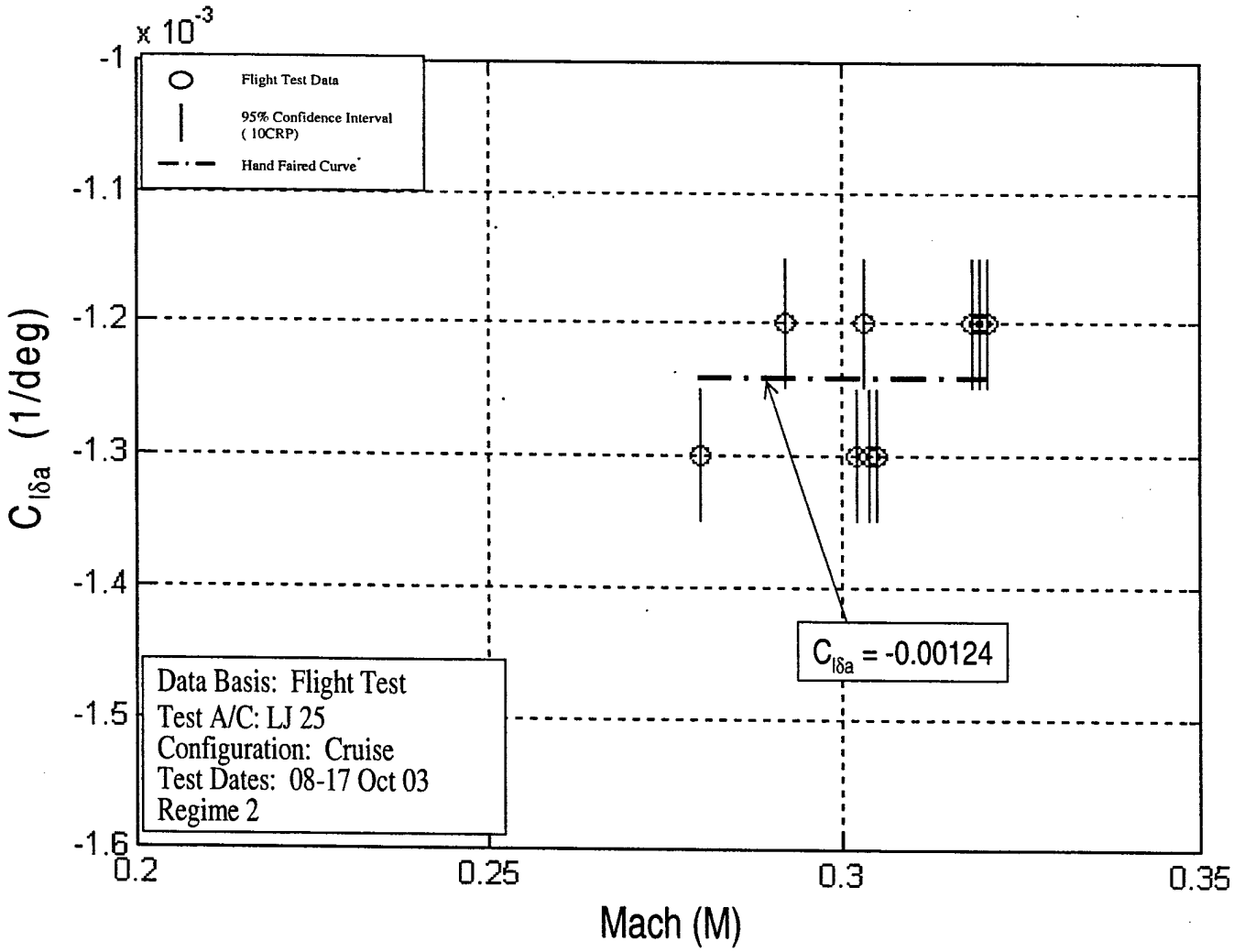

Figure F51: Learjet 25 $C_{l\delta a}$ vs. Mach Regime 2, Project HAVE TRIM

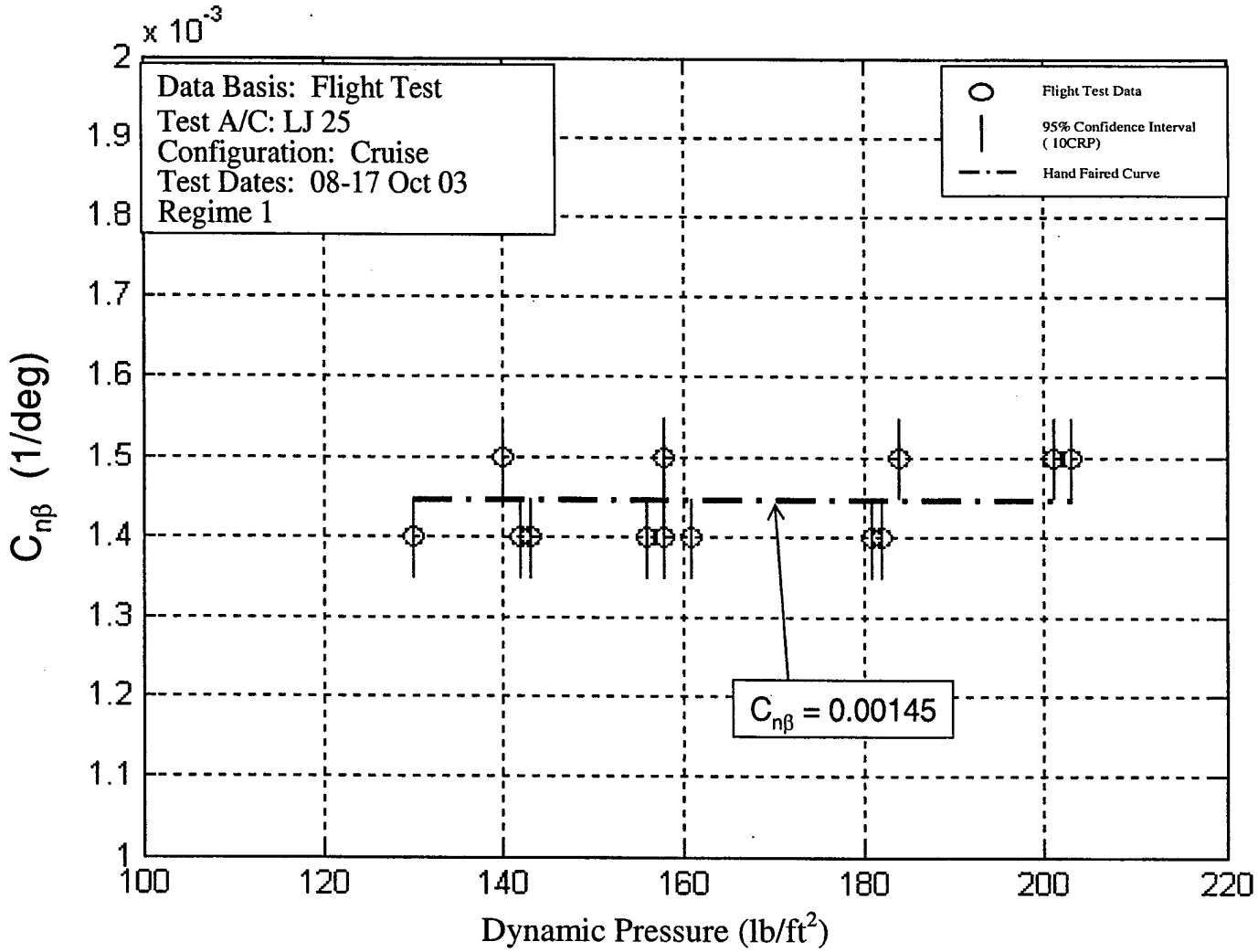

Figure F52: Learjet 25 $C_{n\beta}$ vs. q Regime 1, Project HAVE TRIM

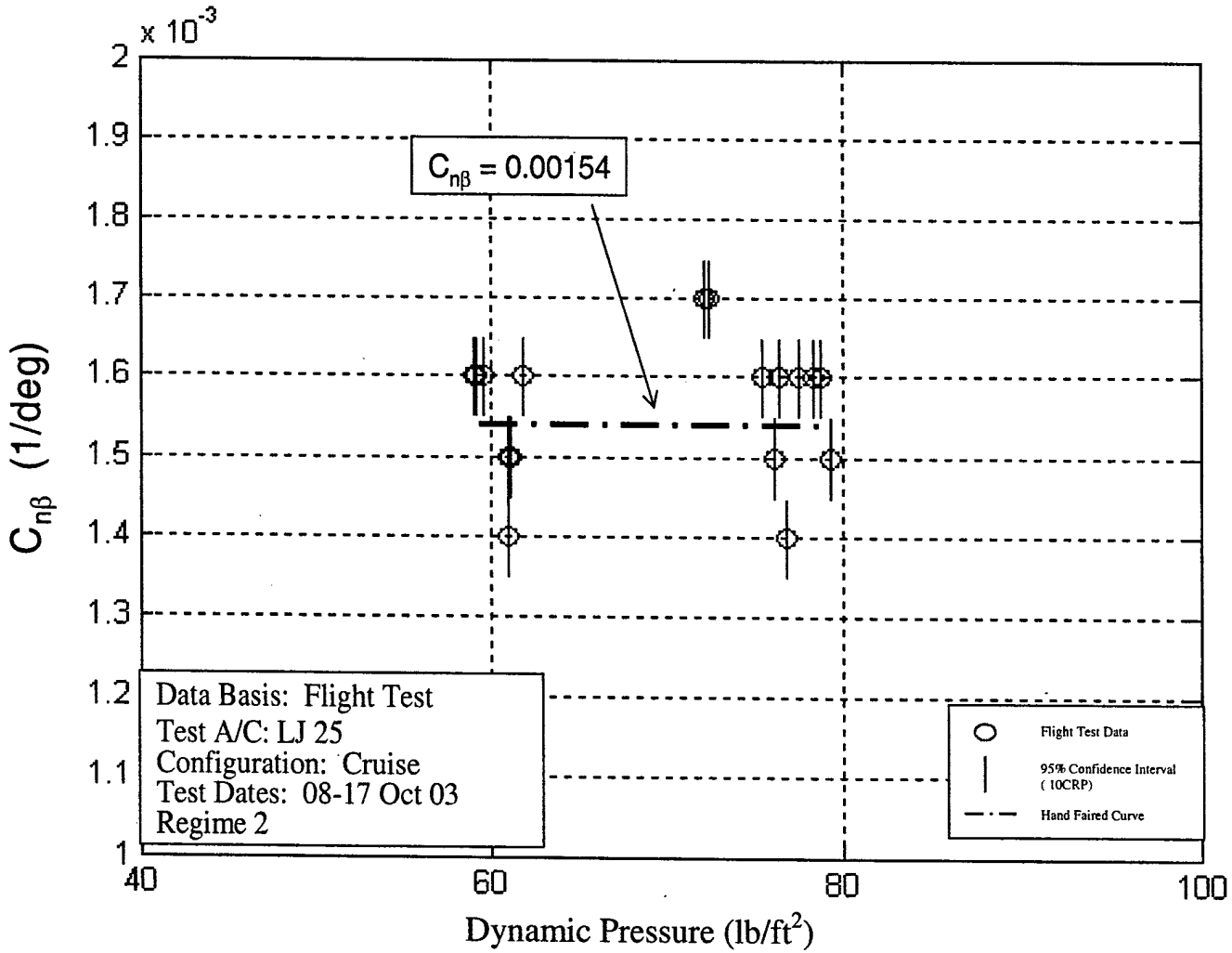

Figure F53: Learjet 25 $C_{n\beta}$ vs. q Regime 2, Project HAVE TRIM

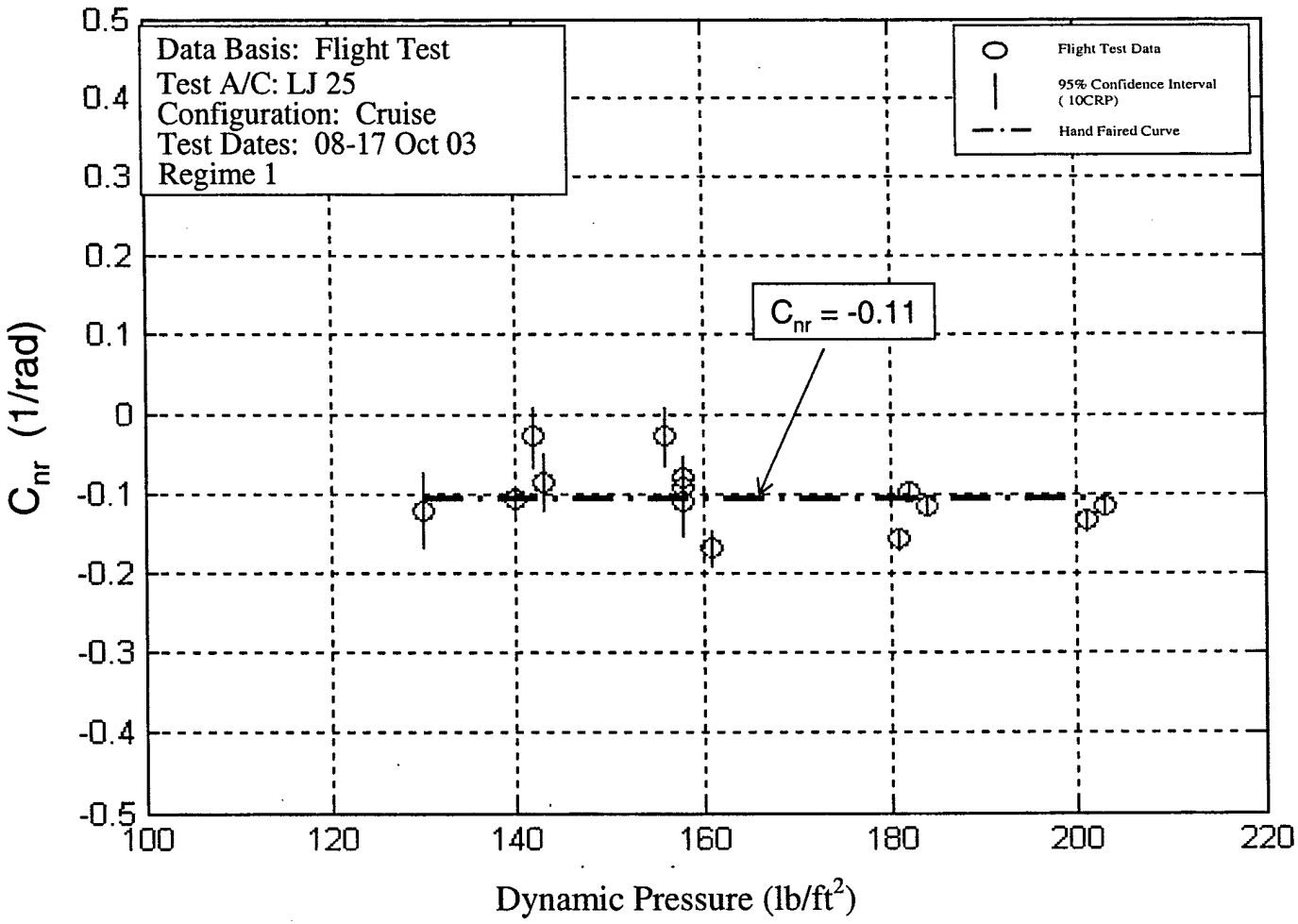

Figure F54: Learjet 25 C_{nr} vs. q Regime 1, Project HAVE TRIM

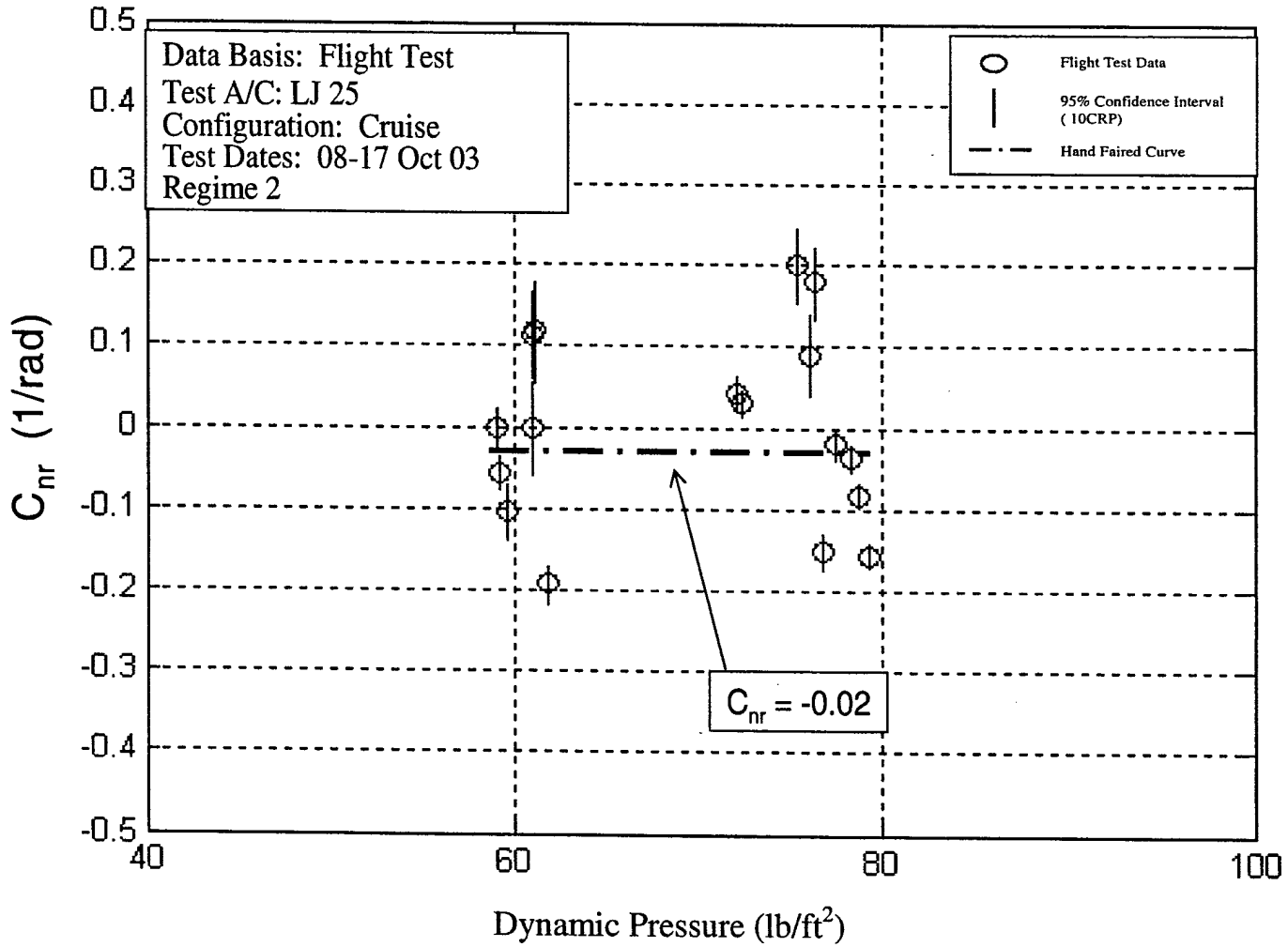

Figure F55: Learjet 25 C_{nr} vs. q Regime 2, Project HAVE TRIM

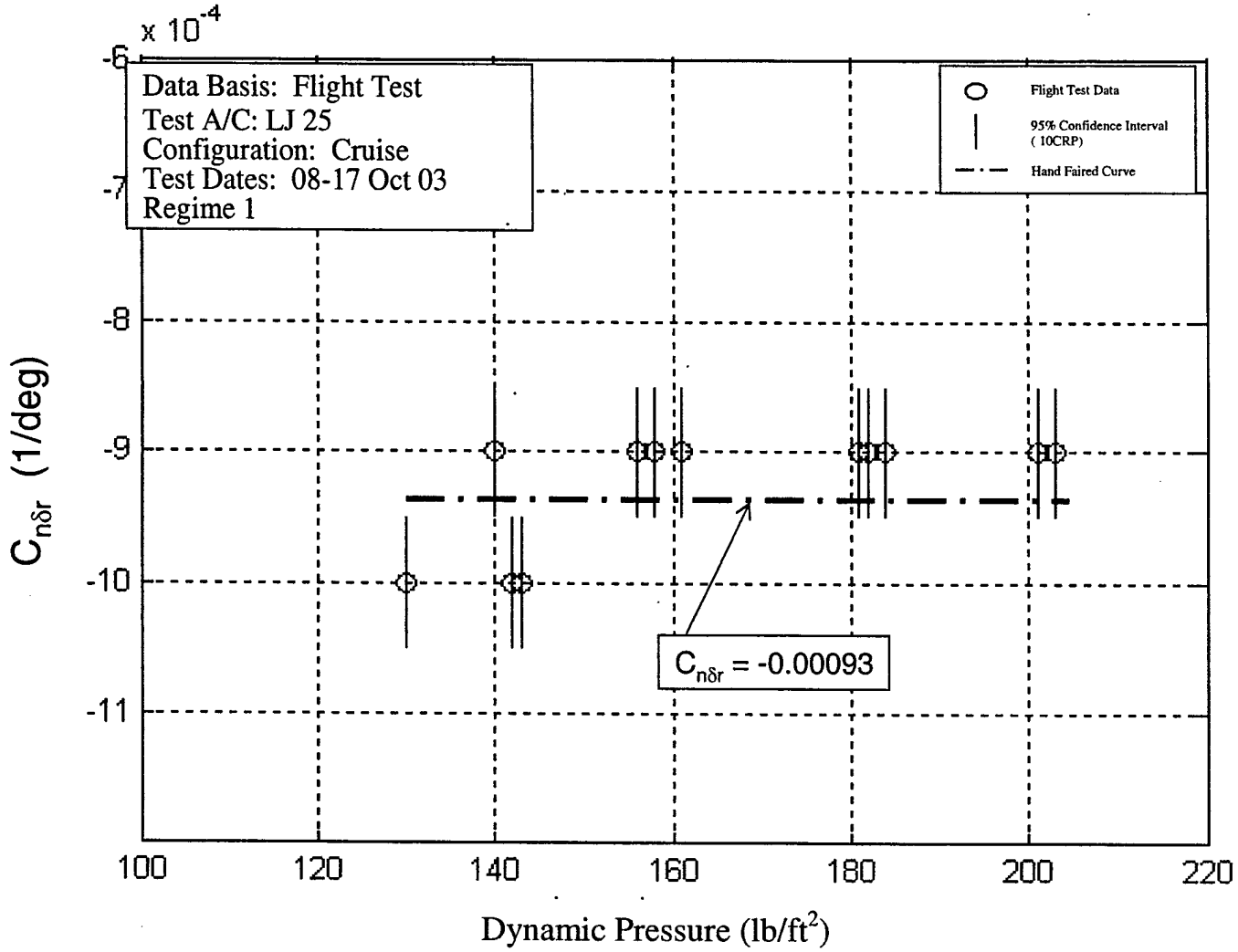

Figure F56: Learjet 25 $C_{n\delta r}$ vs. q Regime 1, Project HAVE TRIM

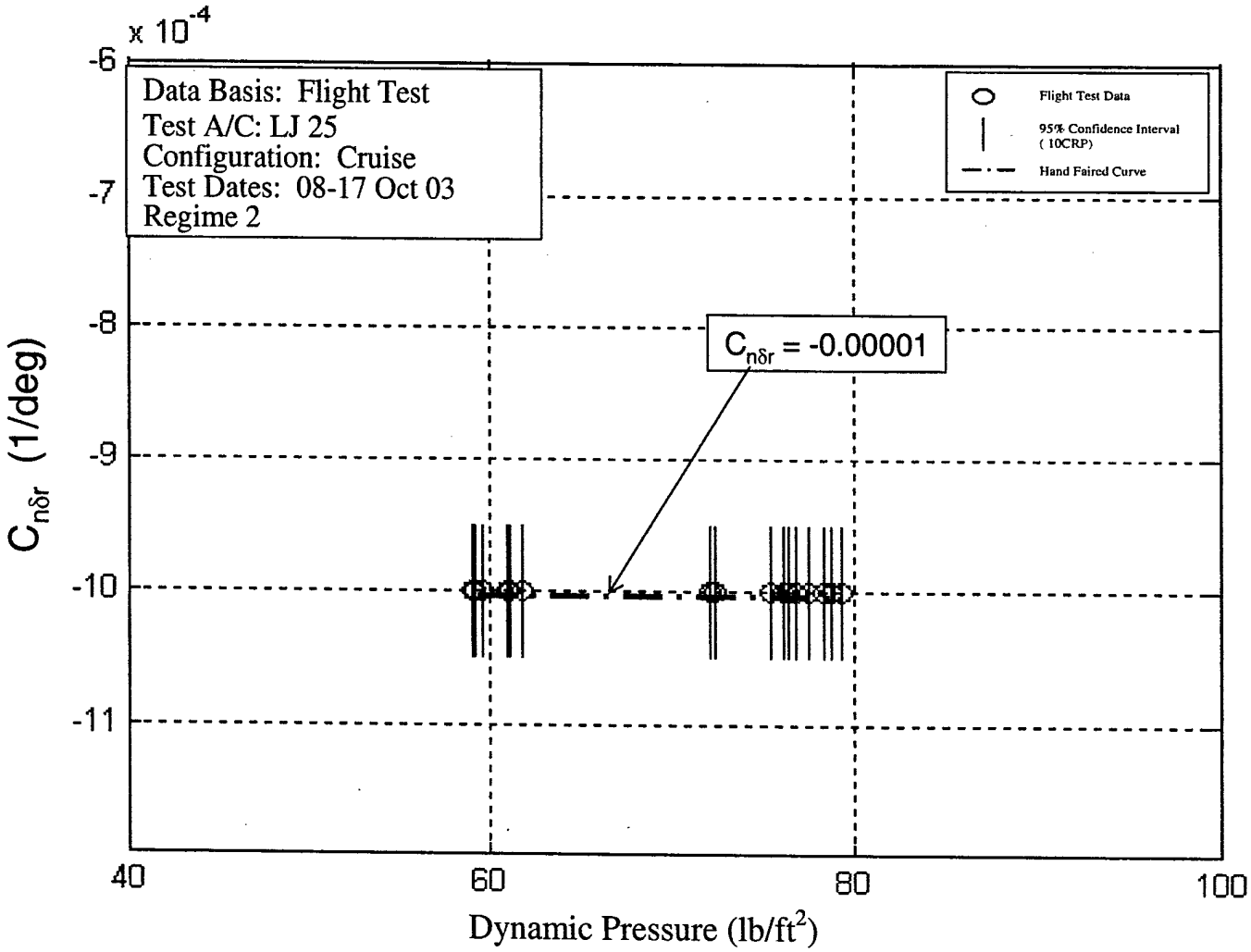

Figure F57: Learjet 25 $C_{n\delta r}$ vs. q Regime 2, Project HAVE TRIM

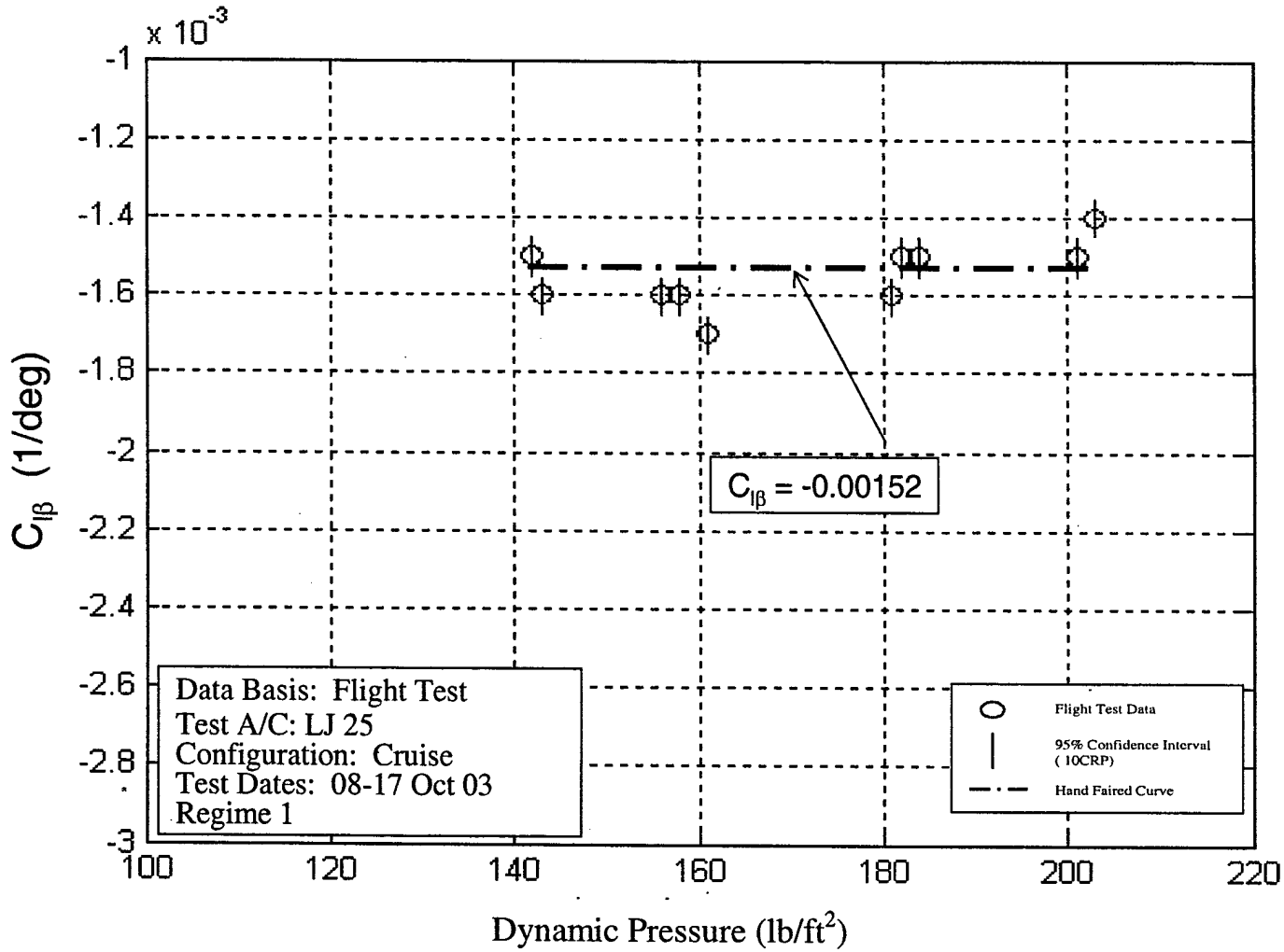

Figure F58: Learjet 25 $C_{l\beta}$ vs. q Regime 1, Project HAVE TRIM

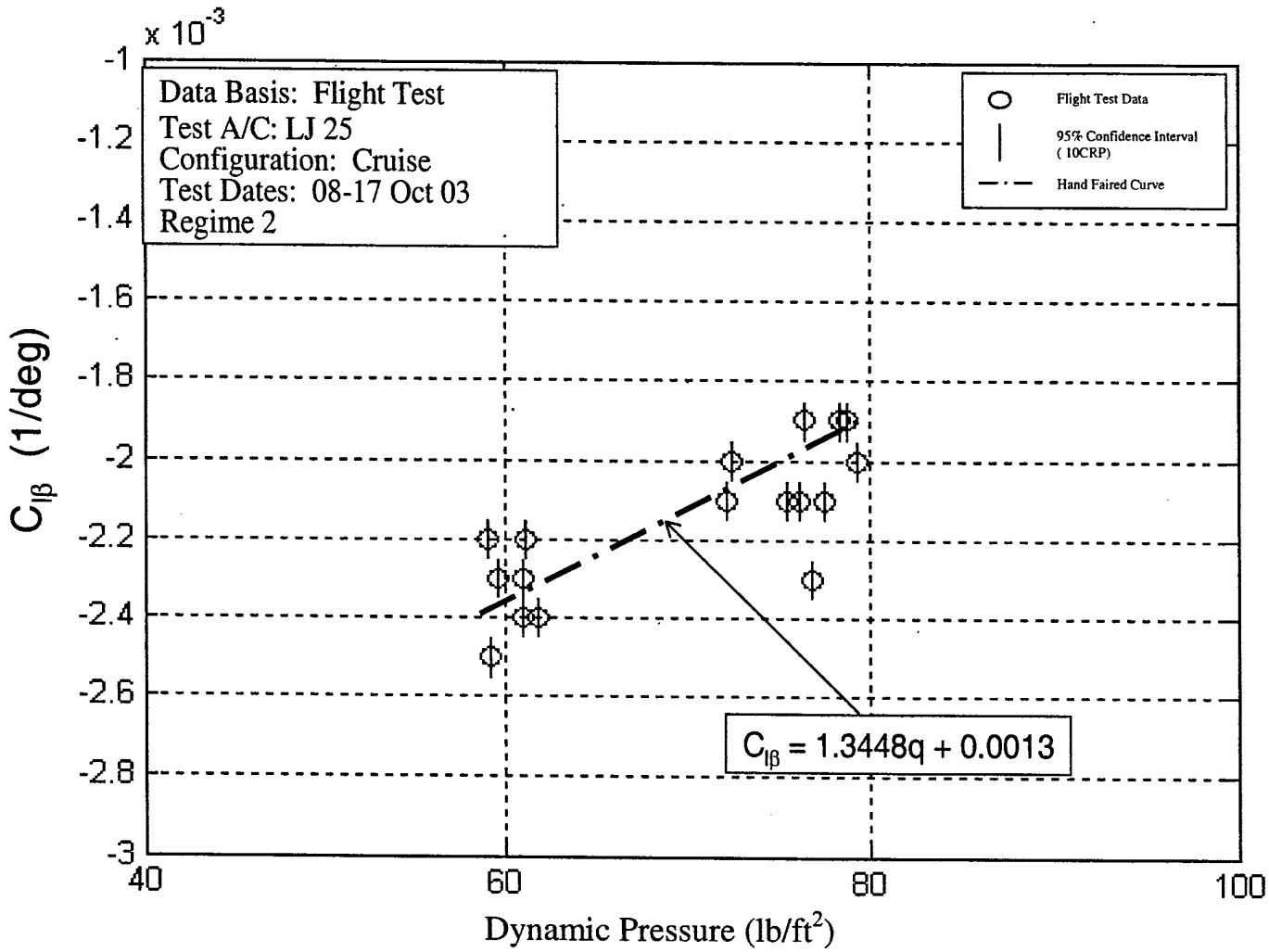

Figure F59: Learjet 25 $C_{l\beta}$ vs. q Regime 2, Project HAVE TRIM

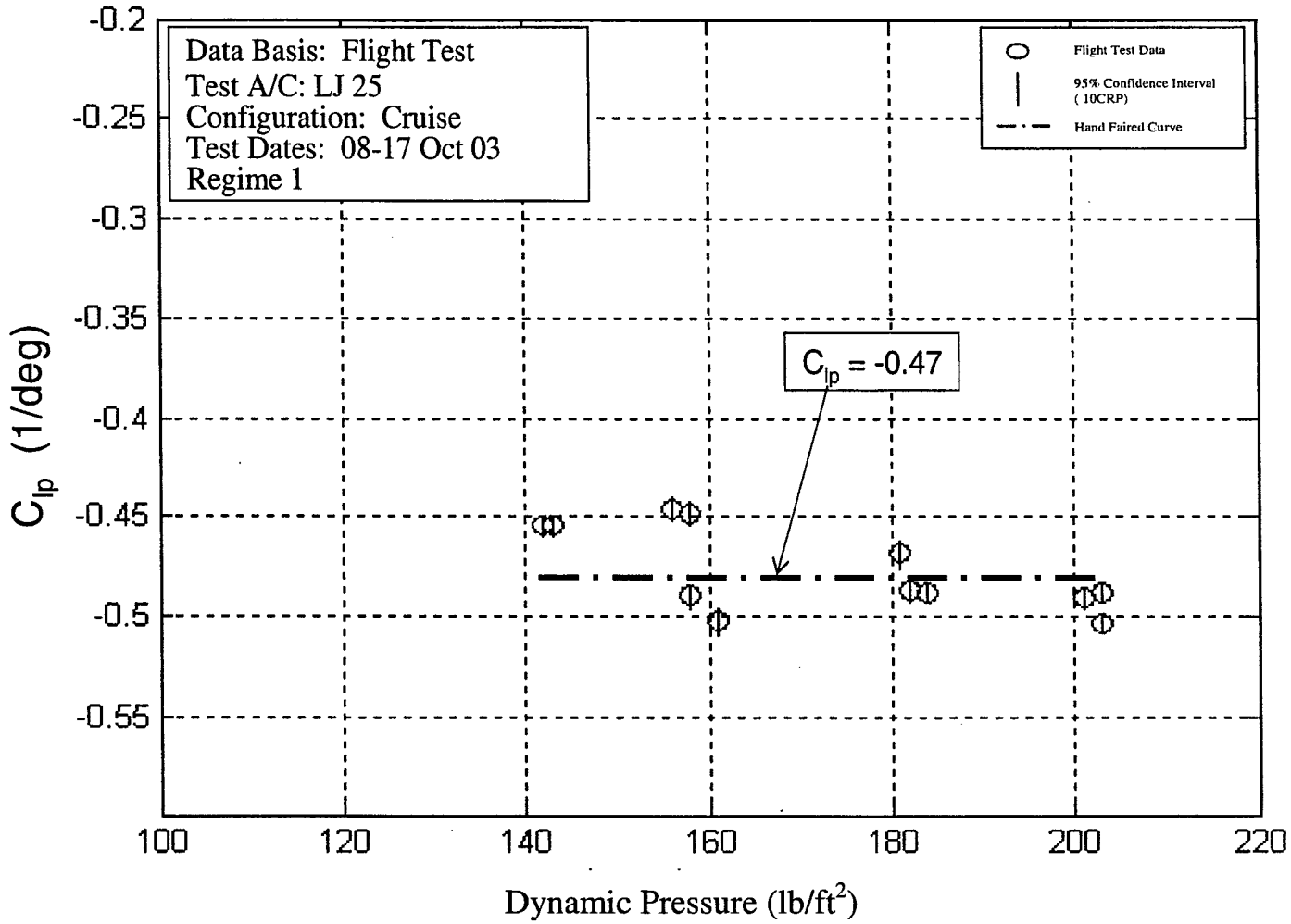

Figure F60: Learjet 25 C_{lp} vs. q Regime 1, Project HAVE TRIM

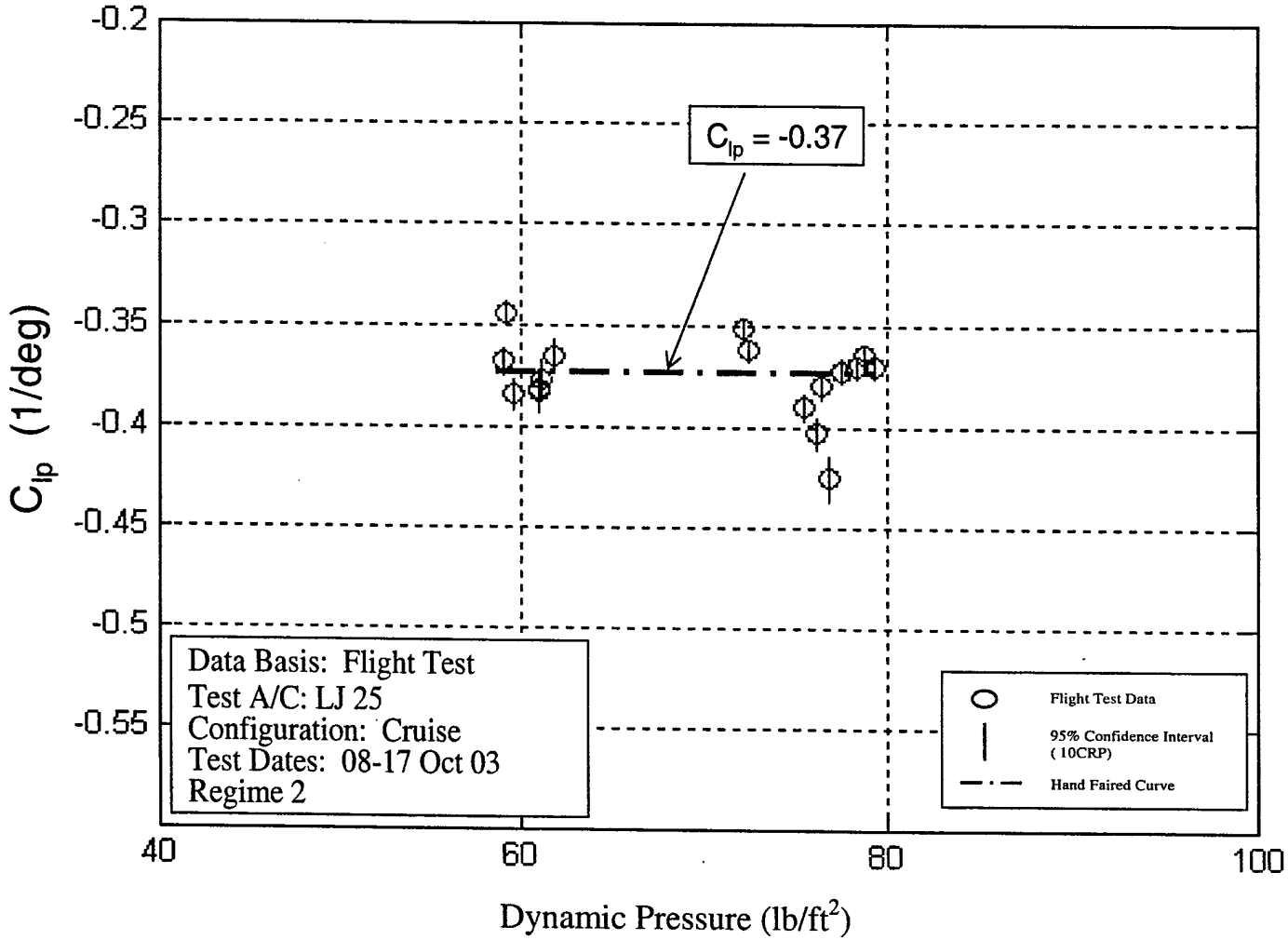

Figure F61: Learjet 25 C_{lp} vs. q Regime 2, Project HAVE TRIM

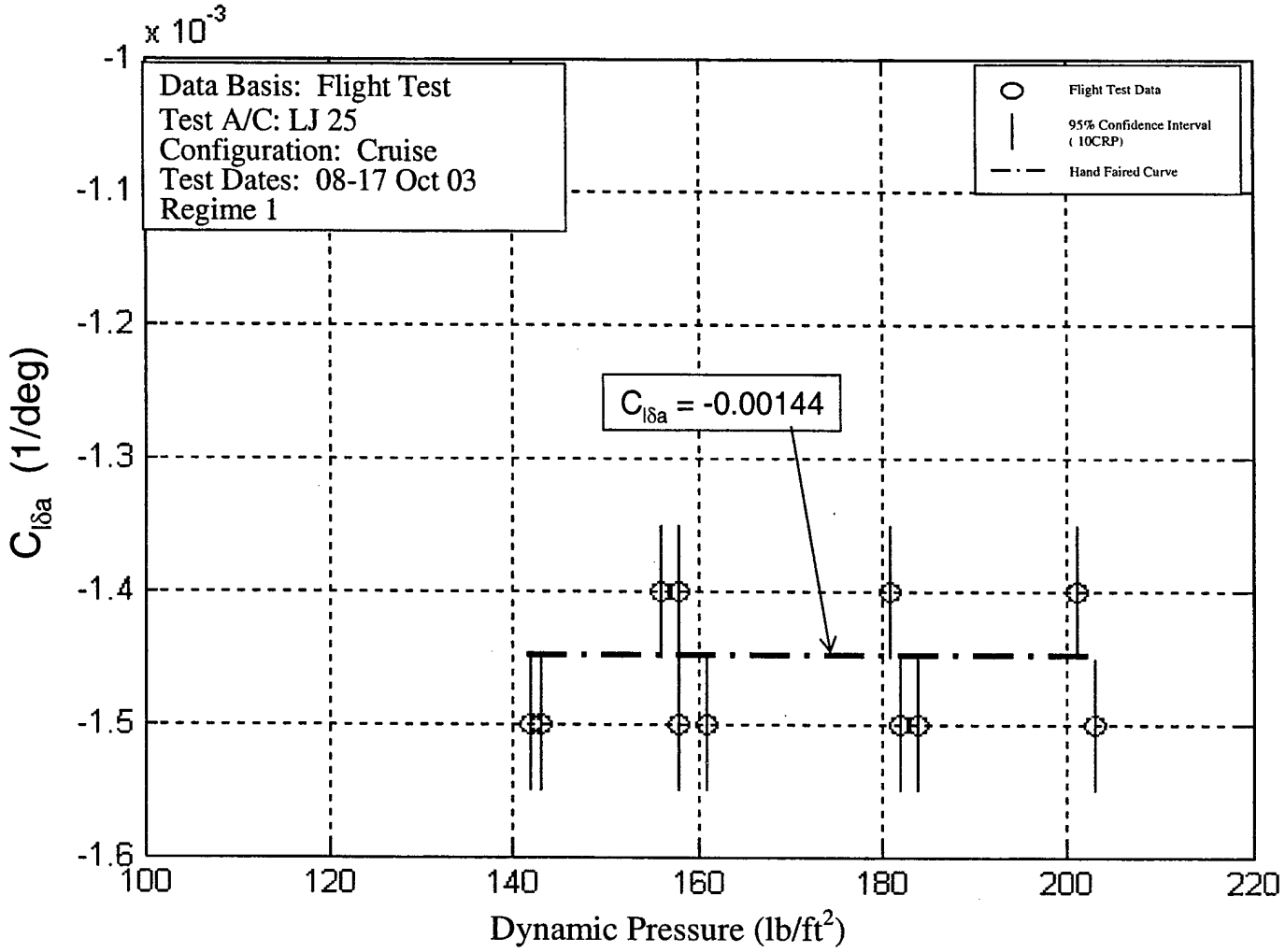

Figure F62: Learjet 25 $C_{l\delta a}$ vs. q Regime 1, Project HAVE TRIM

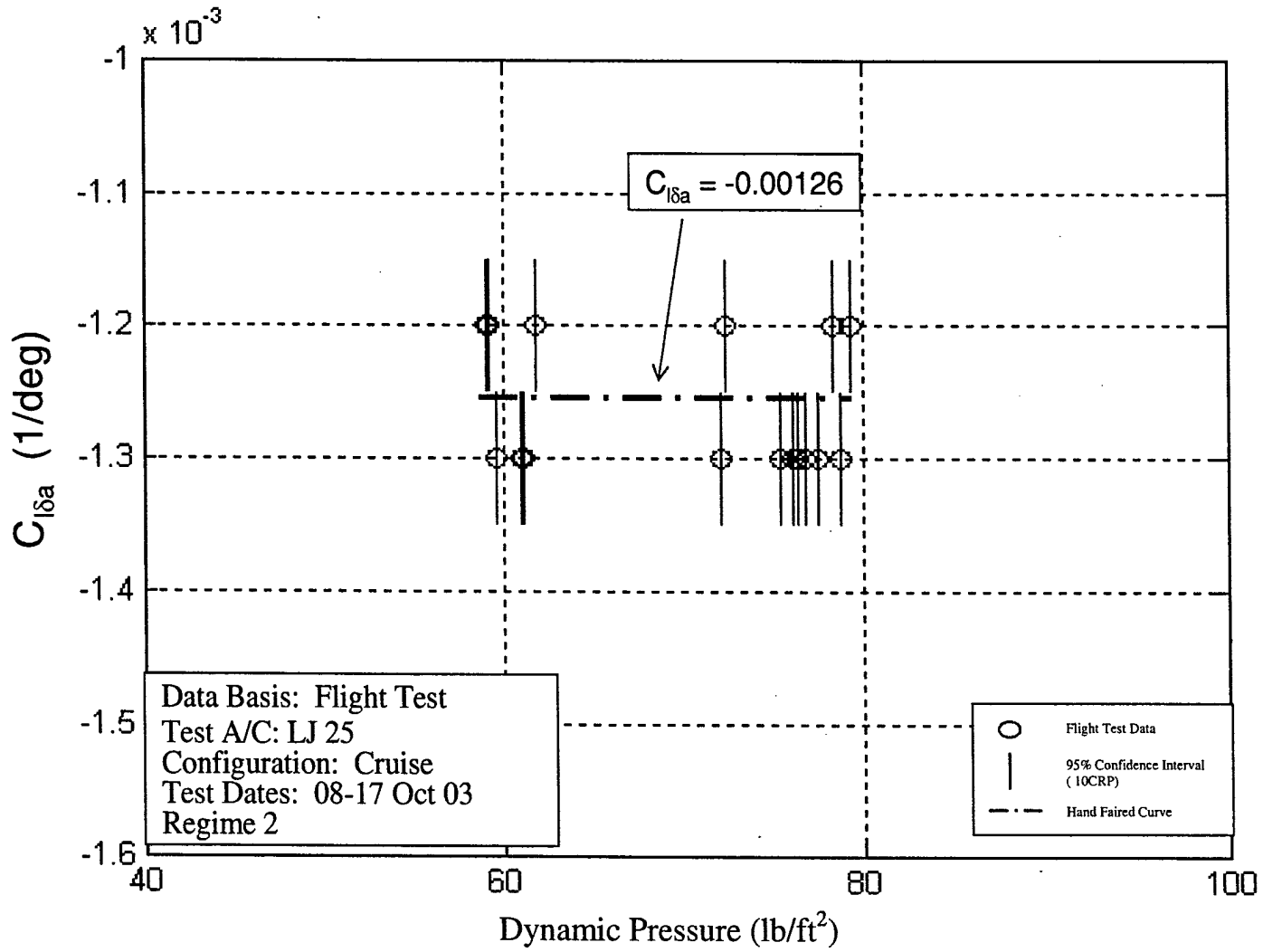

Figure F63: Learjet 25 $C_{l\delta a}$ vs. q Regime 2, Project HAVE TRIM

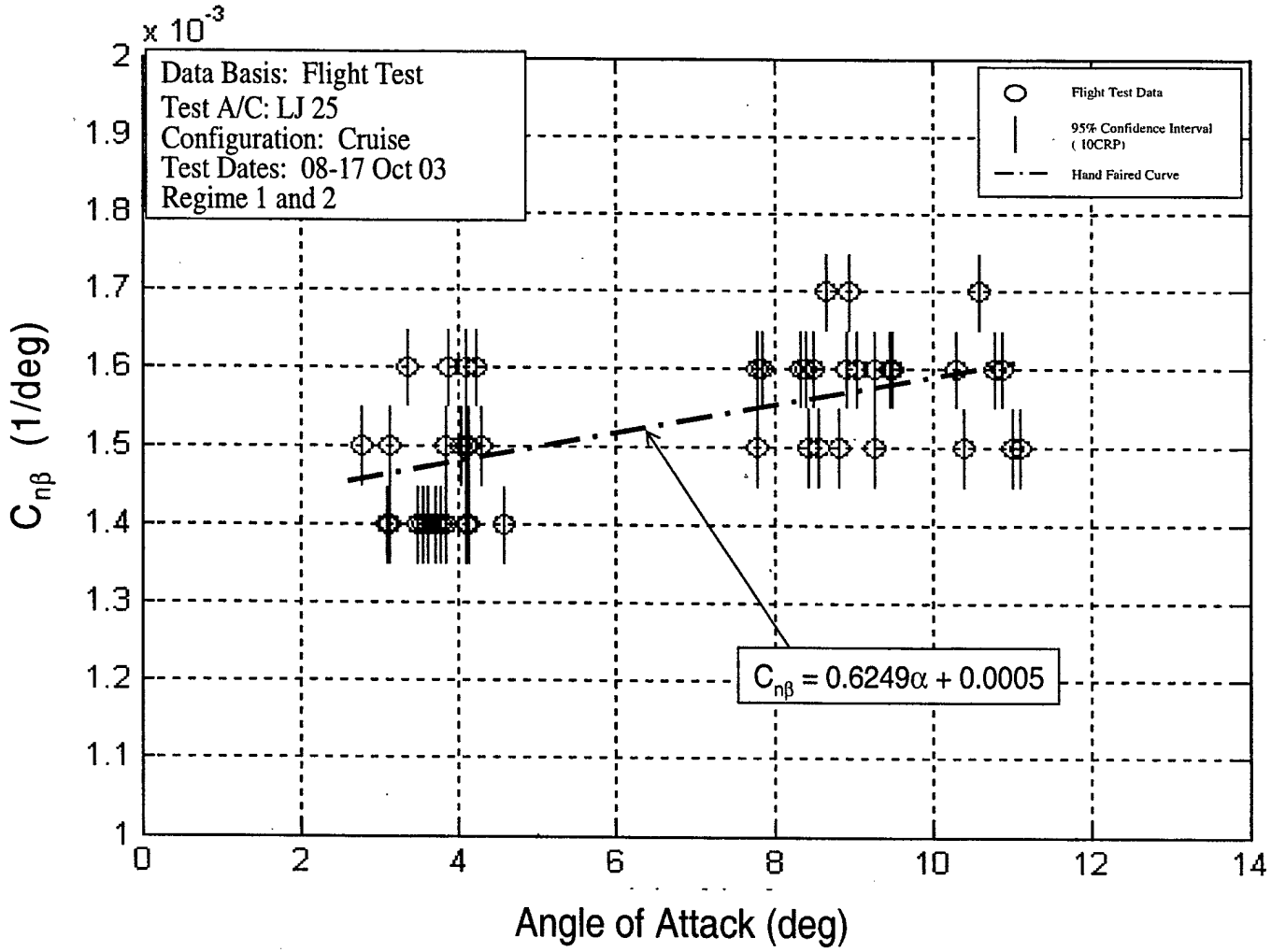

Figure F64: Learjet 25 $C_{n\beta}$ vs. α, Project HAVE TRIM

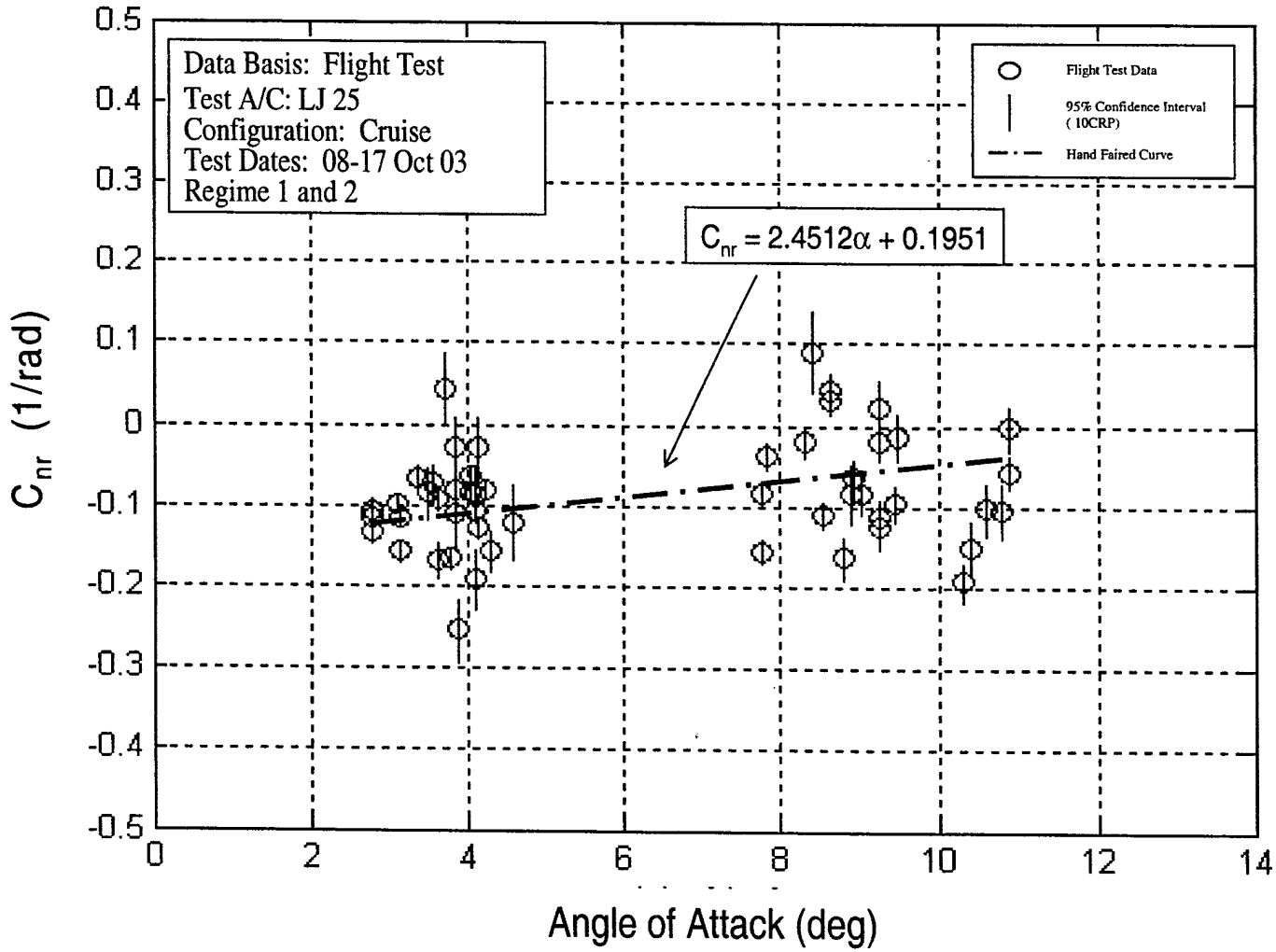

Figure F65: Learjet 25 C_{nr} vs. α, Project HAVE TRIM

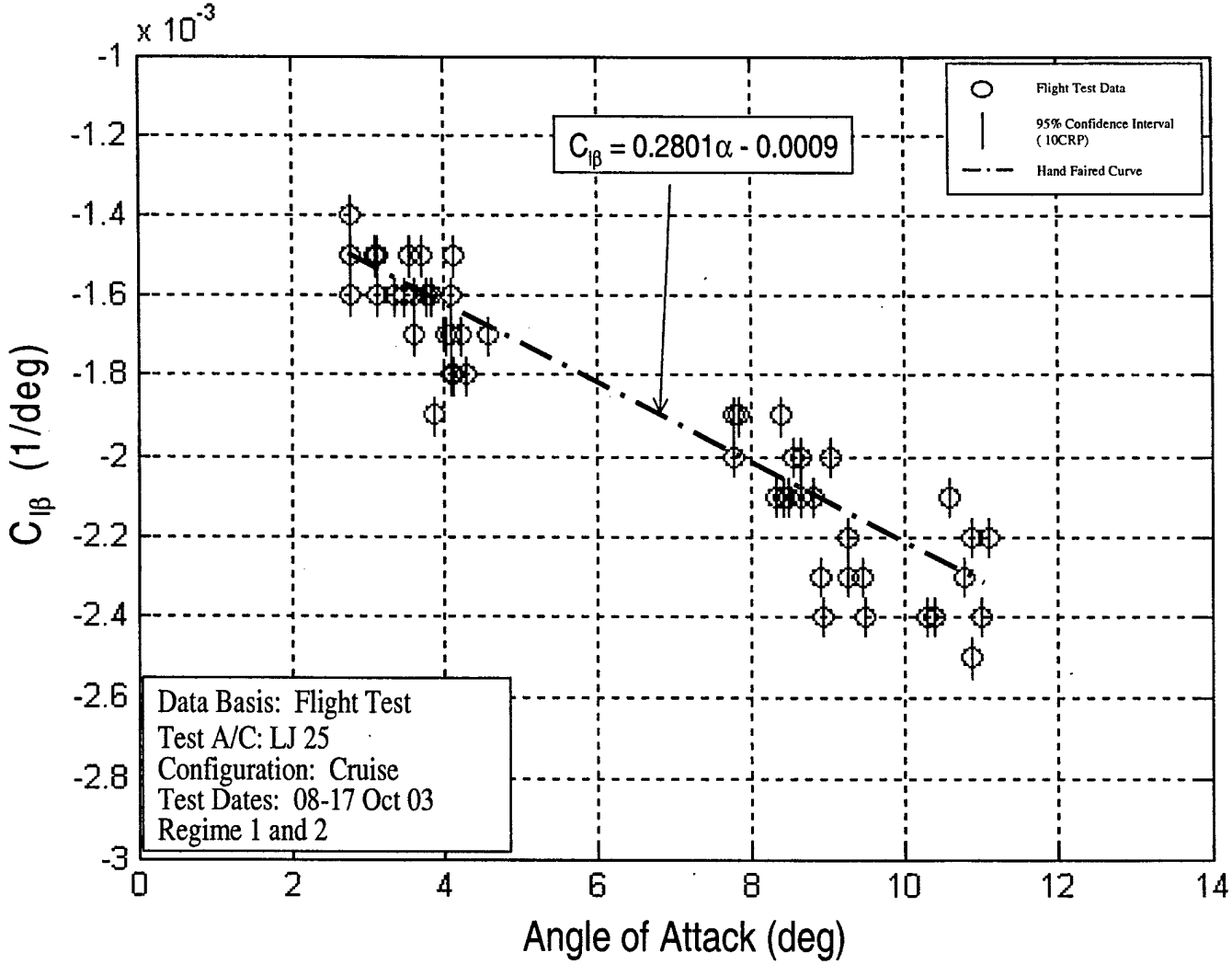

Figure F66: Learjet 25 $C_{l\beta}$ vs. α, Project HAVE TRIM

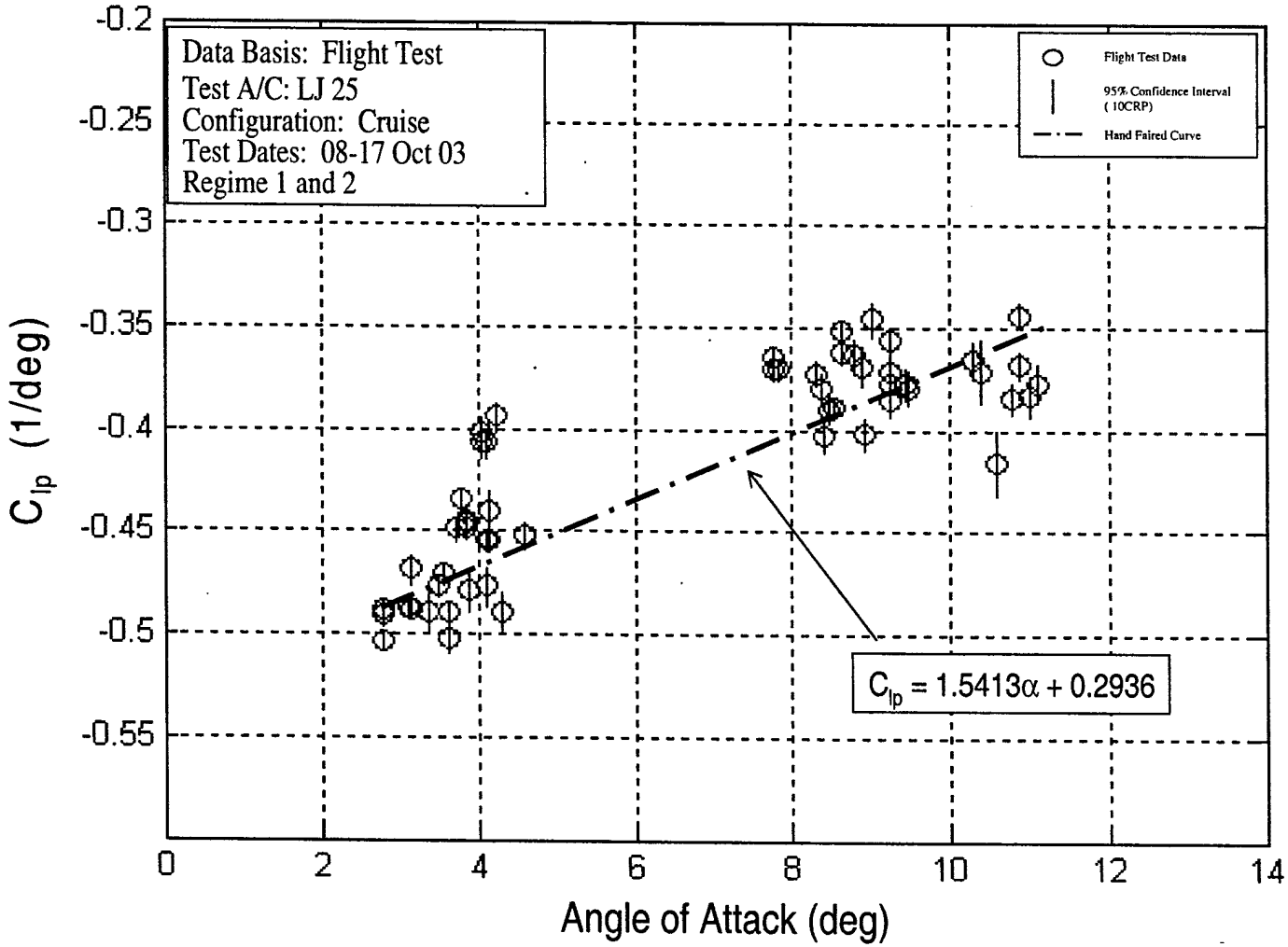

Figure F67: Learjet 25 C_{lp} vs. α, Project HAVE TRIM

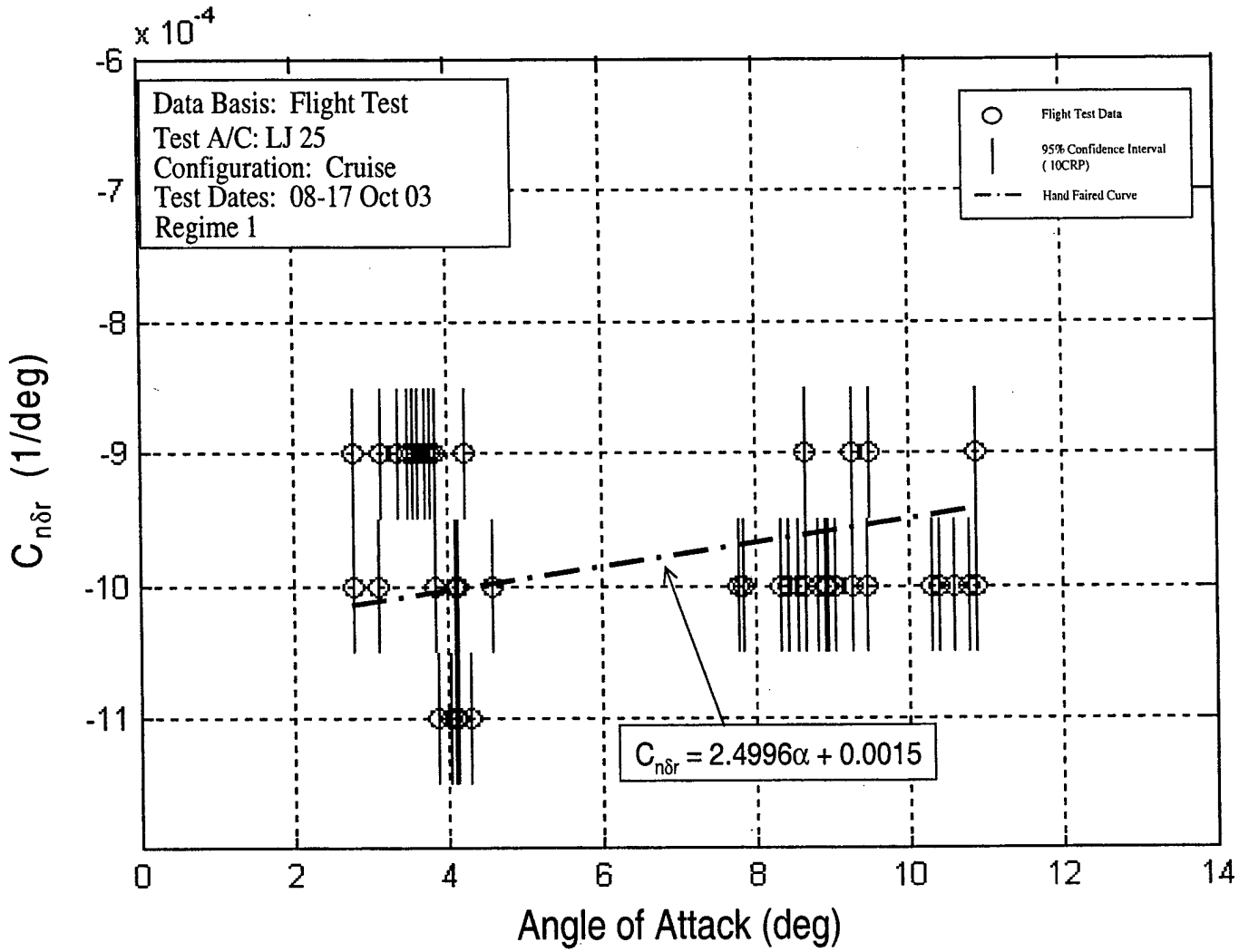

Figure F68: Learjet 25 $C_{n\delta r}$ vs. α, Project HAVE TRIM

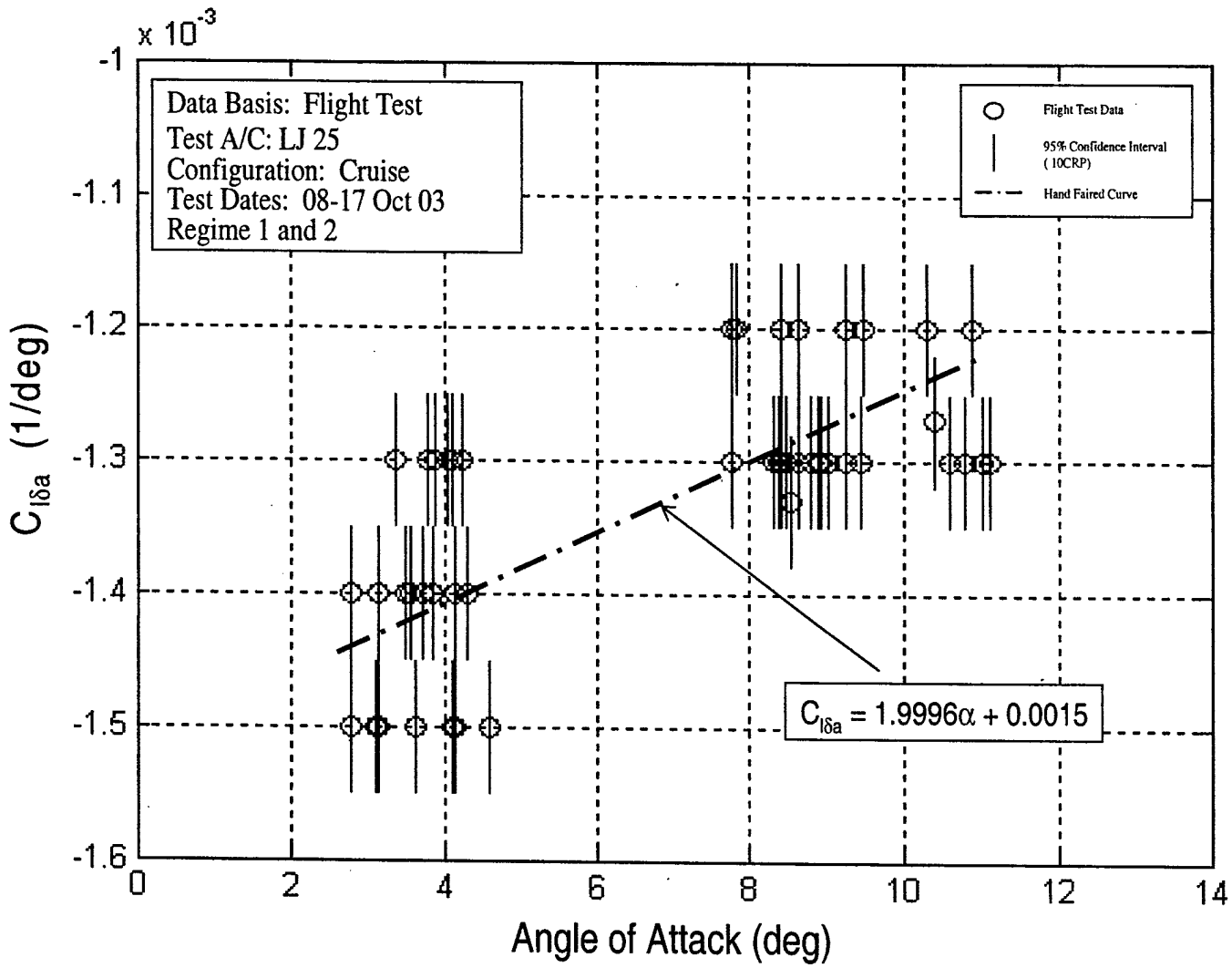

Figure F69: Learjet 25 $C_{l\delta a}$ vs. α, Project HAVE TRIM

APPENDIX G – DERIVATIVES LIST

Test Condition		Mach	qbar (lb/ft^2)	kias	alpha (deg)	Altitude (ft)	cla	cl0	cm0	cmde	cmq	clde	cma
Asymmetric Thrust	0%	0.401	159	441	4.06	10501	0.08413	0.01615	0.05115	-0.01438	-14.61725	0.00653	-0.01453
	10%	0.432	158	466	4.07	14575	0.08573	0.01145	0.04960	-0.01598	-14.81667	0.00690	-0.01503
	20%	0.439	163	475	3.76	14586	0.08504	0.00964	0.05367	-0.01498	-15.23000	0.00677	-0.01606
	30%	0.436	159	470	4.15	14740	0.08363	0.01365	0.05204	-0.01474	-15.16250	0.00691	-0.01556
Bank Angle	0 deg	0.444	164	478	3.75	14900	0.08475	0.00410	0.05345	-0.01470	-15.05000	0.00695	-0.01570
	15 deg	0.447	165	481	3.80	15157	0.08954	-0.00122	0.05722	-0.01606	-15.88000	0.00632	-0.01708
	30 deg	0.437	159	471	4.24	15000	0.08448	0.01912	0.05186	-0.01484	-15.04000	0.00680	-0.01570
	45 deg	0.437	159	471	4.90	14857	0.08418	0.04420	0.05074	-0.01464	-14.16000	0.00672	-0.01558
	60 deg	0.435	158	469	6.06	14843	0.08346	0.09682	0.04334	-0.01504	-14.20000	0.00522	-0.01452
5 deg Climb		0.434	156	468	4.09	15144	0.08408	0.02146	0.04882	-0.01464	-14.84000	0.00678	-0.01462
Max Angle Climb		0.435	159	471	3.75	14875	0.08658	0.01688	0.04775	-0.01525	-15.48333	0.00662	-0.01590
5 deg Descent		0.441	163	475	3.99	14643	0.08683	-0.00418	0.05638	-0.01443	-15.07500	0.00605	-0.01623
Push Over	0.4 g	0.440	163	481	1.54	14738	0.08796	-0.01179	0.05583	-0.01380	-13.67500	0.00645	-0.01713
	0.6 g	0.441	165	481	2.15	14543	0.09133	-0.00210	0.05399	-0.01373	-14.81429	0.00539	-0.01613
	0.8 g	0.443	164	482	3.14	14900	0.08896	0.00674	0.05351	-0.01379	-14.42857	0.00620	-0.01563
	1.0 g	0.437	158	471	3.98	15167	0.08937	-0.00135	0.05417	-0.01537	-15.28333	0.00607	-0.01617
Beta	0 deg	0.432	156	469	4.29	14800	0.08631	0.00610	0.05323	-0.01476	-15.06515	0.00644	-0.01552
	2 deg	0.442	163	479	4.09	14833	0.08631	0.00610	0.05323	-0.01476	-15.06515	0.00644	-0.01552
	-2 deg	0.448	165	486	3.87	15200	0.08631	0.00610	0.05323	-0.01476	-15.06515	0.00644	-0.01552
	4 deg	0.438	160	475	4.00	14920	0.08631	0.00610	0.05323	-0.01476	-15.06515	0.00644	-0.01552
Constant Mach, 0.44	10K	0.443	201	492	2.96	9729	0.09105	-0.00700	0.05718	-0.01362	-15.58333	0.00610	-0.01663
	12.5K	0.441	181	483	3.34	12100	0.08963	-0.00442	0.05493	-0.01453	-15.23333	0.00617	-0.01567
	15K	0.438	159	473	3.95	14994	0.08713	0.00333	0.05220	-0.01453	-15.17500	0.00600	-0.01484
	17.5K	0.438	145	468	4.11	17517	0.08653	0.00828	0.05810	-0.01505	-15.75000	0.00648	-0.01680
	20K	0.438	130	461	4.68	20083	0.08626	0.01506	0.05814	-0.01574	-15.46000	0.00688	-0.01660
Constant q	10K .40M	0.396	161	438	3.99	9687	0.08413	0.01615	0.05115	-0.01438	-14.62500	0.00653	-0.01453
	12.5K .42M	0.415	160	455	3.94	12257	0.08740	0.00158	0.05618	-0.01560	-15.62500	0.00615	-0.01628
	17.5K .46M	0.461	160	493	3.83	17471	0.08738	0.00410	0.05290	-0.01463	-15.42500	0.00650	-0.01523
	20.0K .48M	0.488	161	518	3.70	20200	0.08966	0.00444	0.05456	-0.01464	-15.80000	0.00656	-0.01552
Constant Altitude, 15K	190 KIAS	0.378	119	403	5.55	14907	0.08082	0.03675	0.04908	-0.01592	-15.14545	0.00658	-0.01455
	205 KIAS	0.413	142	444	4.48	14947	0.08420	0.01506	0.05231	-0.01537	-15.44000	0.00628	-0.01511
	220 KIAS	0.442	162	477	3.72	15050	0.08698	0.00548	0.05415	-0.01460	-15.31000	0.00623	-0.01569
	235 KIAS	0.469	184	508	3.49	14833	0.08871	0.00060	0.05350	-0.01378	-14.91250	0.00588	-0.01489
	250 KIAS	0.499	206	542	3.06	15125	0.09126	-0.00659	0.05400	-0.01319	-15.25000	0.00599	-0.01503

Table G1: Longitudinal Derivatives – Regime 1

Test Condition		Mach	qbar (lb/ft^2)	kias	alpha (deg)	Altitude (ft)	crcla	crcl0	crcm0	crcmde	crcmq	crclde	crcma
Asymmetric Thrust	0%	0.401	159	441	4.06	10501	0.00068	0.00288	0.00020	0.00010	0.16070	0.00025	0.00005
	10%	0.432	158	466	4.07	14575	0.00073	0.00310	0.00022	0.00010	0.16783	0.00030	0.00003
	20%	0.439	163	475	3.76	14586	0.00071	0.00281	0.00021	0.00009	0.16800	0.00029	0.00004
	30%	0.436	159	470	4.15	14740	0.00065	0.00303	0.00021	0.00009	0.15575	0.00030	0.00004
Bank Angle	0 deg	0.444	164	478	3.75	14900	0.00070	0.00280	0.00020	0.00010	0.15300	0.00030	0.00000
	15 deg	0.447	165	481	3.80	15157	0.00074	0.00298	0.00024	0.00010	0.18460	0.00030	0.00008
	30 deg	0.437	159	471	4.24	15000	0.00068	0.00316	0.00024	0.00010	0.16860	0.00030	0.00004
	45 deg	0.437	159	471	4.90	14857	0.00074	0.00388	0.00036	0.00010	0.19120	0.00030	0.00008
	60 deg	0.435	158	469	6.06	14843	0.00084	0.00606	0.00062	0.00010	0.21880	0.00034	0.00010
5 deg Climb		0.434	156	468	4.09	15144	0.00070	0.00310	0.00020	0.00010	0.15980	0.00030	0.00002
Max Angle Climb		0.435	159	471	3.75	14875	0.00073	0.00302	0.00022	0.00010	0.17350	0.00030	0.00003
5 deg Descent		0.441	163	475	3.99	14643	0.00075	0.00310	0.00020	0.00010	0.17050	0.00030	0.00005
Push Over	0.4 g	0.440	163	481	1.54	14738	0.00096	0.00159	0.00020	0.00010	0.27175	0.00033	0.00011
	0.6 g	0.441	165	481	2.15	14543	0.00101	0.00223	0.00019	0.00010	0.24243	0.00037	0.00010
	0.8 g	0.443	164	482	3.14	14900	0.00083	0.00264	0.00021	0.00010	0.19829	0.00030	0.00009
	1.0 g	0.437	158	471	3.98	15167	0.00072	0.00293	0.00023	0.00010	0.17250	0.00030	0.00005
Beta	0 deg	0.432	156	469	4.29	14800	0.00070	0.00285	0.00021	0.00010	0.16280	0.00028	0.00003
	2 deg	0.442	163	479	4.09	14833	0.00070	0.00285	0.00021	0.00010	0.16280	0.00028	0.00003
	-2 deg	0.448	165	486	3.87	15200	0.00070	0.00285	0.00021	0.00010	0.16280	0.00028	0.00003
	4 deg	0.438	160	475	4.00	14920	0.00070	0.00285	0.00021	0.00010	0.16280	0.00028	0.00003
Constant Mach, 0.44	10K	0.443	201	492	2.96	9729	0.00075	0.00235	0.00020	0.00008	0.19533	0.00028	0.00007
	12.5K	0.441	181	483	3.34	12100	0.00065	0.00240	0.00018	0.00008	0.16367	0.00025	0.00005
	15K	0.438	159	473	3.95	14994	0.00061	0.00255	0.00018	0.00006	0.14375	0.00023	0.00002
	17.5K	0.438	145	468	4.11	17517	0.00075	0.00335	0.00025	0.00010	0.19425	0.00030	0.00005
	20K	0.438	130	461	4.68	20083	0.00078	0.00396	0.00032	0.00010	0.20160	0.00030	0.00010
Constant q	10K .40M	0.396	161	438	3.99	9687	0.00068	0.00288	0.00020	0.00010	0.16050	0.00025	0.00005
	12.5K .42M	0.415	160	455	3.94	12257	0.00068	0.00280	0.00025	0.00010	0.17125	0.00023	0.00008
	17.5K .46M	0.461	160	493	3.83	17471	0.00060	0.00255	0.00020	0.00010	0.15825	0.00023	0.00000
	20.0K .48M	0.488	161	518	3.70	20200	0.00066	0.00262	0.00020	0.00010	0.16460	0.00030	0.00000
Constant Altitude, 15K	190 KIAS	0.378	119	403	5.55	14907	0.00064	0.00388	0.00030	0.00010	0.14718	0.00021	0.00003
	205 KIAS	0.413	142	444	4.48	14947	0.00063	0.00302	0.00020	0.00010	0.14800	0.00022	0.00003
	220 KIAS	0.442	162	477	3.72	15050	0.00070	0.00279	0.00022	0.00008	0.16500	0.00026	0.00003
	235 KIAS	0.469	184	508	3.49	14833	0.00061	0.00230	0.00015	0.00005	0.14400	0.00026	0.00001
	250 KIAS	0.499	206	542	3.06	15125	0.00068	0.00209	0.00011	0.00008	0.15875	0.00029	0.00003

Table G2: Longitudinal Cramer-Rao Bounds – Regime 1

Test Condition		Mach	qbar (lb/ft^2)	kias	alpha (deg)	Altitude (ft)	cnb	cnda	cndr	cnr	clb	clda	cldr	clp	cyb
Asymmetric Thrust	0%	0.401	159	441	4.06	10501	0.00160	-0.00005	-0.00105	-0.10115	-0.00170	-0.00140	0.00040	-0.39160	-0.01325
	10%	0.432	158	466	4.07	14575	0.00150	-0.00005	-0.00080	-0.16950	-0.00200	-0.00165	0.00030	-0.58650	-0.01375
	20%	0.439	163	475	3.76	14586	0.00160	-0.00008	-0.00090	-0.06055	-0.00168	-0.00128	0.00033	-0.42775	-0.01360
	30%	0.436	159	470	4.15	14740	0.00155	0.00000	-0.00085	-0.09360	-0.00170	-0.00130	0.00030	-0.40050	-0.01385
Bank Angle	0 deg	0.444	164	478	3.75	14900	0.00143	0.00000	-0.00090	-0.11907	-0.00157	-0.00137	0.00030	-0.43467	-0.01287
	15 deg	0.447	165	481	3.80	15157	0.00140	0.00000	-0.00090	-0.12380	-0.00150	-0.00140	0.00040	-0.44500	-0.01235
	30 deg	0.437	159	471	4.24	15000	0.00150	0.00000	-0.00090	-0.11950	-0.00165	-0.00140	0.00040	-0.44150	-0.01330
	45 deg	0.437	159	471	4.90	14857	0.00140	-0.00005	-0.00100	-0.17500	-0.00195	-0.00155	0.00045	-0.48200	-0.01330
	60 deg	0.435	158	469	6.06	14843	0.00140	-0.00005	-0.00100	-0.17500	-0.00195	-0.00155	0.00045	-0.48200	-0.01330
5 deg Climb		0.434	156	468	4.09	15144	0.00143	-0.00003	-0.00090	-0.14000	-0.00175	-0.00135	0.00030	-0.44000	-0.01323
Max Angle Climb		0.435	159	471	3.75	14875	0.00140	0.00000	-0.00095	-0.11950	-0.00140	-0.00130	0.00030	-0.41300	-0.01255
5 deg Descent		0.441	163	475	3.99	14643	0.00150	0.00005	-0.00090	-0.11040	-0.00175	-0.00160	0.00040	-0.49250	-0.01240
Push Over	0.4 g	0.440	163	481	1.54	14738	0.00148	-0.00004	-0.00093	-0.14552	-0.00167	-0.00142	0.00036	-0.44900	-0.01319
	0.6 g	0.441	165	481	2.15	14543	0.00148	-0.00004	-0.00093	-0.14552	-0.00167	-0.00142	0.00036	-0.44900	-0.01319
	0.8 g	0.443	164	482	3.14	14900	0.00148	-0.00004	-0.00093	-0.14552	-0.00167	-0.00142	0.00036	-0.44900	-0.01319
	1.0 g	0.437	158	471	3.98	15167	0.00148	-0.00004	-0.00093	-0.14552	-0.00167	-0.00142	0.00036	-0.44900	-0.01319
Beta	0 deg	0.432	156	469	4.29	14800	0.00145	-0.00010	-0.00085	-0.27800	-0.00185	-0.00140	0.00035	-0.48200	-0.01355
	2 deg	0.442	163	479	4.09	14833	0.00173	-0.00010	-0.00083	-0.28233	-0.00203	-0.00133	0.00030	-0.45467	-0.01313
	-2 deg	0.448	165	486	3.87	15200	0.00185	-0.00010	-0.00090	-0.27500	-0.00210	-0.00130	0.00025	-0.44500	-0.01485
	4 deg	0.438	160	475	4.00	14920	0.00152	-0.00002	-0.00086	-0.18600	-0.00150	-0.00138	0.00044	-0.44080	-0.01468
Constant Mach, 0.44	10K	0.443	201	492	2.96	9729	0.00150	0.00000	-0.00087	-0.11833	-0.00143	-0.00147	0.00037	-0.49400	-0.01323
	12.5K	0.441	181	483	3.34	12100	0.00143	0.00000	-0.00090	-0.12257	-0.00153	-0.00147	0.00037	-0.48133	-0.01323
	15K	0.438	159	473	3.95	14994	0.00136	0.00000	-0.00090	-0.09552	-0.00162	-0.00144	0.00034	-0.46620	-0.01326
	17.5K	0.438	145	468	4.11	17517	0.00140	0.00000	-0.00100	-0.05690	-0.00155	-0.00150	0.00040	-0.45400	-0.01325
	20K	0.438	130	461	4.68	20083	0.00140	0.00000	-0.00100	0.07650	-0.00170	-0.00150	0.00040	-0.45200	-0.01410
Constant q	10K .40M	0.396	161	438	3.99	9687	0.00130	0.00000	-0.00090	-0.10070	-0.00143	-0.00123	0.00030	-0.39800	-0.01243
	12.5K .42M	0.415	160	455	3.94	12257	0.00140	-0.00007	-0.00090	-0.14667	-0.00153	-0.00130	0.00030	-0.43567	-0.01317
	17.5K .46M	0.461	160	493	3.83	17471	0.00133	0.00000	-0.00090	-0.02090	-0.00153	-0.00140	0.00030	-0.45200	-0.01343
	20.0K .48M	0.488	161	518	3.70	20200	0.00137	0.00000	-0.00090	-0.05853	-0.00150	-0.00140	0.00040	-0.47100	-0.01307
Constant Altitude, 15K	190 KIAS	0.378	119	403	5.55	14907	0.00120	-0.00003	-0.00083	-0.03890	-0.00143	-0.00115	0.00030	-0.34675	-0.01310
	205 KIAS	0.413	142	444	4.48	14947	0.00144	-0.00002	-0.00094	-0.05970	-0.00180	-0.00144	0.00036	-0.47120	-0.01318
	220 KIAS	0.442	162	477	3.72	15050	0.00143	0.00000	-0.00090	-0.08385	-0.00155	-0.00150	0.00040	-0.48775	-0.01310
	235 KIAS	0.469	184	508	3.49	14833	0.00130	-0.00010	-0.00090	-0.21800	-0.00160	-0.00120	0.00020	-0.43200	-0.01350

Table G3: Lateral-Directional Derivatives – Regime 1

Test Condition		Mach	qbar (lb/ft^2)	kias	alpha (deg)	Altitude (ft)	crcnb	crcnda	crcndr	crcnr	crclb	crclda	crcldr	crclp	crcyb
Asymmetric Thrust	0%	0.401	159	441	4.06	10501	0.00010	0.00010	0.00010	0.00435	0.00010	0.00010	0.00010	0.00200	1.22380
	10%	0.432	158	466	4.07	14575	0.00010	0.00010	0.00010	0.00360	0.00010	0.00010	0.00010	0.00290	1.36500
	20%	0.439	163	475	3.76	14586	0.00010	0.00010	0.00010	0.00340	0.00010	0.00010	0.00010	0.00203	1.60350
	30%	0.436	159	470	4.15	14740	0.00010	0.00010	0.00010	0.00240	0.00010	0.00010	0.00010	0.00150	1.41500
Bank Angle	0 deg	0.444	164	478	3.75	14900	0.00010	0.00010	0.00010	0.00197	0.00010	0.00010	0.00010	0.00120	0.49767
	15 deg	0.447	165	481	3.80	15157	0.00010	0.00010	0.00010	0.00175	0.00010	0.00010	0.00010	0.00120	0.98200
	30 deg	0.437	159	471	4.24	15000	0.00010	0.00010	0.00010	0.00200	0.00010	0.00010	0.00010	0.00125	0.70800
	45 deg	0.437	159	471	4.90	14857	0.00010	0.00010	0.00010	0.00315	0.00010	0.00010	0.00010	0.00200	0.84650
	60 deg	0.435	158	469	6.06	14843	0.00010	0.00010	0.00010	0.00315	0.00010	0.00010	0.00010	0.00200	0.84650
5 deg Climb		0.434	156	468	4.09	15144	0.00010	0.00010	0.00010	0.00365	0.00010	0.00010	0.00010	0.00165	0.54975
Max Angle Climb		0.435	159	471	3.75	14875	0.00010	0.00010	0.00010	0.00320	0.00010	0.00010	0.00010	0.00130	0.64750
5 deg Descent		0.441	163	475	3.99	14643	0.00010	0.00010	0.00010	0.00240	0.00010	0.00010	0.00010	0.00165	1.20850
Push Over	0.4 g	0.440	163	481	1.54	14738	0.00010	0.00010	0.00010	0.00443	0.00010	0.00010	0.00010	0.00159	0.88443
	0.6 g	0.441	165	481	2.15	14543	0.00010	0.00010	0.00010	0.00443	0.00010	0.00010	0.00010	0.00159	0.88443
	0.8 g	0.443	164	482	3.14	14900	0.00010	0.00010	0.00010	0.00443	0.00010	0.00010	0.00010	0.00159	0.88443
	1.0 g	0.437	158	471	3.98	15167	0.00010	0.00010	0.00010	0.00443	0.00010	0.00010	0.00010	0.00159	0.88443
Beta	0 deg	0.432	156	469	4.29	14800	0.00010	0.00010	0.00010	0.00600	0.00010	0.00010	0.00010	0.00205	1.39500
	2 deg	0.442	163	479	4.09	14833	0.00010	0.00010	0.00010	0.00933	0.00010	0.00010	0.00010	0.00210	2.44333
	-2 deg	0.448	165	486	3.87	15200	0.00010	0.00010	0.00010	0.00840	0.00010	0.00010	0.00010	0.00235	2.71500
	4 deg	0.438	160	475	4.00	14920	0.00010	0.00010	0.00010	0.00838	0.00010	0.00010	0.00010	0.00192	1.42480
Constant Mach, 0.44	10K	0.443	201	492	2.96	9729	0.00010	0.00010	0.00010	0.00280	0.00010	0.00010	0.00010	0.00097	0.52467
	12.5K	0.441	181	483	3.34	12100	0.00010	0.00010	0.00010	0.00260	0.00010	0.00010	0.00010	0.00123	0.58133
	15K	0.438	159	473	3.95	14994	0.00010	0.00010	0.00010	0.00596	0.00010	0.00010	0.00010	0.00130	0.25088
	17.5K	0.438	145	468	4.11	17517	0.00010	0.00010	0.00010	0.00765	0.00010	0.00010	0.00010	0.00120	0.11470
	20K	0.438	130	461	4.68	20083	0.00010	0.00010	0.00010	0.00990	0.00010	0.00010	0.00010	0.00140	-0.28200
Constant q	10K .40M	0.396	161	438	3.99	9687	0.00010	0.00010	0.00010	0.00307	0.00010	0.00010	0.00010	0.00110	0.44667
	12.5K .42M	0.415	160	455	3.94	12257	0.00010	0.00010	0.00010	0.00300	0.00010	0.00010	0.00010	0.00123	-0.07833
	17.5K .46M	0.461	160	493	3.83	17471	0.00010	0.00010	0.00010	0.00847	0.00010	0.00010	0.00010	0.00120	0.12440
	20.0K .48M	0.488	161	518	3.70	20200	0.00010	0.00010	0.00010	0.00720	0.00010	0.00010	0.00010	0.00120	0.24100
Constant Altitude, 15K	190 KIAS	0.378	119	403	5.55	14907	0.00010	0.00010	0.00010	0.00708	0.00010	0.00010	0.00010	0.00145	0.51680
	205 KIAS	0.413	142	444	4.48	14947	0.00010	0.00010	0.00010	0.00534	0.00010	0.00010	0.00010	0.00190	0.66960
	220 KIAS	0.442	162	477	3.72	15050	0.00010	0.00010	0.00010	0.00540	0.00010	0.00010	0.00010	0.00110	0.42125
	235 KIAS	0.469	184	508	3.49	14833	0.00010	0.00010	0.00010	0.00440	0.00010	0.00010	0.00010	0.00120	0.23000

Table G4: Lateral-Directional Cramer-Rao Bounds – Regime 1

Test Condition		Mach	qbar (lb/ft^2)	kias	alpha (deg)	Altitude (ft)	cla	cl0	cm0	cmde	cmq	clde	cma
Asymmetric Thrust	0%	0.30	76.75	317	8.41	14900	0.07378	0.07728	0.08888	-0.01710	-15.05000	0.00560	-0.01258
	20%	0.30	72.43	309	8.72	14975	0.07378	0.07728	0.08888	-0.01710	-15.05000	0.00560	-0.01258
	30%	0.31	77.35	321	8.10	15000	0.07378	0.07728	0.08888	-0.01710	-15.05000	0.00560	-0.01258
Bank Angle	0 deg	0.30	75.93	316	9.25	14900	0.07378	0.07728	0.08888	-0.01710	-15.05000	0.00560	-0.01258
	15 deg	0.30	75.93	316	9.25	14900	0.07325	0.08187	0.08382	-0.01680	-14.36667	0.00547	-0.01217
	30 deg	0.30	75.93	316	9.25	14900	0.07210	0.10930	0.07836	-0.01712	-14.80000	0.00558	-0.01198
5 deg Climb		0.30	75.93	316	9.25	14900	0.07475	0.08335	0.07078	-0.01833	-12.87500	0.00613	-0.01248
10 deg Climb		0.30	75.93	316	9.25	14900	0.07273	0.10870	0.08028	-0.01633	-13.70000	0.00653	-0.01400
3 deg Descent		0.30	75.93	316	9.25	14900	0.07462	0.05507	0.09857	-0.01712	-15.25000	0.00597	-0.01415
Push Over	0.4 g	0.30	75.93	316	9.25	14900	0.08400	-0.02235	0.09455	-0.01555	-13.52500	0.00550	-0.01368
	0.6 g	0.30	75.93	316	9.25	14900	0.08677	-0.02533	0.08730	-0.01563	-15.96667	0.00490	-0.01277
	0.8 g	0.30	75.93	316	9.25	14900	0.08245	-0.00410	0.09170	-0.01525	-13.55000	0.00550	-0.01355
Beta	0 deg	0.30	75.18	316	9.70	14975	0.07378	0.07728	0.08888	-0.01710	-15.05000	0.00560	-0.01258
	2 deg	0.29	71.40	306	10.50	14650	0.07378	0.07728	0.08888	-0.01710	-15.05000	0.00560	-0.01258
	4 deg	0.30	75.80	317	9.18	15100	0.07378	0.07728	0.08888	-0.01710	-15.05000	0.00560	-0.01258
	-4 deg	0.30	76.93	317	9.09	14575	0.07378	0.07728	0.08888	-0.01710	-15.05000	0.00560	-0.01258
	6 deg	0.30	73.77	309	9.66	14467	0.07378	0.07728	0.08888	-0.01710	-15.05000	0.00560	-0.01258
Constant Mach, 0.30	12.5K	0.30	80.42	313	7.72	12440	0.07546	0.03674	0.08966	-0.01672	-13.70000	0.00580	-0.01414
	15K	0.30	75.70	314	8.39	14875	0.07541	0.04473	0.09180	-0.01684	-14.90000	0.00636	-0.01436
	17.5K	0.32	68.93	323	9.28	20100	0.07240	0.06443	0.08147	-0.01697	-14.16667	0.00593	-0.01350
	20K	0.30	60.10	297	10.97	19850	0.06832	0.12680	0.07018	-0.01730	-14.98000	0.00638	-0.01226
Constant q	10K .27M	0.27	73.95	287	8.97	9975	0.07325	0.05925	0.09290	-0.01658	-14.45000	0.00605	-0.01443
	12.5K .28M	0.28	72.60	293	9.02	12167	0.07546	0.03674	0.08966	-0.01672	-13.70000	0.00580	-0.01414
	17.5K .31M	0.30	68.18	309	9.48	17550	0.07526	0.05470	0.08118	-0.01756	-15.38750	0.00594	-0.01324
	20.0K .33M	0.32	68.93	323	9.28	20100	0.07700	0.02657	0.08650	-0.01870	-16.33333	0.00593	-0.01437
Constant Altitude, 15K	135 KIAS	0.27	63.20	285	10.78	14750	0.07124	0.09572	0.07666	-0.01758	-15.10000	0.00600	-0.01286
	150 KIAS	0.30	75.93	316	9.25	14900	0.07480	0.06853	0.08318	-0.01707	-15.08333	0.00560	-0.01227
	165 KIAS	0.33	91.63	351	7.33	14933	0.08130	0.01868	0.08830	-0.01618	-15.10000	0.00552	-0.01245

Table G5: Longitudinal Derivatives – Regime 2

Test Condition		Mach	qbar (lb/ft^2)	kias	alpha (deg)	Altitude (ft)	crcla	crcl0	crcm0	crcmde	crcmq	crclde	crcma
Asymmetric Thrust	0%	0.30	76.75	317	8.41	14900	0.00075	0.00772	0.00050	0.00010	0.15183	0.00023	0.00002
	20%	0.30	72.43	309	8.72	14975	0.00075	0.00772	0.00050	0.00010	0.15183	0.00023	0.00002
	30%	0.31	77.35	321	8.10	15000	0.00075	0.00772	0.00050	0.00010	0.15183	0.00023	0.00002
Bank Angle	0 deg	0.30	75.93	316	9.25	14900	0.00075	0.00772	0.00050	0.00010	0.15183	0.00023	0.00002
	15 deg	0.30	75.93	316	9.25	14900	0.00072	0.00730	0.00050	0.00008	0.14850	0.00020	0.00003
	30 deg	0.30	75.93	316	9.25	14900	0.00080	0.00840	0.00054	0.00010	0.16420	0.00028	0.00002
5 deg Climb		0.30	75.93	316	9.25	14900	0.00100	0.00945	0.00125	0.00010	0.26325	0.00028	0.00013
10 deg Climb		0.30	75.93	316	9.25	14900	0.00088	0.00743	0.00060	0.00010	0.19350	0.00028	0.00005
3 deg Descent		0.30	75.93	316	9.25	14900	0.00063	0.00613	0.00042	0.00008	0.14033	0.00020	0.00002
Push Over	0.4 g	0.30	75.93	316	9.25	14900	0.00115	0.00435	0.00055	0.00010	0.34850	0.00030	0.00015
	0.6 g	0.30	75.93	316	9.25	14900	0.00120	0.00597	0.00057	0.00010	0.30500	0.00030	0.00010
	0.8 g	0.30	75.93	316	9.25	14900	0.00125	0.00740	0.00075	0.00010	0.28500	0.00030	0.00015
Beta	0 deg	0.30	75.18	316	9.70	14975	0.00075	0.00772	0.00050	0.00010	0.15183	0.00023	0.00002
	2 deg	0.29	71.40	306	10.50	14650	0.00075	0.00772	0.00050	0.00010	0.15183	0.00023	0.00002
	4 deg	0.30	75.80	317	9.18	15100	0.00075	0.00772	0.00050	0.00010	0.15183	0.00023	0.00002
	-4 deg	0.30	76.93	317	9.09	14575	0.00075	0.00772	0.00050	0.00010	0.15183	0.00023	0.00002
	6 deg	0.30	73.77	309	9.66	14467	0.00075	0.00772	0.00050	0.00010	0.15183	0.00023	0.00002
Constant Mach, 0.30	12.5K	0.30	80.42	313	7.72	12440	0.00074	0.00692	0.00060	0.00010	0.17460	0.00020	0.00010
	15K	0.30	75.70	314	8.39	14875	0.00067	0.00598	0.00053	0.00010	0.17167	0.00020	0.00006
	17.5K	0.32	68.93	323	9.28	20100	0.00070	0.00747	0.00070	0.00010	0.17467	0.00020	0.00010
	20K	0.30	60.10	297	10.97	19850	0.00074	0.00836	0.00090	0.00010	0.20580	0.00020	0.00008
Constant q	10K .27M	0.27	73.95	287	8.97	9975	0.00070	0.00648	0.00063	0.00010	0.17200	0.00020	0.00010
	12.5K .28M	0.28	72.60	293	9.02	12167	0.00074	0.00692	0.00060	0.00010	0.17460	0.00020	0.00010
	17.5K .31M	0.30	68.18	309	9.48	17550	0.00060	0.00606	0.00050	0.00010	0.15000	0.00020	0.00000
	20.0K .33M	0.32	68.93	323	9.28	20100	0.00067	0.00660	0.00057	0.00010	0.17100	0.00020	0.00003
Constant Altitude, 15K	135 KIAS	0.27	63.20	285	10.78	14750	0.00062	0.00694	0.00064	0.00010	0.17640	0.00020	0.00004
	150 KIAS	0.30	75.93	316	9.25	14900	0.00057	0.00530	0.00037	0.00008	0.12865	0.00020	0.00000
	165 KIAS	0.33	91.63	351	7.33	14933	0.00055	0.00403	0.00025	0.00005	0.12583	0.00020	0.00000

Table G6: Longitudinal Cramer-Rao Bounds – Regime 2

Test Condition		Mach	qbar (lb/ft^2)	kias	alpha (deg)	Altitude (ft)	cnb	cnda	cndr	cnr	clb	clda	cldr	clp	cyb
Asymmetric Thrust	0%	0.30	76.75	317	8.41	14900	0.00145	0.00005	-0.00100	-0.01308	-0.00160	-0.00145	0.00040	-0.38325	-0.0149
	20%	0.30	72.43	309	8.72	14975	0.00148	0.00003	-0.00100	-0.05880	-0.00200	-0.00135	0.00040	-0.37100	-0.0142
	30%	0.31	77.35	321	8.10	15000	0.00135	0.00000	-0.00100	-0.10780	-0.00185	-0.00130	0.00040	-0.37000	-0.0132
Bank Angle	0 deg	0.30	75.93	316	9.25	14900	0.00160	-0.00005	-0.00097	-0.12203	-0.00243	-0.00133	0.00037	-0.37600	-0.0140
	15 deg	0.30	75.93	316	9.25	14900	0.00160	-0.00005	-0.00097	-0.12203	-0.00243	-0.00133	0.00037	-0.37600	-0.0140
	30 deg	0.30	75.93	316	9.25	14900	0.00160	-0.00005	-0.00097	-0.12203	-0.00243	-0.00133	0.00037	-0.37600	-0.0140
5 deg Climb		0.30	75.93	316	9.25	14900	0.00160	-0.00005	-0.00097	-0.12203	-0.00243	-0.00133	0.00037	-0.37600	-0.0140
10 deg Climb		0.30	75.93	316	9.25	14900	0.00160	-0.00005	-0.00097	-0.12203	-0.00243	-0.00133	0.00037	-0.37600	-0.0140
3 deg Descent		0.30	75.93	316	9.25	14900	0.00160	-0.00005	-0.00097	-0.12203	-0.00243	-0.00133	0.00037	-0.37600	-0.0140
Push Over	0.4 g	0.30	75.93	316	9.25	14900	0.00160	-0.00005	-0.00097	-0.12203	-0.00243	-0.00133	0.00037	-0.37600	-0.0140
	0.6 g	0.30	75.93	316	9.25	14900	0.00160	-0.00005	-0.00097	-0.12203	-0.00243	-0.00133	0.00037	-0.37600	-0.0140
	0.8 g	0.30	75.93	316	9.25	14900	0.00160	-0.00005	-0.00097	-0.12203	-0.00243	-0.00133	0.00037	-0.37600	-0.0140
Beta	0 deg	0.30	75.18	316	9.70	14975	0.00153	-0.00005	-0.00098	-0.03143	-0.00238	-0.00135	0.00035	-0.39075	-0.0140
	2 deg	0.29	71.40	306	10.50	14650	0.00160	-0.00005	-0.00100	-0.12600	-0.00245	-0.00125	0.00035	-0.39350	-0.0135
	4 deg	0.30	75.80	317	9.18	15100	0.00163	0.00007	-0.00113	-0.18797	-0.00143	-0.00190	0.00047	-0.11630	-0.0143
	-4 deg	0.30	76.93	317	9.09	14575	0.00120	0.00000	-0.00103	0.00103	-0.00218	-0.00118	0.00028	-0.35600	-0.0130
	6 deg	0.30	73.77	309	9.66	14467	0.00130	0.00000	-0.00107	-0.22467	-0.00150	-0.00133	0.00040	-0.24937	-0.0131
Constant Mach, 0.30	12.5K	0.30	80.42	313	7.72	12440	0.00138	0.00002	-0.00100	-0.06548	-0.00182	-0.00140	0.00040	-0.41480	-0.0138
	15K	0.30	75.70	314	8.39	14875	0.00161	0.00000	-0.00100	0.00774	-0.00216	-0.00130	0.00040	-0.38500	-0.0141
	17.5K	0.32	68.93	323	9.28	20100	0.00157	0.00000	-0.00100	-0.07210	-0.00223	-0.00120	0.00040	-0.37767	-0.0135
	20K	0.30	60.10	297	10.97	19850	0.00153	0.00008	-0.00100	0.01137	-0.00232	-0.00127	0.00038	-0.33133	-0.0149
Constant q	10K .27M	0.27	73.95	287	8.97	9975	0.00160	-0.00005	-0.00100	-0.00570	-0.00260	-0.00130	0.00035	-0.45600	-0.0132
	12.5K .28M	0.28	72.60	293	9.02	12167	0.00153	-0.00003	-0.00103	-0.10613	-0.00233	-0.00123	0.00037	-0.40133	-0.0134
	17.5K .31M	0.30	68.18	309	9.48	17550	0.00165	-0.00002	-0.00102	-0.01687	-0.00237	-0.00127	0.00040	-0.37300	-0.0146
	20.0K .33M	0.32	68.93	323	9.28	20100	0.00157	0.00000	-0.00100	-0.07210	-0.00223	-0.00120	0.00040	-0.37767	-0.0135
Constant Altitude, 15K	135 KIAS	0.27	63.20	285	10.78	14750	0.00165	-0.00008	-0.00100	-0.01445	-0.00275	-0.00120	0.00030	-0.38825	-0.0144
	150 KIAS	0.30	75.93	316	9.25	14900	0.00160	-0.00005	-0.00097	-0.12203	-0.00243	-0.00133	0.00037	-0.37600	-0.0140
	165 KIAS	0.33	91.63	351	7.33	14933	0.00153	-0.00010	-0.00103	0.04233	-0.00223	-0.00153	0.00040	-0.43067	-0.0134
	180 KIAS	0.36	106.86	380	6.35	14700	0.00134	-0.00003	-0.00101	-0.18273	-0.00217	-0.00146	0.00037	-0.44000	-0.0135

Table G7: Lateral-Directional Derivatives – Regime 2

Test Condition		Mach	qbar (lb/ft^2)	kias	alpha (deg)	Altitude (ft)	crcnb	crcnda	crcndr	crcnr	crclb	crclda	crcldr	crclp	crcyb
Asymmetric Thrust	0%	0.30	76.75	317	8.41	14900	0.00000	0.00000	0.00000	0.00745	0.00000	0.00000	0.00000	0.00205	0.0002
	20%	0.30	72.43	309	8.72	14975	0.00000	0.00000	0.00000	0.00593	0.00000	0.00000	0.00000	0.00148	0.0002
	30%	0.31	77.35	321	8.10	15000	0.00000	0.00000	0.00000	0.00410	0.00000	0.00000	0.00000	0.00155	0.0002
Bank Angle	0 deg	0.30	75.93	316	9.25	14900	0.00000	0.00000	0.00000	0.00722	0.00000	0.00000	0.00000	0.00267	0.0002
	15 deg	0.30	75.93	316	9.25	14900	0.00000	0.00000	0.00000	0.00722	0.00000	0.00000	0.00000	0.00267	0.0002
	30 deg	0.30	75.93	316	9.25	14900	0.00000	0.00000	0.00000	0.00722	0.00000	0.00000	0.00000	0.00267	0.0002
5 deg Climb		0.30	75.93	316	9.25	14900	0.00000	0.00000	0.00000	0.00722	0.00000	0.00000	0.00000	0.00267	0.0002
10 deg Climb		0.30	75.93	316	9.25	14900	0.00000	0.00000	0.00000	0.00722	0.00000	0.00000	0.00000	0.00267	0.0002
3 deg Descent		0.30	75.93	316	9.25	14900	0.00000	0.00000	0.00000	0.00722	0.00000	0.00000	0.00000	0.00267	0.0002
Push Over	0.4 g	0.30	75.93	316	9.25	14900	0.00000	0.00000	0.00000	0.00722	0.00000	0.00000	0.00000	0.00267	0.0002
	0.6 g	0.30	75.93	316	9.25	14900	0.00000	0.00000	0.00000	0.00722	0.00000	0.00000	0.00000	0.00267	0.0002
	0.8 g	0.30	75.93	316	9.25	14900	0.00000	0.00000	0.00000	0.00722	0.00000	0.00000	0.00000	0.00267	0.0002
Beta	0 deg	0.30	75.18	316	9.70	14975	0.00000	0.00000	0.00000	0.01070	0.00000	0.00000	0.00000	0.00278	0.0002
	2 deg	0.29	71.40	306	10.50	14650	0.00000	0.00000	0.00000	0.00680	0.00000	0.00000	0.00000	0.00320	0.0002
	4 deg	0.30	75.80	317	9.18	15100	0.00000	0.00000	0.00000	0.00930	0.00000	0.00000	0.00000	0.00797	0.0001
	-4 deg	0.30	76.93	317	9.09	14575	0.00000	0.00000	0.00000	0.00878	0.00000	0.00000	0.00000	0.00388	0.0003
	6 deg	0.30	73.77	309	9.66	14467	0.00000	0.00000	0.00000	0.01083	0.00000	0.00000	0.00000	0.00317	0.0002
Constant Mach, 0.30	12.5K	0.30	80.42	313	7.72	12440	0.00000	0.00000	0.00000	0.00524	0.00000	0.00000	0.00000	0.00188	0.0002
	15K	0.30	75.70	314	8.39	14875	0.00000	0.00000	0.00000	0.00658	0.00000	0.00000	0.00000	0.00169	0.0002
	17.5K	0.32	68.93	323	9.28	20100	0.00000	0.00000	0.00000	0.00587	0.00000	0.00000	0.00000	0.00160	0.0002
	20K	0.30	60.10	297	10.97	19850	0.00000	0.00000	0.00000	0.00863	0.00000	0.00000	0.00000	0.00170	0.0002
Constant q	10K .27M	0.27	73.95	287	8.97	9975	0.00000	0.00000	0.00000	0.00725	0.00000	0.00000	0.00000	0.00295	0.0003
	12.5K .28M	0.28	72.60	293	9.02	12167	0.00000	0.00000	0.00000	0.00563	0.00000	0.00000	0.00000	0.00193	0.0002
	17.5K .31M	0.30	68.18	309	9.48	17550	0.00000	0.00000	0.00000	0.00672	0.00000	0.00000	0.00000	0.00183	0.0002
	20.0K .33M	0.32	68.93	323	9.28	20100	0.00000	0.00000	0.00000	0.00587	0.00000	0.00000	0.00000	0.00160	0.0002
Constant Altitude, 15K	135 KIAS	0.27	63.20	285	10.78	14750	0.00000	0.00000	0.00000	0.00595	0.00000	0.00000	0.00000	0.00188	0.0002
	150 KIAS	0.30	75.93	316	9.25	14900	0.00000	0.00000	0.00000	0.00722	0.00000	0.00000	0.00000	0.00267	0.0002
	165 KIAS	0.33	91.63	351	7.33	14933	0.00000	0.00000	0.00000	0.00610	0.00000	0.00000	0.00000	0.00267	0.0002
	180 KIAS	0.36	106.86	380	6.35	14700	0.00000	0.00000	0.00000	0.00567	0.00000	0.00000	0.00000	0.00254	0.0001

Table G8: Lateral-Directional Cramer-Rao Bounds – Regime 2

This page intentionally left blank.

APPENDIX H – PLOTS SUPPORTING DETERMINATION OF MODEL SENSITIVITY TO STABILITY DERIVATIVE VARIATION

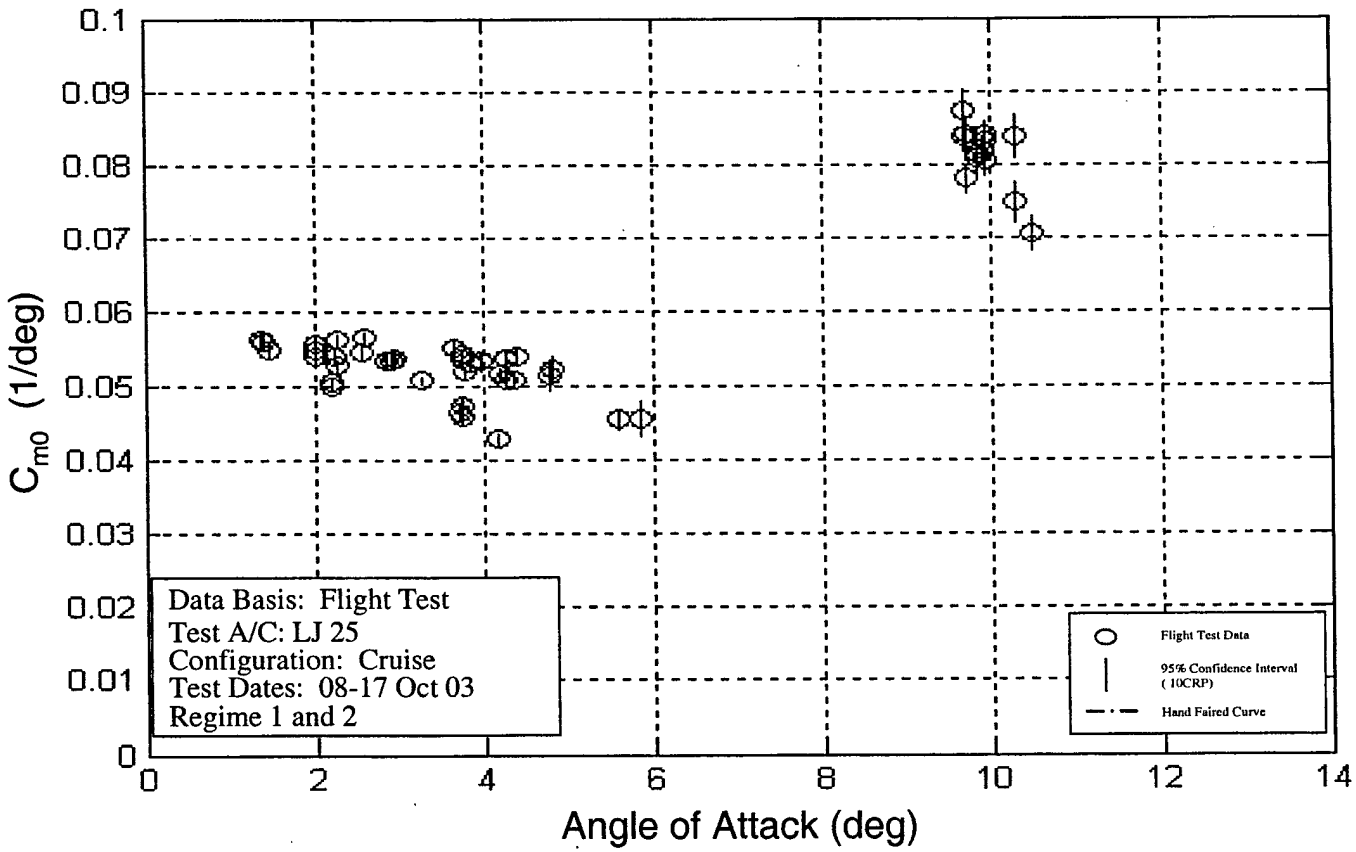

Figure H1: Learjet 25 C_{m0} vs α, Project HAVE TRIM

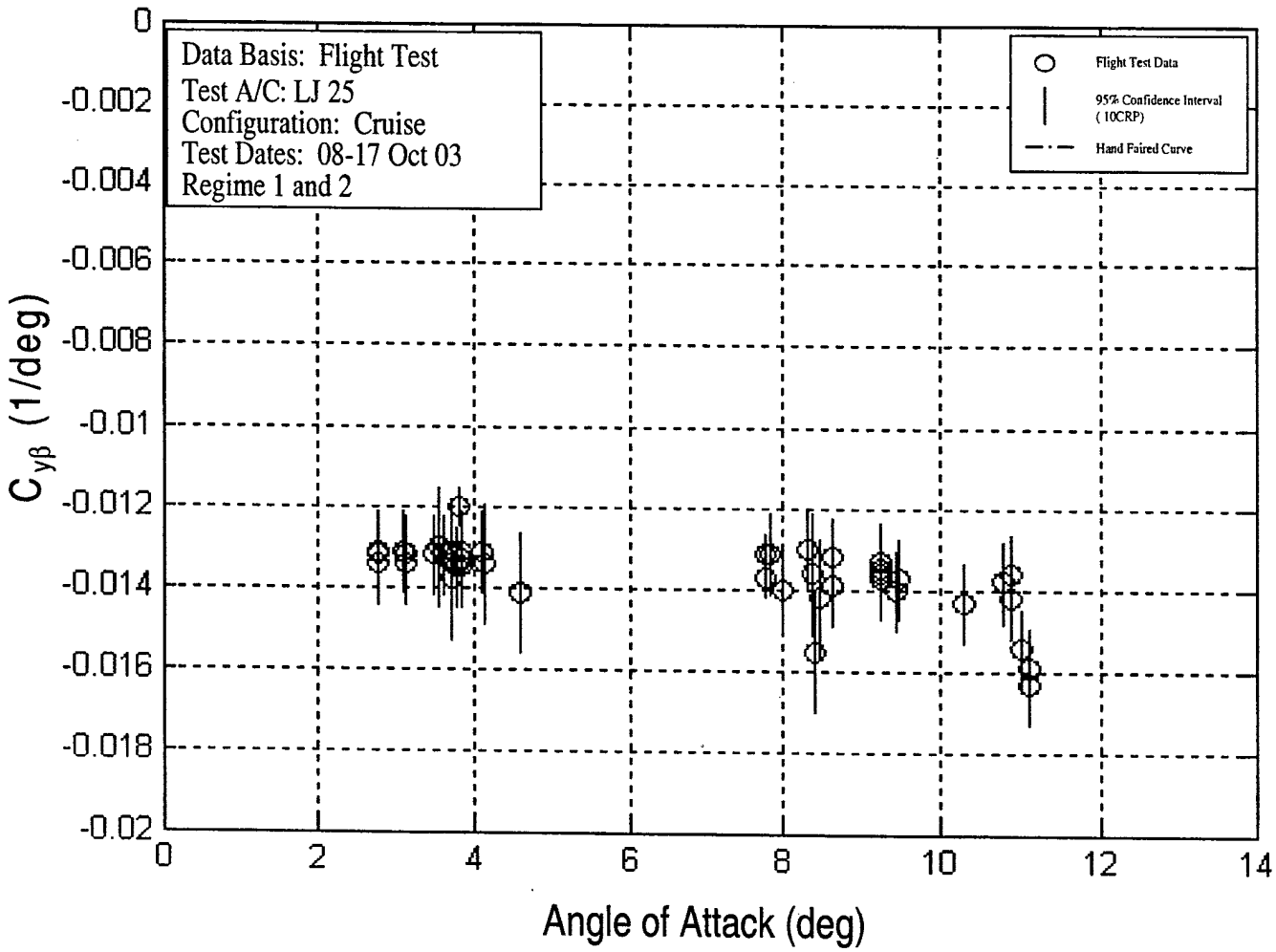

Figure H2: Learjet 25 $C_{y\beta}$ vs α, Project HAVE TRIM

This page intentionally left blank.

APPENDIX I – THESIS FLIGHT CONTROL EQUATIONS

The following equations are from the unpublished Master's thesis by Capt G. Miller and are used to predict δ's. They are collectively referred to as the "model EOM" or simply, the "model" in the HAVE TRIM Final Technical Information Memorandum.

Longitudinal control surface equation:

$$\delta_e = \frac{c_7(z_T\cos\alpha_T + x_T\sin\alpha_T)(T_1+T_2) - C_{m_{pr}}PR - C_{m_{p^2r^2}}(R^2-P^2)}{C_{m_{\delta_e}} c_7 \bar{q}c} - \frac{C_{m_o} + C_{m_\alpha}\alpha + C_{m_{\dot\alpha}}\dot\alpha + C_{m_q}Q}{C_{m_{\delta_e}}}$$

where:

$c_7 = \frac{1}{I_{yy}}$

x_T = horizontal (x-axis) distance from thrust center to center of gravity
z_T = vertical distance from thrust center to center of gravity
T_1 = Thrust from right engine
T_2 = Thrust from left engine
q = Dynamic pressure
c = Wing chord
α_T = Angle of thrust from x_{body} axis
I_{yy} = Moment of inertia about y_{body} axis

Lateral-Directional control surface equations:

$$\begin{bmatrix}\delta_a\\ \delta_r\end{bmatrix} = \frac{\begin{bmatrix} c_r(c_3C_{l_{\delta_r}} + c_4C_{n_{\delta_r}}) - c_p(c_9C_{n_{\delta_r}} + c_4C_{l_{\delta_r}}) \\ c_p(c_9C_{n_{\delta_a}} + c_4C_{l_{\delta_a}}) - c_r(c_3C_{l_{\delta_a}} + c_4C_{n_{\delta_a}})\end{bmatrix}}{\bar{q}b[(c_3C_{l_{\delta_a}} + c_4C_{n_{\delta_a}})(c_9C_{n_{\delta_r}} + c_4C_{l_{\delta_r}}) - (c_3C_{l_{\delta_r}} + c_4C_{n_{\delta_r}})(c_9C_{n_{\delta_a}} + c_4C_{l_{\delta_a}})]}$$

where:

$$c_p = C_{l_{pq}}PQ + C_{l_{qr}}QR + c_3y_T\sin\alpha_T(T_2-T_1) + c_4y_T\cos\alpha_T(T_2-T_1) +$$
$$+\bar{q}b[c_3(C_{l_p}P + C_{l_r}R + C_{l_\beta}\beta) + c_4(C_{n_p}P + C_{n_r}R + C_{n_\beta}\beta)]$$
$$c_r = C_{n_{pq}}PQ - C_{n_{qr}}QR + c_9y_T\cos\alpha_T(T_2-T_1) + c_4y_T\sin\alpha_T(T_2-T_1) +$$
$$+\bar{q}b[c_9(C_{n_p}P + C_{n_r}R + C_{n_\beta}\beta) + c_4(C_{l_p}P + C_{l_r}R + C_{l_\beta}\beta)]$$
$$c_3 = \frac{I_{zz}}{I_{xx}I_{zz} - I_{xz}^2}$$

$$c_4 = \frac{I_{xz}}{I_{xx}I_{zz} - I_{xz}^2}$$

$$c_9 = \frac{I_{xx}}{I_{xx}I_{zz} - I_{xz}^{\ 2}}$$

y_T = horizontal (y-axis) distance from thrust center to center of gravity
b = Wing span
I_{xx} = Moment of inertia about x_{body} axis
I_{zz} = Moment of inertia about z_{body} axis
I_{xz} = Product of inertia about x_{body} axis and z_{body} axis
C_{l_pq} = Product derivative
C_{l_qr} = Product derivative
C_{n_pq} = Product derivative
C_{n_qr} = Product derivative

The following assumptions were made to derive the equations:

- The sum of the forces on the vehicle are zero, so there is no translational acceleration.
- The sum of the moments on the vehicle are zero, so there is no angular acceleration.
- All aerodynamic forces are linear. The equations do not account for aerodynamic effects near stall and at high speed, when aerodynamic compressibility effects occur.
- Longitudinal and lateral-directional equations are decoupled.
- The mass properties of the vehicle do not change during the maneuver. The center of gravity and moments of inertia remains constant.
- Ideal atmosphere: no gusts or disturbances, and the atmosphere can be modeled by the standard atmosphere.
- The stability derivatives are constant throughout the trim point.

APPENDIX J – PARAMETERS LIST

Aerodynamic Parameters (symbol) [units]	Resolution	Uncertainty
Aircraft Weight (W) [lbs.]	*From fuel flow and zero fuel wt.	
Aircraft Airspeed (V) [kts]	0.0305	±0.5%
Pressure Altitude (h) [ft]	19.5	±0.4%+25 ft
Asymmetric Thrust (ΔT) [% right engine]	*From Engine Pressure Ratio	
Glide Path Angle (γ) [deg]	*From α and θ	
Sideslip Angle (β) [deg]	0.00098	±1.0%
Aircraft Turn Rate (ω_ψ) [deg/s]	*From P, Q and R	
Aircraft Pitch Rate (ω_θ) [deg/s]	*From P, Q and R	
Angle of Attack (α) [deg]	0.00098	±1.0%
Pitch Angle (θ) [deg]	0.00439	±1.0 deg
Bank Angle (ϕ) [deg]	0.00439	±1.0 deg
Acceleration in X-body Axis (n_x) [g's]	0.00005	±0.07%
Acceleration in Y-body Axis (n_y) [g's]	0.00005	±0.07%
Acceleration in Z-body Axis (n_z) [g's]	0.00024	±0.07%
Rotation about X-body Axis (P) [deg/s]	0.00488	±2.3%
Rotation about Y-body Axis (Q) [deg/s]	0.00195	±2.3%
Rotation about Z-body Axis (R) [deg/s]	0.00195	±2.3%

Control Surface Deflections (symbol) [units]	Resolution	Uncertainty
Aileron Surface Deflection (δ_a) [deg]	0.00195	±1.0%
Elevator Surface Deflection (δ_e) [deg]	0.00098	±1.0%
Rudder Surface Deflection (δ_r) [deg]	0.00195	±1.0%

Longitudinal Stability Derivatives (symbol) [units]	Initial Value
Lift coefficient slope ($C_{L\alpha}$) [1/rad]	5.386
Zero lift coefficient (C_{L0}) [--]	0.097
Zero lift drag coefficient (C_{D0}) [--]	0.0235
Zero lift pitching moment coefficient (C_{m0}) [--]	0.031
Pitch stability ($C_{m\alpha}$) [1/rad]	-0.7792
Pitch damping (C_{mq}) [sec/rad]	-11.918
Pitch control power ($C_{m\delta e}$) [1/rad]	-0.8995

Lateral-Directional Stability Derivatives (symbol) [units]	Initial Value
Dihedral effect ($C_{l\beta}$) [1/rad]	-0.0802
Lateral damping (C_{lp}) [sec/rad]	-0.4160
Lateral control power ($C_{l\delta a}$) [1/rad]	-0.0596
Weather-cock stability ($C_{n\beta}$) [1/rad]	0.0900
Directional damping (C_{nr}) [sec/rad]	-0.1914
Directional control power ($C_{n\delta r}$) [1/rad]	-0.0487
Adverse yaw derivative ($C_{n\delta a}$) [1/rad]	0.0011
Adverse roll due rudder deflection ($C_{l\delta r}$) [1/rad]	0.0195
Roll coupling due to yaw rate (C_{lr}) [1/rad]	0.311
Yaw coupling due to roll rate (C_{np}) [1/rad]	-0.0395
Yaw derivative due to sideslip ($C_{n\beta}$) [1/rad]	0.090

APPENDIX K – WORKING WITH PEST

Overall

PEST was just one of the four applications of the Parameter Identification software package. In order to run PEST and calculate the derivatives four steps were followed: project manager shield, time history editor shield, parameter estimation shield and output generator shield. In the next sections these steps will be briefly described and the lessons learned highlighted[7]. Each data point run required about 20 minutes.

Project Manager

The Project Manager allowed for setting the constants (the predicted value for the derivatives) the instrumentation correction and the variables from which the aerodynamic model was calculated. PEST did not actually need a good prediction for the derivatives, but these predictions were used as initial values to start the iterations to calculate the stability derivatives. This iteration process stopped when a minimum in the specific cost function was reached. A bad initial value could cause PEST to converge to a local minimum of the cost function instead of the actual absolute minimum. Therefore, since a good set of stability derivatives was not available except for one flight condition, it was decided to use the derivatives related to that condition as a prediction for all the PEST runs.

The instrument corrections page allowed entering the compensations for CG position and aircraft accelerations. Throughout the runs it was observed that PEST gave a relatively high importance to the instrument corrections, and if the time histories did not match, it was sometimes related to an incorrect compensation for CG position and accelerations. The constants page regarded mass properties (moments of inertia, total aircraft mass), airplane constants (chord, wing span) and CG position. This last parameter was related to the instrument corrections page. Whatever CG position the instrument corrections were related to, that position was constant for the entire test program. Therefore the shift between the current position and the reference position was entered in the constant page. The response page allowed for selecting the variables the derivatives were calculated from and the weight of each of those variables. The initial plan was to run PEST a few times, find the weights for each run, calculate the arithmetic averages of the weights and take them as constant for the rest of the runs. However PEST was more sensitive with regard to the weights. Thus, the weights were calculated and fine tuned for each run instead of using averaged values. This was a very time consuming process.

The instrument corrections were assumed to be zero: the LEARJET-25 instrument readings were corrected for the CG position; the compensation for the aircraft accelerations were unknown, so they were set to zero.

[7] For further details see reference 2, PCPID Users manual

The response biases were all set to zero and "false" except the variables "qbias" and "anbias" for the longitudinal case, and "pbias" and "aybias" for the lateral-directional case.

Figures K1 and K2 are taken from the "response" page; they show an initial value for the weightings (column 3), used in the longitudinal and lateral-directional runs respectively. Whenever the variable was not active ("false"), the weight was zero.

alpha	3.217475258	T	10.00000000
an	.9983353436	T	50.00000000
ax	.0000000000	F	.0000000000
ay	-.8385201002E-02	F	70.00000000
beta	-.7414613823E-01	F	12.00000000
p	.1324628093	F	.7000000000
pdot	.0000000000	F	.0000000000
phi	.9372345189	F	3.000000000
q	.3766008385E-01	T	7.000000000
qdot	.0000000000	F	.0000000000
r	-.3129701718E-02	F	17.00000000
rdot	.0000000000	F	.0000000000
theta	3.428782131	T	31.00000000
v	493.6345704	F	.0000000000

Figure K1: Response Page (longitudinal case)

alpha	3.813589847	F	10.00000000
an	1.024682433	F	68.00000000
ax	.0000000000	F	.0000000000
ay	-.9803207908E-02	T	150.0000000
beta	.8259362778E-01	T	10.00000000
p	1.142827776	T	1.500000000
pdot	.0000000000	F	.0000000000
phi	5.166373475	T	25.00000000
q	.1623322571	F	6.000000000
qdot	.0000000000	F	.0000000000
r	.6112072420	T	10.00000000
rdot	.0000000000	F	.0000000000
theta	4.250552107	F	26.00000000
v	445.7449425	F	.0000000000

Figure K2: Response Page (lateral-directional case)

Time history editor

The time history editor allowed for the selection of the time slice from which the derivatives were calculated. A lesson learned for the test team was that PEST truncated the time history if too many points were selected, resulting in a bad estimation of the derivatives. Therefore, if the time spacing between the PTI rudder doublets and the PTI aileron doublets was too long, the resulting time history was not used. The time spacing that was found to permit a better estimation of the derivatives was 1 second.

PEST

The most important checks accomplished before actually running PEST was to make sure the variables that PEST was asked to calculate the derivatives from, were active. The way to perform the check was to read the initial dialogue lines that PEST displayed and insure that all of the active variables would not show up in the list of unknown channels. If one of the variables selected in the response page of the PSF manager shield was on that list, it was necessary to open an ASCII file called "plot setup" to determine the active variables. Therefore, before running PEST, this file was opened and a cross-check between the PSF manager page and the lines of this file was performed.

Output generator

In the output generator, the derivatives that were just calculated were displayed in the "text output" page, together with the 10CRP. Also, the computed and flight data time histories were plotted. The characteristics used to evaluate the accuracy in the estimation were the peak-to-peak time spacing and amplitude. The derivatives plot displayed the derivatives that were just calculated with the 95% confidence interval. If the estimation was deemed satisfactory then the entire set of data were saved in a data base; for each run the flight conditions, the derivatives and the CR bounds were saved automatically in the data base. In order to get the 95% confidence for each derivative, the bounds had to be multiplied by 10. Another lesson learned was that the data base assigned only a 6-digit space for each number. If the derivatives or the CR bounds were less than 0.00001 the value displayed on the data base was 0. Thus, if further data analysis was required, a cross-check with the test output page for each run was necessary as was a manual data entry of the actual value.

APPENDIX L – PROGRAMMED TEST INPUT DESCRIPTION

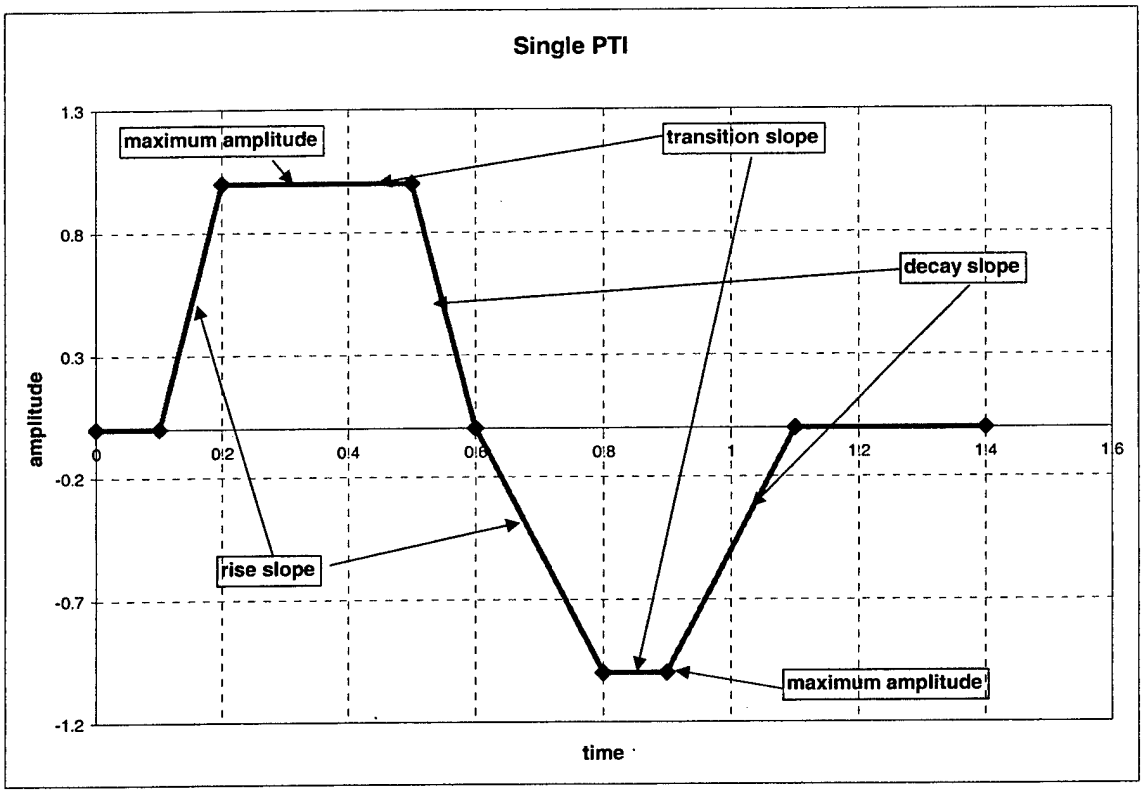

Figure L1: Programmed Test Input

Figure L1 shows an example of doublet PTI. The rise, transition, amplitude and decay slope were set on board and could be changed. The symmetry of the PTI in time was changed, as shown above, in order to make the positive part different from the negative. For a double PTI, the one used for lateral/directional derivatives investigation, the time between the rudder doublet and the aileron doublet could be varied too.

This page intentionally left blank.

APPENDIX M – GROUND SIM AND PTI SHAPING

The test team could have started flight test sooner after the aircraft arrived on station if more ground work had been done in advance. The test team had coordinated what variables were needed to perform the data reduction and obtain the trim conditions and stability derivatives. After the aircraft arrived, the test team discovered that the exact settings and names of the variables had to match precisely for the data to transfer between the program the aircraft used to save data and PEST. The test team spent considerable time changing variable names and order, such that PEST could recognize the data files. A sample file from the contractor previous to the aircraft arriviving would have been very useful. The test team could have reviewed the file and check that the proper variables were available to PEST and that they were in the right order. The test team took a full additional day to get the data issues worked out before flight testing.

PTI shaping was another issue that the test team faced. The test team found no way to predict what the PTI should look like prior to flight, in terms of either magnitude or symmetry. Symmetry was adjusted such that the aircraft completed the maneuver at as close to the initial trim condition as possible. Symmetry was measured in percent, from 0.00 to 1.00. Symmetry ranged from .45 to .48 for test maneuvers. This corresponded to a shorter initial input followed by a longer second input. The longer second input presumably helped overcome the rates generated by the first input.

The following discussion on PTI amplitude applies most specifically to the LEARJET-25, but may have some practical application to other flight testing. The test team had to choose amplitudes that would get measurable responses, but not trip off the variable stability system. Problems were encountered in Regime 1 at high beta when inputting the yaw doublet and under increased G loading in the constant altitude turn. The test team had planned to test up to 9 degrees of sideslip, approaching the VSS sideslip limit. Actual testing showed that it was only practical to go to 4° sideslip and amplitude of the PTI was reduced to half of the amplitude of the other conditions. The rolling moment safety trip kicked off the VSS system prior to the maximum sideslip. Test points at 60° bank were accomplished with a 20% reduction in the PTI pitch amplitude, and 66° bank points were not attempted. Table N1 is a summary of the amplitudes and symmetries used. Regime 2 did not need to have the doublets adjusted.

Regime 1		Pitch	Roll	Yaw
SLUF	Amp	7	15	10
	Period	0.6 sec	0.8 sec	1.0 sec
	Sym	0.45	0.47	0.49
Banked turns	Amp	4	10	7
	Period	0.6 sec	0.8 sec	1.0 sec
	Sym	0.45	0.48	0.46
Push Over 0.4g	Amp	4	10	10
	Period	0.6 sec	0.8 sec	1.0 sec
	Sym	0.45	0.48	0.46
Regime 2		Pitch	Roll	Yaw
SLUF	Amp	7	15	10
	Period	0.6 sec	0.8 sec	1.0 sec
	Sym	0.45	0.45	0.45

Table M1: PTI Summary

The final issue addressed by the test team was the lat-dir doublets were initially too long to be analyzed by PEST. The end of the maneuver was cut off, losing important data. The solution was to sequence the doublets such that by one test conductor input, the roll doublet was triggered followed shortly afterwards (1 second) by the yaw doublet. This was determined to be the best technique for getting the lat-dir stability derivatives.

APPENDIX N – IN FLIGHT LESSONS LEARNED

General

Record the cockpit intercom for qualitative comments and data.
Any flight 135 KIAS or slower should be performed at a maximum of 3000 lbs of fuel remaining to allow the VSS to remain engaged.

Configuration

Ensure that the correct stabilator position is verified after each engagement of the VSS.
Ensure that the stabilator is set to Manual during VSS engagement so that it does not automatically trim.
Return stabilator trim to Auto during administrative phases of flight. Otherwise, the stabilator will cause a fairly violent pitch up or down after a VSS trip if displaced from the trim airspeed.
Check the flaps are in the full up position periodically because they tend to droop.
Only the two heavier CG subsets were attainable.

Asymmetric Thrust Points

The maximum achievable thrust asymmetry in level flight was around 30%. Idle occurs around 61%.

Sideslip

Use the safety pilot to trim the rudder to establish the desired sideslip angle.
Maximum sideslip was around 5 degrees before the VSS would disengage due to side force.
Begin the rudder doublet away from the sideslip to help ensure the VSS remains engaged.
Decrease the PTI rudder doublet amplitude when approaching large sideslip values (we decreased the magnitude from 9 to 4.5).
An engine flamed out during the recovery from a prolonged sideslip with 500 lbs of fuel remaining in each wing tank (1500 lbs total fuel). The Veridian experts decided that the flameout was due to fuel starvation with less than full fuel in the wing fuel tanks. The crew limited future sideslips to greater than 3000 lbs of fuel remaining (full wing tanks). No subsequent problems were discovered.

Climbs and Descents

Maximum dive angle was approximately 3 degrees with idle thrust.
Maximum climb angle was approximately 10 degrees with maximum thrust.
Approximately 3000 feet of altitude was required to establish a trimmed climb.
Approximately 1500 feet of altitude was required to establish a trimmed idle descent.

Turns

In Region 1, the maximum bank angle possible prior to VSS automatic disengagement was 60 degrees.
In Region 2, the maximum bank angle possible prior to VSS automatic disengagement was 30 degrees.

Decrease the PTI elevator doublet amplitude when approaching large bank angle values (we decreased the magnitude from 5 to 4).

Pitch Rate

Hand fly pitch rate points.

In order to enter the pitch rate points begin at level flight about 50 KIAS above the data band. Establish a 12 degree climb using the safety pilot to set and adjust the throttles as necessary. At about 15 KIAS above the data band, begin the bunt. We gained about 500 feet from the initiation of the bunt to the apex altitude. Perform the PTI approaching wings level.

PTI and PEST

Allow a maximum of 2 seconds between aileron and rudder doublets. The smaller the pause between doublets, the easier the data is to analyze in PEST. Perform 3 of each type of doublet at each condition consecutively. This allows for easier PEST analysis because weightings do not have to be changed between each data point.

APPENDIX O – POINTS OF CONTACT

Requesting Agency

Department of Aeronautics & Astronautics,
Air Force Institute of Technology (AFIT/ENY)
2590 P Street, Suite 201
Wright-Patterson AFB, OH 45433-7765

Agency Representative: Lt Col David Jacques, USAF AFIT/ENY
DSN 785-3636 ext 4636
E-mail: david.jacques@afit.af.edu

Responsible Test Organization

The RTO for this project is the 412th Test Wing. The HAVE TRIM team will accomplish all testing and evaluation. The test team consists of two student test pilots, one student flight test navigator (FTN), and two student flight test engineers (FTEs).

Project Manager

Captain Gary Miller
USAF TPS/EDA
DSN 527-9968/9970/3000, COMM (661) 277-9968/9970/3000
E-mail: Gary.Miller4@edwards.af.mil

Advanced Information Engineering Services (formerly Veridian)

Mr Russ Easter
Advanced Information Engineering Services Instructor Pilot (IP)
COMM (716) 310-0278
Email: jeaster@buffalo.veridian.com

USAF TPS

Mr Russell Erb
USAF TPS/EDP
DSN 527-8829, COMM (661) 277-8829/3000
E-mail: russell.erb@edwards.af.mil

NASA Dryden

Mr Chris Nagy
Aerospace Engineer / NASA Dryden
COMM (661) 276-2626
E-mail: @dfrc.nasa.gov

This page intentionally left blank.

LIST OF ABBREVIATIONS, ACRONYMS, AND SYMBOLS

AFFTC – Air Force Flight Test Center
AFIT – Air Force Institute of Technology
AFRL – Air Force Research Laboratory
Alpha (α) – Angle of Attack
Beta (β) – Sideslip angle
CA – California
C_{do} – Coefficient of drag at $\alpha = 0$
Centurion – Test Pilot School student in Class 03A, The Wright Stuff, celebrating 100 years of powered flight.
CG – Aircraft Center of Gravity, measured in %MAC
$C_{L\alpha}$ – Lift curve slope
$C_{l\beta}$ – Rolling moment coefficient due to β
$C_{l\delta a}$ – Rolling moment coefficient due to aileron deflection
$C_{l\delta r}$ – Rolling moment coefficient due to rudder deflection
C_{L0} – Coefficient of lift at $\alpha = 0$
C_{lp} – Rolling moment coefficient due to rolling moment
$C_{m\alpha}$ – Pitching moment coefficient due to α
$C_{m\delta e}$ – Pitching moment coefficient due to elevator deflection
C_{mo} – Pitching moment coefficient at $\alpha = 0$
C_{mq} – Pitching moment coefficient due to pitch rate
$C_{n\beta}$ – Yawing moment coefficient due to β
$C_{n\delta a}$ – Yawing moment coefficient due to aileron deflection
$C_{n\delta r}$ – Yawing moment coefficient due to rudder deflection
C_{nr} – Yawing moment coefficient due to yaw rate
CRP – Cramer-Rao parameter
Delta (δ) – Generic flight control surface deflection
Delta a (δ_a) – Aileron Control Surface Deflection
Delta e (δ_e) – Elevator Control Surface Deflection
Delta r (δ_r) – Rudder Control Surface Deflection
DSN – Defense Services Network
EOM – Equations Of Motion
FTE – Flight Test Engineer
FTN – Flight Test Navigator
FTT – Flight Test Technique
Gamma (γ) – Flight path angle, climb/dive angle
h – height
HAVE TRIM – Project title bestowed upon this testing by the test team.
JON – Job Order Number
JP-5/JP-8 – Jet Fuel
LJ-25 – Learjet 25, the test aircraft
M – Mach number
MAC – Mean Aerodynamic Chord
MOP(s) – Measure(s) Of Performance

n_x – Load Factor in x-body axis
n_y – Load Factor in y-body axis
n_z – Load Factor in z-body axis
P – Aircraft Roll Rate
PRR – Preliminary Report of Results
OH – Ohio
PA – Pressure Altitude
PEST – Parameter Estimation software
Phi (ϕ) – Euler Bank Angle
PRR – Preliminary Report of Results
PTI – Programmed Test Input
q – Dynamic Pressure
Q – Aircraft Pitch Rate
R – Aircraft Yaw Rate
R1 – Region / Regime 1
R2 – Region / Regime 2
RTO – Responsible Test Organization
SHSS – Steady-Heading Sideslip
SLUF – Straight and Level, Unaccelerated Flight
SPORT – Space Positioning and Orientation Radar Tracking
sqrt – Square root
T – Thrust
Theta (θ) – Euler Pitch Angle
TIM – Technical Information Memorandum
TPS – Test Pilot School
TPS/DOR – Test Pilot School Operations Desk
UAV – Unmanned Aerial Vehicle
v – Volts
V – Velocity
VDC – Volts, Direct Current
VMC – Visual Meteorological Conditions
VSS – Variable Stability System installed on the test aircraft
V_{stall} – Stall Airspeed
W – Aircraft Weight
WUT – Wind-up Turn
10CRP – Ten times Cramer-Rao parameter
95 SPTG/LGS – 95th Logistics Squadron, Edwards AFB

REFERENCES

1. *Gates Learjet 25B/25C FAA Approved Airplane Flight Manual*, 8/19/70, Change 27

2. *Personal Computer Parameter Identification User Manual, V2.3*

3. *Trimmed Equilibrium Flight Inner- and Outer-Loop Control Laws,* unpublished thesis by Gary Miller for Air Force Institute of Technology

DISTRIBUTION LIST

Distribution	Number of Copies
412 TW/ENTL Attn: Ms. Lamb 307 E. Popson Ave, Bldg 1400, Rm 110 Edwards AFB CA 93524-6630	1
USAF TPS/EDT Attn: Mr. Gary Aldrich 220 South Wolfe Ave, Bldg 1220 Edwards AFB CA 93524-6485	1
USAF TPS/EDC Attn: Ms Dottie Meyer 220 S Wolfe Ave, Bldg 1220 Edwards AFB CA 93524-6485	1
AFFTC/HO 305 E Popson Ave, Bldg 1405 Edwards AFB CA 93523-6595	1
Advanced Engineering Systems Inc. Attn: Mr. Russ Easter 150 North Airport Drive Buffalo, New York 14225-1436	1
USAF TPS/ED Attn: Capt Gary D. Miller 220 South Wolfe Ave, Bldg 1220 Edwards AFB CA 93524-6485	5
	Total : 10